VOLUME 80 DECEMBER 30, 1976 NUMBER 27

JPCHAx

THE JOURNAL OF PHYSICAL CHEMISTRY

PUBLISHED BIWEEKLY BY THE AMERICAN CHEMICAL SOCIETY

THE JOURNAL OF

PHYSICAL CHEMISTRY

Published by the
AMERICAN CHEMICAL SOCIETY
BOOKS AND JOURNALS DIVISION
D. H. Michael Bowen, Director

Editorial Department: Charles R. Bertsch, Head; Marianne C. Brogan, Associate Head; Celia B. McFarland, Joseph E. Yurvati, Assistant Editors
Graphics and Production Department: Bacil Guiley, Head
Research and Development Department: Seldon W. Terrant, Head

Advertising Office: Centcom, Ltd., 50 W. State St., Westport, Conn. 06880.

Published biweekly by the American Chemical Society at 20th and Northampton Sts., Easton, Pennsylvania 18042. Second class postage paid at Washington, D.C. and at additional mailing offices.

Editorial Information

Instructions for authors are printed in the first issue of each volume. Please conform to these instructions when submitting manuscripts.

Manuscripts for publication should be submitted to *The Journal of Physical Chemistry*, Department of Chemistry, University of Minnesota, Minneapolis, Minn. 55455. Correspondence regarding **accepted papers and proofs** should be directed to the Editorial Department at the ACS Easton address.

Page charges of $60.00 per page are assessed for papers published in this journal. Ability to pay does not affect acceptance or scheduling of papers.

Bulk reprints or photocopies of individual articles are available. For information write to Business Operations, Books and Journals Division at the ACS Washington address.

Requests for **permission to reprint** should be directed to Permissions, Books and Journals Division at the ACS Washington address. The American Chemical Society and its Editors assume no responsibility for the statements and opinions advanced by contributors.

Subscription and Business Information

1976 Subscription rates—including surface postage

	U.S.	PUAS	Canada, Foreign
Member	$24.00	$29.75	$30.25
Nonmember	96.00	101.75	102.25
Supplementary material	15.00	19.00	20.00

Air mail and air freight rates are available from Membership & Subscription Services, at the ACS Columbus address.

New and renewal subscriptions should be sent with payment to the Office of the Controller at the ACS Washington address. **Changes of address** must include both old and new addresses with ZIP code and a recent mailing label. Send all address changes to the ACS Columbus address. Please allow six weeks for change to become effective. **Claims** for missing numbers will not be allowed if loss was due to failure of notice of change of address to be received in the time specified; if claim is dated (a) North America—more than 90 days beyond issue date, (b) all other foreign—more than 1 year beyond issue date; or if the reason given is "missing from files". Hard copy claims are handled at the ACS Columbus address.

Microfiche subscriptions are available at the same rates but are mailed first class to U.S. subscribers, air mail to the rest of the world. Direct all inquiries to Business Operations, Books and Journals Division, at the ACS Washington address or call (202) 872-4444. **Single issues** in hard copy and/or microfiche are available from Special Issues Sales at the ACS Washington address. Current year $4.75. Back issue rates available from Special Issues Sales. **Back volumes** are available in hard copy and/or microform. Write to Special Issues Sales at the ACS Washington address for further information. **Microfilm** editions of ACS periodical publications are available from volume 1 to the present. For further information, contact Special Issues Sales at the ACS Washington address. **Supplementary material** must be ordered directly from Business Operations, Books and Journals Division, at the ACS Washington address.

Microfiche	U.S.	PUAS, Canada	Other Foreign
Photocopy	$2.50	$3.00	$3.50
1–7 pages	4.00	5.50	7.00
8–20 pages	5.00	6.50	8.00

Orders over 20 pages are available only on microfiche, 4 × 6 in., 24X, negative, silver halide. Orders must state photocopy or microfiche if both are available. Full bibliographic citation including names of all authors and prepayment are required. Prices are subject to change.

American Chemical Society
1155 16th Street, N.W.
Washington, D.C. 20036
(202) 872-4600

Member & Subscription Services
American Chemical Society
P.O. Box 3337
Columbus, Ohio 43210
(614) 421-7230

Editorial Department
American Chemical Society
20th and Northampton Sts.
Easton, Pennsylvania 18042
(215) 258-9111

Notice to Authors last printed in the issue of January 1, 1976

THE JOURNAL OF

PHYSICAL CHEMISTRY

Volume 80, Number 27 December 30, 1976

JPCHAx 80(27) 2929–3030 (1976)

ISSN 0022-3654

There is no supplementary material for this issue

* In papers with more than one author, the asterisk indicates the name of the author to whom inquiries about the paper should be addressed.

AUTHOR INDEX

THE JOURNAL OF

PHYSICAL CHEMISTRY

Volume 80

JANUARY—JUNE 1976

PAGES 1–1518

JPCHAx 80(1–13) 1–1518 (1976)
ISSN 0022-3654

THE JOURNAL OF PHYSICAL CHEMISTRY

Volume 80

JULY—DECEMBER 1976

PAGES 1519–3030

JPCHAx 80(14–27) 1519–3030 (1976)
ISSN 0022-3654

THE JOURNAL OF
PHYSICAL CHEMISTRY

VOLUME 80, NUMBER 27 DECEMBER 30, 1976

Hydrogen Bonding in Polar Liquid Solutions. 1. Development of Kirkwood's Dielectric Theory in Terms of a Chemical Model[1a]

Ernest Grunwald*[1b] and Kee-Chuan Pan†

Department of Chemistry, Brandeis University, Waltham, Massachusetts 02154 *(Received June 23, 1976)*

Publication costs assisted by the Petroleum Research Fund

Kirkwood's dielectric theory, applied to dilute solutions, is developed in terms of a parameter $\mu_{2,app}$, called *the apparent dipole moment of the solute*. $\mu_{2,app}^2$ can be calculated directly from experimental data and equals $g_2\mu_2^2 + c_1{}^0\mu_1^2\,(dg_1/dc_2)$; μ_1, μ_2 denote intrinsic dipole moments, g_1, g_2 dipole correlation factors, and c_1, c_2 concentrations of solvent and solute species, respectively. A chemical model is introduced which assumes that dipole correlation between solute and solvent is considerable only in case of molecular complex formation. As a consequence, $\mu_{2,app}^2 - \mu_2^2$ is dissected neatly into additive contributions from (1) solvation of the solute; (2) transfer of solvent molecules into solvation shells from the bulk solvent; and (3) change in dipole correlation in the bulk solvent.

Introduction to Series of Papers

The effects of solutes on hydrogen bonding in hydroxylic solvents are so intricate that experimental probes all too often tell us only whether a given solute is "structure-making" or "structure-breaking". The dielectric constant, when interpreted in terms of Kirkwood's dielectric theory,[2] gives information about dipole alignment and hence can elucidate the specific geometrical structure of hydrogen-bonded complexes. The sharpness of the resulting picture can be further improved if the dielectric measurements are complemented by spectroscopic and other data.

In this series we are developing an approach, centered on dielectric measurements, for deducing specific hydrogen-bonded structure in solutions in hydroxylic solvents. Although our measurements include a variety of hydrogen-bond donors and acceptors and solvents ranging from nonpolar to polar to polar–hydroxylic, the primary substrate will be 1-octanol. The choice of 1-octanol was attractive because (1) the conductivity of the pure liquid is low enough to permit precise measurements of dielectric increments for dilute solutions; (2) dielectric and other properties of the pure liquid are accurately known[3] and indicate molecular interactions conforming approximately to the model of a freely rotating hydrogen-bonded chain;[3,4] (3) the study is readily extended to isomeric liquid octanols whose dielectric properties are quite different.[3]

Kirkwood's exact dielectric theory is so general that, unless the information we seek is already available, simplifying assumptions must be introduced before the theory can be applied. In this paper (part 1 of the series), we shall formulate the theory for convenient application to dilute solutions and introduce a simplifying assumption which we call the *chemical model*. In part 2, we shall apply this formulation to examine the structure of complexes resulting from the interaction of 1-octanol with various donors and acceptors in nonhydroxylic solvents. In part 3, we shall examine the effects of non-hydrogen-bonding solutes on the dielectric constants of several hydroxylic solvents. In part 4, we shall report data for dilute solutions of various hydrogen-bonding solutes in 1-octanol. Finally, in part 5, we shall analyze the data obtained in part 4 and deduce specific hydrogen-bond structural information for solvent and solute.

Terminology and Definitions

When Kirkwood's theory is applied to one-component liquids,[2-7] the dipole alignment is accounted for by means of the correlation factor g, whose definition is as follows. Let μ be the (scalar) molecular dipole moment, $\boldsymbol{\mu}$ the corresponding molecular dipole vector and $\bar{\boldsymbol{\mu}}$ the vector sum (Figure 1) of $\boldsymbol{\mu}$ and the net dipole moment of the surrounding sphere of

† Present address: Department of Chemistry, Tamkang College of Arts and Science, Tamsui, Taiwan 251, Republic of China.

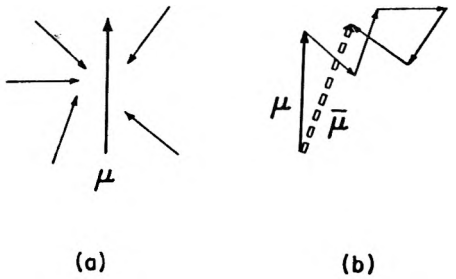

Figure 1. (a) μ and localized dipoles around it. (b) $\bar{\mu}$ is the vector sum of μ and all molecular dipoles around it. In practice, only those dipoles within the effective range of interaction from the central molecule need be considered.

molecules, whose radius in theory approaches infinity. Let $\mu\cdot\bar{\mu}$ denote the scalar product, and let $\langle\mu\cdot\bar{\mu}\rangle$ denote the statistical average, taken over all molecules of the given species. Then g is defined by

$$g = \langle\mu\cdot\bar{\mu}\rangle/\mu^2 \tag{1-1}$$

When there is more than one component,[8] it is instructive to introduce a separate factor g_i for each component, as follows:

$$g_i = \langle\mu_i\cdot\bar{\mu}_i\rangle/{\mu_i}^2 \tag{1-2}$$

$\bar{\mu}_i$ now denotes the vector sum of μ_i, the dipole vector of the ith molecule, and the net dipole moment of the surrounding sphere of molecules, which comprises molecules of all species. This formulation enables us to express the polarization of the liquid solution as a sum of additive terms for the individual components:[2]

$$f(\epsilon) \equiv (\epsilon - 1)(2\epsilon + 1)/9\epsilon = \sum c_i P_i \tag{1-3a}$$

$$P_i = \frac{4}{3}\pi N_0[\alpha_i + g_i{}^{\varphi}\mu_i{}^2/3kT] \tag{1-3b}$$

Here ϵ denotes dielectric constant of the liquid solution, c_i concentration, P_i molar polarization, α_i molecular polarizability, and ${}^{\varphi}\mu_i$ the molecular dipole moment of the ith species of molecules in the given solution.

In general, ${}^{\varphi}\mu_i$ is somewhat greater than the intrinsic moment μ_i of the isolated molecule. The ratio, $\mu_i/{}^{\varphi}\mu_i$, may be calculated from Onsager's reaction field[9] strictly only if all g_i's are unity, and even then may require ad hoc assumptions about molecular size and shape.[10] We decided to adopt the relation

$$h \equiv \mu_i/{}^{\varphi}\mu_i = 1 - [(n^2 - 1)/(n^2 + 2)]\cdot 2(\epsilon - 1)/(2\epsilon + 1) \tag{1-4}$$

which is one of the possibilities suggested by Kirkwood[2] and has also been used by others.[8-10] (In (1-4), n denotes the refractive index of the *solution*.) Equation 1-4 can be derived by applying Onsager's reaction field to a dipole imbedded in a polarizable cavity whose properties are those of the macroscopic solution.[2] It has been shown in previous work,[11] and will be shown in the present series, that eq 1-4 is reasonably accurate in practical applications.

A valid relationship between ${}^{\varphi}\mu_i$ and μ_i is necessary in order to calculate g_i, and thence to deduce structural information. However, the relationship should be based entirely on experimental data and should not require the making of arbitrary assumptions about microscopic or structural parameters. Equation 1-4 satisfies this criterion.

Application to Dilute Solutions

Let component 1 be the solvent and 2 be the solute. Let V_1 denote the molar volume of the pure solvent, V_2 the apparent molar volume of the solute, and $c_1 = (1 - c_2V_2)/V_1$ the solvent concentration. In this notation, (1-3a) becomes

$$f(\epsilon) = P_1/V_1 + c_2[P_2 - (V_2P_1/V_1)] \tag{1-5}$$

where P_1 and P_2 are functions of c_2.

To obtain an expression that is accurate up to terms of first order in c_2, we write $(i = 1, 2) P_i = P_i{}^0 + c_2(dP_i/dc_2)_{c_2=0}$, $f(\epsilon) = f(\epsilon_0) + c_2[(df/d\epsilon)(d\epsilon/dc_2)]_{c_2=0}$, $f(\epsilon_0) = P_1{}^0/V_1$, and $(df/d\epsilon)_{c_2=0} = (2\epsilon_0{}^2 + 1)/9\epsilon_0{}^2$. Equation 1-5 thus reduces to

$$\frac{(2\epsilon_0{}^2 + 1)}{9\epsilon_0{}^2}\left(\frac{d\epsilon}{dc_2}\right)_{c_2=0} = P_2{}^0 - V_2f(\epsilon_0) + \frac{1}{V_1}\left(\frac{dP_1}{dc_2}\right)_{c_2=0} \tag{1-6}$$

It should be noted that $P_1{}^0$ denotes the molar polarization of the pure solvent, while $P_2{}^0$ denotes the molar polarization of the solute in an infinitely dilute solution. To solve for $(dP_1/dc_2)_{c_2=0}$, we introduce (1-3b) and (1-4). The quantities α_i and μ_i are constant, by definition, but g_1, g_2, and $h(n,\epsilon)$ are functions of c_2. In writing[11] the final result (1-7), it is convenient to use the following parameters: $c_1{}^0 = 1/V_1$; $\varphi = (n^2 - 1)/(n^2 + 2)$ for the solution; $\varphi_0 = (n_0{}^2 - 1)/(n_0{}^2 + 2)$ for the pure solvent; $R_1 = 4\pi N_0\alpha_1/3 = \varphi_0V_1$; $R_2 = 4\pi N_0\alpha_2/3$; $h_0 = 1 - 2\varphi_0(\epsilon_0 - 1)/(2\epsilon_0 + 1)$. In principle, R_1 is the molar refraction of the solvent and R_2 is the apparent molar refraction of the dilute solute. In practice we shall use molar refractions of the pure substances obtained at the sodium D line.

$$\mu_2{}^2 = (9kTh_0{}^2/4\pi N_0)\left\{\frac{d\epsilon}{dc_2}\left(\frac{2\epsilon_0{}^2 + 1}{9\epsilon_0{}^2} - \frac{12\varphi_0[f(\epsilon_0) - \varphi_0]}{h_0(2\epsilon_0 + 1)^2}\right)\right.$$
$$\left. + V_2f(\epsilon_0) - R_2 - \frac{4[f(\epsilon_0) - \varphi_0](R_2 - \varphi_0V_2)(\epsilon_0 - 1)}{(2\epsilon_0 + 1)h_0}\right\}$$
$$- [\mu_2{}^2(g_2 - 1) + c_1{}^0\mu_1{}^2(dg_1/dc_2)] \tag{1-7}$$

Note that the right-hand side of (1-7) separates terms without g factors, which can be obtained experimentally, from terms with g factors, which can be used to probe molecular interactions. Because of this, it is useful to introduce a parameter $\mu_{2,app}$, which will be called *apparent dipole moment*.

Apparent Dipole Moment

$\mu_{2,app}$ is defined as follows:

$$\mu_{2,app}{}^2 = (9kTh_0{}^2/4\pi N_0)\left\{\frac{d\epsilon}{dc_2}\left(\frac{2\epsilon_0{}^2 + 1}{9\epsilon_0{}^2} - \frac{12\varphi_0[f(\epsilon_0) - \varphi_0]}{h_0(2\epsilon_0 + 1)^2}\right)\right.$$
$$\left. + V_2f(\epsilon_0) - R_2 - \frac{4[f(\epsilon_0) - \varphi_0](R_2 - \varphi_0V_2)(\epsilon_0 - 1)}{(2\epsilon_0 + 1)h_0}\right\} \tag{1-8}$$

Note that $\mu_{2,app}$ is a function solely of experimental quantities. On substituting in (1-7) and rearranging, we obtain

$$\mu_{2,app}{}^2 = g_2\mu_2{}^2 + c_1{}^0\mu_1{}^2(dg_1/dc_2)_{c_2=0} \tag{1-9}$$

The apparent dipole moment defined here should not be confused with the term "apparent dipole moment" as used in the older literature.[12] The older term is simply the dipole moment measured in nonpolar solvents and calculated by Debye's second method.[13] The present usage is analogous to such familiar usage as "apparent molar volume" or "apparent solvation number". In the absence of dipole correlation, $g_1 =$

$g_2 \equiv 1$ and $dg_1/dc_2 = 0$. It can then be seen from (1-9) that, under such conditions, $\mu_{2,app}$ reduces to μ_2. When there is dipole correlation, $\mu_{2,app}$ may deviate greatly from μ_2. Indeed, $\mu_{2,app}^2$ may be a negative quantity!

Chemical Model

The definition of the correlation factor g_i is so general that, in order to deduce specific structural information, one has to introduce additional assumptions. We shall assume that dipole correlation between solute and solvent is considerable only if there is molecular complex formation between the two kinds of molecules, and that the relative concentrations of complexed and uncomplexed species conform to the laws of mass action and thermodynamics. We shall call this assumption the *chemical model.*

Thus the solute molecules may be divided into two groups: a fraction $1 - f$ remains uncomplexed, with correlation factor = 1; and a fraction f forms complexes with solvent molecules, with correlation factor g_{2a}. The overall average g_2 is given by

$$g_2 = fg_{2a} + (1 - f) \tag{1-10}$$

Similarly, the solvent molecules may be divided into two groups: those that remain in the bulk solvent (correlation factor g_{11}), and those that exist in solute–solvent complexes (correlation factor g_{12}). Let c_1 and c_2 denote the concentrations of the formal components, regardless of complexing, and let m denote the average solvation number of the solvent–solute complexes. Then the fraction of all solvent molecules combined in solvent–solute complexes is mfc_2/c_1, and the overall average g_1 is given by

$$g_1 = (1 - mfc_2/c_1)g_{11} + (mfc_2/c_1)g_{12} \tag{1-11}$$

In principle, g_{11} and g_{12} are functions of c_2. On expanding in Taylor's series about $c_2 = 0$ (i.e., $g_{11} = g_{11}^0 + c_2 (dg_{11}/dc_2) + \ldots$) and neglecting higher order terms in c_2, we obtain

$$g_1 = g_{11}^0 + (g_{12}^0 - g_{11}^0)(mfc_2/c_1) + c_2(dg_{11}/dc_2)_{c_2=0} \tag{1-12}$$

Finally, we take the derivative of (1-12), evaluate at $c_2 = 0$, and substitute in (1-9):

$$\mu_{2,app}^2 - \mu_2^2 = f(g_{2a} - 1)\mu_2^2 + mf(g_{12}^0 - g_{11}^0)\mu_1^2 + c_1^0\mu_1^2 (dg_{11}/dc_2)_{c_2=0} \tag{1-13}$$

Equation 1-13 neatly dissects $\mu_{2,app}^2 - \mu_2^2$ into three additive contributions: μ_2^2 with its associated change of correlation factor; μ_1^2 with the associated change of correlation factor as a fraction (fmc_2/c_1) of the solvent molecules becomes associated with solute molecules; and a term comprising the solute-induced changes in dipole correlation in the bulk solvent. We shall call the third term the *solute-induced medium effect* (SIME).

$(\mu_{2,app}^2 - \mu_2^2)$ and $d\epsilon/dc_2$ are both indications of the change of polarity. However, a positive $\mu_{2,app}^2 - \mu_2^2$ means that the overall *interaction* makes the system become more polar than it was before interaction, while a positive $d\epsilon/dc_2$ means that the system with solute is more polar than that without solute.

To examine the structure of solvent–solute complexes, we need to know the interdependent parameters g_2, g_{12}^0, f, and m. Equation 1-13 shows that these parameters are accessible only if the solute-induced medium effect (proportional to dg_{11}/dc_2) is known or can be predicted: the SIME is the key. We shall examine SIME's in hydroxylic solvents in parts 3 and 5.

References and Notes

(1) (a) Acknowledgment is made to the donors of the Petroleum Research Fund, administered by the American Chemical Society, for support of this work; (b) John Simon Guggenheim Fellow, 1975–1976.
(2) (a) J. G. Kirkwood, *J. Chem. Phys.*, **7**, 911 (1939); (b) *Trans. Faraday Soc.*, **A42**, 7 (1946).
(3) (a) W. Dannhauser, *J. Chem. Phys.*, **48**, 1911 (1968); (b) G. P. Johari and W. Dannhauser, *ibid.*, **48**, 5114 (1968).
(4) G. Oster and J. G. Kirkwood, *J. Chem. Phys.*, **11**, 175 (1943).
(5) C. P. Smyth, "Dielectric Behavior and Structure", McGraw-Hill, New York, N.Y., 1955.
(6) J. A. Pople, *Proc. R. Soc. London, Ser. A*, **205**, 163 (1951).
(7) (a) G. H. Haggis, J. B. Hasted, and T. J. Buchanan, *J. Chem. Phys.*, **20**, 1452 (1952); (b) J. B. Hasted in "Dielectric and Related Molecular Processes", (A Specialist Periodical Report) Vol. 1, The Chemical Society, London, 1972, p 121.
(8) (a) G. Oster, *J. Am. Chem. Soc.*, **68**, 2036 (1946); (b) *ibid.*, **66**, 948 (1944); (c) J. G. Kirkwood in "Proteins, Amino Acids, and Peptides", E. J. Cohn and J. T. Edsall, Ed., New York, 1943, Chapter 12.
(9) L. Onsager, *J. Am. Chem. Soc.*, **58**, 1486 (1933).
(10) C. J. F. Böttcher, "Theory of Electric Polarisation", Elsevier, Amsterdam, 1952.
(11) E. Grunwald and A. Effio, *J. Solution Chem.*, **4**, 373 (1973). This paper also describes a more detailed derivation of eq 1-7.
(12) R. J. W. Le Fevre, "Dipole Moments", 3d ed, Methuen, London, 1953.
(13) P. Debye, "Polar Molecules", Dover Publications, New York, N.Y., 1945.

Hydrogen Bonding in Polar Liquid Solutions. 2. 1-Octanol in Nonhydroxylic Solvents[1a]

Kee-Chuan Pan and Ernest Grunwald* [1b]

Department of Chemistry, Brandeis University, Waltham, Massachusetts 02154 *(Received June 23, 1976)*

Publication costs assisted by the Petroleum Research Fund

Association constants (K_{ij}) and electric dipole moments (μ_{ij}) of 1:1 hydrogen-bonded complexes of 1-octanol with a series of ligands were measured in benzene, and apparent dipole moments ($\mu_{c,app}$) of some of these complexes were measured with 1-octanol being the solute and the pure ligand being the solvent. Results for hydrogen bonding of 1-octanol in benzene at 25 °C are (ligand, K_{ij} (M^{-1}), μ_{ij}): dimethyl sulfoxide, 7.5, 4.56 D; acetone, 1.1, 4.07 D; benzaldehyde, 0.75, 4.14 D; pyridine, 2.5, 3.73 D; chloroform, 0.85, 2.63 D; methyl isobutyl ketone (MIK), 1.1, 3.94 D. Results for 1:1 octanol–solvent complexes at 25 °C are (solvent, dielectric constant, $\mu_{c,app}$): pyridine, 12.4, 3.62 D; chloroform, 4.81, 2.68 D; MIK, 13.11, 3.99 D. In each case, $\mu_{c,app} \approx \mu_{ij}$ in benzene, suggesting that the structure of these complexes is quite insensitive to the dielectric constant of the solvent. The values of μ_{ij} in benzene conform rather well to a model of free rotation about the hydrogen-bond axis and negligible charge transfer on complex formation.

Before considering dielectric data for solutions of hydrogen-bonding ligands in liquid 1-octanol, we wish to examine the nature of the interaction of 1-octanol with these and similar ligands in nonhydroxylic solvents of varying polarity. Dipole moments for hydrogen-bonded complexes were measured in benzene solution, as well as under conditions where 1-octanol is a dilute solute and the other hydrogen-bonding ligand is the solvent.

Hydrogen-Bonded Complexes in Benzene

Experimental results needed for the calculation of electric dipole moments are listed in Table I. The measurements were made under conditions where self-association of 1-octanol is negligible. Association constants (K_{ij}) of 1-octanol (OctOH) with dimethyl sulfoxide (DMSO), acetone, benzaldehyde, pyridine, and methyl isobutyl ketone (MIK) were measured spectrophotometrically, using the first overtone[2] of the monomer OH stretching band of 1-octanol at 1430 nm. In each case a benzene solution of OctOH and the other ligand was compared with an otherwise identical solution containing OctOD in place of OctOH, thus compensating for absorption other than that assignable to the OH group.[3] The data for each system are reproduced adequately by the assumption of 1:1 complex formation,[4] although for the interaction of DMSO with OctOH the formation of 1:2 complexes cannot be clearly ruled out. The standard errors of precision of the association constants are on the order of 20%; the resulting errors in dipole moments for the complexes are within 0.1 D.

For CCl_3H-OctOH, the 1:1 association constant was obtained by fitting the dielectric data.

Dielectric constants were measured for dilute solutions of the ligands alone and in combination. In each case, the difference $\Delta\epsilon$ between the dielectric constant of the solution and that of the pure solvent was a linear function of molar concentrations,

$$\Delta\epsilon = S_{OctOH}[OctOH] + S_L[L] + S_{OctOH-L}[OctOH-L] \quad (2\text{-}1)$$

S_i denotes the molar dielectric increment ($d\epsilon/dc_i$) of the ith species. S_{OctOH} and S_L were obtained from experiments using these solutes alone. $S_{OctOH-L}$ was obtained by analysis of $\Delta\epsilon$ for solutions containing both solutes, using the values of S_{OctOH}, S_L, and K_{ij}.

For the calculation of dipole moments one also needs apparent molar volumes (V_i) and molar refractions (R_i). Values of V_i obtained for the uncomplexed ligands are listed in Table I. For R_i we used the molar refractions of the pure liquids at the sodium D line. For the complexes we assumed that $V_{ij} = V_i + V_j$ and that $R_{ij} = R_i + R_j$.

As shown in Table I, dipole moments calculated in the standard way by Debye's second method[5] are in substantial agreement with apparent dipole moments according to eq 1-8, as expected for a nonpolar solvent. It is worth noting, however, that the latter values are consistently ~0.1 D greater than the former. In the following we shall use the values obtained by Debye's method, in order that our results be comparable with the previous literature.

Structure of Hydrogen-Bonded Complexes

The final column of Table I lists predicted dipole moments of the complexes, based on a model which assumes a linear hydrogen bond with "free" rotation[6] about the hydrogen-bond axis, and which neglects any dipole enhancement owing to hydrogen bonding.[7] On that basis μ_{ij} for the complex is given by eq 2-2, where α denotes the angle between the hydrogen-bond axis and μ_i, and β denotes the angle between the hydrogen-bond axis and μ_j (see Figure 1).

$$\mu_{ij}^2 = \mu_i^2 + \mu_j^2 + 2\mu_i\mu_j \cos\alpha \cos\beta \quad (2\text{-}2)$$

For OctOH, on the basis of bond moments,[8] an angle of 43° was adopted when this ligand acts as H-bond donor in the presence of carbonyl compounds, DMSO, and pyridine, and of 55.5° when it acts as H-bond acceptor toward CCl_3H. For carbonyl compounds and DMSO, the angle was 60°; for pyridine and CCl_3H, it was 0°. Values of μ_i and μ_j for the free ligands were taken from our own measurements (Table I).

On the whole, agreement between prediction based on this free rotation model and experiment is quite satisfactory. The mean of μ_{ij}(exptl) − μ_{ij}(pred) is 0.05 D, with a mean deviation of 0.15 D.

Hydrogen Bonding in Polar Nonhydroxylic Solvents

We now wish to consider the hydrogen-bonded complexes that are formed when 1-octanol exists as a dilute solute in the solvents pyridine, MIK, or chloroform. At 25 °C, dielectric constants of these solvents range from 4.8 to 13.1, and dipole

TABLE I: Experimental Results and Calculated Dipole Moments in Benzene at 25.0 °C

Substrate (*i*, *ij*)	S_i, S_{ij}, M^{-1}	V_i, V_{ij}, cm^3/mol	K_{ij}, M^{-1}	μ_i, μ_{ij}, D[a]	$\mu_{i,app}$, $\mu_{ij,app}$[b]	μ_{ij} (free rot.)[c]
Octanol	0.340	164		1.76	1.88	
DMSO	*1.91*	*66.0*		*3.91*	*4.08*	
OctOH–DMSO	2.50	230	7.5	4.56	4.73	4.84
Acetone	0.93	74.8		2.80	2.90	
OctOH–acetone	1.94	239	1.1	4.07	4.22	3.81
PhCHO	1.14	101		3.04	3.17	
OctOH–PhCHO	2.06	265	0.75	4.14	4.31	4.03
Pyridine	0.612	81.1		2.23	2.33	
OctOH–pyridine	1.65	245	2.5	3.73	3.88	3.72
$CHCl_3$	0.173	81.0		1.24	1.32	
OctOH–$CHCl_3$	0.780	245	0.85	2.63	2.76	2.67
Methyl isobutyl ketone (MIK)	0.84	127		2.69	2.79	
OctOH–MIK	1.80	291	1.1	3.94	4.09	3.72

[a] Calculated from experimental data by Debye's method. [b] Calculated from experimental data using eq 1-8 of part 1. [c] Predicted according to eq 2-2.

TABLE II: Hydrogen Bonding of 1-Octanol in Polar Nonhydroxylic Solvents at 25 °C

Solvent	ϵ_0	g_{11}^0	S_{OctOH}, M^{-1}	V_c,[b] cm^3/mol	$\mu_{c,app}$,[b] D	μ_c,[c] D
Pyridine	12.4	1.009[a]	−0.52	239	3.62	3.73
$HCCl_3$	4.81	1.125[a]	0.30	238	2.68	2.63
MIK	13.11	1.347[a]	−0.90	284	3.99	3.94

[a] Calculated according to eq 1-3 and 1-4 and intrinsic dipole moments as listed in Table I. [b] For 1:1 solute–solvent complex; in applying eq 1-8, V_2 becomes $V_c = V_2 + V_1$; R_2 becomes $R_c = R_2 + R_1$. [c] Measured in benzene. Denoted by μ_{ij} in Table I.

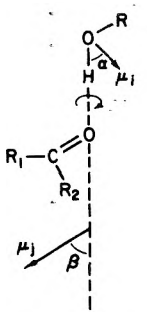

Figure 1. Model for prediction of μ_{ij}, illustrated for complex formation between 1-octanol and a ketone. Angles α and β are drawn as described in the text.

correlation factors range from 1.0 for pyridine to 1.35 for MIK[9] (Table II). Using association constants listed in Table I, we reckon that at least 90% of the OctOH molecules form H-bonded complexes with solvent molecules. The actual fractions are probably even closer to unity, because $\Delta\mu^2 > 0$ and hence K_{ij} is expected to increase with the dielectric constant.[10]

In the following, we shall assume that each OctOH molecule is hydrogen bonded to one solvent molecule. On that basis it turns out that apparent dipole moments for the octanol complexes in the polar solvents are remarkably close to dipole moments for the same complexes obtained in benzene.

Results are listed in Table II, where the subscript c denotes the 1:1 octanol–solvent complex. Apparent dipole moments ($\mu_{c,app}$) were calculated according to eq 1-8, by letting the properties of the solute species be those of the 1:1 complex; that is, the apparent molar volume of the solute is $V_c = V_2 + V_1$, and its molar refraction is $R_2 + R_1$.[11]

There are various ways of interpreting the remarkably close agreement between $\mu_{c,app}$ in the polar solvents and μ_c in benzene for the complexes described in Table II. On the one hand, one may argue that μ_c in the polar solvents and μ_c in benzene *should* be equal. It then follows that $\mu_{c,app} = \mu_c$ in the polar solvents, so that the introduction of the solute produces no dipole correlation effects other than those inherent in the formation of the 1:1 complex. This is a plausible conclusion for nonhydroxylic solvents. Alternatively, the premise and conclusion of the preceding argument may be reversed. Finally, one may adopt both premises and accept the agreement as evidence for the validity of the theory leading to eq 1-8. In view of the wide range of dielectric properties of the solvents, and of donor–acceptor and dipolar properties of the solutes (Table II), we believe that all three interpretations are at least approximately valid.

Experimental Section

Materials. Reagent-grade commercial samples of solvents and solutes were further purified by drying and double distillation, under reduced pressure if necessary.[12] Octanol-*O-d* was prepared by isotopic exchange, by twice stirring with a large molar excess of D_2O. The octanol-rich phase was separated, dried over molecular sieves, and distilled at reduced pressure. The NMR spectrum of the final product showed no OH-proton resonance.

Dielectric Measurements. Cells and measuring techniques described in earlier publications from this laboratory were used.[13] However, the basic measuring apparatus was simplified and improved by elimination of the external Gertsch ratio transformer for conductance balancing, expansion of the conductance measuring range of the General Radio Type 1615A capacitance bridge, and use of a phase-sensitive de-

tector with matched oscillator (General Radio Type 1238 and 1316).

The conductance measuring range of the General Radio Type 1615A bridge was expanded to 10 μmhos (110 μmhos with external standard of 100 μmhos) by essentially the method of Addison and Stalinski,[14] but omitting the new external switch described by these authors. We merely substituted a matched pair of 9096-ohm resistors for R245 and R246,[15] thus generating measuring ranges of ±10 μmhos and ±1 μmho, with resolutions of 1 and 0.1 nmho, respectively. As a result of this modification, the relationship between bridge reading and conductance becomes nonlinear, as described in the Instruction Manual,[15] but that is a trivial inconvenience. Less trivial is the fact that the conductance-balancing network now has a significant equivalent capacitance, C_{eq}, which must be added to the reading of the capacitance-balancing network if accurate results are to be obtained. In determining this capacitance, C_{eq}, as a function of conductance reading, we used as primary standard a carefully mounted and shielded 100.027-μmho resistor whose effective capacitance had been determined by Dr. John Hersh of the General Radio Standards Laboratory, and independently by ourselves, to be 0.14 ± 0.05 pF at 10 kHz. The equivalent circuit for reproducing C_{eq} as a function of R_N, the bridge resistance in ohms as defined in the Instruction Manual,[15] is more complicated than suggested by Addison and Stalinski.[14] We used the empirical equation,

$$C_{eq}(\text{pF}) = 4.12 \times 10^{-5} R_N - 3.11 \times 10^{-7} R_N^2 + 0.017 \times (\text{decimal part of } R_N/100) \quad (2\text{-}3)$$

which reproduced the calibration data with a standard deviation of 0.003 pF.

Specific conductivities (in $\text{ohm}^{-1}\ \text{cm}^{-1}$) of the solvents were: $<1 \times 10^{-12}$ for benzene, 8×10^{-11} for $CHCl_3$, $\sim 1.8 \times 10^{-9}$ for methyl isobutyl ketone (MIK), and 3.6×10^{-8} for pyridine. Although in $CHCl_3$, and especially in MIK, the conductivity increased considerably with 1-octanol concentration, the effect of the free ions on $\Delta\epsilon$[16,17] was estimated to be less than 2% of the experimental $\Delta\epsilon$ in every case.

Plots of $\Delta\epsilon$ vs. c_2 for 1-octanol in the three polar solvents were straight lines through the origin over the entire experimental range, up to ~1.8 M. Values of $S_{OctOH} = d\epsilon/dc_2$ in Table II are based on no less than six concentrations.

Near-Infrared Spectrophotometry. Spectra were taken at room temperature (~23 °C) with a Perkin-Elmer Hitachi Model 323 spectrophotometer. Tightly stoppered, 0.5-cm matched cells were used. By comparing otherwise identical solutions of OctOH and OctOD, all absorbances except for the OH absorbance were compensated in the region ~1430 nm. Under the experimental conditions (<0.2 M 1-octanol in benzene), the first overtone of the OH stretching band of OctOH monomer was a sharp peak. OH stretching absorbance due to hydrogen-bonded complexes was relatively weak, as expected.[2] Concentrations of the hydrogen-bond acceptor ligands were usually 0.3–0.7 times those of OctOH.

Acknowledgment. We thank Mr. Amit Wadhwaney for technical assistance.

References and Notes

(1) (a) Acknowledgment is made to the donors of the Petroleum Research Fund, administered by the American Chemical Society, for support of this work; (b) John Simon Guggenheim Fellow, 1975–1976.
(2) W. A. P. Luck and W. Ditter, *J. Mol. Struct.*, 1, 261 (1967).
(3) C. Bourderon and C. Sandorfy, *J. Chem. Phys.*, 59, 2527 (1973).
(4) For a consistent related study, see D. Hadzi, H. Ratajczak, and L. Sobczyk, *J. Chem. Soc. A*, 48 (1967).
(5) P. Debye, "Polar Molecules", Dover Publications, New York, N.Y., 1945.
(6) Inherent in the free-rotation model is the assumption that the characteristic time period for relative rotation about the hydrogen-bond axis is short compared to the dielectric relaxation time, and that the time-average of $\sin(\alpha - \beta)$ is zero. See ref 7a, p 512.
(7) (a) E. Grunwald, S. Highsmith, and T.-P. I, in "Ions and Ion Pairs in Organic Reactions", M. Szwarc, Ed., Wiley-Interscience, New York, N.Y., 1974, p 462 ff; (b) H. Ratajczak, *J. Phys. Chem.*, 76, 3000 (1972).
(8) C. P. Smyth, "Dielectric Behavior and Structure", McGraw-Hill, New York, N.Y., 1955.
(9) R. H. Cole, *J. Chem. Phys.*, 9, 251 (1941).
(10) J. Jadzyn and J. Malecki, *Acta Phys. Pol. A*, 41, 599 (1972).
(11) An alternative method of calculation, which leads to the identical final result, is based on eq 1-13 and illustrates the use of g factors and of the chemical model. After obtaining $\mu_{2,app}$ according to (1-8), one introduces the assumptions that $f = 1$ and $m = 1$. It then follows that $(g_2 - 1)\mu_2^2 = (g_{12}^0 - 1)\mu_1^2 = \langle \mu_2 \cdot \mu_1 \rangle$, the latter being the average scalar product for the 1:1 complex. It is readily shown that $\mu_1^2 + \mu_2^2 + 2\langle \mu_1 \cdot \mu_2 \rangle = \mu_c^2$ (cf. eq 2-2) and that $\mu_{c,app}^2 = \mu_{2,app}^2 + g_{11}^0 \mu_1^2$. The final result is $\mu_{c,app}^2 = \mu_c^2 + c_1^0 \mu_1^2 (dg_{11}/dc_2)$, showing that $\mu_{c,app} = \mu_c$ if $dg_{11}/dc_2 = 0$.
(12) J. A. Riddick and W. B. Bunger, "Organic Solvents", 3d ed, Wiley-Interscience, New York, N.Y., 1970.
(13) E. Grunwald and A. Effio, *J. Solution Chem.*, 4, 373 (1973).
(14) J. R. Addison and P. Stalinski, *Rev. Sci. Instrum.*, 45, 1296 (1974).
(15) Instruction Manuel: Type 1615A Capacitance Bridge, General Radio Co., West Concord, Mass., 1963, p 33.
(16) S. Highsmith and E. Grunwald, *J. Phys. Chem.*, 78, 1431 (1974).
(17) L. Onsager and S. W. Provencher, *J. Am. Chem. Soc.*, 90, 3134 (1968).

Hydrogen Bonding in Polar Liquid Solutions. 3. Effects of Non-Hydrogen-Bonding Solutes on the Dielectric Constant of Hydroxylic Solvents[1a]

Ernest Grunwald,*[1b] Stephen P. Anderson, Adan Effio, Stephen E. Gould, and Kee-Chuan Pan

Department of Chemistry, Brandeis University, Waltham, Massachusetts 02154 *(Received June 26, 1976)*

Publication costs assisted by the Petroleum Research Fund and the National Science Foundation

Dielectric constants have been measured for dilute solutions of the solutes benzene, 1,4-di-*tert*-butylbenzene, chlorobenzene, nitrobenzene, benzonitrile, and CCl_4 in the solvents 1-octanol, 5-methylheptanol-3, and acetic acid. Apparent dipole moments of the solutes differ considerably from intrinsic dipole moments: values of $\mu_{2,app}^2 - \mu_2^2$ range from +11 to −10 D^2. Results are reproduced by the empirical equation, $\mu_{2,app}^2 - \mu_2^2 = AV_2 + B\mu_2^2$, in which the parameters A and B are found to vary greatly with the solvent: $A < 0 < B$. The results reflect solute-induced changes in hydrogen-bonded solvent structure; for non-hydrogen-bonding solutes, $\mu_{2,app}^2 - \mu_2^2 = c_1^0\mu_1^2 (dg_{11}/dc_2)$, where g_{11} is the dipole correlation factor of the solvent molecules. Mechanisms by which the addition of a solute may modify g_{11} are discussed.

Introduction

Apparent dipole moments of non-hydrogen-bonding solutes such as chlorobenzene, CCl_4, or 1,4-di-*tert*-butylbenzene, in hydroxylic solvents such as 1-octanol or acetic acid, often differ considerably from intrinsic dipole moments. Solutes such as these are not likely to form discrete solvation complexes. Thus, in terms of the chemical model (part 1),[2] $f = 0$ and eq 1–13 reduces to

$$\mu_{2,app}^2 - \mu_2^2 = c_1^0\mu_1^2 (dg_{11}/dc_2)_{c_2=0,f=0} \qquad (3\text{-}1)$$

According to (3-1), when $f = 0$, any significant difference between $\mu_{2,app}^2$ and μ_2^2 implies a nonzero dg_{11}/dc_2 and is therefore a solute-induced medium effect.

We visualize the following mechanisms by which the addition of a non-hydrogen-bonding solute may modify the average dipole correlation among the solvent molecules in a hydroxylic solvent. (1) The addition of solute causes a dilution of the solvent. By the law of mass action, this shifts the equilibrium among the solvent complexes so as to favor solvent species with lower association numbers. (2) The addition of solute causes a change in the dielectric constant (ϵ) and in other macroscopic measures of polar character. The change in polar character in turn affects the *equilibrium constants* for solvent–solvent complex formation, so that an increase in polar character will favor the formation of more polar complexes. (3) Hydrogen bonding among hydroxylic molecules often leads to the formation of substantial chains or three-dimensional molecular networks. The addition of solute molecules, of characteristic size and shape, may interfere with the preferred packing or freedom of motion of such solvent polymers.

In this paper, solute-induced medium effects will be examined in three hydroxylic solvents of widely different properties: 1-octanol (OctOH, $\epsilon_0 = 10.01$ at 25 °C), 5-methylheptanol-3 (5-MH3, $\epsilon_0 = 3.88$ at 25 °C), and acetic acid (HAc, $\epsilon_0 = 6.265$ at 25 °C). Solutes include benzene (PhH), 1,4-di-*tert*-butylbenzene (DTB), CCl_4, chlorobenzene (PhCl), benzonitrile (PhCN), and nitrobenzene ($PhNO_2$). These solutes are aprotic substances whose hydrogen-bond acceptor affinity may be neglected. Because of a recent claim that the acceptor affinity of the nitro group in *p*-nitroaniline is significant,[3] we measured the spectral absorption of benzene solutions of OctOH and $PhNO_2$ in the first overtone region of the OH stretching band around 1430 nm, without obtaining any evidence for OctOH–$PhNO_2$ hydrogen-bond complex formation.

TABLE I: Dielectric Measurements for Non-Hydrogen-Bonding Solutes in Hydroxylic Solvents

Solvent[a] (ϵ_0)	Solute[a]	Highest c_2, M	S_2, M^{-1}	$\mu_{2,app}^2 - \mu_2^2$, D^2 [b]	dg_{11}/dc_2, M^{-1} [b,c]
OctOH (10.01)	$PhNO_2$	0.31	0.89	−4.04	−0.21
	PhCl	0.38	−1.07	−4.22	−0.22
	PhH	0.23	−1.45	−4.49	−0.23
	DTB	0.044	−3.41	−9.88	−0.51
5-MH3 (3.88)	$PhNO_2$	0.30	3.58	11.0	0.62
	PhCl	0.32	0.32	1.04	0.058
	PhH	0.28	−0.15	0.14	0.008
	DTB	0.063	−0.57	−0.96	−0.054
HAc (6.265)	$PhNO_2$	0.13	1.90	0.24	0.005
	PhCN	0.06	2.02	1.12	0.023
	PhCl	0.24	−0.54	−3.44	−0.070
	PhH	0.22	−0.82	−3.13	−0.064
	DTB	0.25	−1.98	−7.34	−0.15
	CCl_4	0.10	−1.11	−4.70	−0.096

[a] OctOH = 1-octanol; 5-MH3 = 5-methylheptanol-3; HAc = acetic acid; Ph = C_6H_5; DTB = 1,4-di-*tert*-butylbenzene. [b] Values of μ_1, μ_2, and other properties used in the calculations are listed in Table II. [c] Eq 3-1.

Results

Experimental plots of dielectric constant ϵ vs. c_2 were linear or, in a few cases, showed slight curvature. Initial slopes $S_2 = (d\epsilon/dc_2)_{c_2=0}$ and other relevant data are listed in Table I. The calculation of $\mu_{2,app}^2$ is based on eq 1–8, using physical properties as listed in Table II. The calculation of dg_{11}/dc_2 is based on eq 3-1.

The accuracy of S_2 is within 0.1 (M^{-1}). The corresponding error in $\mu_{2,app}^2 - \mu_2^2$ is ~0.5 D^2, while actual values range from +11 to −10. It is clear that the differences between $\mu_{2,app}^2$ and μ_2^2 are real.

On comparing $\mu_{2,app}^2 - \mu_2^2$ in a given solvent (Table I) with physical properties of the solutes (Table II), certain trends

TABLE II: Physical Properties (25 °C) Used in Calculation of Apparent Dipole Moments

Solute or solvent[a]	V_2, V_1, cm³/mol	R_2, R_1, cm³/mol	μ_2, μ_1, D
$PhNO_2$	105.0	33.42	3.93
PhCl	102.2	31.16	1.58
PhH	89.4	26.2	0
DTB	221	63.8	0
PhCN	103.1	31.70	3.93
CCl_4	97.1	26.46	0
HAc	57.54	13.01	1.68
OctOH	158.4	40.71	1.76
5-MH3	158.6	40.32	1.68

[a] For definition of abbreviations, see footnote in Table I.

TABLE III: Least-Squares Data Fitting According to Eq 3-2

Solvent[a]	A, D^2 cm^{-3}	B	Std dev, D^2 [b]	Correlation coeff
OctOH	−0.0451	0.0477	0.38	0.982
5-MH3	−0.0041	0.736	0.45	0.993
HAc	−0.0362	0.286	0.77	0.939
	(−0.0344)[c]	(0.273)[c]	0.51	0.977

[a] OctOH = 1-octanol; 5-MH3 = 5-methylheptanol-3; HAc = acetic acid. [b] By comparison, the experimental error is ~0.5 D^2. [c] Exclude CCl_4.

may be noted: for nonpolar solutes the values of $(\mu_{2,app}^2 - \mu_2^2)$ decrease with increasing V_2, while, for polar solutes of comparable V_2, the values increase with μ_2. A negative value indicates that dg_{11}/dc_2 is negative; i.e., the added solute causes the *solvent* to become less polar.[4]

Discussion

In principle the values of dg_{11}/dc_2 are predictable, but the required model of hydrogen-bonded solvent structure and of solvent–solute interaction must be quite detailed. In the absence of such information, we searched for an appropriate empirical function for fitting the experimental values of $\mu_{2,app}^2 - \mu_2^2$. Equation 3-2, in which A and B are parameters characteristic of the solvent, is adequately successful.

$$\mu_{2,app}^2 - \mu_2^2 = AV_2 + B\mu_2^2 \qquad (3\text{-}2)$$

Least-squares adjusted values of A and B, and measures of quality of fit, for the present solvents are listed in Table III. The standard deviations of fit are compatible with the experimental error. A and B are of opposite sign; the magnitudes of A and B vary greatly, each by more than an order of magnitude; and there is a consistent trend for $-A$ to decrease when B increases.[5]

The choice of V_2 and μ_2^2 as independent variables in an empirical correlation is at least partly suggested by theory. Of the three mechanisms for solute-induced medium effects considered in the Introduction, the effect of a decrease in solvent concentration, per molar solute, is proportional to V_2. The change in polar character of the solution, per molar solute, depends primarily on μ_2^2. Steric interference with the hydrogen-bonded solvent structure, per molar solute, should be more specific. However, the underlying interactions are van der Waals interactions, for which various mathematical models are available.[6] Thus it is not implausible for interactions which depend specifically on the solute's polarizability to produce effects which, in dilute solution, vary approximately as V_2 and are thus gathered up by the term AV_2. Specific polar effects should vary approximately as μ_2 (rather than μ_2^2). However, the fit of the relation, $\mu_{2,app}^2 - \mu_2^2 = A'V_2 + B'\mu_2$, is distinctly inferior to that of (3-2).

Experimental Section

Materials. Reagent-grade acetic acid was further purified by recrystallization, as described previously.[7] The conductivity of the pure liquid was 40–50 nmhos/cm.

1-Octanol (Fisher certified reagent) was distilled twice under nitrogen at reduced pressure: density, 0.821 g/cm³ at 25 °C; ϵ_0 = 10.01 at 24.9 °C: conductivity, 0.4–0.8 nmho/cm.

5-Methylheptanol-3 (J. T. Baker Chemical Co.) was purified by double distillation under nitrogen at reduced pressure. The structural formula of this alcohol contains two asymmetric carbon atoms, hence permits two diastereomeric *d,l* pairs. The solvent actually used in this work was a somewhat variable mixture, probably of the two diastereomers, because the dielectric constant of different batches varied over a 3% range. However, dielectric increments were always measured using solvent from the same batch. In one experiment, a small batch was especially purified by careful vacuum fractionation with a spinning-band column. The near-infrared spectrum and S_2 for chlorobenzene, measured using this batch, were practically indistinguishable from properties measured with a batch resulting from normal double-vacuum distillation: $n^{25}D$ 1.4222; ρ^{25} 0.821.

Nitrobenzene (Fisher certified reagent) was recrystallized twice and then distilled twice under nitrogen at reduced pressure. The conductivity of the purified liquid was about 5 nmhos/cm and the dielectric constant 34.68 at 24.9 °C.

Chlorobenzene (Fisher certified reagent) was dried over phosphorus pentoxide and then distilled twice under nitrogen at atmospheric pressure.

1,4-Di-*tert*-butylbenzene (Aldrich), mp 77.9 °C, was recrystallized three times from ethanol and dried under vacuum.

Benzene (Eastman Organic Chemicals spectrograde) was distilled twice under nitrogen at atmospheric pressure.

Benzonitrile (Eastman White Label) was distilled, bp 90 °C (31 mm).

Carbon tetrachloride (reagent grade) was used without further purification.

Dielectric measurements were made over a period of several years, during which the instrumentation was gradually improved. Most of the data were obtained using the apparatus described by Grunwald and Effio;[8] some of the results reported for OctOH and 5-MH3 were checked or obtained using the apparatus described in part 2. Measurements in acetic acid were somewhat less precise than in the alcohol solvents, owing to the higher conductivity.

Solutions were prepared quantitatively under anhydrous conditions, using a glove box flushed with dry nitrogen. Near-infrared spectra were measured as described in part 2.

References and Notes

(1) (a) Acknowledgment is made to the donors of the Petroleum Research Fund, administered by the American Chemical Society, for partial support of this work. Grateful acknowledgment is also made to the National Science Foundation for support of this work in the initial stages; (b) John Simon Guggenheim Memorial Fellow, 1975–1976.
(2) Parts 1 and 2 of this series are immediately preceding papers in this issue. Equations beginning with 1 or 2 (e.g., eq 1-8) will be found in those papers.
(3) M. J. Kamlet and R. W. Taft, *J. Am. Chem. Soc.*, **98**, 377 (1976); see espe-

cially the discussion following eq 18.
(4) The use of the parameter $\mu_{2,app}^2$ in the examination of dg_1/dc_2 may be avoided by letting $dg_1/dc_2 = (\partial g_1/\partial \epsilon)(d\epsilon/dc_2) + (\partial g_1/\partial c_1)(dc_1/dc_2)$, and evaluating the partial derivatives from eq 1-3.
(5) These empirical conclusions do not apply generally to hydroxylic solvents. For instance, in octanoic acid ($\epsilon_0 = 2.46$) $\mu_{2,app}^2 - \mu_2^2$ is close to zero for a wide range of solutes: T.-P. I and E. Grunwald, *J. Am. Chem. Soc.*, **98**, 1351 (1976).
(6) See, for example, J. H. Hildebrand and R. L. Scott, "The Solubility of Nonelectrolytes", Reinhold, New York, N.Y., 1950.
(7) M. R. Crampton and E. Grunwald, *J. Am. Chem. Soc.*, **93**, 2987 (1971).
(8) E. Grunwald and A. Effio, *J. Solution Chem.*, **2**, 373 (1973).

Hydrogen Bonding in Polar Liquid Solutions. 4. Effect of Hydrogen-Bonding Solutes on Dielectric Constant and Solvent Structure in 1-Octanol[1a]

Ernest Grunwald,*[1b] Kee-Chuan Pan, and Adan Effio

Department of Chemistry, Brandeis University, Waltham, Massachusetts 02154 *(Received June 23, 1976)*

Publication costs assisted by the Petroleum Research Fund

Dielectric constant (ϵ) was measured as a function of concentration at 24.9 °C for the following hydrogen-bonding solutes in 1-octanol: benzaldehyde, acetone, $(t\text{-Bu})_2CO$, $(i\text{-Bu})COCH_3$, $(CH_3)_2SO$, pyridine (Py), 2,4- and 2-6-$(t\text{-Bu})_2$Py, 2-$(i\text{-Pr})$-6-$(t\text{-Bu})$Py, $CHCl_3$, and $(C_2H_5)_3COH$. Molar dielectric increments ($d\epsilon/dc_2$ at $c_2 = 0$) were generally negative even though ϵ for the majority of the pure liquid solutes is greater than ϵ for 1-octanol. Solute-induced medium effects differed considerably from the relationship established for non-hydrogen-bonding solutes. Adopting a hydrogen-bonded chain model for 1-octanol, the mean chain length was found, by near-infrared spectroscopy, to be 27.7 at 25 °C. Adopting a model for sitewise equilibrium between free OH-donor sites, free O-acceptor sites, and OH·O hydrogen-bonded sites, the sitewise association constant $K = 117$ (M^{-1}) at 25 °C; $\Delta H° = -8.58$ kcal, $\Delta S° = -19.3$ gibbs/mol of hydrogen bonds. The sitewise equilibrium model predicts a marked breakdown of hydrogen-bonded solvent structure in the presence of hydrogen-bonding solutes.

In part 3 we considered the effects of non-hydrogen-bonding solutes on dipole correlation in hydroxylic solvents.[2] We shall now consider the effects of hydrogen-bonding solutes, which according to our data are even more complicated. For illustration, Figure 1 shows dielectric constant ϵ as a function of c_2 for dimethyl sulfoxide (DMSO, $\mu_2 = 3.91$ D) in 1-octanol (OctOH, $\mu_1 = 1.76$ D). If DMSO were a non-hydrogen-bonding solute, with solute-induced medium effects given by eq 3-2, the relation between ϵ and c_2 would follow the dashed line in Figure 1, whose slope is positive. If DMSO and OctOH were forming a 1:1 complex whose dipole moment, as reported in part 2, is 4.56 D, and if solute-induced medium effects were again given by (3-2), the slope would be approximately zero. By contrast, the experimental slope at low concentrations is negative!

Pure DMSO ($\epsilon_0 = 46.7$)[3] is much more polar than OctOH ($\epsilon_0 = 10.01$). Thus the slope of ϵ vs. c_2 cannot remain negative indefinitely. As shown in Figure 1, $d\epsilon/dc_2$ changes sign at $c_2 \approx 0.24$ M.

Because DMSO is known to be an efficient hydrogen-bond acceptor,[4] we expect the formation of solvation complexes of the general formula DMSO–$(OctOH)_m$. The solvation number m may be an integer or an average for a distribution, and m may vary with c_2. If this is granted, then the negative initial slope allows of two interpretations: (1) Solvation complexes of DMSO in OctOH are markedly less polar than expected from the structure of the 1:1 complex in benzene. (2) Hydrogen bonding between DMSO and OctOH couples the DMSO molecules to the hydrogen-bonded solvent structure and thereby introduces a new kind of solute-induced medium effect that lowers the dielectric constant. Having found in part 2 that dipole moments of OctOH–L complexes, for typical ligands L, are quite insensitive to the solvent medium, we consider the *first* interpretation to be *less* probable.

In this paper we shall report dielectric constants for a variety of hydrogen-bonding solutes in 1-octanol and show that the behavior of DMSO is part of a perplexing general pattern. We shall then consider the hydrogen-bonded structure of the solvent and show, by straightforward application of principles of chemical equilibrium, that hydrogen bonding to a solute greatly reduces the average aggregation number. In 1-octanol, such "structure breaking" of the solvent is attended by a decrease in the dielectric constant. In part 5 we shall develop these concepts into a quantitative theory.

Experimental Dielectric Constants

Typical plots of $\Delta\epsilon = \epsilon - \epsilon_0$ vs. c_2 for hydrogen-bonding solutes in 1-octanol are shown in Figures 1–3. Results for all solutes are listed in Table I.

Because the pyridine solutes ionize as bases in water, it is worth noting that ionization according to

$$Py + HOOct \rightleftarrows PyH^+ \cdot OOct^- \rightleftarrows PyH^+ + OOct^-$$

was found to be negligible. The evidence for this is that the conductivity of the solutions remained in all cases essentially the same as that of the solvent, about 0.4–0.8 nmho/cm. Free-ion concentrations as small as 10^{-5} M could have been detected easily. Ion-pair dissociation constants for hydro-

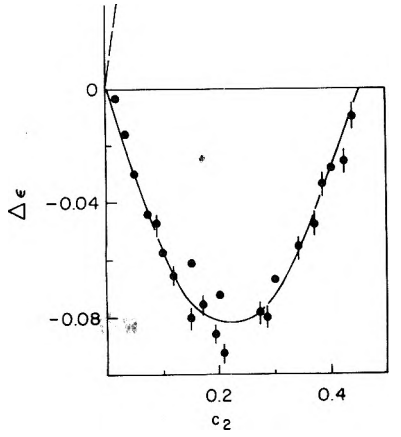

Figure 1. Plot of $\Delta\epsilon$ vs. c_2 for dimethyl sulfoxide in 1-octanol at 24.9 °C: solid circles, data of KCP; lined circles, data of AE. Dashed line shows the relationship for a non-hydrogen-bonding solute with the same μ_2, V_2, and R_2 as dimethyl sulfoxide.

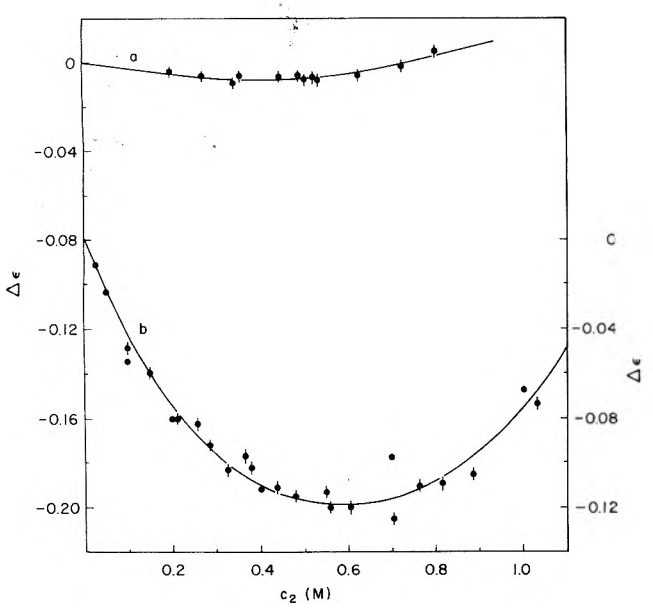

Figure 2. $\Delta\epsilon$ vs. c_2 for (a) pyridine; (b) acetone (ordinate on right) in 1-octanol at 25 °C: solid circles, data of KCP; lined circles, data of AE.

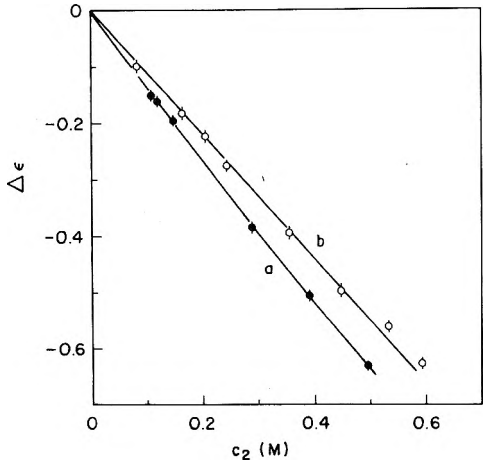

Figure 3. $\Delta\epsilon$ vs. c_2 for (a) 2,4-di-*tert*-butylpyridine; (b) di-*tert*-butyl ketone, in 1-octanol at 24.9 °C.

gen-bonded ion pairs such as $PyH^+ \cdot X^-$ in 1-octanol are in the range 10^{-6}–10^{-5} M.[5]

Plots of $\Delta\epsilon$ vs. c_2 are of three types: (A) $\Delta\epsilon = S_2c_2$; (B) $\Delta\epsilon = S_2c_2 + J_2c_2^2$ ($J_2c_2^2$ is relatively small); (C) $\Delta\epsilon$ vs. c_2 shows marked, characteristic curvature and passes through a minimum. In cases A and B the initial slopes S_2, as listed in Table I, are accurate to 0.1 M^{-1} or better; in case C the standard errors of S_2 are greater, but should be within 0.3 M^{-1}.

If one may generalize from the results in Table I, the type of relationship between $\Delta\epsilon$ and c_2 depends on the magnitude of V_2. Solutes with relatively large V_2 (>170 cm^3/mol) show linear or nearly linear plots, as illustrated in Figure 3, while solutes with small V_2 (<110 cm^3/mol) show curved plots, as illustrated in Figures 1 and 2.

Table I also lists various derived quantities. Except for the solute triethylcarbinol, which acts both as hydrogen-bond donor and acceptor, values of $\mu_{2,app}^2 - \mu_2^2$ are uniformly negative. Correction for solute-induced medium effects according to (3-2) raises the values, as shown in the right-hand column, but in most cases leaves statistically significant, large deviations from zero. (For non-hydrogen-bonding solutes in 1-octanol, the standard deviation, after correction according to (3-2), was 0.4 D^2.)

Solvent Structure

Judging by the relatively high dielectric constant[6] and viscosity,[3] liquid 1-octanol consists largely of linear hydrogen-bonded chains, $(ROH)_n$. The Kirkwood correlation factor g_1^0 for the pure liquid is 2.805 (based on $\epsilon_0 = 10.01$ and $\mu_1 = 1.76$ D), while the method of Kirkwood and Oster[7] predicts a value of 2.25 for linear alcohol chains with free rotation around the hydrogen bonds but excluding OH·O bending. The viscosity of 1-octanol, 0.076 P at 25 °C, is about ten times greater than that of the non-hydrogen-bonded isomorph, *n*-nonane.

In the following, we shall adopt a hydrogen-bonded chain model, as indicated in (4-1). The average chain length $\bar{n}$ can

$$\mathrm{R}\text{–}\mathrm{O}_X\mathrm{H}\cdot\left(\mathrm{R}\text{–}\mathrm{OH}\right)_{n-2}\cdot\mathrm{R}\text{–}(\mathrm{OH})_D \qquad (4\text{-}1)$$

then be obtained by measuring the concentration of $(OH)_D$ terminal groups. This can be done approximately by analyzing the first overtone of the OH stretching band of liquid OctOH. In the overtone, the absorption band due to "free" OH groups (in which the H atom is *not* hydrogen-bonded to another atom) is relatively strong and can be resolved even in the presence of considerably greater concentrations of OH·O groups.[8]

Figure 4 shows the first-overtone OH-stretching absorption of liquid OctOH, referenced against liquid OctOD, at 25 °C. The sharp prominence, whose λ_{max} of ≈1430 nm virtually coincides with λ_{max} of octanol monomer in benzene, is assigned to the terminal "free" OH groups $[(OH)_D$ in (4-1)].[8-10] The remaining broad absorption is assigned to OH·O groups. To estimate actual concentrations, we measured the optical density of the sharp prominence, interpolating the broad absorption as a baseline, and used the molar extinction coefficient of octanol monomer at the 1430 nm maximum in benzene. Results obtained in this way at various temperatures are listed in Table II. The average chain length $\bar{n} = c_1^0/[(OH)_D]$.

Stepwise association constants for chain formation will be defined as follows.

TABLE I: Dielectric Constants of Solutions of Hydrogen-Bonding Solutes in 1-Octanol at 24.9 °C

Solute[a]	Highest c_2, M	Type[b] of plot	S_2, M^{-1}	V_2[c]	R_2[c]	μ_2, D	$\mu_{2,app}^2 - \mu_2^2$, D^2 [d]	$\mu_{2,app}^2 - AV_2 - (1 + B)\mu_2^2$ [e]
C_6H_5CHO	1.01	C	−0.43	101.7	32.05	3.04	−7.2	−3.0
$(CH_3)_2CO$	2.0	C	−0.39	74.0	16.18	2.80	−5.8	−2.8
$(t\text{-Bu})_2CO$	0.59	A	−1.17	173.4	43.61	2.79	−5.3	2.1
MIK	2.0	C	−0.68	127	30.05	2.69	−4.1	1.3
$(CH_3)_2SO$	0.49	C	−0.63	71.3	20.16	3.91	−15.5	−13.0
Py	0.80	C	−0.02	80.9	24.09	2.23	−1.2	2.3
2,6-$(t$-Bu$)_2$Py	0.71	A	−2.61	220[i]	61.7[j]	1.32[k]	−6.5	3.3
2,4-$(t$-Bu$)_2$Py	0.49	B	−1.36[f]	220	61.7	2.32[k]	−2.4	7.2
2-(i-Pr)-6-(t-Bu)Py	0.50	B	−2.36[g]	203[i]	57.1	1.5	−6.4	2.7
$CHCl_3$	1.0	A	−1.12	81.0	21.38	1.24	−4.5	−0.9
$(C_2H_5)_3COH$	0.88	B	−0.47[h]	139.2	35.8	1.6	2.2	8.4

[a] MIK = methyl isobutyl ketone; Py = pyridine. [b] A: $\Delta\epsilon = S_2c_2$; B: $\Delta\epsilon = S_2c_2 + J_2c_2^2$; C: $\Delta\epsilon$ vs. c_2 goes through a minimum in the experimental range. [c] In cm^3/mol; from data in ref 3, unless otherwise indicated. [d] Equation 1-8. [e] Corrected for solute-induced medium effects according to eq 3-2; for 1-octanol, $A = -0.0451$, $B = 0.0477$. [f] $J_2 = 0.170$. [g] $J_2 = 0.200$. [h] $J_2 = -0.099$. [i] Estimated from known effect of *tert*-butyl or isopropyl substituent on V_2 or R_2 of benzene. [j] n_D from H. C. Brown and B. Kanner, *J. Am. Chem. Soc.*, **88**, 986 (1966). [k] Measured in benzene solution by Barry Knishkowy, Brandeis University.

TABLE II: $(OH)_D$ Terminal Group Concentration of 1-Octanol Chains, Based on "Sharp-Band" Intensity at 1430 nm, and Derived Stepwise Association Constant

Temp, °C	$[(OH)_D]$, M	$\bar{n}$	K,[a] M^{-1}
25	0.23	27.7	117
39	0.30	21.1	67
80	0.74	8.5	10.2
88	0.81	7.8	8.4

[a] Equation 4-7.

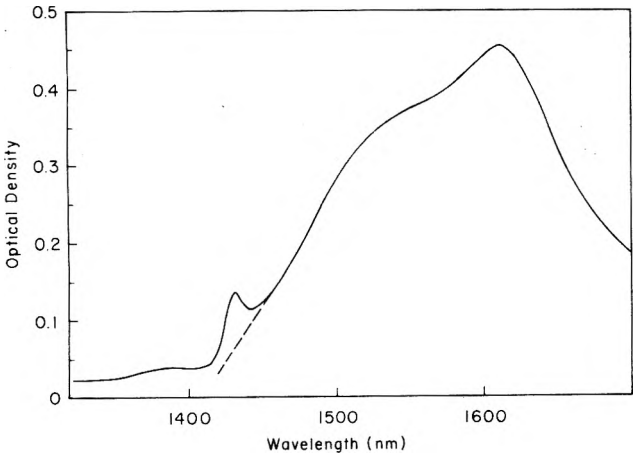

Figure 4. Near-infrared absorption spectrum of pure liquid 1-octanol (OctOH) vs. OctOD in the first overtone region of the OH-stretching vibration at 25 °C.

$$ROH + (ROH)_{n-1} \overset{K_n}{\rightleftharpoons} (ROH)_n \quad (4\text{-}2)$$

$$K_n = [(ROH)_n]/[ROH][(ROH)_{n-1}] \quad (4\text{-}3)$$

Because of the high average chain length (Table II), it is both plausible and mathematically convenient to assume that the stepwise association constants are all equal.

$$K_n = K;\ n = 2, 3, \ldots \quad (4\text{-}4)$$

Let $x = [(OH)_D]$ and c_1 = formal alcohol concentration. Then,

$$x = [ROH](1 + K[ROH] + K^2[ROH]^2 + \ldots)$$
$$x = [ROH]/(1 - K[ROH]) \quad (4\text{-}5)$$

$$c_1 = [ROH](1 + 2K[ROH] + 3K^2[ROH]^2 + \ldots)$$
$$c_1 = [ROH]/(1 - K[ROH])^2 \quad (4\text{-}6)$$

On solving these equations for K, we obtain

$$K = (c_1 - x)/x^2 \quad (4\text{-}7)$$

Values of K were calculated from the $(OH)_D$-terminal group concentrations derived from the infrared spectra. Results are included in Table II. From the linear plot of log K vs. T^{-1} we obtain $\Delta H° = -8.58$ kcal; $\Delta S° = -19.3$ gibbs/mol (molar standard states). $\Delta H°$ is comparable to values obtained calorimetrically for other strong OH·O bonds.[4a] On the other hand, K is at least 20 times greater than stepwise association constants K_2, K_3, and K_4 reported for dilute solutions of octanol in CCl_4. Geiseler et al.[11] report that (in our notation) $K_2 = 1.1$, $K_3 = 5.4$, $K_4 = 4.6$ (M^{-1}) at 30 °C, while Coggeshall and Saier[12] report that $K_2 = 1.4$ and that the average association constant for nearby higher oligomers is about 3 (M^{-1}). The relatively high value of K for stepwise association in the pure liquid may be due to electrostatic stabilization of the polar chains by the higher dielectric constant.

Solvent Structure Breaking by Hydrogen-Bonding Solutes

Although eq 4-7 was derived by summing over molar concentrations, K is in fact a *sitewise* association constant. Referring again to (4-1), let $x = [(OH)_D]$, the concentration of free hydrogen-bond donor sites, as before; let $y = [O_X]$, the concentration of free acceptor sites, and $z = [OH·O]$, the concentration of hydrogen bonds. Then, for the sitewise equilibrium, $(OH)_D + O_X \rightleftarrows OH·O$,

$$K = z/(xy) \quad (4\text{-}8)$$

In the pure solvent, $x = y$ and $z = c_1 - x$; hence (4-8) reduces to (4-7). We now wish to show that (4-8) remains valid in the presence of hydrogen-bond acceptor or donor solutes, and that it implies solvent structure breaking.

For definiteness, consider a hydrogen-bond acceptor solute X. For consistency with the above, we shall assume that the $(OH)_D$·X association constants are independent of chain length

$$(ROH)_n + X \rightleftarrows (ROH)_n\cdot X \quad (4\text{-}9)$$

$$K_{X,n} = [(ROH)_n\cdot X]/[X][(ROH)_n] \quad (4\text{-}10)$$

$$K_{X,n} = K_X;\ n = 1, 2, 3, \ldots \quad (4\text{-}11)$$

Stoichiometry and eq 4-3, 4-4, 4-10, and 4-11 then lead to the following expressions for c_1, y, and the OH·X hydrogen-bond concentration $y - x$.

$$c_1 = [ROH] + 2[(ROH)_2] + 3[(ROH)_3] + \ldots + [ROH\cdot X] + 2[(ROH)_2\cdot X] + \ldots \quad (4\text{-}12)$$

$$c_1 = [ROH](1 + K_X[X])/(1 - K[ROH])^2$$

$$y = [ROH] + [(ROH)_2] + [(ROH)_3] + \ldots + [ROH\cdot X] + [(ROH)_2\cdot X] + \ldots \quad (4\text{-}13)$$

$$y = [ROH](1 + K_X[X])/(1 - K[ROH])$$

$$[OH\cdot X]_{total} = (y - x) = [ROH\cdot X] + [(ROH)_2\cdot X] + \ldots$$

$$(y - x) = K_X[X][ROH]/(1 - K[ROH]) \quad (4\text{-}14)$$

From (4-13) and (4-14), it follows that

$$x = [ROH]/(1 - K[ROH]) \quad (4\text{-}15)$$

$$K = (c_1 - y)/(xy) \quad (4\text{-}16)$$

Recalling that X is the only solute present, it follows that y is equal to the total concentration of chains $[(ROH)_n$ and $(ROH)_n\cdot X]$. The average chain length $\bar{n}_X$ in the presence of X is therefore given by

$$\bar{n}_X = c_1/y \quad (4\text{-}17)$$

Similarly, $(c_1 - y)$ is equal to the total concentration z of OH·O hydrogen bonds. Thus (4-16) is equivalent to (4-8).

The preceding approach is readily extended to solute species (D) that function as hydrogen-bond donors (in that case, $\bar{n}_D = c_1/x$) and to mixed solutes, provided that the solute molecules attach themselves only to the terminal groups of the alcohol chains. Bifunctional solute molecules, such as triethylcarbinol in the present study, can enter the solvent chains and produce qualitatively different effects.

Returning to the simpler problem of a single hydrogen-bond acceptor solute X, eq 4-16 and 4-17 indicate a marked breakdown in solvent structure as X is added. For example, pure OctOH at 25 °C has an average chain length $\bar{n}$ of 27.7. When to this solvent, 0.3 M of a solute X is added for which $K_X = 50\ M^{-1}$, the average chain length $\bar{n}_X$ becomes 16.1, about 40% smaller than in the original solvent! This marked breakdown of solvent structure is a simple consequence of a shift in the sitewise equilibrium $(OH)_D + O_X \rightleftarrows OH\cdot O$. The addition of X causes formation of OH·X hydrogen bonds. This leads to a reduction in the concentration x of free $(OH)_D$ terminal groups and a concomitant increase in y and decrease in $\bar{n}$, in accordance with (4-16) and (4-17). In the following paper we shall consider the effect of the breakdown in solvent structure on g_1 and on the dielectric constant.

Experimental Section

Details of dielectric and near-infrared spectral measurements have been described in part 2. Details of 1-octanol purification have been described in part 3.

Dimethyl sulfoxide (Baker Analyzed Reagent) was recrystallized once and then distilled twice under nitrogen at a reduced pressure at which the boiling point was less than 90 °C.

Acetone (Baker spectrophotometric grade) was dried over magnesium sulfate and then distilled twice under nitrogen at atmospheric pressure. 2,2,4,4-Tetramethyl-3-pentanone (di-*tert*-butyl ketone, Chemical Samples Co.) was dried over magnesium sulfate and then distilled under nitrogen at reduced pressure.

Benzaldehyde (Fisher certified reagent) was distilled twice under nitrogen at reduced pressure, care being taken to protect the distillate from exposure to bright light.

Pyridine (Fisher certified reagent) was dried over KOH and then distilled twice under nitrogen at atmospheric pressure.

2,4- and 2,6-di-*tert*-butylpyridine and 2-isopropyl-6-*tert*-butylpyridine (Chemical Samples Co.) were distilled under nitrogen at reduced pressure.

3-Ethyl-3-pentanol (Et_3COH, Baker analyzed reagent) was distilled twice under nitrogen at reduced pressure.

Chloroform and methyl isobutyl ketone (both reagent grade) were purified by drying and double distillation.

References and Notes

(1) (a) Acknowledgment is made to the donors of the Petroleum Research Fund, administered by the American Chemical Society, for support of this work; (b) John Simon Guggenheim Fellow, 1975–1976.
(2) Parts 1–3 directly precede this article. Equations appearing therein are numbered accordingly. For instance, eq 1-8 appears in part 1, etc.
(3) J. A. Riddick and W. B. Bunger, "Organic Solvents", 3d ed, Wiley-Interscience, New York, N.Y., 1970.
(4) See, for examples, (a) E. M. Arnett, L. Joris, E. Mitchell, T. S. S. R. Murty, T. M. Gorrie, and P. v. R. Schleyer, *J. Am. Chem. Soc.*, **92**, 2365 (1970); (b) R. S. Drago, N. O'Bryan, and G. C. Vogel, *ibid*, **92**, 3924 (1970); (c) part 2 of this series.
(5) S. Highsmith and E. Grunwald, *J. Phys. Chem.*, **78**, 1431 (1974).
(6) (a) W. Dannhauser, *J. Chem. Phys.*, **48**, 1911 (1968); (b) G. P. Johari and W. Dannhauser, *ibid.*, **48**, 5114 (1968).
(7) G. Oster and J. G. Kirkwood, *J. Chem. Phys.*, **11**, 175 (1943).
(8) W. A. P. Luck and W. Ditter, *J. Mol. Struct.*, **1**, 261 (1967).
(9) Inasmuch as the intensity of the first overtone, relative to that of the fundamental, is an index of oscillator anharmonicity, we expect a greater anharmonic frequency shift for the "free" OH band than for the OH·O band.
(10) C. Bourderon and C. Sandorfy, *J. Chem. Phys.*, **59**, 2527 (1973).
(11) G. Geiseler, J. Fruwert, and E. Stöckel, *Z. Phys. Chem. (Frankfurt am Main)* **32**, 330 (1962).
(12) N. D. Coggeshall and E. L. Saier, *J. Am. Chem. Soc.*, **73**, 5414 (1951).

Hydrogen Bonding in Polar Liquid Solutions. 5. Theory of Dipole Correlation for Chain-Associated Solvents Containing Hydrogen-Bonding Solutes. Application to 1-Octanol[1a]

Kee-Chuan Pan and Ernest Grunwald* [1b]

Department of Chemistry, Brandeis University, Waltham, Massachusetts 02154 *(Received June 23, 1976)*

Publication costs assisted by the Petroleum Research Fund

Assuming a freely rotating hydrogen-bonded chain structure for the solvent, with solute molecules hydrogen-bonded to the chain terminals, and equilibrium constants conforming to the model of sitewise equilibrium, expressions are obtained for dipole correlation factors of solvent and solute and for the solute-induced medium effect, at $c_2 = 0$. The theory is used to analyze dielectric constant data for the following solutes in 1-octanol: acetone, methyl isobutyl ketone, benzaldehyde, dimethyl sulfoxide, pyridine, and chloroform. The theory leads to values of the pairwise dipole moment μ_{12} (which is analogous to the dipole moment for a 1:1 complex) which are in quite reasonable agreement (10% discrepancy) with dipole moments for the corresponding 1:1 complexes measured in benzene.

For definiteness, consider a dilute solution of a hydrogen-bond acceptor solute (X) in a hydrogen-bond, chain-associated alcohol solvent (ROH). Let $\bar{n}$ denote the mean number of solvent molecules per chain. Let f denote the fraction of solute molecules that are associated with solvent chain terminals, and g_{2a} denote the dipole correlation factor of these molecules. For the complementary fraction $1 - f$ of unsolvated X molecules, $g_{2u} = 1$, by hypothesis of the chemical model.[2] Let g_{12}^0 and g_{11}^0 denote the dipole correlation factors of *solvent* molecules in chains with and without terminal X molecules, respectively. Equation 1-13 then takes the form,[2]

$$\mu_{2,app}^2 - \mu_2^2 = f(g_{2a} - 1)\mu_2^2 + \bar{n}f(g_{12}^0 - g_{11}^0)\mu_1^2 + c_1^0\mu_1^2 (dg_{11}/dc_2)_{c_2=0} \quad (5\text{-}1)$$

Dipole Correlation Factors

In this section we shall express g_{2a}, g_{12}, and g_{11} as sums of pairwise dipole correlations, first for a general chain model, then for chain models in which *specific* interactions are limited to nearest neighbors, or to nearest as well as next-nearest neighbors. The scheme for labeling chain sites is shown in Figure 1. The chains are of variable length, the chain-length ν following a probability distribution function p_ν such that

$$\sum_{\nu=1}^{\infty} p_\nu = 1$$

We shall use primed symbols if the chain contains a terminal X molecule, and unprimed symbols if it does not.

On applying the general definition (1-2), we then write for solute molecules attached to chains of ν links,

$$g_{2a}^{(\nu)} = \left\langle \boldsymbol{\mu}_2' \cdot \left(\boldsymbol{\mu}_2' + \sum_{\iota=\alpha}^{\nu} \boldsymbol{\mu}_{1\iota}'\right) \right\rangle \Big/ \mu_2^2 \quad (5\text{-}2)$$

The average g_{2a} for the solute is given by $g_{2a} = \Sigma_\nu p_\nu' g_{2a}^{(\nu)}$. Introducing (5-2), we obtain:

$$g_{2a} = \left\langle \left\langle \boldsymbol{\mu}_2' \cdot \left(\boldsymbol{\mu}_2' + \sum_{\iota=\alpha}^{\nu} \boldsymbol{\mu}_{2}'\right) \right\rangle \right\rangle \Big/ \mu_2^2 \quad (5\text{-}3)$$

where $\langle\langle\ \rangle\rangle$ denotes an ensemble average over both chain conformation and chain length.

To obtain g_{12} for the solvent molecules in chains terminating in X, we need a double summation. Let $g_{12}^{(\nu)}$ denote the *average* dipole correlation factor for the ν solvent molecules in chains of ν links.

$$g_{12}^{(\nu)} = \nu^{-1} \left\langle \sum_{\iota=\alpha}^{\nu} \boldsymbol{\mu}_{1\iota}' \cdot \left(\boldsymbol{\mu}_2' + \sum_{\kappa=\alpha}^{\nu} \boldsymbol{\mu}_{1\kappa}'\right) \right\rangle \Big/ \mu_1^2 \quad (5\text{-}4)$$

The average g_{12} for the ensemble is $(\Sigma_\nu p_\nu' \nu g_{12}^{(\nu)}/\Sigma_\nu \nu p_\nu')$, and is obtained from (5-4), recalling that $\Sigma_\nu \nu p_\nu' = \bar{n}'$.

$$g_{12} = \left\langle \left\langle \sum_{\iota=\alpha}^{\nu} \boldsymbol{\mu}_{1\iota}' \cdot \left(\boldsymbol{\mu}_2' + \sum_{\kappa=\alpha}^{\nu} \boldsymbol{\mu}_{1\kappa}'\right) \right\rangle \right\rangle \Big/ \bar{n}'\mu_1^2 \quad (5\text{-}5)$$

The average g_{11} for solvent chains not terminating in X is obtained similarly. The result is,

$$g_{11} = \left\langle \left\langle \sum_{\iota=\alpha}^{\nu} \left(\boldsymbol{\mu}_{1\iota} \cdot \sum_{\kappa=\alpha}^{\nu} \boldsymbol{\mu}_{1\kappa}\right) \right\rangle \right\rangle \Big/ \bar{n}\mu_1^2 \quad (5\text{-}6)$$

For the general chain model, the distribution function p_ν may be different from p_ν', and dipole correlations such as $\langle\langle \boldsymbol{\mu}_{1\iota} \cdot \boldsymbol{\mu}_{1\kappa} \rangle\rangle$ may change upon addition of X.

A great simplification results if it is assumed that specific interactions within the chain are limited to nearest neighbors. Such a model is consistent with two explicit features of the forthcoming calculations: (1) Stepwise association constants are independent of chain length, as expressed in (4-4) and (4-11), with the result that a sitewise equilibrium formulation becomes valid. (2) Each hydrogen-bond strength is independent of the state of the adjacent hydrogen bonds, so that free rotation about hydrogen bonds is permitted. Consequences are that p_ν and p_ν', $\bar{n}$ and $\bar{n}'$, and solvent–solvent dipole correlations $\langle \boldsymbol{\mu}_{1\iota} \cdot \boldsymbol{\mu}_{1\kappa} \rangle$ and $\langle \boldsymbol{\mu}_{1\iota}' \cdot \boldsymbol{\mu}_{1\kappa}' \rangle$ between any pair of sites in chains of any length, all become equal.

On introducing these consequences into (5-3), (5-5), and (5-6), one obtains for the "nearest-neighbor" model

$$(g_{2a} - 1)\mu_2^2 = \bar{n}(g_{12} - g_{11})\mu_1^2 = \left\langle \left\langle \boldsymbol{\mu}_2' \cdot \sum_{\iota=\alpha}^{\nu} \boldsymbol{\mu}_{1\iota}' \right\rangle \right\rangle \quad (5\text{-}7)$$

Substituting this result in (5-1) leads to

$$\mu_{2,app}^2 - \mu_2^2 = \left[2f \left\langle \left\langle \boldsymbol{\mu}_2' \cdot \sum_{\iota=\alpha}^{\nu} \boldsymbol{\mu}_{1\iota}' \right\rangle \right\rangle + c_1^0\mu_1^2 (dg_{11}/dc_2) \right]_{c_2=0} \quad (5\text{-}8)$$

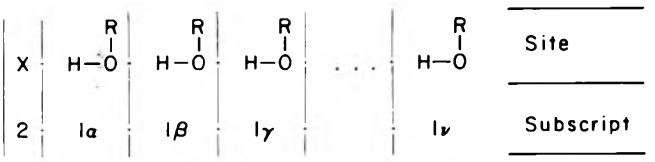

Figure 1. Notation for hydrogen-bonding sites.

Equation 5-8 becomes useful if f and dg_{11}/dc_2 can be evaluated independently.

In order to account for the properties of *covalent* chain polymers, it is necessary to consider specifically not only nearest- but also next-nearest-neighbor interactions.[3] For hydrogen-bonded chain polymers, it is likely that next-nearest-neighbor interaction will also have to be considered specifically in order to achieve broad scope. We are currently applying Flory's rotational isomeric state approximation and statistical formalism[3] to liquid alcohols and find that this approach can reproduce nearly all of the perplexing features of the dielectric constant of the isomeric octanols.[4]

From the present point of view, the introduction of specific next-nearest-neighbor interactions requires the following formal changes. (1) The sitewise equilibrium model is no longer rigorously correct. Equation 4-4 must be changed so that $K_n = K$ for $n \geq 3$ but $K_2 \neq K$; (4-11) must be changed so that $K_{X,n} = K_X$ for $n \geq 2$ but $K_{X,1} \neq K_X$. However, chemical considerations require that neither K_2 and K, nor $K_{X,1}$ and K_X, will be greatly different. Thus, unless $\bar{n}$ is near unity, the sitewise equilibrium model should continue to be an acceptable approximation. (2) In (5-8), the first term on the right must be expanded to allow for specific differences in interactions with the α site, as follows:

$$\mu_{2,\mathrm{app}}^2 - \mu_2^2 = \left\{2f\left[\left\langle\left\langle(\mu_2' + \mu_{1\alpha}')\cdot\sum_{\iota=\alpha}^{\nu}\mu_{1\iota}'\right\rangle\right\rangle - \left\langle\left\langle\mu_{1\alpha}\cdot\sum_{\iota=\alpha}^{\nu}\mu_{1\iota}\right\rangle\right\rangle\right] + c_1^0\mu_1^2\,(dg_{11}/dc_2)\right\}_{c_2=0} \quad (5\text{-}8a)$$

Solute-Induced Medium Effect

The term $c_1^0\mu_1^2\,(dg_{11}/dc_2)$ in (5-8) represents the solute-induced medium effect (SIME). As shown previously, the SIME may be dissected into a general component, represented for non-hydrogen-bonding solutes by the empirical relation $AV_2 + B\mu_2^2$ (part 3), and (for hydrogen-bonding solutes) an additional solvent structure-breaking component (part 4). In this section we shall combine the two components to obtain the total SIME.

Let us admit at once that by using the empirical relation $AV_2 + B\mu_2^2$, we are introducing an extratheoretical element into a purportedly theoretical calculation. This introduces no logical inconsistency, because we are not mixing imcompatible models, but it does introduce some risk of error, because we are obliged to apply the empirical relation outside its most narrowly defined domain. We see no way of avoiding this risk.

We reckon the *general* component of the SIME as follows:

For the unsolvated fraction	$(AV_2 + B\mu_2^2)(1 - f)$
For the solvated fraction	$(AV_2 + B\mu_2^2)f(Z - 1)/Z$
Total	$(AV_2 + B\mu_2^2)(1 - f/Z)$

In the above, Z is the coordination number of the liquid quasi-lattice surrounding an unsolvated solute molecule. The factor $(Z - 1)/Z$ appearing in the expression for the solvated fraction allows for the fact that one of the Z lattice sites is hydrogen-bonded to a solvent chain terminal and thus is precluded from producing an SIME.

We obtain the solvent structure-breaking (SB) component of the SIME on the basis of (5-9).

$$(\mathrm{SIME})_{\mathrm{SB}} = [\mu_1^2 c_1^0\,(dg_{11}/d\bar{n})\cdot(d\bar{n}/dc_2)_{\mathrm{SB}}]_{c_2=0} \quad (5\text{-}9)$$

To obtain $dg_{11}/d\bar{n}$ in this expression, we need an explicit structural model of the solvent chains. To obtain $(d\bar{n}/dc_2)_{\mathrm{SB}}$, we use the sitewise equilibrium model of part 4. We express the free OH site concentration x first in terms of stoichiometry, then in terms of (4-16) and (4-17).

$$x = y - [\mathrm{OH}\cdot\mathrm{X}] = c_1/\bar{n} - fc_2 \quad (5\text{-}10a)$$

$$x = (\bar{n} - 1)/K \quad (5\text{-}10b)$$

Eliminating x and differentiating:

$$\frac{d\bar{n}}{dc_2}\left(\frac{1}{K} + \frac{c_1}{\bar{n}^2}\right) = -f - c_2\frac{df}{dc_2} + \frac{1}{\bar{n}}\frac{dc_1}{dc_2} \quad (5\text{-}11)$$

Equation 5-11 may be simplified because (1) $d\bar{n}/dc_2$ is required at $c_2 = 0$; (2) the term containing dc_1/dc_2 represents the effect of dilution of the solvent by the added solute. This is a general effect, independent of f, and thus is already included in the general component of the SIME. On introducing the simplified expression into (5-9) and adding it to the expression for the general component, we obtain for the total SIME:

$$\mu_1^2 c_1^0\left(\frac{dg_{11}}{dc_2}\right)_{c_2=0} = (AV_2 + B\mu_2^2)\left(1 - \frac{f}{Z}\right) - \frac{\mu_1^2 f K c_1^0 \bar{n}^2}{Kc_1^0 + \bar{n}^2}\left(\frac{dg_{11}}{d\bar{n}}\right)_{c_2=0} \quad (5\text{-}12)$$

Explicit Model for Solvent Chains

Oster and Kirkwood[5] have shown that a model of OH·O hydrogen-bonded chains, with free rotation around the hydrogen-bond axis but excluding OH·O bending, comes close to fitting experimental g factors for a series of normal alcohols. We shall adopt this model, but introduce an adjustable parameter to obtain precise agreement with g_1 for pure 1-octanol at the experimental temperature of 25 °C.

Structural features of the model are shown in Figure 2. As in part 2, α and β are the angles between the hydrogen-bond axis and the molecular dipole axis of donor and acceptor molecule, respectively. On applying bond moments tabulated by Smyth,[6] for 1-octanol $\alpha = 43°$ and $\beta = 55.5°$. $(\pi - \gamma)$, the angle between adjacent hydrogen bonds, should be near the tetrahedral angle. However, we shall treat γ as an adjustable parameter. Using this model, the average g factor for the molecules in a chain of n units is given by

$$g_n = 1 + \frac{2\cos\alpha\cos\beta}{n}[(n-1) + (n-2)\cos\gamma + (n-3)\cos^2\gamma + \ldots + (\cos\gamma)^{n-2}]$$

$$g_n = 1 + \frac{2\cos\alpha\cos\beta}{(1-\cos\gamma)}\left(1 - \frac{1 - n\cos^n\gamma}{n(1-\cos\gamma)}\right) \quad (5\text{-}13)$$

For fairly long chains such as we are considering, $n\cos^n\gamma \ll 1$ and may be neglected, leaving a linear relationship between g_n and $1/n$. The ensemble average of g_n thus is a linear function of the ensemble average of $1/n$, which for a sitewise equilibrium ensemble is practically equal to $1/\bar{n}$.[7] We thus obtain, for the ensemble average,

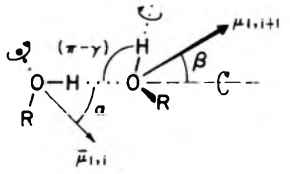

Figure 2. Explanation of angles used in the explicit model.

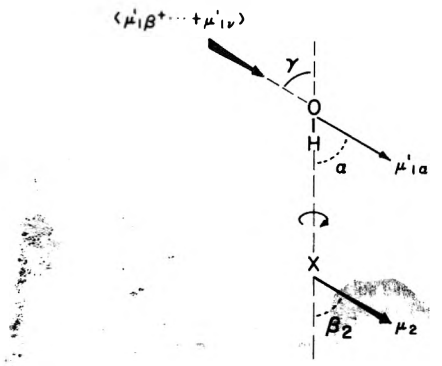

Figure 3. Explanation of angles near the site of the solute.

$$g_{\bar{n}} = 1 + \frac{2\cos\alpha\cos\beta}{(1-\cos\gamma)}\left(1 - \frac{1}{\bar{n}(1-\cos\gamma)}\right) \quad (5\text{-}14)$$

On introducing the numerical values $\alpha = 43°$, $\beta = 55.5°$, $\bar{n} = 27.7$, and $g_{\bar{n}} = 2.805$ at 25 °C, we find that $\cos\gamma = 0.5807$. Thus for 1-octanol at 25 °C,

$$g_{\bar{n}} = 2.976 - 4.712/\bar{n} \quad (5\text{-}15)$$

The value of the parameter $\cos\gamma$ leads to $\pi - \gamma = 125.5°$, significantly greater than the expected near-tetrahedral value. This indicates that the free-rotation model is adequate only in first approximation. Equation 5-15 will be used in the calculation of the solvent structure-breaking component of the SIME.

Next we wish to obtain an explicit expression for the solvent–solute dipole correlation term in (5-8). We shall again consider a model of free rotation about the hydrogen-bond axes, and a solute X which is a hydrogen-bond acceptor. Notation for vectors and angles is indicated in Figure 3. For convenience, we shall regard $\mu_{1\nu}'$ as fixed and the other dipoles in the chain as rotating about their respective hydrogen bond axes. On that basis, the average vector $\langle\mu_{1\beta}' + \ldots + \mu_{1\nu}'\rangle$ for the chain is directed along the hydrogen-bond axis joining the 1α and 1β sites. Also, in computing $\langle\mu_2'\cdot\Sigma\mu_{1i}'\rangle$ for the chain, we may first find the average component of $\Sigma\mu_{1i}'$ along the OH·X hydrogen-bond axis, and then multiply by $\mu_2\cos\beta_2$. Thus, for a solute X attached to a chain of n solvent molecules,

$$\left\langle \mu_2' \cdot \sum_i \mu_{1i}' \right\rangle = \mu_2\cos\beta_2(\mu_1\cos\alpha + \langle\mu_{1\beta}' + \ldots + \mu_{1\nu}'\rangle\cos\gamma)$$

$$= \mu_2\cos\beta_2\,\mu_1\cos\alpha\,(1 + \cos\gamma + \cos^2\gamma + \ldots + \cos^{n-1}\gamma)$$

$$\left\langle \mu_2' \cdot \sum_i \mu_{1i}' \right\rangle = \frac{\mu_1\mu_2\cos\alpha\cos\beta_2}{(1-\cos\gamma)}(1 - \cos^n\gamma) \quad (5\text{-}16)$$

For chains of the length we are considering, $\cos^n\gamma$ is negligible compared to unity. Thus the result, (5-16), is practically independent of chain length and expresses also the ensemble average. On introducing this result into (5-8), expressing the SIME according to (5-12) and $dg_{11}/d\bar{n}$ according to (5-15), and introducing numerical values for 1-octanol at 25 °C, we obtain

$$\mu_{2,\mathrm{app}}^2 - \mu_2^2 = 4.77f\mu_1\mu_2\cos\alpha\cos\beta_2 + (AV_2 + B\mu_2^2)(1 - f/Z) - 7.16f \quad (5\text{-}17)$$

For hydrogen-bond donor solutes such as $CHCl_3$, the factor $\cos\alpha\cos\beta_2$ is replaced by $\cos\beta\cos\alpha_2$. As reported in part 3, $A = -0.0451$ D^2 cm^{-3} mol and $B = 0.0477$ for 1-octanol at 25 °C. The lattice coordination number Z is relatively unimportant to the final result; we shall arbitrarily adopt the value $Z = 6$. Thus the only remaining unknown is the solvated fraction f.

For the solutes that we shall consider, the hydrogen-bonding affinity in nonpolar solvents is comparable to, or greater than, that of 1-octanol (part 2). It is reasonable to expect that *relative* association constants will not vary greatly with the solvent. For 1-octanol, the statistically corrected sitewise association constant in the pure liquid at 25 °C is ½·117, or 58 (M^{-1}). By comparison, if K_X were as small as 20 (M^{-1}), f would be 0.82. If $K_X > 58$, $f > 0.93$. Judging that f will be close to unity, we shall simply adopt a uniform value of $f = 1$.

Application

An analysis of experimental data in terms of the present theory is shown in Table I. Values of $\mu_{2,\mathrm{app}}^2 - \mu_2^2$ in 1-octanol were taken from part 4. Only those solutes are listed for which association constants, and dipole moments, for 1:1 complexes with 1-octanol in benzene are known (part 2).[8]

Values of the SIME, listed in the next column of Table I, are generally quite negative. The solvent structure-breaking component ($-7.16f$ in eq 5-17, or ≈ -7.16 D^2) accounts for nearly three-fourths of the total and thus is quite important.

TABLE I: Analysis of Apparent Dipole Moments for Hydrogen-Bonding Solutes in 1-Octanol at 25 °C

Solute	$\mu_{2,\mathrm{app}}^2 - \mu_2^2$, D^2 [a]	SIME, D^2 [b]	$2\mu_1\mu_2\cos\alpha\cos\beta_2$		μ_{12}, D	
			OctOH[c]	Benzene[d]	OctOH[e]	Benzene[f]
Acetone	−5.8	−9.6	1.6	5.6	3.5	4.07
MIK	−4.1	−11.6	3.1	5.2	3.7	3.94
C_6H_5CHO	−7.2	−10.6	1.4	4.8	3.7	4.14
$(CH_3)_2SO$	−15.5	−9.2	−2.6	2.6	4.0	4.56
Pyridine	−1.2	−10.0	3.7	5.8	3.4	3.73
$CHCl_3$	−4.5	−10.1	2.4	2.3	2.7	2.63

[a] From part 4. [b] $(AV_2 + B\mu_2^2)(1 - f/Z) - 7.16f$; $f = 1$ throughout. [c] $(\mu_{2,\mathrm{app}}^2 - \mu_2^2 - \mathrm{SIME})(1 - \cos\gamma)$; $\cos\gamma = 0.581$. [d] $\mu_{12}^2 - \mu_1^2 - \mu_2^2$; see eq 2-2. [e] Equation 5-18. [f] From part 2.

The next column lists values of $2\mu_1\mu_2 \cos\alpha \cos\beta_2$ (for $CHCl_3$, $2\mu_1\mu_2 \cos\beta \cos\alpha_2$), calculated from the experimental ($\mu_{2,app}^2 - \mu_2^2$) and the theoretical SIME according to (5-17). These values should be comparable to ($\mu_{12}^2 - \mu_1^2 - \mu_2^2$) measured in benzene, since the dipole moments of the complexes conform fairly well to a free-rotation model (eq 2-2). This comparison places great demands on the present theory, requiring simultaneous adherence to sitewise equilibrium and free-rotation models. Bearing this in mind, the results are encouraging. Except for DMSO, values calculated from the 1-octanol data via (5-17) are positive and of the same order of magnitude as those in benzene.

A more familiar, and perhaps more realistic, comparison is that of μ_{12}, calculated according to

$$\mu_{12} = (\mu_1^2 + \mu_2^2 + 2\mu_1\mu_2 \cos\alpha \cos\beta_2)^{1/2} \qquad (5\text{-}18)$$

Values thus calculated from the 1-octanol data should be comparable to measured dipole moments for the 1:1 complexes in benzene. As shown in the final columns of Table I, agreement of the two sets of dipole moments is better than semiquantitative. Discrepancies range from 2 to 15% and average about 10%. If we recall the perplexing aspects of the original data, that polar solutes such as acetone or DMSO added at low concentrations to 1-octanol actually *lower* the dielectric constant, it becomes clear that the present approach goes a long way toward accounting for this complex phenomenon.

References and Notes

(1) (a) Acknowledgment is made to the donors of the Petroleum Research Fund, administered by the American Chemical Society, for support of this work; (b) John Simon Guggenheim Fellow, 1975-1976.
(2) Parts 1-4 directly precede this article. Equations appearing therein are numbered accordingly. For instance, eq 4-6 appears in part 4, etc.
(3) P. J. Flory, "Statistical Mechanics of Chain Molecules", Wiley-Interscience, New York, N.Y., 1969.
(4) (a) W. Dannhauser, *J. Chem. Phys.*, **48**, 1911 (1968); (b) G. P. Johari and W. Dannhauser *ibid.*, **48**, 5114 (1968).
(5) G. Oster and J. G. Kirkwood, *J. Chem. Phys.*, **11**, 175 (1943).
(6) C. P. Smyth, "Dielectric Behavior and Structure", McGraw-Hill, New York, N.Y., 1955.
(7) Equation 4-5 implies a distribution function $p_n = r(1 - r)^{n-1}$, where $r^{-1} = \bar{n}$. We replace p_n by a continuous function $P(x) = \exp(-rx)$. Then

$$1/n = \lim_{t\to -1} \int_0^\infty x^t \exp(-rx)\,dx / \int_0^\infty \exp(-rx)\,dx = r = 1/\bar{n}$$

(8) Data are also reported in part 4 for several solutes with bulky alkyl substituents near the hydrogen-bonding site. Although there is some doubt whether a model of free rotation about the hydrogen-bond axis will be a good approximation for these solutes, we have nevertheless calculated μ_{12}(OctOH) and μ_{12}(benzene) via eq 5-17 and 5-18. Values thus obtained for μ_{12} (in Debye units) are: *t*-Bu_2CO–OctOH, 3.77 (3.80); 2,6-*t*-Bu_2Py–OctOH, 2.92 (2.56); 2,4-*t*-Bu_2Py–OctOH, 3.72 (3.39); 2-*t*-Bu-6-*i*-PrPy–OctOH, 3.04 (2.70). (Values in parentheses denote μ_{12} predicted for the free-rotation model in benzene.) The fairly good agreement throughout does not establish the validity of the free-rotation model, because deviations could be similar in the two solvents. Direct measurements of μ_{12} in benzene by the methods of part 2 would be required.

Phase Transitions of the Anion Radical Salts of $[(C_6H_5)_3PCH_3]_{1-x}^+[(C_6H_5)_3AsCH_3]_x^+(TCNQ)_2^{\cdot -}$ ($0 \leq x \leq 1$). The Thermodynamic Properties of the Solid Solutions

Yoichi Iida

Department of Chemistry, Faculty of Science, Hokkaido University, Sapporo, 060, Japan *(Received August 16, 1976)*

The thermodynamic properties of the solid-state phase transitions were investigated with anion radical salts containing mixed cations represented by $[(C_6H_5)_3PCH_3]_{1-x}^+[(C_6H_5)_3AsCH_3]_x^+(TCNQ)_2^{\cdot -}$ ($0 \leq x \leq 1$). The properties of Gibbs free energy and entropy were examined for the solid solutions of these TCNQ anion radical salts. The experimental relations of the magnitude of the heat of transition and the entropy change associated with the phase transition to the composition parameter were explained by applying a thermodynamical theory of the ideal solid–solution model. In this case, the solid solutions have four possible phases ($\alpha\gamma$, $\beta\gamma$, $\alpha\delta$, and $\beta\delta$ phases). The phase transitions of those TCNQ anion radical salts observed at 1 atm pressure were assigned to the $\alpha\gamma \rightarrow \beta\gamma$ transition.

Introduction

Much attention has been paid to the solid anion radical salts of 7,7,8,8-tetracyanoquinodimethane (TCNQ) because of their prominent electronic properties.[1-16] In particular, the anion radical salt of methyltriphenylphosphonium, $[(C_6H_5)_3PCH_3]^+(TCNQ)_2^{\cdot -}$, is known to undergo a phase transition at 315.7 K under 1 atm pressure in the solid state.[4-12] Heat-capacity measurements of this phase transition have been made by Kosaki et al.[8] The transition has thus been found to be first order. The enthalpy and the total entropy change associated with the phase transition were experimentally determined to be 485.18 cal/mol and 1.7206 cal/deg mol, respectively.[8] On the other hand, the methyltriphenylarsonium salt, $[(C_6H_5)_3AsCH_3]^+(TCNQ)_2^{\cdot -}$, although it exhibits electronic properties almost identical with those of the phosphonium salt, is known to have no such phase transition up to the decomposition temperature of about 480 K under 1 atm pressure.[5,7,10-12]

One can prepare the anion radical salts containing the mixed cations represented by $[(C_6H_5)_3PCH_3]_{1-x}^+[(C_6H_5)_3AsCH_3]_x^+(TCNQ)_2^{\cdot -}$ ($0 \leq x \leq 1$).[4] For these solid solutions, we investigated in a previous paper the effect of the chemical composition upon the phase transition phenomenon with a

differential scanning calorimeter (DSC).[10] It was found that the transition temperature, T_c, is increased, while the magnitude of the heat of the transition, ΔH, is decreased progressively with an increase in the composition parameter, x, and that the phase transition disappears with $x = 1.00$. These thermodynamic behaviors vs. the composition parameter are illustrated in Figure 1. Figure 2 shows the relation of the magnitude of the molar entropy change estimated for the phase transition, ΔS, to the composition parameter. It is interesting to see that ΔS decreases almost linearly with an increase of x, converging to zero at $x = 1.00$.

In the present paper, a thermodynamical theory of solid solution was applied to the anion radical salts of $[(C_6H_5)_3PCH_3]_{1-x}^+[(C_6H_5)_3AsCH_3]_x^+(TCNQ)_2^{\cdot-}$ ($0 \leq x \leq 1$) in order to understand these experimental results of the thermodynamic properties. The relations of the magnitude of the heat of transition and the entropy change associated with the phase transition to the composition parameter were well explained by using an ideal solid solution approximation. These theoretical considerations are quite useful for investigating the mechanism of the phase transitions of those TCNQ anion radical salts.

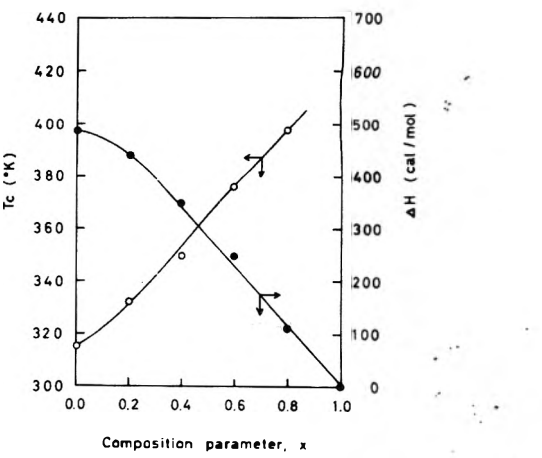

Figure 1. Experimental relations of the transition temperature, T_c, and of the magnitude of the heat of the phase transition, ΔH, to the composition parameter, x, in $[(C_6H_5)_3PCH_3]_{1-x}^+[(C_6H_5)_3AsCH_3]_x^+(TCNQ)_2^{\cdot-}$ ($0 \leq x \leq 1$).

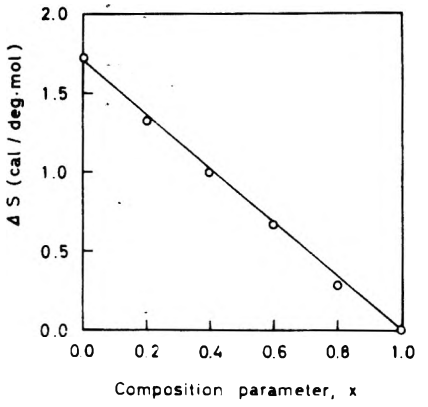

Figure 2. The relation of the total entropy change at the phase transition, ΔS, to the composition parameter, x, in $[(C_6H_5)_3PCH_3]_{1-x}^+[(C_6H_5)_3AsCH_3]_x^+(TCNQ)_2^{\cdot-}$ ($0 \leq x \leq 1$). The open circles indicate the observed values, while the solid line represents the theoretical relation estimated from eq 4 and 9. See text.

Theoretical

First, let us consider the crystal structures of the component anion radical salts of $[(C_6H_5)_3PCH_3]^+(TCNQ)_2^{\cdot-}$ and $[(C_6H_5)_3AsCH_3]^+(TCNQ)_2^{\cdot-}$. We define the phases of $[(C_6H_5)_3PCH_3]^+(TCNQ)_2^{\cdot-}$ below and above the transition temperature as α and β phases, respectively. According to the X-ray diffraction studies by McPhail et al.,[13] the crystal structure of the α phase is triclinic (space group $P\bar{1}$), consisting of tetrads of TCNQ molecules and methyltriphenylphosphonium cations. The unit cell data are $a = 9.01$ Å, $b = 12.82$, $c = 18.02$, $\alpha = 121.48°$, $\beta = 90.80°$, $\gamma = 97.52°$, and $Z = 2$ with unit cell volume of 1751 Å^3. On the other hand, the crystal structure of the β phase has been determined by Konno and Saito.[14] It is also triclinic, and the lattice constants are very much similar to those of the α phase. The volume of the unit cell of the β phase is less than that of the α phase by 4.2 Å^3.[17] Because of this very small change in cell dimensions, a single crystal specimen transforms into the β phase without any breaking. The structure of the β phase is closely related to that of the α phase, but a difference was found in the conformation of the methyltriphenylphosphonium cation with respect to the intramolecular rotation of the phenyl groups.[14]

The crystals of the $[(C_6H_5)_3AsCH_3]^+(TCNQ)_2^{\cdot-}$ anion radical salt do not undergo phase transition at 1 atm pressure. We define the phase of this salt at 1 atm pressure as the γ phase. The crystal structure of the γ phase is also triclinic (space group $P\bar{1}$) and isomorphous to the α phase of the phosphonium salt.[13] The unit cell data of the γ phase are $a = 9.01$ Å, $b = 12.89$, c = 18.18, $\alpha = 121.80°$, $\beta = 90.58°$, $\gamma = 97.30°$, and $Z = 2$ with a unit cell volume of 1772 Å^3.[13] Although there is no phase transition at 1 atm pressure, the $[(C_6H_5)_3AsCH_3]^+(TCNQ)_2^{\cdot-}$ salt undergoes phase transition when one applies a pressure.[7] We define the high-pressure phase of this salt as the δ phase. By the use of the observed p–T phase diagram, Merkl et al. estimated the unit cell volume of the δ phase to be 1760.3 Å^3, which is smaller than that of the γ phase by 11.7 Å^3.[7]

These crystal data show very slight difference in the crystal structures among the four phases of the component anion radical salts. Moreover, the methyltriphenylphosphonium cation is very similar to the methyltriphenylarsonium cation, and the ion radii of both cations are much alike.[13] For the salts of $[(C_6H_5)_3PCH_3]_{1-x}^+[(C_6H_5)_3AsCH_3]_x^+(TCNQ)_2^{\cdot-}$, we can obtain solid solutions in the whole range from $x = 0.00$ to 1.00. On the basis of these facts, our solid solutions will be of substitutional type, and both cations seem to be randomly arranged in the solid solutions. Thus, we can assume the ideal mixing of the two component anion radical salts. To a first approximation, an ideal solid solution model is applicable to our system. For the phase transition of solid solutions, we can further expect that the phase transition does not change the manner of ideal mixing, because the methyltriphenylphosphonium and methyltriphenylarsonium cations are so bulky that we cannot expect the cation exchange in the phase transition. In this respect, it is important to note that the phase transition of our system is not the usual order–disorder phase transition with respect to the mixing of two components. On the basis of these considerations, there are four possible phases ($\alpha\gamma$, $\beta\gamma$, $\alpha\delta$, and $\beta\delta$) for solid solutions of $[(C_6H_5)_3PCH_3]_{1-x}^+[(C_6H_5)_3AsCH_3]_x^+(TCNQ)_2^{\cdot-}$ ($0 \leq x \leq 1$). Hereafter, we denote the Gibbs free energies per mol for the α and β phases of the pure phosphonium salt as $G_1^{\alpha}(T,p)$ and $G_1^{\beta}(T,p)$, respectively, while those for the γ and δ phases of the pure arsonium salt as $G_2^{\gamma}(T,p)$ and $G_2^{\delta}(T,p)$, respectively. They are functions of the temperature, T, and the pressure,

p. Then, the Gibbs free energies of the solid solution per mol for the $\alpha\gamma$, $\beta\gamma$, $\alpha\delta$, and $\beta\delta$ phases can be expressed by

$$G^{ij}(T,p) = n_1 G_1^{i}(T,p) + n_2 G_2^{j}(T,p) + RT(n_1 \ln n_1 + n_2 \ln n_2) \qquad (i = \alpha, \beta; j = \gamma, \delta) \quad (1)$$

where n_1 and n_2 ($n_1 + n_2 = 1$) are the mole fractions of component $[(C_6H_5)_3PCH_3]^+(TCNQ)_2^{\cdot -}$ and $[(C_6H_5)_3AsCH_3]^+(TCNQ)_2^{\cdot -}$, respectively.

For the solid solutions where $0 < x < 1$, the phase below the transition temperature at 1 atm can be firmly assigned to the $\alpha\gamma$ phase, because this phase forms a uniform phase and faces the α phase at $x = 0.00$ and the γ phase at $x = 1.00$ (see Figure 1). On the other hand, the phase above the transition temperature of the solid solutions at 1 atm also forms a uniform phase. However, there are two possible candidates for this high-temperature phase, that is, the $\beta\gamma$ phase or the $\beta\delta$ phase. In order to determine the character of the high-temperature phase, we can use the relations of the magnitude of the heat of transition and the entropy change associated with the phase transition to the composition parameter of the solid solutions.

For the solid solution with a composition of n_1 and n_2, if the high-temperature phase is the $\beta\delta$ phase, that is, if the phase transition is described in terms of the $\alpha\gamma \rightarrow \beta\delta$ process, the entropy change per mol, $\Delta S(T_c)$, and the heat of transition per mol, ΔH, at transition temperature, T_c, are given from eq 1 as

$$\Delta S(T_c) = -\left[\frac{\partial(G^{\beta\delta} - G^{\alpha\gamma})}{\partial T}\right]_{p,n_i} = n_1 \Delta S_1(T_c) + n_2 \Delta S_2(T_c) \quad (2)$$

$$\Delta H = n_1 \Delta H_1 + n_2 \Delta H_2 \quad (3)$$

where $\Delta S_1(T_c) = S_1^{\beta}(T_c) - S_1^{\alpha}(T_c)$ is the entropy difference per mol between the β and α phases of the phosphonium salt; $\Delta S_2(T_c) = S_2^{\delta}(T_c) - S_2^{\gamma}(T_c)$ is that between the δ and γ phases of the arsonium salt; $\Delta H_1 = H_1^{\beta} - H_1^{\alpha}$ and $\Delta H_2 = H_2^{\delta} - H_2^{\gamma}$ are the entalpy differences per mol for each phases. Similarly, if the high-temperature phase of the solid solution is the $\beta\gamma$ phase and the phase transition is of the $\alpha\gamma \rightarrow \beta\gamma$ process, $\Delta S(T_c)$ and ΔH are given by

$$\Delta S(T_c) = n_1 \Delta S_1(T_c) \quad (4)$$

$$\Delta H = n_1 \Delta H_1 \quad (5)$$

Let us compare these relations with the experimental results of Figures 1 and 2, which show that, for the phase transition of $[(C_6H_5)_3PCH_3]^+(TCNQ)_2^{\cdot -}$ where $n_1 = 1$ and $n_2 = 0$, $\Delta S(T_c) = \Delta S_1(T_c) = 1.7206$ cal/deg mol and $\Delta H = \Delta H_1 = 485.18$ cal/mol at $T_c = 315.7$ K. For the solid solution, if the phase transition is $\alpha\gamma \rightarrow \beta\gamma$ and if $\Delta S_1(T_c)$ remains constant, eq 4 clearly shows that the entropy change per mol, $\Delta S(T_c)$, will decrease linearly with a decrease of n_1, converging to zero at pure $[(C_6H_5)_3AsCH_3]^+(TCNQ)_2^{\cdot -}$ where $n_1 = 0$ and $n_2 = 1$. This theoretical prediction agrees well with the experimental results given in Figure 2. Moreover, eq 5 shows that the ΔH of the solid solution is the greatest at $n_1 = 1.00$ and decreases progressively with the decrease of n_1, converging to zero at $n_1 = 0$. This also explains well the experimental result of Figure 1.

On the other hand, if the phase transition of the solid solution is $\alpha\gamma \rightarrow \beta\delta$, eq 2 and 3 clearly show that, when the composition parameter goes to $n_1 = 0$ and $n_2 = 1$, $\Delta S(T_c)$ and ΔH will not converge to zero but have the values of $\Delta S(T_c) = \Delta S_2(T_c)$ and $\Delta H = \Delta H_2$. These $\Delta S_2(T_c) = S_2^{\delta}(T_c) - S_2^{\gamma}(T_c)$ and $\Delta H_2 = H_2^{\delta} - H_2^{\gamma}$ values should be large, because there exists a significant unit-cell volume difference of 11.7 Å^3 between the δ and γ phases of $[(C_6H_5)_3AsCH_3]^+(TCNQ)_2^{\cdot -}$. Thus, the mechanism of $\alpha\gamma \rightarrow \beta\delta$ phase transition cannot explain our experimental results of Figures 1 and 2. On the basis of these considerations, for solid solutions of $[(C_6H_5)_3PCH_3]_{1-x}^+[(C_6H_5)_3AsCH_3]_x^+(TCNQ)_2^{\cdot -}$ ($0 \leq x \leq 1$) the high-temperature phase at 1 atm is found to be the $\beta\gamma$ phase, and the phase transition is assigned to the $\alpha\gamma \rightarrow \beta\gamma$ process.

Discussion

We have to note that the value of $\Delta S_1(T_c) = S_1^{\beta}(T_c) - S_1^{\alpha}(T_c)$ in eq 4 does not necessarily remain constant in $0 < n_1 < 1$, because $S_1^{\beta} - S_1^{\alpha} = 1.7206$ cal/deg mol is the value at $T_0 = 315.7$ K, and the $S_1^{\beta} - S_1^{\alpha}$ value in eq 4 is the value at the T_c temperature of the phase transition of the solid solution, where T_c is always higher than T_0 as is shown in Figure 1. These situations are schematically demonstrated in Figure 3, which illustrated the relations of G_1^{α} and G_1^{β} in pure $[(C_6H_5)_3PCH_3]^+(TCNQ)_2^{\cdot -}$ and of $G^{\alpha\gamma}$ and $G^{\beta\gamma}$ in the solid solution to the temperature under a constant pressure of 1 atm. In Figure 3, $S_1^{\beta} - S_1^{\alpha} = 1.7206$ cal/deg mol is related to the slope values of G_1^{β} and G_1^{α} with respect to the temperature at $T_0 = 315.7$ K, where the G_1^{α} and G_1^{β} curves intersect. On the other hand, for the solid solution, the $S_1^{\beta} - S_1^{\alpha}$ value in eq 4 is related to the slope values of G_1^{β} and G_1^{α} with respect to the temperature at T_c, where the $G^{\alpha\gamma}$ and $G^{\beta\gamma}$ curves intersect but the G_1^{α} and G_1^{β} curves no longer intersect. One can express the S_1^{α} and S_1^{β} values at T_c by the use of Taylor expansion around $T_0 = 315.7$ K:

$$S_1^{\alpha}(T_c) = S_1^{\alpha}(T_0) + S_1^{\alpha\prime}(T_0)(T_c - T_0) + \frac{1}{2!} S_1^{\alpha\prime\prime}(T_0)(T_c - T_0)^2 + \ldots \quad (6)$$

$$S_1^{\beta}(T_c) = S_1^{\beta}(T_0) + S_1^{\beta\prime}(T_0)(T_c - T_0) + \frac{1}{2!} S_1^{\beta\prime\prime}(T_0)(T_c - T_0)^2 + \ldots \quad (7)$$

so that we have

$$S_1^{\beta}(T_c) - S_1^{\alpha}(T_c) = S_1^{\beta}(T_0) - S_1^{\alpha}(T_0) + (S_1^{\beta\prime}(T_0) - S_1^{\alpha\prime}(T_0))(T_c - T_0) + \frac{1}{2!}(S_1^{\beta\prime\prime}(T_0) - S_1^{\alpha\prime\prime}(T_0))(T_c - T_0)^2 + \ldots \quad (8)$$

where $S_1^{\beta}(T_0) - S_1^{\alpha}(T_0) = 1.7206$ cal/deg mol and $S'(T_0)$, $S''(T_0)$, etc. indicate the derivatives with respect to temperature at T_0.

The experimental fact that the ΔS value decreases linearly with a decrease of n_1, as is shown in Figure 2, means that $S_1^{\beta}(T_c) - S_1^{\alpha}(T_c)$ remains practically constant even though T_c varies from T_0. This evidently indicates that, although both $S_1^{\alpha}(T_c)$ and $S_1^{\beta}(T_c)$ are, in general, functions including higher-order terms of T_c, for $S_1^{\beta}(T_c) - S_1^{\alpha}(T_c)$ these higher-order terms almost cancel with each other and only the constant term remains. Then we have from eq 8

$$S_1^{\beta}(T_c) - S_1^{\alpha}(T_c) \approx S_1^{\beta}(T_0) - S_1^{\alpha}(T_0) = 1.7206 \text{ cal/deg mol}$$

$$S_1^{\beta\prime}(T_0) - S_1^{\alpha\prime}(T_0) \approx 0$$

$$S_1^{\beta\prime\prime}(T_0) - S_1^{\alpha\prime\prime}(T_0) \approx 0 \quad (9)$$

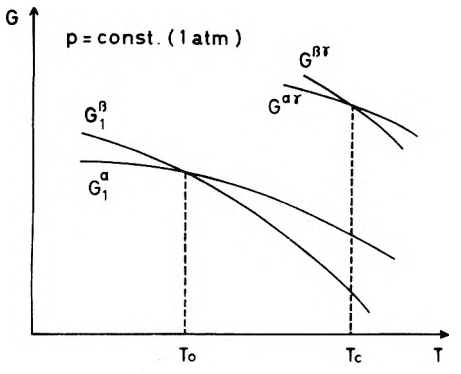

Figure 3. Schematic representation of the relation of the Gibbs free energy to the temperature, T, under a constant pressure of 1 atm in $[(C_6H_5)_3PCH_3]_{1-x}^{+}[(C_6H_5)_3AsCH_3]_x^{+}(TCNQ)_2^{\cdot-}$ $(0 \leq x \leq 1)$. G_1^{α} and G_1^{β} indicate the Gibbs free energies for pure $[(C_6H_5)_3PCH_3]^{+}(TCNQ)_2^{\cdot-}$, while $G^{\alpha\gamma}$ and $G^{\beta\gamma}$, those for the solid sclution. The G_1^{α} and G_1^{β} vs. T curves intersect at $T_0 = 315.7$ K, but the $G^{\alpha\gamma}$ and $G^{\beta\gamma}$ vs. T curves intersect at the T_c temperature.

On the basis of these theoretical considerations, we can well understand the experimental relation of Figure 2 for solid solutions of $[(C_6H_5)_3PCH_3]_{1-x}^{+}[(C_6H_5)_3AsCH_3]_x^{+}(TCNQ)_2^{\cdot-}$ $(0 \leq x \leq 1)$.

Another thing we have to note is that eq 5 shows a linear relationship between ΔH and n_1, while the experimental relation between them has a slight hump as is shown in Figure 1. One reason for this is that we used the ideal solid–solution model to derive eq 5 and ignored the effect of heat of mixing between the two components. Therefore, the deviation of eq 5 from the experimental result may be due to the difference of heat of mixing between the $\alpha\gamma$ and $\beta\gamma$ phases. However, since this effect becomes negligibly small at the two extremes of $n_1 = 1.00$ and of $n_2 = 1.00$, our assignment of the $\alpha\gamma \rightarrow \beta\gamma$ phase transition is still valid for the phase transition of our solid solutions.

Concluding Remarks

The mechanism of the $\alpha\gamma \rightarrow \beta\gamma$ phase transition of $[(C_6H_5)_3PCH_3]_{1-x}^{+}[(C_6H_5)_3AsCH_3]_x^{+}(TCNQ)_2^{\cdot-}$ $(0 \leq x \leq 1)$ solid solutions means that only the phase change of $\alpha \rightarrow \beta$ of the phosphonium salt is involved and the γ phase of the arsonium salt does not vary through the phase transition. This implies that, for the phase transition of the solid solutions, a significant structural change (especially the intramolecular rotation of the phenyl groups) will take place in the methyltriphenylphosphonium part, while no change will be found in the methyltriphenylarsonium cations. In this respect, we have to note the significance of eq 8. If we investigate only the phase transition of pure $[(C_6H_5)_3PCH_3]^{+}(TCNQ)_2^{\cdot-}$ where $n_1 = 1$, information is quite limited to the term of $S_1^{\beta}(T_0) - S_1^{\alpha}(T_0)$ at $T_0 = 315.7$ K. However, studies of the phase transitions of solid solutions provide us with valuable knowledge on the entropy change of the α and β phases of $[(C_6H_5)_3PCH_3]^{+}(TCNQ)_2^{\cdot-}$, $S_1^{\beta}(T_c) - S_1^{\alpha}(T_c)$, at temperatures other than $T_0 = 315.7$ K. This kind of information is also useful for investigating the behaviors of the Gibbs free energies for the α and β phases of $[(C_6H_5)_3PCH_3]^{+}(TCNQ)_2^{\cdot-}$, G_1^{α} and G_1^{β}, at temperatures other than $T_0 = 315.7$ K.

References and Notes

(1) D. B. Chesnut and W. D. Phillips, *J. Chem. Phys.*, **35**, 1002 (1961).
(2) M. T. Jones and D. B. Chesnut, *J. Chem. Phys.*, **38**, 1311 (1963).
(3) W. J. Siemons, P. E. Bierstedt, and R. G. Kepler, *J. Chem. Phys.*, **39**, 3523 (1963).
(4) L. R. Melby, R. J. Harder, W. R. Hertler, W. Mahler, R. E. Benson, and W. E. Mochel, *J. Am. Chem. Soc.*, **84**, 3374 (1962).
(5) R. G. Kepler, *J. Chem. Phys.*, **39**, 3528 (1963).
(6) Y. Iida, M. Kinoshita, M. Sano, and H. Akamatu, *Bull. Chem. Soc. Jpn.*, **37**, 428 (1964).
(7) A. W. Merkl, R. C. Hughes, L. J. Berliner, and H. M. McConnell, *J. Chem. Phys.*, **43**, 953 (1965).
(8) A. Kosaki, Y. Iida, M. Sorai, H. Suga, and S. Seki, *Bull. Chem. Soc. Jpn.*, **43**, 2280 (1970).
(9) Y. Iida, *Bull. Chem. Soc. Jpn.*, **44**, 3344 (1971).
(10) Y. Iida, *Bull. Chem. Soc. Jpn.*, **43**, 578, 3685 (1970).
(11) Y. Iida, *J. Phys. Soc. Jpn.*, **30**, 583 (1971); *J. Chem. Phys.*, 59, 1607 (1973).
(12) Y. Suzuki and Y. Iida, *Bull. Chem. Soc. Jpn.*, **46**, 683 (1973).
(13) A. T. McPhail, G. M. Semeniuk, and D. B. Chesnut, *J. Chem. Soc. A*, 2174 (1971).
(14) M. Konno and Y. Saito, *Acta Crystallogr., Sect. B*, **29**, 2815 (1973).
(15) A. J. Epstein, S. Etemad, A. F. Garito, and A. J. Heeger, *Phys. Rev. B*, **5**, 952 (1972).
(16) E. Ehrenfreund, E. F. Rybaczewski, A. F. Garito, and A. J. Heeger, *Phys. Rev. Lett.*, **28**, 873 (1972).
(17) We used the experimental results on the pressure effect on the phase transition of the phosphonium salt performed by Goll and Phillips (*J. Chem. Phys.*, **43**, 1076 (1965)), who reported the pressure coefficient to be $(\partial T_c/\partial p) = -0.02$ K/atm. By applying Clapeyron–Clausius equation and using the ΔH and T_c values of the phase transition, which are taken from ref 8, we have $(\partial T_c/\partial p) = T_c(V^{\beta} - V^{\alpha})/\Delta H$, where V^{β} and V^{α} are crystal volumes of the β and α phases, respectively. This equation leads to $V^{\beta} - V^{\alpha} = -4.2$ Å^3/unit cell. On the other hand, Konno and Saito (ref 14) reported the $V^{\beta} - V^{\alpha}$ value as -2.2 Å^3/unit cell by X-ray analyses.

Equilibrium Studies with Ca/Sr Zeolite A

H. Gaus* and W. Lutze

Hahn-Meitner-Institut für Kernforschung Berlin GmbH, Bereich Kernchemie und Reaktor, 1 Berlin 39, West Germany

(Received June 2, 1976)

Publication costs assisted by Hahn-Meitner-Institut für Kernforschung Berlin GmbH

The Sr/Ca ion exchange isotherm as well as the related water content in zeolite A is described by a model based on the number of configurations for a certain composition of the unit cell. When these compositions and arrangements are described by ideal mass action laws, for the total system there results an overall activity, which depends on the composition. Fitting the constants of the ideal mass action laws to the experimental curve shows that these constants do not deviate from unity when the change of cell composition is accompanied by a change in water content. It is likely that configuration effects cause the deviations. As to the uptake of water, the data are best described by assuming a successive uptake of three water molecules along with the first three strontium ions.

Introduction

We present an investigation to study ion-exchange equilibria in the system Sr/Ca zeolite A, based on measurements by Fischbach.[1] Many inorganic ion-exchangers show selectivity phenomena. In some cases it was possible to relate pronounced selectivity of mineral ion-exchangers to structural changes[2] occurring at critical ionic ratios in the solid. However, in the zeolite A system there is no evidence for structural changes of the framework when charging the original sodium form with either strontium or calcium or both species. There is also no ion sieve effect to be expected. Both ions are small enough to fit into the large cavities, these having a window width of 4.2 Å. Nevertheless, varying arrangements or local accommodation of the respective cations on energetically different sites in the cavities of the unit cell as discussed by other authors[3,4] could lead to ion selectivity, and varying water content could also have a certain effect. Therefore, Fischbach measured the equilibrium isotherm for the Ca/Sr ion exchange along with the water content of the zeolite as a function of the Ca/Sr ratio.

The Na ions in Na-A were replaced by other ions at 95 °C by using 1 N solutions of the appropriate chlorides labeled with radioactive isotopes. Various Sr/Ca compositions of the zeolite were obtained by contacting it with mixed alkaline earth salt solutions. The composition of the exchanger phase was determined by measuring the radioactivity either in the solid or in the liquid. The water content of the crystals was derived from weight losses after heating the crystals up to about 550 °C. Table I gives the water content of the unit cell for various Ca/Sr-charged forms of zeolite A.

Figure 1 shows the equilibrium isotherm for Sr/Ca at 95 °C. It can be seen that the zeolite exhibits a slight selectivity for Sr in the range of Sr fractions above 0.2 in the solution. It can be seen from Table I that the selectivity for Sr is accompanied by an increased water content in the solid. This is opposite to what can be expected from ion hydration in aqueous salt solutions. There Sr is less hydrated than Ca and a decreasing water content in the zeolite with increasing Sr would not be surprising.

A model has been developed on the basis of the law of mass action to describe the shape of the exchange isotherm for the respective ions and the related water content.

Theoretical Treatment

In this section we try to describe the slight selectivity for Sr and the variation of the water content using the mass action law. We treat the crystallographic microcell with six cations (Sr or Ca) at definite locations as a "molecule". Such a molecule with a certain number of Sr and of Ca ions may form another molecule of different composition by means of a "chemical reaction", namely, ion and water exchange with its environment. In addition we assume that at equilibrium each "molecule" contains a definite number of water molecules which depends on the ionic species present. One would assume that in a microcell with, for example, two Sr and four Ca ions a certain configuration is favored energetically, e.g., the Sr ions on opposite places. However, as there is only a slight selectivity and as we wish to keep the description as simple as possible, we assume at first that with a fixed number of Sr and Ca ions any configuration is equally probable. This means if a "molecule" passes into another configuration by a unimolecular reaction, the constant of the mass action law is unity. The microcells are considered to be fixed in the lattice. Therefore, we have different configurations not only concerning the positions of the Sr and Ca ions relative to each other within one cell but also relative to the coordinates of the lattice. That is, denoting the number of Ca and Sr ions in the cell as n_1 and n_2, respectively, and assuming N possible locations for the cations ($N \geq n_1 + n_2$) there are

$$z(n_1 n_2) = \frac{N!}{n_1! n_2! (N - n_1 - n_2)!}$$

possible configurations. Assuming

$$n_1 + n_2 = 6 \tag{1}$$

we may eliminate n_2 and write

$$z(n_1 n_2) = \frac{6!}{n_1!(6 - n_1)!} \frac{N!}{6!(N - 6)!} = \binom{6}{n_1} \binom{N}{N - 6} \tag{2}$$

Now we consider a given quantity of solid zeolite in equilibrium with an aqueous salt solution containing Ca and Sr ions. We denote the $z(n_1,n_2)$ different configurations with $\alpha, \beta, \ldots,$

TABLE I: Equilibrium Unit Cell Content of Sr/Ca-Loaded Zeolites A at 95 °C

Ionic fraction, $\bar{C}_{Sr}$	Water content of unit cell
0	30.4 H_2O
0.35	31.9 H_2O
0.68	33.2 H_2O
0.86	33.5 H_2O
1	33.4 H_2O
Commercial form	28.0 H_2O

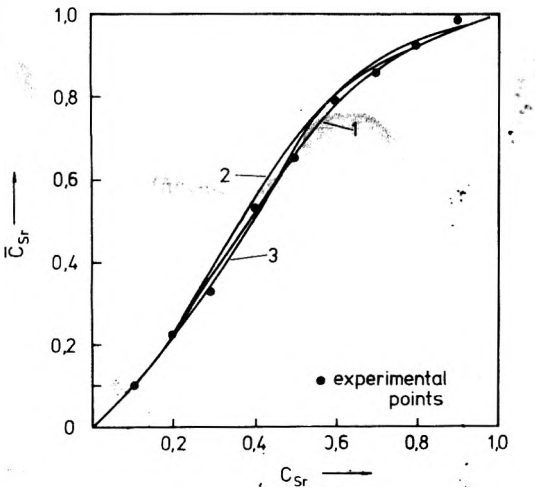

Figure 1. Equilibrium isotherm for Sr zeolite + Ca^{2+} = Ca zeolite + Sr^{2+} at 95 °C: curve 1, according to eq 7a with $\kappa = 2.5$; curve 2, according to eq 7a with $\kappa = 3$; curve 3, acccrding to eq 7b.

the number of cells with (n_1,n_2) composition in a certain configuration α by $x_\alpha(n_1,n_2)$, and the quotient (number of Sr ions):(number of Ca ions) in the liquid and in the solid by ζ and $\bar{\zeta}$, respectively. Then our assumption is that the amounts of the $x_\alpha(n_1,n_2)$ are given by the law of mass action. Relating these amounts to $x_\eta(6,0)$ as a common factor we get

$$\begin{aligned} x_\alpha(5,1) &= \zeta x_\eta(6,0)\kappa_1 \\ x_\beta(4,2) &= \zeta^2 x_\eta(6,0)\kappa_2 \\ x_\gamma(3,3) &= \zeta^3 x_\eta(6,0)\kappa_3 \\ x_\delta(2,4) &= \zeta^4 x_\eta(6,0)\kappa_4 \\ x_\epsilon(1,5) &= \zeta^5 x_\eta(6,0)\kappa_5 \\ x_\vartheta(0,6) &= \zeta^6 x_\eta(6,0)\kappa_6 \end{aligned} \tag{3}$$

Here the κ_i are the appropriate equilibrium constants of the mass action law including eventually a quotient corresponding to the exchange of one or more water molecules. Further the κ_i contain a quotient of the four activity factors if necessary as the x and ζ refer to concentrations and not to activities. However, it seems that these factors cancel, because one may use simple concentration-independent values for the κ's; see eq 7 below. Nevertheless, for the total solid one overall activity will result relative to the solution. The derivation of this overall activity is the purport of the present section.

As mentioned, we assume the κ_i also independent of the configuration α, i.e.

$$x_\alpha(n_1,n_2) = x_\beta(n_1,n_2) \tag{4}$$

also for $\alpha = \beta$. Then the total number $x(n_1,n_2)$ of cells with (n_1,n_2) composition is

$$x(n_1,n_2) = z(n_1,n_2)x_\alpha(n_1,n_2)$$

According to this relation one may also write eq 3 for the total $x(n_1,n_2)$ replacing $x_\alpha, \ldots, x_\vartheta$ by the corresponding x/z. Physically this means to consider the configurations as unknown and the z factors then appearing in (3) as resulting from an entropy term $\exp(\Delta S/k)$ belonging to the equilibrium constants κ with $S = k \log z$.

Our aim is to determine $\bar{\zeta}$ as a function of ζ. To this end according to (4) we multiply the eq 3 with the corresponding frequencies (2) and with the corresponding n_2 and add up the terms to obtain the number of Sr ions in the solid. The same procedure with n_1 yields the number of Ca ions. By division we get $\bar{\zeta}$. Dividing by ζ we obtain after simplification

$$\frac{\bar{\zeta}}{\zeta} = \frac{\kappa_1 + 5\zeta\kappa_2 + 10\zeta^2\kappa_3 + 10\zeta^3\kappa_4 + 5\zeta^4\kappa_5 + \zeta^5\kappa_6}{1 + 5\zeta\kappa_1 + 10\zeta^2\kappa_2 + 10\zeta^3\kappa_3 + 5\zeta^4\kappa_4 + \zeta^5\kappa_5} \tag{5}$$

For all $\kappa_i = 1$ there is $\bar{\zeta} = \zeta$. The right side contains the mentioned total activity of the solid, i.e., a fraction of activity factors, in the notation of Ekedahl, Högfeldt, and Sillen[5]

$$\frac{\bar{\zeta}}{\zeta} = K_{21}\frac{\gamma_1 f_2}{\gamma_2 f_1} \tag{6}$$

where γ and f refer to the solid and liquid, respectively. In eq 5 a concentration dependence of this activity may result with constant κ's. It is caused by the variation of the frequencies $z(n_1n_2)$ with changing concentration.

Now we try to get evidence about the κ's from the empirical plot. By trial and error it turns out rather safely that one has to put

$$\kappa_1 = \kappa_2 = \kappa_3 = 1, \quad \kappa_4 = \kappa, \quad \kappa_5 \geq \kappa^2, \quad \kappa_6 \geq \kappa\kappa_5 \tag{7}$$

with $\kappa \approx 2$–3. For instance

$$\kappa_4 = \kappa, \quad \kappa_5 = \kappa^2, \quad \kappa_6 = \kappa^3, \quad \kappa = 2.5 \text{ or } 3 \tag{7a}$$

reproduces the measurements fairly well. From the additional water content (see below) one could take into consideration, that the last three κ_i are the frequencies to put three water molecules on i places; however, only the half of these values fit the plot

$$\kappa_4 = \frac{1}{2}\binom{4}{3} = 2, \quad \kappa_5 = \frac{1}{2}\binom{5}{3} = 5, \quad \kappa_6 = \frac{1}{2}\binom{6}{3} = 10 \tag{7b}$$

In Figure 1 there is plotted

$$\bar{C}_{Sr} = \frac{\bar{\zeta}}{1 + \bar{\zeta}}$$

as a function of $C_{Sr} = \zeta/(1 + \zeta)$ for some values of κ_i.

Concerning the water contents the measurements show (see Figure 2) that passing from the (6,0) composition (Ca only) to the (0,6) form (Sr only) three water molecules per cell are accommodated additionally. They further suggest that this is finished before the (0,6) composition is reached, already the (2,4) form should contain the three waters. Then the most simple assumption is that the additional-water case coincides with $\kappa_i = 1$ and the no-additional-water case with $\kappa_i \neq 1$. Then, together with the first three Sr ions, there is respectively one water molecule brought into the cell; i.e., up to $n_2 = 3$ there are n_2 additional water molecules.

For the total amount $\bar{y}$ of additional water per cell of the solid one gets in this case and with (7a)

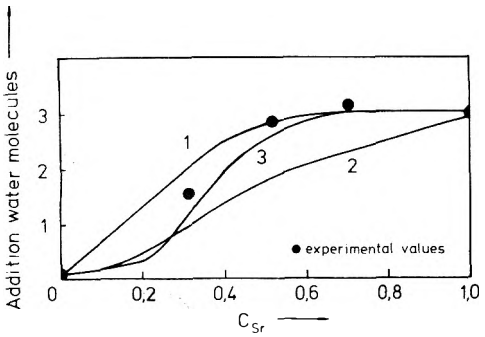

Figure 2. Addition of water molecules: curve 1, successive uptake of three waters with the first three Sr's; curve 2, uptake of one water with every second Sr; curve 3: uptake of three waters with the third Sr.

$$\bar{y} = \frac{1.6\zeta + 2.15\zeta^2 + 3(20\zeta^3 + 15\zeta^4\kappa + 6\zeta^5\kappa^2 + \zeta^6\kappa^3)}{1 + 6\zeta + 15\zeta^2 + 20\zeta^3 + 15\zeta^4\kappa + 6\zeta^5\kappa^2 + \zeta^6\kappa^3} \quad (8)$$

For other assumptions the form of the corresponding expression for $\bar{y}$ is obvious. Formulas like (8) are not very sensitive against a variation of the value of κ. In Figure 2 $\bar{y}$ is plotted as a function of $\zeta/(1 + \zeta)$.

Discussion

The foregoing treatment is based on the assumption of a crystalline structure with cells being occupied by six exchangeable cations, which in the cell may form different configurations formally described by the occupation of $N \geq 6$ different places. Fluctuations in the occupation numbers of the cells are not taken into account explicitly. Such a strong crystalline structure (possibly $N = 6$) may be favored energetically by local electroneutrality. It is in accordance with the measurements of Barrer[6] and Hoinkis.[7] On the other hand Fischbach concluded from his investigations a structure with 6.5 ions per cell. Then one has to assume at least cells with six and cells with seven ions or even larger deviations from the mean value, which means a weaker crystalline structure of the cations. Concerning the above calculation it seems rather sure that one may get similar results also for $n_1 + n_2 = 7$ in eq 1. However, it is only worth going into further calculations if a more detailed knowledge of the structure of Ca- and Sr-charged zeolite A is available. In this case also one may consider eventually more detailed schemes, e.g., different numbers of possible locations for the species 1 and 2. It was pointed out to us, that such an effect possibly causes the change of the water content. Here we do not try to explain the assumed water input with the first three Sr's.

Concerning the values of the κ's a possible explanation of eq 7 arises if one may distinguish between free water in the solid and water's belonging to the cell "molecule". Denoting, e.g., [511] as a cell configuration with 5 Cs, 1 Sr, and 1 additional water, one gets, from the first equation and the last two equation of (3), eliminating ζ

$$\frac{[153][511]}{[063][600]\kappa^{-1}} = 1$$

This is a mass action law, the constant of which is unity, for the corresponding reaction in the solid if κ^{-1} is the number of free water molecules per cell inside the solid. According to Table I with $\kappa^{-1} = 2.5^{-1} = 0.4$ one gets 30 for the water content of a [600] cell. However, in view of the mentioned possible deviations from a fixed cell composition and in view of the experimental inaccuracy we consider this interpretation only as compatible with the measurements.

References and Notes

(1) H. Fischbach, Dissertation D-83, Berlin, 1971.
(2) F. Helfferich, "Ionenaustauscher", Vol. 1, Verlag Chemie, Weinheim/Bergstr., Germany, 1959.
(3) D. C. Freeman and D. N. Stamires, *J. Chem. Phys.*, **35**, 799 (1961).
(4) L. Broussard and D. P. Shoemaker, *J. Am. Chem. Soc.*, **82**, 1041–1051 (1960).
(5) E. Ekedahl, E. Hogfeldt, and L. G. Sillen, *Acta Chem. Scand.*, **4**, 556 (1950).
(6) R. M. Barrer, *Trans. Faraday Soc.*, **54**, 1074 (1958).
(7) E. Hoinkis Dissertation, Berlin, 1969.

Carbon-13 Nuclear Magnetic Resonance Observations of Butenes Adsorbed on Alumina

J. F. Kriz and Ian D. Gay*

Department of Chemistry, Simon Fraser University, Burnaby, British Columbia, Canada V5A 1S6
(Received March 16, 1976)

Publication costs assisted by the National Research Council of Canada

^{13}C chemical shifts of 1- and 2-butenes adsorbed on alumina have been measured and compared with those obtained for other adsorbents. Isomerization of butenes has been studied using samples with different surface pretreatment. The catalytic activity was found to be affected by surface OH concentration and the method of sample preparation.

Introduction

This study is part of a research program in which ^{13}C NMR observations have been made of various molecules adsorbed on SiO_2, Al_2O_3, and SiO_2–Al_2O_3 surfaces.[1-3] Previous experiments with adsorbed butenes showed definite chemical shift differences between free and adsorbed molecules.

The kinetics and product distribution of the isomerization of butenes on alumina are well documented.[4] More recently investigations have focused on the surface mechanism for these reactions and the interpretation of results arising from different experimental methods.[5-7] A direct analysis by ^{13}C NMR spectroscopy can be used to monitor such reactions, provided the time necessary to collect one spectrum is short enough compared with the time in which the reactions reach equilibrium. This method has the benefit of permitting the observation of the adsorbed region rather than free reactants or products and possesses the potential to indicate the state of adsorbed intermediates.

We have examined in this way the isomerization of 1-butene and cis–trans interconversions of 2-butenes on alumina samples with different surface pretreatment.

Experimental Section

As in the previous work[2] spectra were measured at 25.2 MHz with a Varian XL-100 spectrometer incorporating a TTI Fourier transform modification, using an external ^{19}F lock. Several proton-decoupled spectra were obtained successively to follow the reaction change. Each spectrum was accumulated from 2000 scans by applying approximately $\pi/3$ pulses at 1.2-s intervals. Preliminary experiments showed that spin–lattice relaxation times (T_1) could be expected in the 0.2–1-s range. Samples were prepared by vacuum degassing of the adsorbate followed by adsorption of butene from the gas phase.[1] Samples were degassed for 48 ± 2 h at various temperatures ranging from 150 to 500 °C. In a separate experiment the mass of an alumina sample was measured as a function of degassing temperature using a vacuum microbalance.[8]

Surface areas and coverages were obtained by BET measurements as previously described.[2] Adsorption measurements and spectrum accumulations were performed at 32 ± 1 °C.

Materials. The first alumina (A) was prepared by adding an excess of a 20% ammonium hydroxide solution to a 20% aluminum nitrate solution at room temperature. The precipitate was washed with distilled water several times. The second alumina (B) was prepared by room-temperature hydrolysis with a small excess of water of a saturated solution of aluminum isopropoxide in isopropyl alcohol. Resulting precipitates were dried and ignited in air at 600 and 700 °C, respectively, cooled, and allowed to rehydrate in air. Surface areas of the two aluminas were 195 and 108 m^2/g, respectively.

The butenes used were CP grade from Matheson of Canada Ltd. and were vacuum-distilled before storing and before adsorption.

Results

Chemical Shifts. Average ^{13}C chemical shifts observed for *cis*- and *trans*-2-butenes and for 1-butene on our alumina samples are presented in Table I. Shifts are relative to the lines in pure liquids and are not corrected for differing diamagnetic susceptibilities. These corrections would amount to −0.5 ppm in all cases.[2] Blanks have been inserted in Table I where some shifts were not determined with precision due to low signal to noise ratios. A systematic investigation of the dependence of these shifts upon degassing temperature and coverage has not been attempted; however, it appears from Table I that a downfield shift for =CH– groups in butenes is larger when higher degassing temperatures are used.

The relative shifts of the $-CH_3$ groups in *trans*-2-butene and *cis*-2-butene seem to remain unchanged upon adsorption on our alumina samples. The =CH– group of the cis isomer shows a relatively larger shift to lower field than that of the trans isomer since the separation between the two lines narrowed from 1.2 ppm for the pure liquids to 0.6 ppm for the adsorbed molecules. This separation was measured from spectra taken during the reaction of *cis*-2-butene where =CH– lines for both butenes were resolved.

Isomerization. Sets of spectra for the isomerization of 1-butene (Figure 1) and *cis*-2-butene (Figure 2) illustrate the manner in which these reactions were monitored. Although all lines for the liquid 1-butene and 2-butenes were resolved, overlapping of $-CH_3$ lines in 1-butene and *cis*-2-butene and =CH– lines in the 2-butenes was usual for the adsorbed butenes due to line broadening.

Peak heights of individual spectra were compared with those for the equilibrium state to estimate the degree of conversion at the time the spectrum was taken. Then first-order rate constants were calculated to obtain parameters of catalytic activity. These are collected in Table II for the surfaces

TABLE I

(a) ^{13}C Chemical Shifts (ppm ± 0.2) of 1-Butene Adsorbed on Alumina Relative to Liquid 1-Butene[a]

Sample (% coverage)	Degassing temp, °C	=CH-	$=CH_2$	$-CH_2-$	$-CH_3$
A (75)	150	−1.7	0.1	0.4	1.1
A (50)	200	−1.6	0.2	0.5	1.1
A (80)	250	−2.0	0.2	0	0.7
A (45)	320	−2.8	0.4	0.5	1.4
B (95)	420	−2.8	0.2	0	1.2
A (55)	500	−4		0.9	

(b) ^{13}C Chemical Shifts (ppm ± 0.2) of *cis*- and *trans*-2-Butenes Adsorbed on Alumina Relative to the Liquids[a]

Sample (% coverage)	Degassing temp, °C	=CH-		$-CH_3$	
		Cis	Trans	Cis	Trans
A (50)	200	−1.0			
B (90)	250	−1.3	−0.6	1.1	1.0
A (45)	320		−1.2		0.9
B (95)	420		−1.6	0.8	0.6
A (55)	500	−2	−0.9	1.4	1.2
A (25)	500		−1.9	0.5	1.0

[a] Chemical shifts of the pure liquid butenes relative to tetramethylsilane may be found in ref 2 and 11.

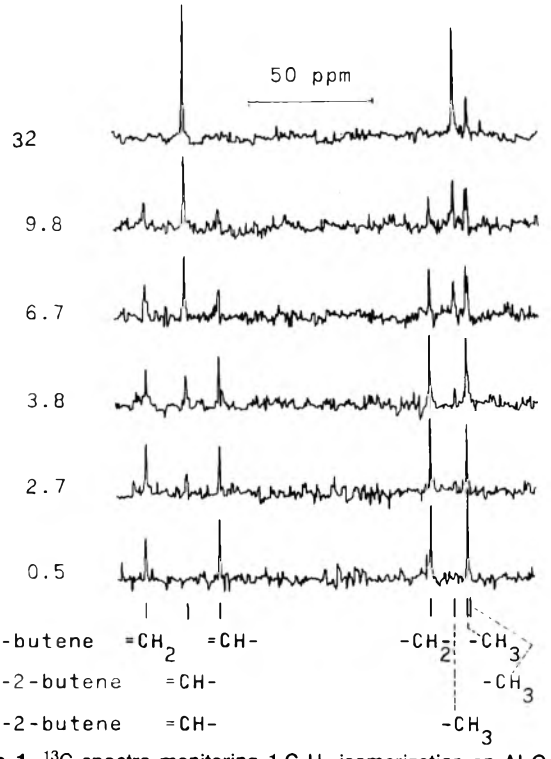

Figure 1. ^{13}C spectra monitoring 1-C_4H_8 isomerization on Al_2O_3-A degassed at 400 °C. Numbers on left indicate time in hours elapsed since sample preparation.

degassed at different temperatures. Errors in values of the rate constants fell in the range of 5–20% for each experiment and the constants therefore offered sufficiently accurate parameters of activity considering the large differences caused by surface pretreatment.

The decrease in mass of our Al_2O_3-A sample with increasing outgassing temperature is shown in Figure 3. Similar diagrams

Figure 2. ^{13}C spectra monitoring *cis*-2-C_4H_8 isomerization on Al_2O_3-B degassed at 250 °C. Numbers on left indicate time in hours elapsed since sample preparation.

for γ-alumina samples were obtained elsewhere[9] and it can be estimated by comparison that monolayer OH coverage should drop to about 60% at 500 °C and reach 100% in the vicinity of 200 °C, where some adsorbed water is also possibly present.

Discussion

It was pointed out previously[2] that ^{13}C chemical shifts of various isomeric butenes adsorbed on pure SiO_2 showed trends parallel to those observed for Na–Y zeolite. Surface treatments of SiO_2 such as Na addition or OH removal caused only small deviations from the shifts on pure SiO_2. It was therefore concluded that the observed shift pattern arises from interaction with some other species, possibly O atoms of the lattice. Further support for this hypothesis is given by the present observations. The chemical shifts of butenes adsorbed on Al_2O_3 show the same trends as those observed on SiO_2; in fact, values of the shifts for the two oxides do not differ appreciably. The characteristic trend is a downfield shift for the =CH– group carbon and an upfield shift for the $-CH_3$ group of adsorbed 1-butene and 2-butenes relative to the liquid. The downfield shift of =CH– in 1-butene appears to be enhanced by OH removal from the alumina surface prior to adsorption. This is in contrast to the case of SiO_2, where dehydroxylation causes the $=CH_2$ line to move downfield with little effect on =CH–.

The above trend in chemical shifts on adsorption with respect to liquids is however not common to all adsorbents. In two separate samples with adsorbed 1- and 2-butenes on charcoal (surface area 512 m^2/g, degassing temperature 400 °C, and coverage 40%) we observed upfield shifts of about 5 ppm for all carbons. Values of these shifts were less accurate (±0.5 ppm) because of extensive line broadening; however, the change in the shift pattern with respect to adsorbed butenes on oxides is quite notable.

TABLE II: Rates of Isomerization

1-Butene			*cis*-2-Butene		
Sample (% coverage)	Degassing temp, °C	k, h^{-1}	Sample (% coverage)	Degassing temp, °C	k, h^{-1}
A (50)	500	0.3	A (50)	400	0.3
A (60)	400	0.2	A (70)	350	0.15
A (50)	340	0.1	A (60)	340	0.15
A (25)	310	0.08	A (60)	325	0.1
A (70)	260	0.01	A (50)	260	0.01
A (50)	200	0.00			
B(95)	420	0.16	B (95)	350	0.35
B (90)	350	0.05	B (90)	250	0.13
B (100)	250	0.00	B (95)	180	0.00

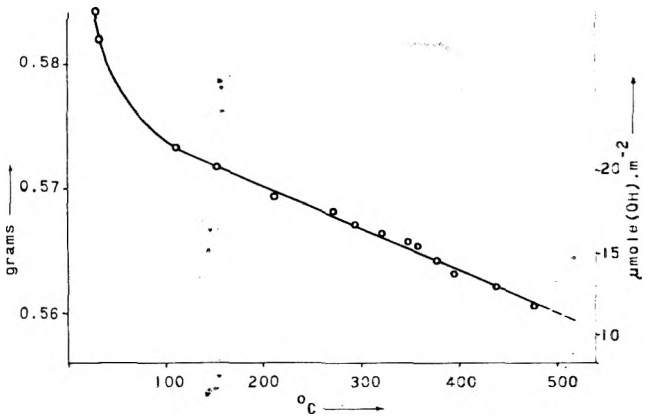

Figure 3. Mass of Al_2O_3-A and estimated OH concentration vs. degassing temperature. Individual readings were at least 24 h apart.

Spectra in Figures 1 and 2 follow isomerization in the adsorbed phase in which the concentration exceeded that in the gas phase by a large factor (more than 50 times). The equilibrium fractional concentrations of 1- and *cis*-2-butene are about 3% and 20%,[4] respectively, and as can be seen from the spectra, the equilibrium concentration of 1-butene was too low to produce a detectable signal. It is assumed that the presence of lines corresponding to possible reaction intermediates was not observed for similar reasons. The strong dependence of the rate of isomerization upon the temperature of surface degassing prior to adsorption is notable. While isomerization reached equilibrium in a few hours after degassing at 500 °C, no observable change was recorded within 1 month after treatment at 200 °C. The rates of 1-butene isomerization increased by more than an order of magnitude by raising the degassing temperature from 250 to 400 °C. The effect on isomerization of *cis*-2-butene was similar when Al_2O_3-A was used; however, the activity of the Al_2O_3-B sample with a smaller surface area appeared to be relatively higher. The large differences in activity can be linked to OH coverage of the surface. It has been suggested earlier[4] that surface hydroxyl protons do not participate in butene isomerization and it appears that 1-butene molecules undergo hydrogen transfer on sites unoccupied by hydroxyls. The difference in selective activity of our two alumina samples, notably between the rates of 1-butene relative to 2-butene isomerization, suggests that other factors resulting from different preparation and pretreatment are involved. Existence of sites with different activity has been demonstrated on the surface of γ-alumina[6] and it is possible that the relative concentration of these sites depends on sample preparation.

The present work, in comparison with that in ref 2, shows that the chemical shift pattern of adsorbed butenes displays only slight differences from one oxide adsorbent to another. This is somewhat in contrast to the results of Michel and coworkers,[10] who found that rather large effects can be produced in zeolite adsorbents by variation of the exchangeable cation. It may be that our present and previous[2] work with pure oxides produced shifts which would be characteristic of the Si–Al–O framework of zeolites, on top of which may be superimposed specific effects due to substituent cations. It should be noted, however, that Na^+ on SiO_2[2] does not produce the large effect found[10] in zeolite and SiO_2–Al_2O_3 catalysts doped with $Na.^+$ This is in agreement with the lack of effect of Na^+ in solution, in contrast to Ag^+.[10] It may be that the observed effects in zeolites and mixed-oxide catalysts arise from some interaction of Na^+ with the effective negative charge of Al in these mixed-oxide systems. Isomerization of 1-butene on alumina was found to proceed on sites unoccupied by OH groups. The surface-selective activity of alumina for isomerization apparently depends on the method of preparation and pretreatment. We have been unable to observe any unstable intermediates in these reactions, and our sensitivity is such that this implies a concentration of less than 5% and/or very broad lines due to immobility.

References and Notes

(1) I. D. Gay, *J. Phys. Chem.*, **78**, 38 (1974).
(2) I. D. Gay and J. F. Kriz, *J. Phys. Chem.*, **79**, 2145 (1975).
(3) I. D. Gay and S. Liang, *J. Catal.*, **44**, 306 (1976).
(4) J. W. Hightower and W. K. Hall, *J. Phys. Chem.*, **71**, 1014 (1967).
(5) G. Gati and H. Knozinger, *Catal. Proc. Int. Congr., 5th, 1972*, 1, 819 (1973).
(6) M. P. Rosynek, W. D. Smith, and J. W. Hightower, *J. Catal.*, **23**, 204 (1971).
(7) T. A. Gilmore and J. J. Rooney, *J. Chem. Soc., Chem. Commun.*, 220 (1975).
(8) J. Landa, *Thesis, Simon Fraser University*, 1976.
(9) B. A. Hendriksen, D. R. Fearce, and R. Rudham, *J. Catal.*, **24**, 82 (1972).
(10) D. Michel, W. Meiler, and H. Pfeiffer, *Catal., Proc. Int. Symp., 1974*, 199 (1975).
(11) J. B. Stothers, "Carbon-13 NMR Spectroscopy", Academic Press, New York, N.Y., 1972.

Electron Spin Resonance Spectra of the Halogen Hexafluorides[1]

A. R. Boate,[2] J. R. Morton, and K. F. Preston*

Division of Chemistry, National Research Council of Canada, Ottawa, Canada K1A 0R9 *(Received June 14, 1976)*

Publication costs assisted by the National Research Council of Canada

The ESR spectra of ClF_6, BrF_6, and IF_6 in solid SF_6 have been reexamined. The observation of formally forbidden or "NMR" transitions for the latter two radicals has permitted the precise determination of their ESR parameters, hitherto known only approximately. Analysis of anisotropic spectra observed at 27 K clearly shows that the halogen hexafluorides possess O_h symmetry. In these radicals the unpaired electron occupies an antibonding a_{1g} orbital consisting primarily of central-atom *ns* and fluorine $2p_\sigma$ atomic orbitals. Temperature dependences noted for the line widths and hyperfine interactions are indicative of the presence of a very low-frequency deformation mode in these molecules. The results of INDO calculations for ClF_6 are in essential agreement with the experimental findings.

Introduction

Since the publication of preliminary data on the ESR spectra of the halogen hexafluorides from this laboratory[3] and elsewhere[4,5] we have given consideration to the proper determination of the spectral parameters of these species. Although a reasonably complete analysis of the spectrum of ClF_6 has been carried out, those of BrF_6 and IF_6 were not properly analyzed because only a single ESR transition was available for each isotopic species. As has been shown elsewhere,[6] this is a situation which arises when a hyperfine interaction (in these cases, that of the central atom) exceeds $\nu/(I + \frac{1}{2})$ MHz, where ν is the microwave frequency of the spectrometer and I is the spin of the nucleus concerned.

An examination of the appropriate energy level diagram has revealed that formally forbidden or "NMR" transitions are available at X-band frequencies for both BrF_6 and IF_6. This report presents data on these transitions, a determination of the hyperfine parameters, and a discussion of the structure of the halogen hexafluoride radicals.

Experimental Section

The raw materials were ClF_3 (Matheson), BrF_5 (Allied Chemical), IF_7 (PCR Inc.), SF_6 (Matheson), and TeF_6 (Ozark-Mahoning). The ClF_3 was converted to ClF_5 by fluorination over CsF;[7] BrF_5 was purified by bubbling fluorine through it immediately prior to use; SF_6 and IF_7 were used as received. Liquid neon was obtained from Canadian Liquid Air Ltd., Montreal.

Samples containing ~5% halogen fluoride in SF_6 were thoroughly degassed and sealed into quartz ESR tubes. Spectra of ClF_6 and BrF_6 were obtained from samples of ClF_5:SF_6 and BrF_5:SF_6, respectively, which had been γ irradiated at 77 K for 1 h in a 9000-Ci ^{60}Co source. The spectrum of IF_6 was obtained by UV photolysis of IF_7:SF_6 with a Schoeffel 1000-W Xe–Hg lamp. Samples with TeF_6 as a matrix were prepared in a similar fashion to those with SF_6.

The ESR spectra were obtained with a Varian E-12 spectrometer fitted with a low-temperature accessory operating in the range 100–200 K; spectra could also be obtained at 27 and 77 K. A cylindrical microwave choke served as a light-pipe for UV photolyses and also enabled us to lower the resonant frequency of the cavity to 8.5 GHz by the introduction of a short length of quartz tubing.

The microwave frequency was measured with a Systron-Donner Type 6057 frequency counter, which also monitored the magnetic field strength via a Varian F-8A proton–deuteron magnetometer.

Results

The appearance of the ESR spectra of these radicals is determined by the large hyperfine interactions of the central atoms. At 110 K in SF_6 isotropic spectra were obtained, consisting of a number of transitions each showing an intensity pattern characteristic of six equivalent spins ½. As the temperature was lowered, each such pattern changed to that of a strong central line accompanied by weaker features attributable to anisotropic interactions with six ^{19}F nuclei equivalent in pairs for all directions of the magnetic field.

Isotropic Spectra. The ^{35}Cl ($I = \frac{3}{2}$) nucleus in ClF_6 gives rise to a hyperfine quartet whose components are centered at 1870 G ($m_I = \frac{3}{2}$), 2447 G ($m_I = \frac{1}{2}$), and 4230 G ($m_I = -\frac{3}{2}$) with a microwave frequency of 9019.2 MHz (Table I). The $m_I = -\frac{1}{2}$ transition falls in the $g = 2$ region where it is masked by the powerful spectra of the sulfur fluorides.[3] At 110 K, the six equivalent ^{19}F nuclei of ClF_6 contribute a seven-line manifold of binomial intensity to each component.[3,4]

In the case of BrF_6, the two bromine isotopes ^{79}Br and ^{81}Br ($I = \frac{3}{2}$) have quite large hyperfine interactions, and their $m_I = -\frac{3}{2}$ transitions overlap near 7150 G.[3,5] The six ^{19}F nuclei are equivalent and have hyperfine interactions of 88.5 G. A determination of the g value and bromine hyperfine interactions cannot be made, however, without measurements on another transition. In such situations it is useful to construct a graph such as that shown in Figure 1, in which the resonance field (H) of various transitions in the $I = \frac{1}{2}$ system is plotted against hyperfine interaction (A).[6] Both A and H are dimensionless being expressed as multiples of $\nu/g\beta$. The $m_I = \pm\frac{3}{2}$ transitions may be plotted with the aid of the equations

$$A = \pm(2 - 2H)/(4 - H) \qquad (1a,b)$$

which are exact except for the neglect of the $\gamma\mathbf{H}\cdot\mathbf{I}$ term in the Hamiltonian. More complex expressions may be derived for the $m_I = \pm\frac{1}{2}$ transitions, but more important here is the transition given by

$$H = (4A - 2)/(2 - A) \qquad (2)$$

This transition is between the $m_I = -\frac{1}{2}$ and $m_I = -\frac{3}{2}$ levels

TABLE I: Spectral Data and ESR Parameters for ClF_6, BrF_6, and IF_6 in SF_6[a]

Radical	Temp, K	ν, MHz	Magnetic field, G			NMR	g	a_M,[b] G	a_F, G
			$m_I = I$	$m_I = I-1$	$m_I = -I$				
$^{35}ClF_6$	110	9019.2[b]	1870.4	2446.8	4229.8		2.0181	775	89.6
$^{35}ClF_6$	27	9093.3	1885.4	2468.5	4271.8		2.0154	783.7	
$^{37}ClF_6$	27	9093.4	2133.3	2650.1	4114.0		2.0152	653.4	
$^{79}BrF_6$	110	9210.9			7077.0	13 986[c]	2.0158	4160	88.5
$^{79}BrF_6$	27	9188.1		Site A	7076.7	14 220[c]	2.0147	4175	
$^{79}BrF_6$	27	9188.1		Site B	7085.4	14 410[c]	2.0148	4191	
$^{79}BrF_6$[d]	27	9191.0			7068.5	14 016[c]	2.0148	4158	
$^{81}BrF_6$	110	9210.9			7254.0	18 330[c]	2.0158	4485	88.5
$^{81}BrF_6$	27	9188.1		Site A	7253.2	18 685[c]	2.0147	4501	
$^{81}BrF_6$	27	9188.1		Site B	7262.4	18 967[c]	2.0148	4519	
$^{81}BrF_6$[d]	27	9191.0			7244.9	18 388[c]	2.0149	4483	
$^{127}IF_6$	110	8798.5			10879	18 569[c,d]	2.0098	6140	150.2
$^{127}IF_6$	27	8807.5		Site A	10944	18 251[e]	2.0105	6237	
						18 379[f]	2.0104	6236	
$^{127}IF_6$	27	8807.5		Site B	10956	18 204[e]	2.0105	6256	
						18 331[f]	2.0104	6255	
$^{127}IF_6$[d]	27	8820.6			10940	18 357[e]	2.0108	6215	
						18 494[f]	2.0106	6214	

[a] Except as otherwise indicated. [b] Precision ±1 in the last significant figure. [c] NMR 1. [d] In TeF_6. [e] NMR 2′. [f] NMR 2″.

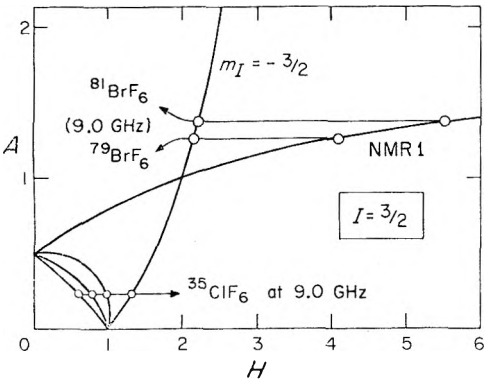

Figure 1. Position of transitions (H) as a function of hyperfine interaction (A), for spin $I = 3/2$. Both H and A are in multiples of $\nu/g\beta$.

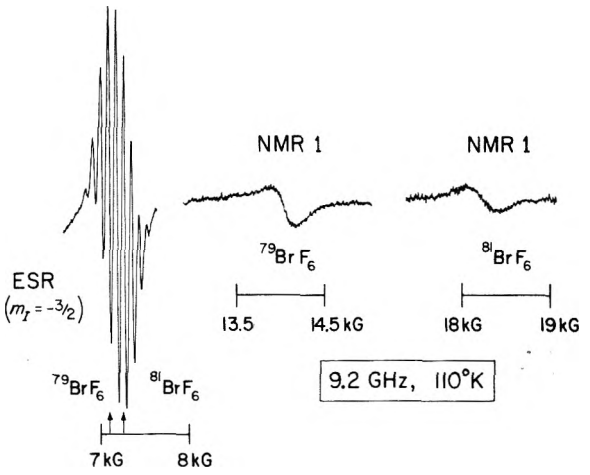

Figure 2. ESR and NMR 1 transitions of $^{79}BrF_6$ and $^{81}BrF_6$ in SF_6 at 9.2 GHz, obtained with identical spectrometer gain.

of $m_s = -1/2$ and (since it involves no change in m_s) may reasonably be described as an "NMR" transition. At 9018 MHz, the $m_I = -3/2$ transition of $^{79}BrF_6$ was centered at 6975 G.[3] Assuming $g = 2.00$, this corresponds to $H = 2.165$ and, from Figure 1 or eq 1b, $A = 1.27$. Similarly it may be calculated from the same transition of $^{81}BrF_6$ that its A is 1.37. It may be predicted from Figure 1 or eq 2 that "NMR 1" transitions for $^{79}BrF_6$ and $^{81}BrF_6$ should be detectable near $H = 4.22$ and 5.52, respectively. Assuming $g \simeq 2.00$, these values correspond to 13.6 and 17.8 kG, respectively. A search in these regions revealed these two transitions (Figure 2), both of which were, however, quite broad ($\Delta H \simeq 200$ G) and lacked ^{19}F hyperfine structure. The experimental data are reported in Table I.

The ^{127}I hyperfine interaction in IF_6 is even larger than the bromine interactions in BrF_6 and, moreover, the situation is exacerbated by the higher spin (5/2) of ^{127}I. At 9020 MHz the $m_I = -5/2$ transition, consisting of a 148-G septet of binomial intensity distribution, was centered at 11 053 G.[3] Assuming a g value of 2.00, this magnetic field corresponds to $H = 3.43$ (in $\nu/g\beta$ units). Use of the equation

$$A = (2H - 2)/(6 - H)$$

yields an approximate value of 1.89 for A, and examination of Figure 3 shows that the NMR 1 transition lies at a completely inaccessible magnetic field. However, with the aid of the Breit–Rabi equations,[9] the other five "NMR" transitions of the $I = 5/2$ system were plotted, and it was found that one of them (NMR 2) should lie at an accessible magnetic field (Figure 3), provided the microwave frequency was below 8.8 GHz. A broad ($\Delta H \simeq 500$ G) transition, also lacking ^{19}F hyperfine structure, was detected at 18 569 G using a microwave frequency of 8798 MHz (Table I).

Anisotropic Spectra. At 27 K the spectra were characterized by sharp central lines accompanied to higher and lower fields by weak features typical of a polycrystalline spectrum (Figure 4). In the cases of BrF_6 and IF_6 in SF_6, the spectra at 27 K were interpreted in terms of two sites for these species.[10] In Figure 5a are shown the central portions of the $m_I = -5/2$ and NMR 2 transitions of IF_6 in SF_6. In this case one site (B) was characterized by a narrower line width and was populated to about half the extent of the other site. When TeF_6 was used as the matrix, only one site was observed for IF_6, as shown in Figure 5b. BrF_6 in TeF_6 also showed only one site.

Discussion

Determination of Spectral Parameters. (a) Isotropic Spectra. The spectral parameters of ClF_6, obtained by di-

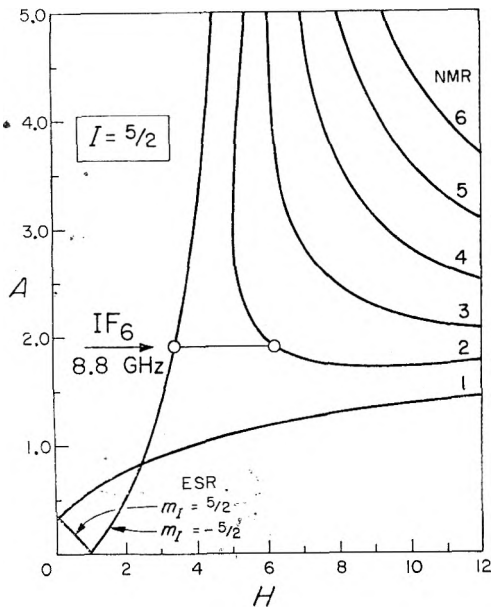

Figure 3. Position of transitions (H) as a function of hyperfine interaction (A), for spin $I = 5/2$. Both H and A are in multiples of $\nu/g\beta$.

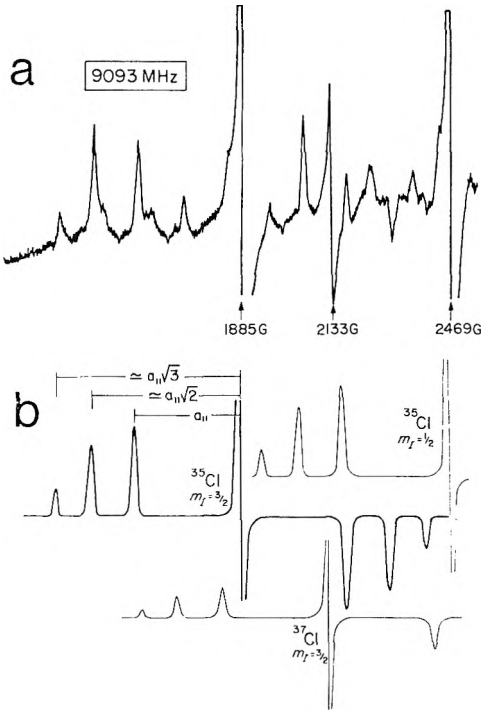

Figure 4. (a) Part of the ESR spectrum of ClF_6 at 27 K, showing the $m_I = 3/2$ transitions of ^{35}Cl and ^{37}Cl. (b) A simulation of same using $a_{\parallel}(F) = 292$ G and $a_{\perp}(F) = -12$ G.

agonalization[11] of the spin matrix, are given in Table I. Owing to the complexity of the ^{19}F hyperfine structure the ^{37}Cl hyperfine interaction could not be determined at 110 K.

For BrF_6 the spectral parameters were obtained from the $m_I = -3/2$ ESR transition and the NMR 1 transition for each isotope. These transitions were more readily handled by iterative solution of the Breit–Rabi equations.[9] At 110 K the ratio a_{81}/a_{79} for BrF_6 was found to be 1.078, in exact agreement with expectation.

In the case of IF_6 two complications arise, one concerning

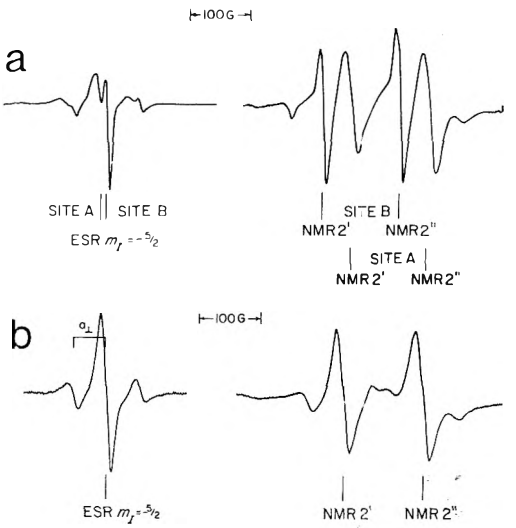

Figure 5. Central portions of the ESR and NMR transitions observed for IF_6 at 27 K: a, in SF_6; b, in TeF_6. Field positions are given in Table I.

the ^{127}I hyperfine interaction and the other involving the ^{19}F hyperfine interactions. The ^{127}I hyperfine interaction a_{127} was determined from the positions (Table I) of the $m_I = -5/2$ and NMR 2 transitions (Figure 3) with the aid of the Breit–Rabi equations. When the $\gamma\mathbf{H}\cdot\mathbf{I}$ term is included in these equations,[12] it is seen that NMR 2 (unlike NMR 1 of BrF_6) is an unresolved doublet, its components arising from the different ($\pm 1/2$) m_s states. Either of the transitions NMR 2′ ($m_s = -1/2$) or NMR 2″ ($m_s = +1/2$) may be combined with the $m_I = 5/2$ transition to yield values of a_{127} and g. Figure 6 was obtained by varying the position of NMR 2′ and 2″ near 18 550 G and plotting the values of a_{127} and g so obtained against the magnetic field. Since we know the unresolved transition to be centered at 18 569 G, Figure 6 reveals that its two components are 136 G apart, $a_{127} = 6140$ G, and $g = 2.0098$.

The second complication is a consequence of the large value of a_{127}, which results in an incomplete Paschen-Back effect, even at 11 kG. The ^{19}F hyperfine interaction obtained by exact diagonalization (Table II) exceeds the observed splittings[3] by ~2 G.

(*b*) *Anisotropic Spectra.* At 27 K the halogen hexafluoride radicals are no longer tumbling and anisotropic spectra are obtained. We attribute the strong central lines to the $m_{I(F)} = 0$ components of each transition. Their positions are determined by hyperfine interaction with the central nucleus alone, an interaction which is evidently isotropic. There was, furthermore, no indication (within the limits imposed by the line width) of anisotropy in the g factor of these species. The isotropic g values and central-atom hyperfine interactions may thus be determined by the methods used above.

For ClF_6 at 27 K the two isotopic species are readily distinguished (Figure 4) and the parameters are given in Table I. The ratio of the two chlorine hyperfine interactions a_{35}/a_{37} is 1.199, in reasonable agreement with the expected value of 1.201.

For BrF_6 there are two sites in SF_6 and the parameters for these as well as for BrF_6 in TeF_6 are reported in Table I.

The spectra of IF_6 at 27 K clearly show the separation predicted above of the transitions NMR 2′ and NMR 2″. In Figure 5 the central lines of each of these transitions are clearly resolved. In Table I the isotropic g values and central-atom hyperfine interactions are reported for IF_6 in SF_6 (both sites) as well as in TeF_6.

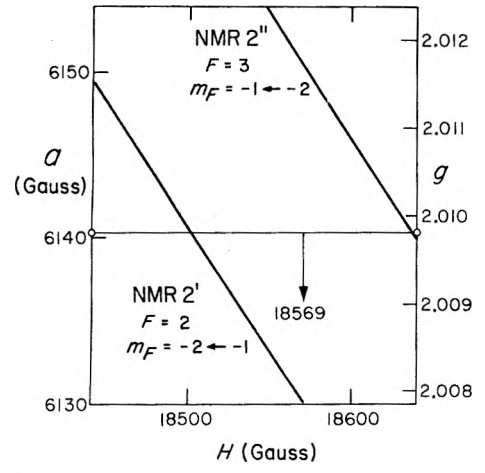

Figure 6. ^{127}I hyperfine interaction (a) and g factor of IF_6 as functions of the positions (H) of NMR 2′ and NMR 2″, obtained using the $m_I = -5/2$ transition at 10 879 G (ν = 8798.5 MHz).

TABLE II: ^{19}F Hyperfine Tensors (Gauss)

Radical	$a_\parallel$	$a_\perp$	a_{iso}	B^a	p_σ spin density^b
ClF_6	292 (10)^c	−12 (10^d)	90	102	0.19
BrF_6	296 (10)	−18 (2)	87^e	105	0.19
IF_6	342 (10)	52 (5)	149^e	97	0.18

^{a} $B = a_{iso} - a_\perp$. ^{b} Estimated using B_0 = 540 G for ^{19}F. ^{c} The numbers in parentheses are estimated errors. ^{d} Perpendicular features not detected; $a_\perp$ estimated from a_{iso} at 110 K. ^{e} $a_{iso} = (a_\parallel + 2a_\perp)/3$.

The anisotropic ^{19}F hyperfine structure accompanying each transition of ClF_6 at 27 K was remarkably simple (Figure 4a). Three absorptions were detected on either side of each central peak whose separations from the latter were approximately in the ratio $1:2^{1/2}:3^{1/2}$. This observation is most readily interpreted in terms of interaction of the unpaired electron with an octahedral arrangement of six ^{19}F nuclei, each of which has a tensor component along the bond ($a_\parallel$) which is much greater than the components perpendicular to the bond ($a_\perp$). Pronounced features in the anisotropic spectrum would be expected when the magnetic field lies along a bond, along a bisector of two bonds, or along a C_3 axis. By neglecting nuclear Zeeman and second and higher order effects, these features are displaced from the central $m_{I(F)} = 0$ line by $a_\parallel$, $(2a_\parallel^2 + 2a_\perp^2)^{1/2}$, and $(3a_\parallel^2 + 6a_\perp^2)^{1/2}$, respectively. Thus if $a_\perp \ll a_\parallel$, the observed anisotropic hyperfine pattern of ClF_6 is accounted for. In Figure 4b are shown the simulated spectra[13] generated by six equivalent $I = 1/2$ nuclei in an octahedral arrangement, each having $a_\parallel$ = 292 G. The value of $a_\perp$ used in the simulation was obtained from the relation $a_{iso} = (a_\parallel + 2a_\perp)/3$.

For BrF_6 and IF_6 additional transitions observed in their ^{19}F anisotropic hyperfine patterns were associated with resolved contributions from the perpendicular components of the hyperfine tensors. The perpendicular features adjacent to the central line of each transition (Figure 5) were very clearly defined and were used to obtain values of $a_\perp$ for these radicals. The components of the ^{19}F hyperfine tensors for the halogen hexafluorides are given in Table II.

The Semioccupied Orbital. As far as can be inferred from their ESR spectra, the halogen hexafluorides are octahedral radicals (O_h symmetry). No evidence has been found either at 110 K or at 27 K to indicate a lower symmetry. On the contrary, the observation at 27 K of sharp, intense lines at the center of each transition confirms the high symmetry of the radicals. We attribute these to the $m_{I(F)} = 0$ components of the transitions, whose resonant fields are orientation independent. This implies that the frozen-in radical has fluorine nuclei which are equivalent in pairs (giving an $I(F) = 0$ component) for every direction of the magnetic field. In other words, the F(2p) contributions to the semioccupied orbital must point toward each other and toward the central atom. This conclusion, together with the fact that the transitions observed at 27 K show no evidence of central-atom or g-factor anisotropy, indicates that the halogen hexafluoride radicals have octahedral symmetry. The good agreement between the measured and simulated spectra of ClF_6 (Figure 4) supports this conclusion.

The orbital of the unpaired electron must have a totally symmetric representation (A_{1g} in O_h) in order to accommodate the exceedingly large central-atom hyperfine interactions. INDO calculations[14] which we have carried out for ClF_6 and the isoelectronic radical SF_6^- in O_h symmetry[8] (Table III) show that the semioccupied orbital is an antibonding combination of central atom (M) ns and fluorine $2p_\sigma$ atomic orbitals (the latter point toward the central atom). While F(2s) atomic orbitals may in principle contribute directly to the a_{1g} molecular orbital, the observed (and predicted) small positive spin density in F(2s) probably arises largely from spin-polarization effects. Spin polarization of F–M bonds by the F($2p_\sigma$) orbitals would be expected to generate a small positive spin density in F(2s) and a small negative spin density in central-atom atomic orbitals.[15]

The results of INDO calculations summarized in Table III imply that in ClF_6, as compared to SF_6^-, there is (a) less unpaired spin in the 3s atomic orbital of the central atom, (b) more unpaired spin in the F($2p_\sigma$) atomic orbitals, and (c) less unpaired spin in F(2s) atomic orbitals.

In view of results (a) and (b), which may be predicted from electronegativity considerations, the last result is somewhat surprising. Indeed, we have noted that the isotropic ^{19}F hyperfine interactions in anion radicals are invariably greater than those of the isoelectronic, neutral radicals. Many examples of this effect can be cited: OPF_3^- (69, 340 G),[16] OSF_3 (51, 252 G);[17] SiF_4^- (81, 310 G),[18] PF_4 (59, 282 G);[19] PF_5^- (207 G),[20] SF_5 (143 G);[21] AsF_5^- (187 G),[20] SeF_5 (118 G);[8] SF_6^- (195 G),[8] ClF_6 (90 G); SeF_6^- (173 G),[8] BrF_6 (89 G); TeF_5^- (212 G),[8] IF_6 (150 G).

We are inclined to regard this phenomenon as Coulombic. These pairs of radicals are isoelectronic, there being lower central nuclear charge in the anionic species. As compared to its neutral analogue, the negative ion will have weaker, and hence more polarizable, bonds. This contention supports our hypothesis that in all of these polyatomic fluorine-containing radicals (neutral and charged) the isotropic ^{19}F hyperfine interactions arise solely via polarization and not via direct F(2s) contributions to the semioccupied molecular orbital.

In order to convert the observed hyperfine interactions into unpaired spin densities it is necessary to use the factors $A_0 = (8\pi/3)\gamma_e\gamma_M|\psi_{ns}|^2(0)$ and $B_0 = \frac{2}{5}\gamma_e\gamma_M\langle r^{-3}\rangle$ as measures of unit central-atom ns and unit fluorine 2p spin densities, respectively. Unfortunately, these conversion factors are not known with any certainty. In a preliminary note[3] we estimated central-atom ns spin densities of 0.46, 0.46, and 0.54 for ClF_6, BrF_6, and IF_6, respectively, using A_0 values derived from Froese's wave function[22] and corrected according to the empirical method of Mackey and Wood.[23] Taking B_0 = 540 G for

TABLE III: Results of INDO I Calculations for ClF_6 and SF_6^- in O_h symmetry

Radical	Bond length, Å	Unpaired spin densities M(3s)	M($3p_{x,y,z}$)	F(2s)	F($2p_\sigma$)
$^{33}SF_6^-$	1.73	0.326	−0.077	0.0074	0.150
$^{35}ClF_6$	1.63	0.244	−0.092	0.0037	0.177

fluorine,[22] we deduce individual F($2p_\sigma$) spin densities of 0.19, 0.19, and 0.18 for ClF_6, BrF_6, and IF_6, respectively, from their anisotropic ^{19}F hyperfine tensors (Table II). With total positive spin densities thus considerably in excess of unity for all three species we are forced to conclude either that there is considerable negative spin density in certain atomic orbitals or that the conversion factors A_0 and/or B_0 are in error. The excellent agreement of the F($2p_\sigma$) spin densities derived from the anisotropic ^{19}F hyperfine tensor of ClF_6 with that obtained from the INDO calculations suggests that B_0, at least, is not seriously in error. The INDO calculations confirm the presence of considerable negative spin density, mainly in the central atom $np_{x,y,z}$ orbitals (Table III).

The g Factors of the Hexafluorides. In O_h symmetry the spin–orbit operator will mix the A_{1g} ground state with a T_{1g} state. Promotion of an electron with spin opposed to that of the unpaired electron from a nearby filled t_{1g} orbital into the semioccupied a_{1g} orbital will result in a positive g shift. The triply degenerate t_{1g} orbital is composed of F($2p_\pi$) atomic orbitals only, no contribution (either s or p) from the central atom being permitted. The g shift, which is determined by the product of atomic orbital coefficients for the a_{1g} and the t_{1g} molecular orbitals, summed over all atoms, is therefore entirely determined by the fluorine contributions. The central atom, whose contribution to a_{1g} is entirely ns (no effect on g), need not be included in the summation. Shown in I are the a_{1g} semioccupied orbital and one of the three degenerate t_{1g} orbitals contributing to the g shift.

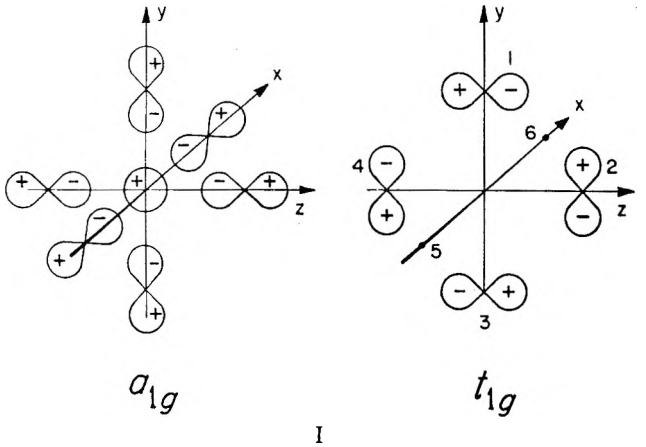

I

Since the three principal axes are equivalent

$$\Delta g_{iso} = \Delta g_{xx} = \frac{2\lambda}{\Delta E}\left[\sum_{i=1}^{6}(a_i t_i)\right]^2$$

where λ is the spin–orbit coupling constant for fluorine (~270 cm^{-1}), the a_i are the coefficients of the F($2p_\sigma$) atomic orbitals in the LCAO description of the semioccupied orbital (a_{1g}), the t_i are the coefficients for the F($2p_\pi$) contributions to the t_{1g} molecular orbital, and ΔE is the energy separation of the ground and excited states.[24] The absence of any central atom contribution to t_{1g} means that $t_i = 1/2$ (i = 1–4) or 0 (i = 5, 6). Hence

$$\Delta g_{iso} = \frac{2\lambda}{\Delta E}[2a_i]^2 = \frac{8\lambda}{\Delta E}a_i^2$$

since the a_i are equal. Using the estimate of 0.19 for the F($2p_\sigma$) spin densities (a_i^2) in ClF_6 together with $\Delta g_{iso}(ClF_6)$ = 0.016 and λ = 270 cm^{-1}, the excitation energy ΔE is calculated to be ~25 650 cm^{-1}, or approximately 3 eV.

The decrease in Δg_{iso} along the series ClF_6, BrF_6, IF_6 is due to a decrease in the factor $a_i^2/\Delta E$. Since the anisotropic ^{19}F hyperfine interactions (Table II) indicate no significant decrease in a_i^2, we presume the effect is primarily due to an increase in ΔE.

Temperature Dependence of Hyperfine Interactions and Line Widths. It may be observed from Table I that the central atom hyperfine interactions of the halogen hexafluorides are lower at 110 K than at 27 K. Further measurements at 77 K and in the isotropic region (up to 120 K for ClF_6 and to 140 K for BrF_6 and IF_6) confirmed this observation. It was found that in all three instances the central-atom hyperfine interaction decreased monotonically with increasing temperature. In BrF_6, for example, the ^{79}Br hyperfine interaction decreased by 10 G between 110 and 133 K.

The decrease in the central-atom hyperfine interaction with temperature is accompanied by an increase in the line widths. For IF_6 in SF_6, for example, the central components of both the ESR and NMR lines have line widths at 27 K of 10 G for the sharp site and 20 G for the broad site. At 110 K the line width of the ESR transition increased to ~100 G and that of the NMR transition to the point where the ^{19}F hyperfine structure was no longer resolved. This broadening trend continued up to 140 K and was also observed for BrF_6.

A possible explanation for the observed temperature dependence of both the hyperfine interactions and the line widths lies in the "pseudo" or "second-order" Jahn–Teller effect.[25] This has been invoked[26,27] for the analogous molecule XeF_6 where the proximity of a T_{1u} excited state to the A_{1g} ground state results in a very "soft" t_{1u} deformation mode. It has been suggested[4] that in the hexafluorides this mixing of states could lead to enhanced spin–lattice relaxation. However, while this might explain the line widths of ClF_6 and of the ESR transitions of BrF_6 and IF_6, it fails to account for the much larger line widths of the NMR transitions of the latter radicals.

We feel that modulation of the central-atom hyperfine interaction by the very low frequency deformation may well account for both the large line widths of the latter transitions and the observed temperature dependence of the line widths and hyperfine interactions. The contribution of such a mechanism to line broadening should be proportional to dH/dA, that is, to the inverse slope of the A vs. H curves (Figures 1, 3). For both BrF_6 and IF_6, dH/dA is considerably larger for the NMR transition than for the ESR transition so that one would expect a greater line width for the former (Figure 2). With increasing temperature and population of excited levels of the t_{1u} vibration, the average amplitude of the deformation will increase, resulting in a greater line width and a larger departure of the hyperfine interactions from their values at absolute zero. The observation that the central-atom hyperfine interactions decrease with increasing temperature is not surprising since the excited $^2T_{1u}$ state admixed into the ground $^2A_{1g}$ state by the t_{1u} deformation will unquestionably have very small central-atom s character.

Acknowledgments. We thank Dr. J. C. Tait for simulation of ESR powder spectra and Dr. S. K. Garg for communication of his results prior to publication.[10]

References and Notes

(1) NRCC No. 15681.
(2) NRCC Research Associate, 1975–1976.
(3) A. R. Boate, J. R. Morton, and K. F. Preston, *Inorg. Chem.*, **14**, 3127 (1975).
(4) K. Nishikida, F. Williams, G. Mamantov, and N. Smyrl, *J. Am. Chem. Soc.*, **97**, 3526 (1975).
(5) K. Nishikida, F. Williams, G. Mamantov, and N. Smyrl, *J. Chem. Phys.*, **63**, 1693 (1975).
(6) A. R. Boate, J. R. Morton, and K. F. Preston, *J. Magn. Reson.*, **24**, 259 (1976).
(7) D. Pilipovich, W. Maya, E. A. Lawton, H. F. Bauer, D. F. Sheehan, N. N. Ogimachi, R. D. Wilson, F. C. Gunderloy, and V. E. Bedwell, *Inorg. Chem.*, **6**, 1918 (1967).
(8) J. R. Morton, K. F. Preston, and J. C. Tait, *J. Chem. Phys.*, **62**, 2029 (1975).
(9) G. Breit and I. I. Rabi, *Phys. Rev.*, **38**, 2082 (1931).
(10) It has recently been shown by ^{19}F NMR experiments between 4 and 94 K that the low-temperature phase of SF_6 possesses two inequivalent sites in a noncubic lattice, populated in the ratio ~3:1 (S. K. Garg, private communication).
(11) Exact diagonalization was achieved using Program 311, Quantum Chemistry Program Exchange, Indiana University, Bloomington, Ind., by J. R. Morton and K. F. Preston.
(12) J. E. Nafe and E. B. Nelson, *Phys. Rev.*, **73**, 718 (1948).
(13) R. Lefebvre and J. Maruani, *J. Chem. Phys.*, **42**, 1480 (1965).
(14) The program used is based on Program 141, Quantum Chemistry Program Exchange, Indiana University, Bloomington, Ind., by P. A. Dobosh. The INDO I parameterization was used.[6]
(15) J. E. Wertz and J. R. Bolton, "Electron Spin Resonance", McGraw-Hill, New York, N.Y., 1972, Chapter 6.
(16) A. R. Boate, J. R. Morton, and K. F. Preston, unpublished data.
(17) J. R. Morton and K. F. Prestor, *J. Chem. Phys.*, **58**, 2657 (1973).
(18) J. R. Morton and K. F. Prestor, *Mol. Phys.*, **30**, 1213 (1975).
(19) R. W. Fessenden and R. H. Schuler, *J. Chem. Phys.*, **45**, 1845 (1966).
(20) A. R. Boate, A. J. Colussi, J. R. Morton, and K. F. Preston, *Chem. Phys. Lett.*, **37**, 135 (1976).
(21) J. R. Morton and K. F. Prestor, *Chem. Phys. Lett.*, **18**, 98 (1973).
(22) C. Froese, *J. Chem. Phys.*, **45**, 1417 (1966).
(23) J. H. Mackey and D. E. Wood, *J. Chem. Phys.*, **52**, 4914 (1970).
(24) P. W. Atkins and M. C. R. Symons, "The Structure of Inorganic Radicals", Elsevier, Amsterdam, 1967, Appendix 3.
(25) R. F. W. Bader, *Mol. Phys.*, **3**, 137 (1960).
(26) L. S. Bartell and R. M. Gavin, *J. Chem. Phys.*, **48**, 2466 (1968).
(27) S. Y. Wang and L. L. Lohr, *J. Chem. Phys.*, **60**, 3901 (1974).

Electron Spin Resonance Investigations of the Triplet Spectra of Rhodamine Dyes and Their Aggregates

Hartmut Schmidt

Institute of Physical Biochemistry of the J. W. Goethe University, D-6000 Frankfurt am Main, West Germany *(Received July 19, 1976)*

The dependence of the ESR spectra of some rhodamine dyes (rhodamine 6G, rhodamine B, sulforhodamine B, rhodamine 110, and acridine red) in their lowest excited triplet states upon the concentration has been investigated in methanol–water solutions at 90 K. The different spectra have been assigned to monomers and dimers (and/or association polymers). Using triplet exciton theory from the spectra it has to be concluded that the molecules within the aggregates are oriented in a translationally nonequivalent manner (twisted sandwich structures). The twisting angles have been calculated.

Introduction

In tunable dye lasers rhodamine compounds are very often used as active media. Consequently during recent years much attention has been focused on their spectroscopic properties. As intersystem crossing to the triplet state of the dyes causes a depopulation of the corresponding excited singlet levels, detrimental to laser action, some investigations concerning these states were carried out by ESR spectroscopy.[1–5] From the ESR spectra the corresponding zero-field splitting (zfs) parameters X, Y, Z[6] were calculated.

However, the authors did not take into consideration that the zfs can depend strongly on the state of aggregation of the compounds if the triplet energy is delocalized within the dye aggregates (triplet excitons).[7–10] We have observed such effects for various acridine[10,11] and cyanine dyes.[12]

On the other hand, because of theoretical reasons[10] the zero-field splitting parameters of the aggregate triplets differ from those of the monomers only if the molecules within the aggregates are oriented in a nontranslationally equivalent manner. Thus from the concentration dependence of the ESR spectra conclusions can be drawn concerning the structure of the dye aggregates. This will be discussed in the present publication.

Theoretical Section

When the triplet energy is delocalized within the dye aggregate (triplet exciton) the spin-Hamiltonian H^* of the dimers (describing the interaction between the magnetic field and the two triplet electrons as well as their dipole–dipole interaction[6,10]) is the average of the Hamiltonians of the identical dye molecules A and B

$$H^* = \tfrac{1}{2}(H_A + H_B) \tag{1}$$

Due to the dimer model of rhodamine B suggested from absorption spectroscopy by Gál, Kelly, and Kurucsev[13] (twisted sandwich structure), it is reasonable to consider the mathematically simplest case that the magnetical principal axes x in both molecules within an aggregate are oriented parallel to each other ($X_A = X_B = X^*$). Thus the angle φ between the

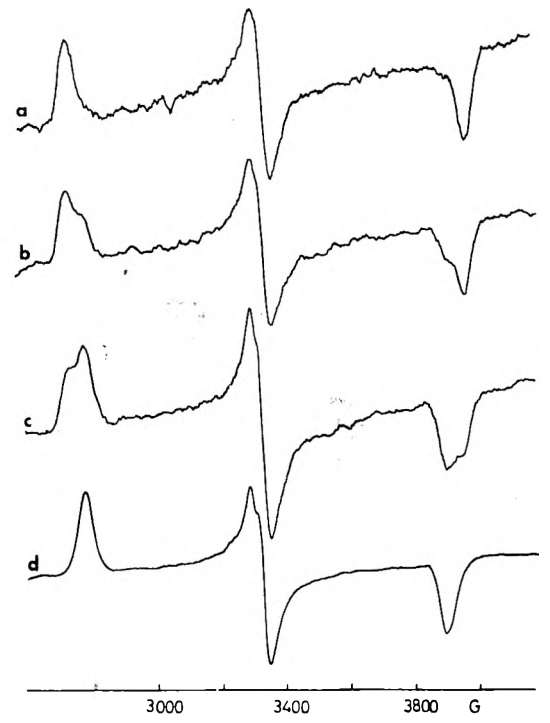

Figure 1. ESR triplet spectra ($\Delta m = 1$) of rhodamine 6G in methanol/water = 8/2 (w/w); temperature 90 K: (a) 5×10^{-5} M, (b) 1×10^{-4} M, (c) 2×10^{-4} M, (d) 5×10^{-4} M.

other axes of neighboring molecules ($\varphi(y_A,y_B) = \varphi(z_A,z_B)$) is calculated[10] by

$$\cos(2\varphi) = 2\frac{(Z^* - Y^*)^2}{(Z - Y)^2} - 1 \qquad (2)$$

X, Y, Z are the zero-field splitting energies of the dye monomers and X^*, Y^*, Z^* are the corresponding parameters of the dimers.

Equation 2 can also be used for higher aggregates with an even number of molecules when there are not more than two differently oriented molecules within the aggregate unit cell. For aggregates with an odd number of molecules the results differ slightly from the dimer case.[10]

Results and Discussion

For rhodamine 6G two different ESR triplet spectra have been observed depending on the dye concentration (Figure 1). (The zero-field splitting calculated from the spectra (Table I) agrees reasonably with that measured by other authors[1-3] under comparable conditions.) The spectra at low and high concentrations can be ascribed to monomers and dimers (and/or association polymers), respectively. With the parameters given in Table I an angle of $\varphi = 17°$ or $(180° - \varphi) = 163°$ is calculated from eq 2. Magnetophotoselection experiments[6] show that the axis parallel for all molecules within the aggregates is the short axis of the xanthene ring system or (more probably from energy reasons) the axis perpendicular to the xanthene plane. (It was assumed that the optical transition moment is oriented parallel to the long axis of the xanthene ring.[13]) The results are consistent with the dimer model of Gál et al.[13]

Similar results have been obtained for most of the other rhodamine dyes as shown in Table I. For these dyes the corresponding zfs parameters (again with the exception of X) depend also on the dye concentration. However, in contrast to rhodamine 6G described above, only one spectrum could be resolved independent of dye concentration. Obviously in these cases the monomer and aggregate spectra do not differ very much. Consequently only small changes in the stationary resonance fields are observed instead of two discrete spectra.

TABLE I: Zero-Field Splitting Energies (cm^{-1} hc)[a]

Compd	Concn[b]	$\mp\lvert Z\rvert$	$\pm\lvert Y\rvert$	$\pm\lvert X\rvert$	φ, deg	τ
Rhodamine 6G	2×10^{-5}	(0.0391)	0.0380	0.0011		
	1×10^{-4}	(0.0391)	0.0380	0.0011		
		(0.0374)	0.0363	0.0011	17	1.4
	1×10^{-3}	(0.0366)	0.0352	0.0014	21	
	1×10^{-1}	(0.0337)	0.0328	0.0009	30	
Rhodamine B	2×10^{-5}	(0.0392)	0.0376	0.0016		
	1×10^{-4}	(0.0394)	0.0375	0.0019		1.3
	1×10^{-2}	(0.0376)	0.0360	0.0016	16	
	1×10^{-1}	(0.0372)	0.0356	0.0016	18	
Sulforhodamine B	1×10^{-4}	0.0379	0.0365	0.0017		0.9
	1×10^{-3}	0.0373	0.0365	0.0017		
Rhodamine 110	1×10^{-4}	0.0429	0.0401	0.0020		1.2
	1×10^{-3}	0.0426	0.0400	0.0026		
	1×10^{-2}	0.0417	0.0392	0.0021	13	
Acridine red	3×10^{-5}	(0.0378)	0.0371	0.0007		
	1×10^{-4}	(0.0380)	0.0367	0.0013		1.5
	1×10^{-3}	(0.0364)	0.0351	0.0013	17	
	1×10^{-2}	(0.0361)	0.0347	0.0014	19	

[a] Experimental error: 0.0005 cm^{-1} hc, in parentheses; calculated from $X + Y + Z = 0$; decay times τ (s); twisting angle φ (equivalent to $180° - \varphi$) of the rhodamine dyes; concentration, M.

In principle for all these dyes, the results of the ESR measurements are consistent with the dimer model of twisted sandwich structures described above. The twisting angle varies for the different dyes and depends slightly on the concentration. However, in contrast to the assumption of Gál et al.[13] it seems more probable from thermodynamic data that the carboxyphenyl substituents of the two molecules within the dimer are in contact with each other. Only then can it be explained that dimerization of rhodamine dyes is associated with a strong increase of dimerization entropy $\Delta S°$ [14] ($\Delta H° \gtrsim 0$) opposite to other dyes without 9-phenyl substituents. E.g., for acridine[15,16] and thiazine dyes[7,18] the standard dimerization enthalpy is strongly negative while the entropy change $\Delta S°$ even gives a small positive contribution to $\Delta G°$. The simplest explanation for this effect is the stronger solvophobic interaction in the case of rhodamine dyes caused by the carboxyphenyl groups touching each other in the dimer.

Experimental Section

The ESR spectra were obtained using a Varian E 12 X-band spectrometer with standard equipment. The microwave frequency was measured with a Systron + Donner counter 1037 and transfer oscillator 1292. The static magnetic field was determined by means of a proton resonance gauss meter. Samples were illuminated by a high-pressure xenon lamp (Osram XBO 1600 W) at about 90 K in a glassy methanol (Merck: p.A.)/water (triple distilled) mixture (80% w/w). All

measurements were carried out in the presence of oxygen. Sharp cut filters (Schott & Gen.) were used to cut off short-wavelength light. To prevent heating of the samples a water cell (15 cm pathlength) and two IR reflecting filters (Schott & Gen., type Tempax 112 and 116) were employed.

Most of the dyes (Eastman Kodak, best commercial grades) were used without further purification. Rhodamine 6G was recrystallized from methanol. The ESR spectra of the purified and unpurified product did not differ.

Acknowledgments. This work was supported by the Deutsche Forschungsgemeinschaft. The author wishes to thank Professor J. Stauff for the continuous encouragement of his work. The technical assistance of Mr. D. Bhandarkar is gratefully acknowledged.

References and Notes

(1) I. H. Leaver, *Photochem. Photobiol.*, **19**, 309 (1974).
(2) M. Yamashita and H. Kashiwagi, *J. Chem. Phys.*, **59**, 2156 (1973).
(3) M. Yamashita, H. Ikeda, and H. Kashiwagi, *J. Chem. Phys.*, **63**, 1127 (1975).
(4) M. Yamashita and H. Kashiwagi, *J. Phys. Chem.*, **78**, 2006 (1974).
(5) F. R. Antonucci and L. G. Tolley, *J. Phys. Chem.*, **77**, 2712 (1973).
(6) S. P. McGlynn, T. Azumi, and M. Kinoshita, "Molecular Spectroscopy of the Triplet State", Prentice-Hall, Englewood Cliffs, N.J., 1969.
(7) H. Sternlicht and H. M. McConnel, *J. Chem. Phys.*, **35**, 1793 (1961).
(8) M. Schwoerer and H. C. Wolf, *Mol. Cryst.*, **3**, 177 (1967).
(9) D. Haarer and H. C. Wolf, *Mol. Cryst. Liq. Cryst.*, **10**, 359 (1970).
(10) H. Schmidt and R. Zellhofer, *Z. Phys. Chem. (Frankfurt am Main)*, **91**, 204 (1974).
(11) H. Schmidt, *Z. Phys. Chem. (Frankfurt am Main)*, **97**, 189 (1975).
(12) H. Rödder, Thesis, Frankfurt, 1976.
(13) M. E. Gál, G. R. Kelly, and T. Kurucsev, *J. Chem. Soc., Faraday Trans. 2*, **69**, 395 (1973).
(14) M. M. Wong and Z. A. Schelly, *J. Phys. Chem.*, **78**, 1891 (1974).
(15) V. Zanker, *Z. Phys. Chem. (Leipzig)*, **199**, 225 (1952).
(16) G. R. Haugen and W. H. Melhuish, *Trans. Faraday Soc.*, **60**, 386 (1964).
(17) E. Rabinowitsch and L. F. Epstein, *J. Am. Chem. Soc.*, **63**, 69 (1941).
(18) P. Mukerjee and A. K. Ghosh, *J. Am. Chem. Soc.*, **92**, 6419 (1970).

Mechanical and Photoelastic Properties of Ethylene–Propylene Copolymers Related to Chain Microstructure

F. de Candia,* R. Russo, and V. Vittoria

Laboratorio di Ricerche su Tecnologia dei Polimeri e Reologia, C.N.R. Via Toiano 2,80072 Arco Felice, Napoli, Italy *(Received June 1, 1976)*

In the present paper the mechanical and photoelastic behavior of two ethylene–propylene copolymers are investigated. The two samples differ in the ethylene amount and in the distribution law of monomeric units. The different molecular microstructure gives rise to different physical properties. Results are discussed in terms of chain–chain interactions.

Introduction

Ethylene–propylene copolymers[1] are widely used as elastomers in many technological applications. However, the interest in this class of polymers is related not only to technological aspects but also to some implications at a fundamental level. In particular the chain microstructure can be changed within a large interval, changing the relative amount of the two monomers and the distribution law. The influence of different microstructures on the physical behavior gives informations about the relations between micro- and macroproperties and therefore can be used to investigate at the molecular level some aspects of the mechanical behavior of rubberlike materials. The aspect that attracts our attention is the effect that supramolecular interactions or aggregations can have on the mechanical behavior. The use of the ethylene–propylene copolymers is suggested by the consideration that a different tendency to give rise to interaction phenomena is surely related to a different ethylene amount and to a different distribution law.

In the present paper the elastic and photoelastic behavior of two ethylene–propylene copolymers has been investigated. The two samples differ in the molar ethylene amount and in the distribution law.

Experimental Section

Materials. In Table I the main characteristics of the analyzed samples are reported. The M_c value was given by the first Mooney–Rivlin constant obtained from a stress–strain plot of swollen samples.[2,3] The ethylene amount was obtained by infrared analysis.[4] The distribution law is alternanting-like for sample A and blocklike for sample B, respectively. Information about the distribution of the two monomer units in the chain is given by the knowledge of the catalytic system and of the polymerization conditions.[5] Anyway it was confirmed by NMR and ir analysis.[5]

Dynamic Mechanical Behavior

Viscoelastic spectra of the two samples were recorded using a vibrational viscoelastometer (Vibron-Toyo Instruments); the working frequency was 110 Hz. The complex modulus E^* and the loss term tan δ were reported as function of the temperature in the temperature range 130–280 K. The physical

TABLE I:

Sample	Ethylene content	Vulcan initiator	Vulcan temp, °C	Vulcan time, min	M_c
A	0.52	Dicumyl peroxide 5%	130	80	24 000
B	0.78	Dicumyl peroxide 5%	115	80	22 000

significance of the terms E^* and tan δ is well known.[6] Obtained results are shown in Figures 1 and 2.

The main transition that is characterized by a strong maximum in tan δ and by a large decrease in E^* is the glass transition T_G, that, in spite of the different composition of the two samples, occurs at 240 and 241 K for samples A and B, respectively. A second transition at about 173 K is visible in the two spectra; this transition temperature, indicated in the literature as $T\gamma$,[6,7] is associated to local movements of polymethylenic sequences and requires sequences not shorter than three or four methylenic units. However the feature we want to point out, and that is very important for the problem examined, regards the behavior of E^* at T_G. As is clear from Figures 1 and 2, the decrease of E^* for sample A is sharp and without any element of discontinuity, while for sample B the decrease is retarded on the temperature scale, discontinuity appears in the slope that gives rise to a harplike shape, as evidenced by the dashed lines.

This behavior can be ascribed to paracrystallinity or crystallinity phenomena, or, more generally, to pronounced interaction phenomena.[8]

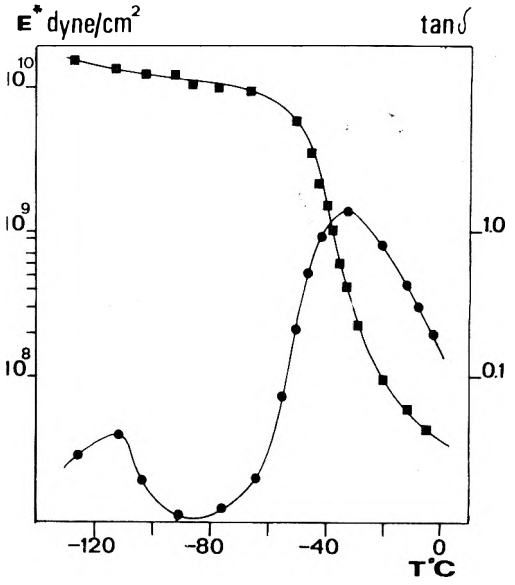

Figure 1. Dynamic-mechanical viscoelastic spectrum of sample A (110 Hz).

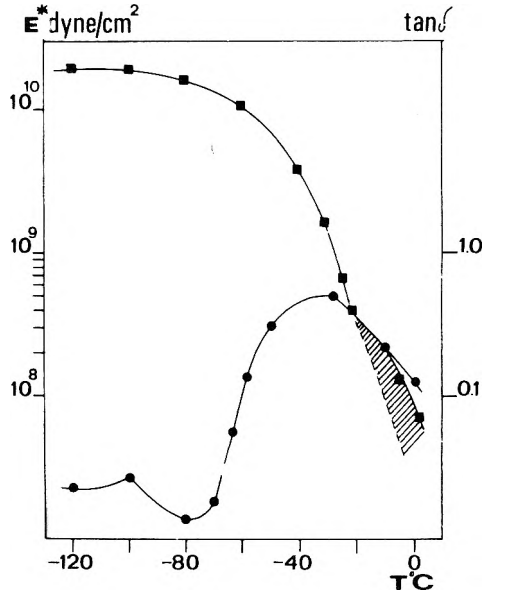

Figure 2. Dynamic-mechanical viscoelastic spectrum of sample B (110 Hz).

Elastic Behavior

Elastic behavior of samples A and B was analyzed in terms of the Mooney–Rivlin equation

$$\tau = 2C_1(\alpha - \alpha^{-2}) + 2C_2(\alpha - \alpha^{-2})\frac{1}{\alpha} \qquad (1)$$

where τ is the force on the cross-section unit, α the strain ratio, and $2C_1$ and $2C_2$ are two constants. Stress–strain measurements were carried out by stretching the sample step-by-step and measuring the stress with 5-min intervals between two successive strain values. The work temperature was 25 °C. For each stress–strain plot Mooney–Rivlin constants were calculated. While for sample A our results indicate no significant effects originating from the mechanical history of the sample, stress–strain data obtained on sample B indicate the presence of very strong and interesting effects connected with the mechanical and thermal history of the examined specimen. All results are summarized in Table II.

Data of Table II were obtained on the same specimen with various thermal and mechanical histories. Group I corresponds to the mechanical responses of the sample without any thermal history after vulcanization. The letters a, b, c, d, and e refer to different successive stress–strain plots. In particular a is the first plot, b the second after 30 min of relaxation at zero load, c the third after 48 h; in a, b, and c the maximum strain value was $\alpha = 2$, in d and e it was 2.5 and it was measured with 30-min intervals. After the mechanical treatments summarized in group I, the sample was kept 1 h at 50 °C and thus showed the mechanical behavior reported in group II of Table II. Finally the data of group III correspond to the mechanical response after a thermal treatment at 135 °C for 15 min. a, b, and c in groups II and III indicate a sequence of mechanical treatments as in group I. The corresponding plots, summarized in terms of the Mooney–Rivlin constants in Table II, are reported in Figures 3–5.

Elastic and Photoelastic Hysteretic Behavior

The photoelastic hysteretic behavior of samples A and B was also investigated. Birefringence measurements were carried out using the Senarmont method[9] to detect the retardation angle, while the stress was obtained by a force transducer. All measurements were performed at 25 °C. The sample was deformed step-by-step in a cyclic way going through the maximum strain value $\alpha = 2$; retardation angle

TABLE II: Mechanical Data Obtained on Sample B[a]

	I		II		III	
	$2C_1$	$2C_2$	$2C_1$	$2C_2$	$2C_1$	$2C_2$
a	0.94	1.50	0.56	1.00	0.13	1.74
b	1.22	0.48	0.89	0.54	0.79	0.74
c	1.34	0.00	1.00	0.24	0.78	0.48
d	1.35	0.00				
e	1.22	0.00				

[a] $2C_1$ and $2C_2$ are reported in kg/cm^2.

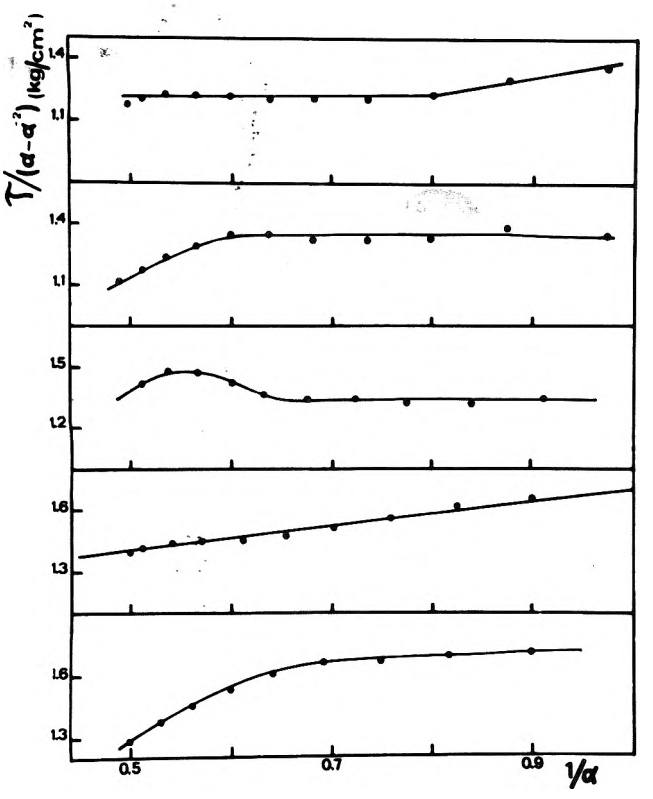

Figure 3. Mooney–Rivlin plots obtained for sample B. From bottom to top Ia, Ib, Ic, Id, Ie.

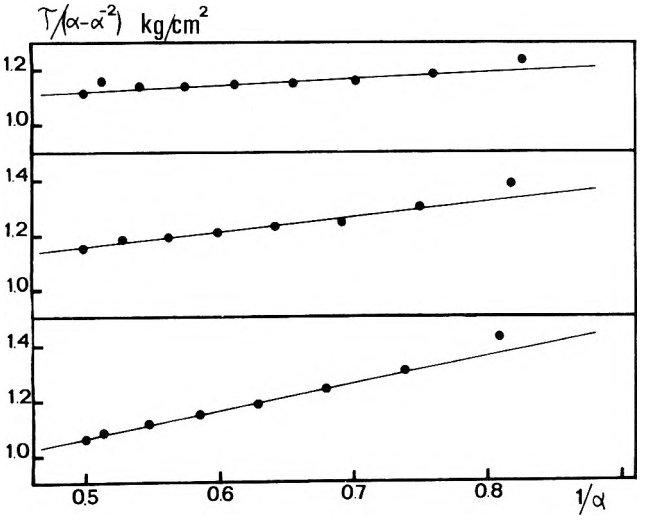

Figure 4. Mooney–Rivlin plots obtained for sample B. From bottom to top IIa, IIb, IIc.

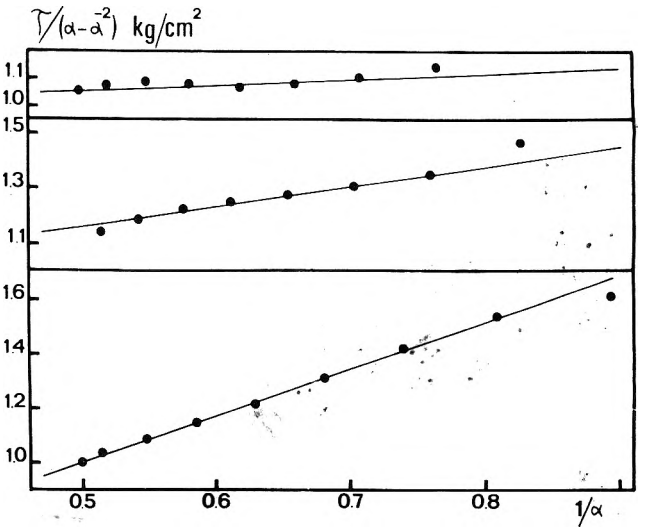

Figure 5. Mooney–Rivlin plots obtained for sample B. From bottom to top IIIa, IIIb, IIIc.

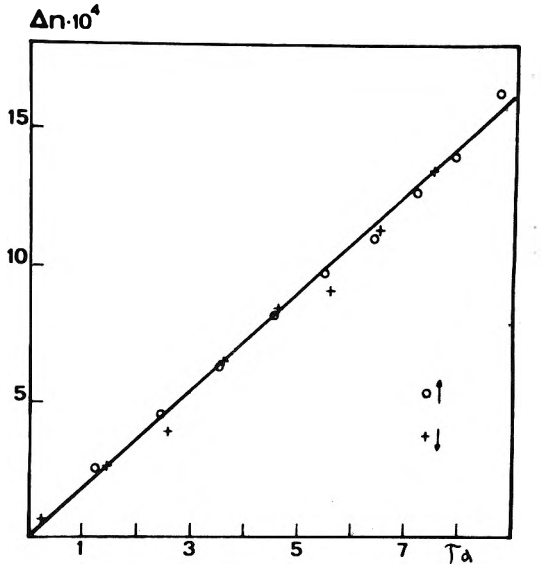

Figure 6. Photoelastic plot of sample A. The birefringence is reported as a function of the true stress.

and stress were detected at each strain value with 5-min intervals between two successive points. Experimental data were reported in terms of birefringence Δn vs. the true stress $\tau\alpha$.

In Figure 6 results obtained on sample A are shown. In Figure 7 we report the photoelastic hysteretic plots observed on sample B. The significance of the symbols Ia, Ib, . . . , IIa, . . . , IIIc is the same as in Table II.

As is clear from Figures 6 and 7, for sample A the Δn vs. $\tau\alpha$ plot is reversible on stretching and relaxing, whereas sample B shows very strong hysteretic effects. For sample B mechanical hysteresis loops were detected, and results are reported in Figure 8. Numerical treatment of the plots of Figures 7 and 8 are collected in Table III. The degree of irreversibility in the two kinds of hysteretic plots is reported in terms of the functions $\phi_{\Delta n}$ and ϕ_τ defined as follows:

$$\phi_{\Delta n} = \left[\int_{\alpha=2}^{\alpha=1} \Delta n \, d\tau\alpha - \int_{\alpha=1}^{\alpha=2} \Delta n \, d\tau\alpha\right] \Big/ \int_{\alpha=2}^{\alpha=1} \Delta n \, d\tau\alpha$$

$$\phi_\tau = \left[\int_{\alpha=1}^{\alpha=2} \tau \, d\alpha - \int_{\alpha=2}^{\alpha=1} \tau \, d\alpha\right] \Big/ \int_{\alpha=1}^{\alpha=2} \tau \, d\alpha$$

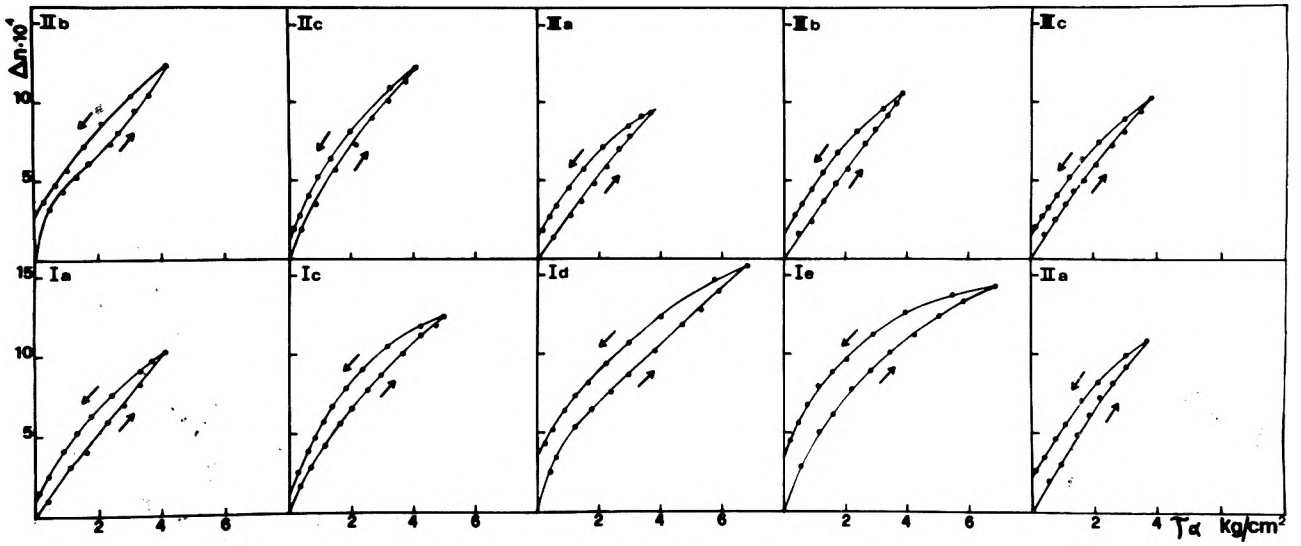

Figure 7. Photoelastic hysteretic plots of sample B. For each plot an indication about the sample history is given.

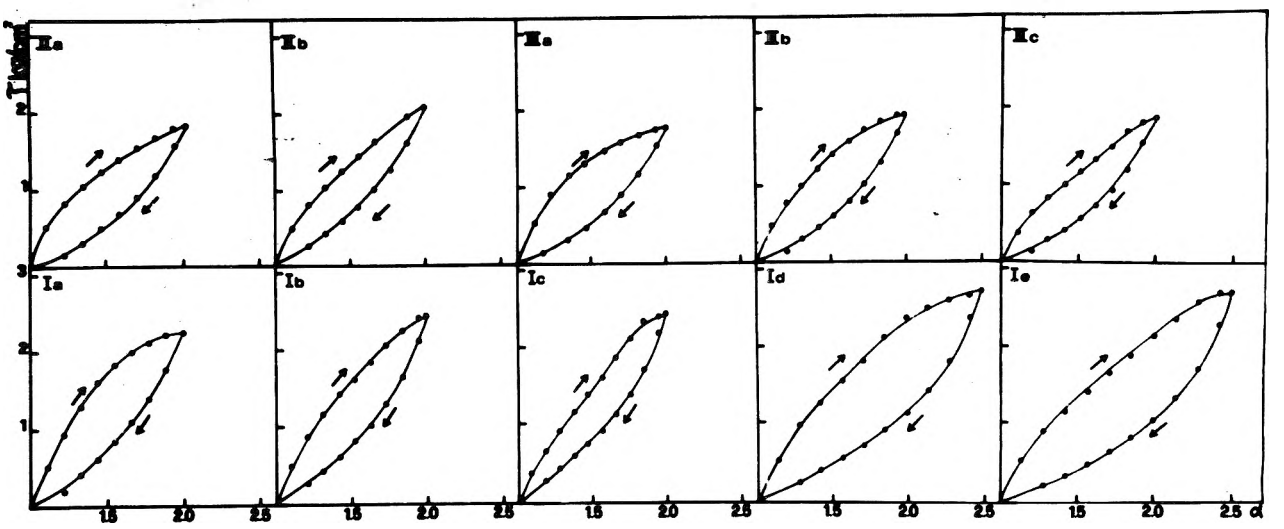

Figure 8. Elastic hysteretic plots of sample B. For each plot an indication about the sample history is given.

Discussion

As stated in the Introduction the main purpose of the present work was to analyze the relationships between the microstructure and the physical behavior for ethylene–propylene samples. The two analyzed samples differ in the ethylene amount, and in the distribution law. This microstructural difference induces very different physical behaviors. In particular the different composition acts directly on the chain–chain interaction or aggregation phenomena. This is clearly supported by the viscoelastic data of Figures 1 and 2 where the shape of the modulus curve at T_G indicates for sample B the presence of some hardening effect that is related to physical crosslinks, such as chain aggregation or paracrystallinity, or crystallinity zones in the sample.[8] In other words the two samples differ in the different tendency to give rise to molecular organization phenomena. This difference has as its main effect that the physical behavior of the sample B is strongly hysteretic when compared with that of sample A. All experimental data obtained in this paper clearly point out this feature. In fact as a starting point we can discuss the indications given by the photoelastic analysis that is summarized in Figures 6 and 7 and in Table III. On the time scale of the experiment, sample A shows a reversible behavior, while for sample B a strong hysteretic photoelastic trend is observable. The trend of Figure 7 indicates that on relaxing the birefringence Δn is reinforced with respect to the true stress $\tau\alpha$, that is the anisotropy of the sample, for equal values of the stress, is greater on relaxing than on stretching. Moreover, the degree of such an irreversibility, that is reported in a quantitative way in Table III, is closely related to the mechanical and thermal history of the sample. It is evident that the term $\phi_{\Delta n}$ decreases when successive mechanical treatments are carried out on the sample (see the sequence Ia–Id); on the other hand, thermal treatment restores practically all of the first photoelastic response, as is clear when Ia, IIa, and IIIa are compared.

In other words, the degree of irreversibility of the photoelastic behavior must be related to a mechanism consistent with this observation, i.e., mechanical treatment can be memorized by the sample, while thermal treatment can cancel this mechanical memory.

A phenomenon such as chain aggregation or paracrystallization induced by strain, irreversible even if the sample is relaxed at zero load for a long time, can be consistent with this picture.

TABLE III: Hysteretic Behavior of Sample B

Sample history	$\phi_{\Delta n}$	ϕ_τ
Ia	0.211	0.429
Ib	0.198	0.415
Ic	0.166	0.347
Id	0.159	0.473
Ie	0.165	0.471
IIa	0.192	0.453
IIb	0.123	0.401
IIc	0.129	0.400
IIIa	0.228	0.487
IIIb	0.200	0.457
IIIc	0.164	0.395

The difference $\Delta\phi_{\Delta n}$ between successive mechanical treatments takes into account the contribution of this irreversible aggregation phenomenon to the hysteretic behavior of the sample. Moreover, this phenomenon contributes to the total number of cross-link points, in fact physical aggregation behaves at mechanical levels in a way not too different from a chemical cross link.

This hardening effect, on one hand, is supported by the viscoelastic behavior, as previously discussed, and, on the other hand, by the quantitative values of the term $2C_1$ of the Mooney equation. In fact in Table II an increase of the $2C_1$ term as a function of the mechanical history of the sample is observable, while the thermal treatment, by a mechanism of aggregation zone melting, produces a decrease of the $2C_1$ value. The relationship between the C_1 term and the cross-linking density is well known,[5] and does not require any explanation. This overall picture is further supported by the data on the ϕ_τ term. The hysteretic mechanical behavior is consistent in the same way with the mechanism proposed for the term $\phi_{\Delta n}$. The apparent disagreement in the data between the values for Ic and Ie is due to the different value of the maximum strain that is 2.5 in cycle e instead of 2 in cycle c.

Up to this point we have discussed in terms of simple aggregation or paracrystallization and not in terms of large crystallization phenomena. This restriction is supported by much experimental evidence. The first is the good macroscopic reversibility of sample deformation. In other words, the mechanical behavior of the sample at the macroscopic level does not give any evidence of plastic behavior that could be consistent with a diffuse and extended crystallization phenomenon. Moreover, when the deformation produces a diffuse crystallization phenomenon, generally a drastic plot upturn appears in the Mooney–Rivlin data, where the C_2 term goes from positive to negative values.[2] Such a behavior is not observed in our experiments, as it is clear in Figures 3–5. On the other hand, if these experimental elements can exclude a high degree of crystallization, the thermograms carried out with a differential scanning calorimeter (DSC II, Perkin-Elmer), analyzing stretched and unstretched samples under all the experimental conditions of Tables II and III, do not give any appreciable evidence of enthalpic change. Taking into account that from the thermograms, in the sensitivity range used (up to 5 mcal/s), also a small amount of crystallinity can be detected, it seems that also a low degree of crystallization can be excluded, and that the observed hysteretic effects are connected with interchains phenomena at a low degree of organizations, or with a very low amount of crystallinity, under the limit of the sensitivity of our measurements.

The photoelastic data, discussed in terms of the photoelastic coefficient, seem to point in the same direction. As is well known[2] the slope of the Δn vs. $\tau\alpha$ plot is directly related to the molecular and structural nature of the material and therefore can be used to obtain information about the presence of a crystalline phase. For ethylene–propylene copolymers, in particular, a quantitative treatment of the photoelastic data was reported,[10] where the contributions of the amorphous and crystalline regions to the photoelastic behavior are reported. This means that a structural change, such as a different amount of the crystalline phase, affects the numerical value of the photoelastic coefficient. In our experiments, as it is clear from Figure 7, this value, calculated from the data obtained by stretching the sample, is practically independent of the mechanical and thermal history of the sample, with the exclusion of cycles Id and Ie, where the maximum strain is increased and where we can observe a drastic distorsion of the curve indicating drastic structural changes. To sum up on this point we can exclude the presence of diffuse crystallization phenomenon during the deformation as a direct cause of the memorization of the mechanical history, while, as previously pointed out, we must believe that the last is related to interchain interactions, not very organized at a structural level, or to a very low degree of crystallization. The last point we want to discuss is another interesting experimental observation that regards the C_2 term of the Mooney equation.

As evidenced by Figures 3–5, even if the shape of the Mooney plots is not regular, a tendency to give rise to a null value for C_2, in large strain intervals, is observable as a function of the mechanical history of the sample.

This is reported in a quantitative way in Table II, where the effect of the thermal treatment on C_2 is also evident. This result, once again, supports the general point of view that the term C_2 is related to chain–chain phenomena in amorphous materials.[11]

Particularly surprising is the direction in which the change of the C_2 value takes place. In fact, the apparent result is that the ideality of the behavior[5] ($C_2 = 0$) increases when the ideality of the sample topology[5] (chain–chain interactions = 0) decreases.

An explanation could be put forward only if the mechanism of the ordering phenomena on C_2 were known. A possible suggestion could be a relation between C_2 and organization phenomena that takes place during the deformation; but such an hypothesis is purely speculative. Another possible correlation could be with the physical cross linking induced by the strain, and that, therefore, takes place in an oriented system. In fact in the past it was found that C_2 decreases when some degree of cross linking is introduced in the strained material.[12] Anyway, the point stressed by this paper is the existence of relations between the second Mooney constant and interchains phenomena, and more generally between mechanical behavior, interchain phenomena, and chain microstructure.

Acknowledgments. We wish to thank Professor A. Zambelli for the polymer preparation and for many helpfull discussions. The contribution of Professor P. A. Temussi in the discussion and in manuscript preparation is also appreciated.

References and Notes

(1) F. P. Baldwin and G. Ver Strate, *Rubber Chem. Technol.*, **45**, 709 (1972).
(2) L. R. G. Treolar, "The Physics of Rubber Elasticity", 3d ed, Oxford University Press, London, 1975.
(3) F. de Candia and L. Amelino, *J. Polym. Sci., Part A2*, **10**, 715 (1972).
(4) J. J. Gardner, C. Cozewith, and G. Ver State, *Rubber Chem. Technol.*, **44**, 1015 (1971).

(5) A. Zambelli, private communication.
(6) N. G. McCrum, B. E. Read, and G. Williams, "Anelastic and Dielectric Effects in Polymeric Solids", Wiley, New York, N.Y., 1967.
(7) F. C. Stehling and L. Mandelkern, *Macromolecules*, **2**, 242 (1970).
(8) A. Valvassori and V. Zamboni, XXIII JUPAC Conference, Boston, Mass., July 1971.
(9) S. Flügge, "Encyclopedia of Physics", Vol. I, Springer-Verlag, Berlin, 1958.
(10) K. Baba and R. S. Stein, *Bull. Am. Phys. Soc., Ser. 2*, **17**, 223 (1972).
(11) K. Dusek and W. Prins, *Adv. Polym. Sci.*, **6**, 1 (1969).
(12) A. Greene, K. J. Smith, and A. Ciferri, *Trans. Faraday Soc.*, **61**, 2772 (1965).

Optically Detected Magnetic Resonance and Spectroscopic Studies of the Lowest Excited Triplet States of Xanthone and Related Molecules in Crystalline Systems

Asok Chakrabarti

Department of Chemistry, State University of New York at Stony Brook, Stony Brook, New York 11794

and Noboru Hirota*

Department of Chemistry, State University of New York at Stony Brook, Stony Brook, New York 11794 and Department of Chemistry, Faculty of Science, Kyoto University, Kyoto, Japan 606 *(Received March 3, 1976; Revised Manuscript Received August 17, 1976)*

The magnetic and dynamic properties of the lowest excited triplet (T_1) state of xanthone trap and xanthone in diphenylmethane and 9,10-dihydroanthracene host crystals were investigated at 1.2 K using the optically detected magnetic resonance (ODMR) technique and phosphorescence emission and excitation spectroscopy. It is unambiguously shown that the T_1 state of xanthone studied here is $^3\pi\pi^*$ state, but in xanthone and diphenylmethane crystals there are two triplet species with different magnetic properties. The total and radiative decay rates from spin sublevels and the sublevel phosphorescence spectra were obtained. The results were discussed in terms of the possible mechanisms of radiative and radiationless transitions. It is suggested that the main radiative mechanism is spin–orbit vibronic involving $^1n\pi^*$, $^1\pi\pi^*$ ($^1B_2$) states and b_1 vibrations. The relationship between the present results and those reported by other workers is discussed.

Introduction

The spectroscopic, photochemical, and magnetic properties of the lowest excited triplet states of aromatic carbonyls have been the topics of much interest in recent years.[1-45] Optically detected magnetic resonance (ODMR) studies at zero field have revealed a number of interesting features concerning the magnetic and dynamic properties of the T_1 states of these molecules.[35-38,40-46] It was shown that the radiative properties of the $^3\pi\pi^*$ aromatic carbonyls depend on many factors such as molecular structure, energy separation between $^3n\pi^*$ and $^3\pi\pi^*$ states (ΔE_{TT}), and the nature of environments.[45] The main radiative mechanism differs markedly depending on these factors within $^3\pi\pi^*$ aromatic carbonyls.[45] Here, we have investigated the T_1 state of xanthone and related molecules in order to clarify the main radiative mechanism and to obtain more information about the relationships between structures and radiative properties of aromatic carbonyls. The main motives of the present study are the following.

(1) In case of $^3\pi\pi^*$ aromatic carbonyls of the benzaldehyde type with small ΔE_{TT} it was found that the vibronic and configurational mixing between $^3n\pi^*$ and $^3\pi\pi^*$ states is the important source of radiative activity.[45] However, different from benzaldehydes the carbonyl group is rigidly held to the planar π-electron system in xanthone. This may make the radiative property of the $^3\pi\pi^*$ state xanthone very different from those of the other $^3\pi\pi^*$ carbonyls. Comparison between the radiative property of xanthone with those of the other aromatic carbonyls appears to be useful in understanding structure–dynamic property relationship.

(2) It is known that xanthone shows dual phosphorescence emissions in rigid glass at 77 K.[47] The nature of the phosphorescing species as well as the origin of the dual emission is still not well established despite wide interest in this phenomenon.[6,10,20,30,47-52] It was recently suggested that the T_1 state of xanthone in 3-methylpentane at 2 K might have a very distorted structure[52] but definitive evidence seems to be lacking. It was hoped that the zero field ODMR studies would help to answer some of these questions.

In this work we have made detailed ODMR studies of xanthone in various single crystal systems. The $S_0 \rightarrow T_1$ absorption studies were also made to supplement ODMR studies.

Experimental Section

(1) *Sample Preparations.* Xanthone was studied in pure crystals (traps), diphenylmethane (DPM), and 9,10-dihydroanthracene (DHA) hosts. Benzophenone and 4-aminobenzophenone were studied in a DPM host. The 4,4′-dimethoxybenzophenone trap was also studied. Molecular structure and the axis systems used here are given in Figure 1. All chemicals except diphenylmethane were recrystallized and zone refined extensively prior to use. Diphenylmethane was purified by repeated distillation.

* Address correspondence to this author at the Department of Chemistry, Faculty of Science, Kyoto University.

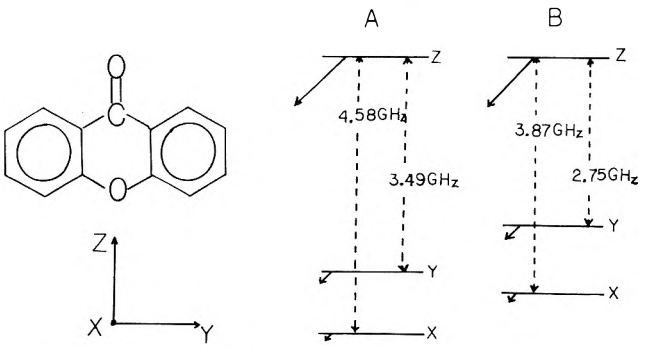

Figure 1. Molecular structure, axis system, and energies of the triplet sublevels.

The single crystals of these systems were grown by the standard Bridgman method. The guest concentration in the initial host–guest mixture was normally about 1% but the actual concentrations in the mixed crystals were considered to be very low, because the solubility of xanthone in DHA and DPM host is rather low.

(2) *ODMR Experiments.* The experimental setup for the present zero field ODMR experiment is essentially the same as that previously reported.[53] A crystalline sample held in a microwave helix at liquid helium temperature was excited by the light from an Osram 500w/2 high-pressure mercury arc lamp, filtered through a $NiSO_4$ + $CoSO_4$ solution, and a Corning uv transmitting filter. The microwave was supplied to the helix through a coaxial cable with a Hewlett-Packard 8690 sweeper. The desired phosphorescence peak was selected with an Engis 60-cm monochromator. We have made the following three types of ODMR experiments at 1.5~1.2 K.

(A) *Steady State Zero Field ODMR Measurements.* The phosphorescence emission was obtained with an ordinary phosphoroscope using a sector which chops the emission at 720 Hz. The signal was detected with an EMI 6256B photomultiplier and a PAR HR8 lock-in amplifier. The microwave was repeatedly swept through the frequencies corresponding to the zero field transitions and the changes in the phosphorescence emission were stored and accumulated on a Varian C-1024.

(B) *Microwave Induced Delayed Phosphorescence (MIDP) Experiments.* The total decay rate (k_i), relative radiative decay rate (k_i^r), and populating rate (P_i) of each spin sublevel were determined at 1.2 K by the standard MIDP technique.[54,55] The vibronic level dependence of k_i^r was studied by determining k_i^r at selected vibronic bands. The chopper module was replaced by a shutter module which opens and closes excitation and emission lights synchronously. The experimental procedures and the methods of data analyses are similar to those given in the literature[53-56] and are not repeated here.

(C) *Microwave Modulated and Sublevel Phosphorescence Spectra.* In order to study the radiative mechanisms in detail it is desirable to obtain phosphorescence spectra from different sublevels separately. We have attempted to do this in the following way.

(1) *Rapid Passage Microwave Modulated Phosphorescence Spectra.* The commonly used method to obtain the vibronic band dependence of the phosphorescence spectra is AM modulated PMDR method.[57-59] However, when the line width of the resonance signal is rather broad, AM modulation can cause the microwave transition of only a small fraction of triplet state molecules. In such systems, much larger changes in phosphorescence intensities can be obtained by rapidly sweeping the microwave repetitively over the entire region of resonance frequencies.[53,60,61] We swept microwave repetitively at the rate of 3 s^{-1} and detected the produced changes with a lock-in amplifier.

The change in phosphorescence intensity (ΔI_{ij}) produced by the rapid passage of microwave transition between i and j spin sublevels under steady state condition is given by[61]

$$\Delta I_{ij} = A(k_i^r - k_j^r)(n_j - n_i) \quad (1)$$

where k_i^r and k_j^r are the radiative decay rates, and n_i and n_j are the populations of the sublevels i and j at the time of microwave sweep. Since we only detect ΔI_{ij}, the spectrum obtained gives $k_i^r - k_j^r$ as a function of emission wavelength. When $k_j^r \ll k_i^r$ the obtained spectrum gives the phosphorescence spectrum from the radiatively dominant sublevel.

(2) *Phosphorescence Sublevel Spectra*[62] *Obtained under Microwave Saturation.* When only one sublevel is decaying rapidly and the spin–lattice relaxation time is very slow compared to the decay rates, phosphorescence emission of the slowly decaying sublevels may be separated conveniently by combining microwave saturation and appropriate delay of the shutter facing to the monochromator.[45] For example, in order to obtain the y sublevel spectrum of xanthone x ⇔ z transition was saturated by continuous sweep of microwave at 500 s^{-1} and the opening of the emission shutter was delayed by 0.4 s so that most of the population in the x and z sublevels decayed before the shutter was open. Under constant saturation of microwave, the populations in the x and z sublevels decay with the decay rate constant $k_a = 1/2(k_x + k_z)$. Hence, in order to separate the y sublevel spectrum of xanthone completely, it is necessary to use a shutter delay of longer than 0.5 s. Under our experimental conditions, it was not possible to eliminate the contribution from the z sublevel emission entirely from the y and x sublevel emissions. Nevertheless, the spectra obtained under microwave saturation and shutter delay are very different from those obtained without them.

(3) *Phosphorescence Excitation Spectra.* The phosphorescence excitation spectra[63,64] were obtained in order to determine the exact locations of the $^3\pi\pi^*$, $^3n\pi^*$, $^1n\pi^*$, and $^1\pi\pi^*$ states of xanthone in pure crystal and diphenylmethane. Our ODMR setup was modified so that an Engis 60-cm monochromator became the excitation monochromator which analyzes the output of the Osram 1000-W xenon lamp. The total phosphorescence emission of the sample was chopped at 720 s^{-1} and detected with an EMI 6256B PM tube and amplified with a PAR HR-8 lock-in amplifier.

Experimental Results

(1) *Phosphorescence Excitation Spectra and Locations of the $^3n\pi^*$, $^1n\pi^*$, and $^1\pi\pi^*$ States.* The phosphorescence excitation spectra of xanthone are shown in Figure 2. The excitation spectrum of xanthone crystal starts at 25 230 cm^{-1}, which is 180 cm^{-1} higher than that of the origin of the phosphorescence spectrum of the crystal at 4.2 K. This difference is reasonable, since the phosphorescence of the crystal is considered to originate from shallow traps. There are two strong absorption bands starting at 26 700 and 27 700 cm^{-1}. In the diphenylmethane host the absorption at 25 200 cm^{-1} is not observable, but the other two absorption bands are very clear. Comparing the intensity changes in going from the pure crystal to the mixed crystal we assign the absorption starting at 27 700 cm^{-1} as the $S_0 \rightarrow {}^1n\pi^*$ ($^1A_2$) absorption, although the peak is about 500 cm^{-1} blue shifted compared to the same absorption determined in 3-MP glass.[47] Then absorptions

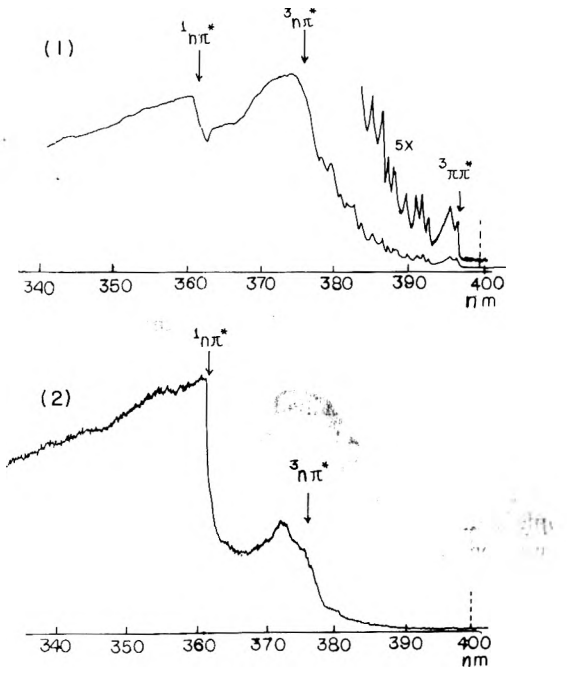

Figure 2. Phosphorescence excitation spectra: (1) pure xanthone crystal, (2) xanthone in diphenylmethane. Vertical dotted lines indicate the locations of the 0–0 bands of phosphorescence spectra.

TABLE I: Energies of the States (cm^{-1})

	Xanthone crystal	Xanthone trap	Xanthone in DPM[a]	Xanthone in 3-MP[c]
$^3\pi\pi^*(^3A_1)$	25 230	25 050[b]	25 020[b]	25 906 (?)
$^3n\pi^*(^3A_2)$	26 700		26 700	?
$^1n\pi^*(^1A_2)$	27 700		27 700	27 050
$^1\pi\pi^*(^1A_1)$				29 450
$^1\pi\pi^*(^1B_2)$				35 280
$\Delta E_{^1T}$	1 470		1 680	Very small
ΔE_{ST}	2 470		2 680	1 144
$\Delta E(^1n\pi^*-^3n\pi^*)$	1 000		1 000	?

[a] DPM represents diphenylmethane. [b] Obtained from the phosphorescence spectra. Others were determined from either excitation or absorption spectra. [c] Obtained by Huber et al. (ref 47).

starting at 26 700 and 25 230 cm^{-1} are assigned as the $S_0 \rightarrow {}^3n\pi^*$ and $S_0 \rightarrow {}^3\pi\pi^*$ absorptions, respectively.

The 0–0 band of the $S_0 \rightarrow {}^3\pi\pi^*$ absorption is very weak, but the vibronic bands gradually gain intensity as they approach the origin of the $^3n\pi^*$ state as shown in Figure 2. This indicates that the radiative transition probability of the $S_0 \rightarrow {}^3\pi\pi^*$ absorption is very small at the 0–0 band, but it gains more intensity through vibronic coupling with the $^3n\pi^*$ state, as the $S_0 \rightarrow {}^3\pi\pi^*$ transition approaches the 0–0 of the $^3n\pi^*$ state. Such a change of the intensity of the vibronic band is known in the cases of conjugative enones[23] and many $^3\pi\pi^*$ substituted benzaldehydes[26,65] and is consistent with the $^3\pi\pi^*$ assignment of the 25 230-cm^{-1} band. The excitation spectrum of xanthone in diphenylmethane does not show the $S_0 \rightarrow {}^3\pi\pi^*$ absorption, but clearly show the $S_0 \rightarrow {}^3n\pi^*$ absorption. The location of the peak is almost identical with the case of pure crystal. The locations of the $^3\pi\pi^*$, $^3n\pi^*$, and $^1n\pi^*$ states determined here are tabulated in Table I and are compared with the data given by Pownal and Huber obtained in rigid matrices.[47]

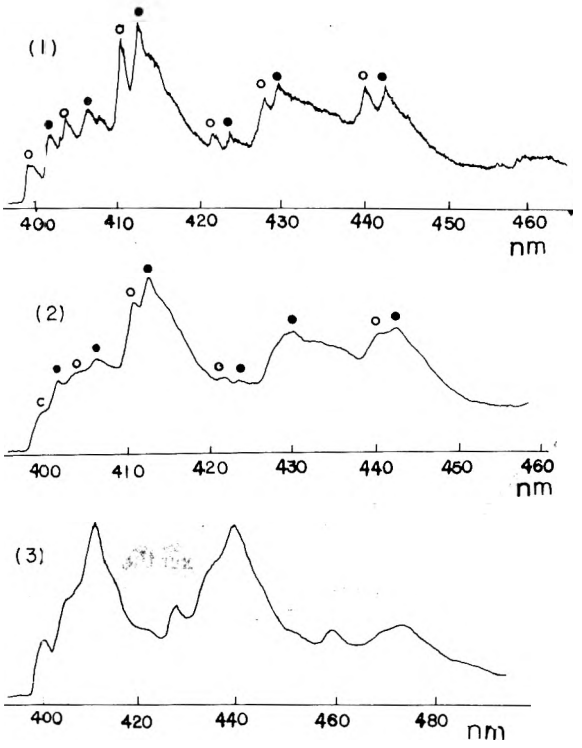

Figure 3. Phosphorescence spectra of xanthone in various hosts at 1.5 K: (1) xanthone trap in xanthone crystal; (2) xanthone in diphenylmethane; (3) xanthone in 9,10-dihydroanthracene. ● and O indicate the vibronic bands belonging to the spectra of different triplet species

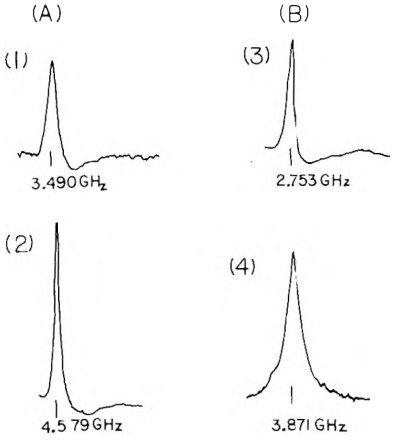

Figure 4. Typical steady state zero field ODMR spectra of a xanthone trap. The spectra were taken by sweeping microwave about 250 times repetitively over 0.3~0.5 GHz in 2.5 s and accumulating the signals on a CAT. (1) and (2) are the signals of A species. (3) and (4) are the signals of B species.

(2) *Phosphorescence Spectra.* The phosphorescence spectra of xanthone obtained in various hosts are shown in Figure 3. In all three hosts the spectra are rather broad. Although the vibrational structures appear to be different depending on the host, this is primarily due to the superposition of the two spectra coming from the two different triplet species as shown in a later section. In all cases the 0–0 bands of the phosphorescence spectra are weak indicating that the main radiative mechanism is possibly vibronic. This is in striking contrast to the cases of many $^3\pi\pi^*$ aromatic carbonyls of the benzaldehyde type.[42,45]

(3) *ODMR Results.* The MIDP results show that the decay

TABLE II: Vibrational Structures of the Phosphorescence Spectra

Xanthone trap (A)		Xanthone trap (B)		Xanthone in 3-MP (2 K)[a]	
ν, cm^{-1}	$\Delta\nu$, cm^{-1}	ν, cm^{-1}	$\Delta\nu$, cm^{-1}	ν, cm^{-1}	$\Delta\nu$, cm^{-1}
25 050		24 882		25 650	
24 760	290	24 590	292	25 350	300
24 360	690	24 230	652	24 980	670
23 720	1330	23 580	1302	24 290	1360
23 392	1658	23 256	1626	23 490	1660
23 100	1658 + 292	22 960	1626 + 296	23 690	1660 + 300
22 717	1658 + 675	22 589	1626 + 667	23 320	1660 + 670

[a] Taken from the data by Pownall, Connors, and Huber (ref 52).

TABLE III: ZFS and Dynamic Properties of the $^3\pi\pi^*$ State of Xanthone

		ν_{00}, cm^{-1}	ZFS,[a] cm^{-1}	P_i(relative) x	y	z	k_i, s^{-1} x	y	z	k_i^r(relative) Band	X	Y	Z
Xanthone trap	A	25 050	D = −0.1345				0.73	2.2	18.5	0–0		~1	1
			E = +0.0181							0–290	0.065		1
										0–670	0.048		1
	B	24 882	D = −0.1103				0.45	1.75	16.0	0–0	0.11	~0.6	1
			E = +0.0186							0–270	0.040	0.30	1
										0–670	0.033	0.15	1
Xanthone in DPM	A	25 020	D = −0.1352	0.07		1	0.73	2.4	17.7	0–0		~1	1
			E = +0.0173							0–290	0.05		1
										0–670	0.03		1
	B	24 895	D = −0.1105	0.04	0.2	1	0.50	1.95	16.0	0–0		~0.7	1
			E = +0.0201							0–290	0.06	~0.4	1
										0–670	0.04	~0.2	1
Xanthone in 9,10-DHA		25 000	D = −0.1095	0.03	0.05	1	0.74	1.7	20	0–0		~1	1
			E = +0.0195							0–670		0.18	1

[a] Note that D is negative because of the choice of our axis system.

rate from either the top or the bottom spin sublevel is the largest one. In view of the results of the other $^3\pi\pi^*$ aromatic carbonyls so far studied[35-37,42,44,45] we assume that the bottom spin sublevel is the slowest decaying one and the x sublevel. The z sublevel is assumed to be the fastest decaying top sublevel as in all other $^3\pi\pi^*$ aromatic carbonyls. Then $k_z \gg k_y > k_x$.

The ODMR results clearly indicate that in xanthone and diphenylmethane hosts there are two different triplet species (we call A and B) characterized by the two different sets of ZFS (Figures 1 and 4). The transition frequencies for the A species are 4.578 and 3.490 GHz in the xanthone crystal, and 4.58 and 3.55 GHz in diphenylmethane.[66] For the B species they are 3.87 and 2.75 GHz in the xanthone crystal and 3.81 and 2.77 GHz in diphenylmethane. These yield D and E values given in Table III. The E values of the two species are similar, but their D values are somewhat different. Their decay rates are also similar. In the case of xanthone in 9,10-dihydroanthracene the properties of the triplet state are similar to those of B species.

Since there are two distinct emitting species, the phosphorescence spectra consist of the superposition of those of two species. However, the spectra which belong to different species can be separated conveniently by taking rapid passage spectra corresponding to the microwave resonance frequencies of the A and B species. These spectra are shown in Figure 5.

The rapid passage spectra clearly show that the spectra of the individual species A and B are similar. The main vibra-

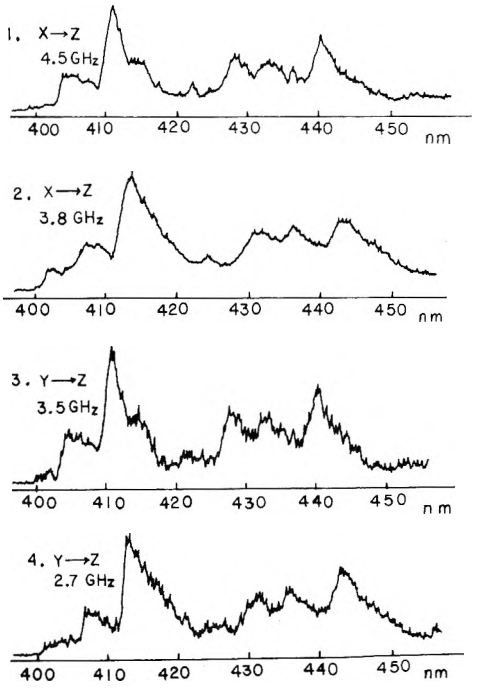

Figure 5. Rapid passage microwave modulated phosphorescence spectra of xanthone trap: (1) modulated by the 4.58-GHz x ↔ z transition of the A species; (2) modulated by the 3.87-GHz x ↔ z transition of the B species; (3) modulated by the 3.50-GHz y ↔ z transition of the A species; (4) modulated by the 2.753-GHz y ↔ z transition of the B species.

tional frequencies obtained from the rapid passage spectra are ~290 and 670 cm^{-1} for both species. These vibrational frequencies are also very similar to those obtained for xanthone in 3-MP glass at 2 K studied by Pownall, Connors, and Huber[52] (Table III), indicating that the nature of the species responsible for the phosphorescence emission obtained by them in 3-MP at 2 K is likely to be similar to those studied here. In pure xanthone and diphenylmethane the 0–0 of the A and B species are separated by about 160 cm^{-1}.

The rapid passage phosphorescence spectra obtained by the z ↔ y and x ↔ z transitions are similar, indicating that the main features of the spectra are determined by k_z^r. The intensities of the 0–0 bands of the rapid passage spectra are weak indicating that k_z^r is small at the 0–0 bands. However, $k_z^r - k_y^r$ of the B species seems to be somewhat larger than that of the A species. Although $k_z^r > k_y^r$ and $k_z^r > k_x^r$ were found for all vibronic bands, k_z^r/k_y^r varies considerably depending on the vibronic bands as shown in Table II.

In Figure 6 the phosphorescence spectra of xanthone obtained under the continuous microwave saturation and shutter delay are shown. These spectra are likely to be contaminated by the z sublevel emission and do not represent the true x and y sublevel spectra. Nevertheless it is clear that the 0–0 and 0–1660 cm^{-1} peaks are relatively much stronger and 0–290 and 0–670 cm^{-1} peaks are weaker in the y sublevel spectrum. These spectra also indicate that the weakness of the 0–0 band is not due to the small Franck–Condon factor caused by distortion.

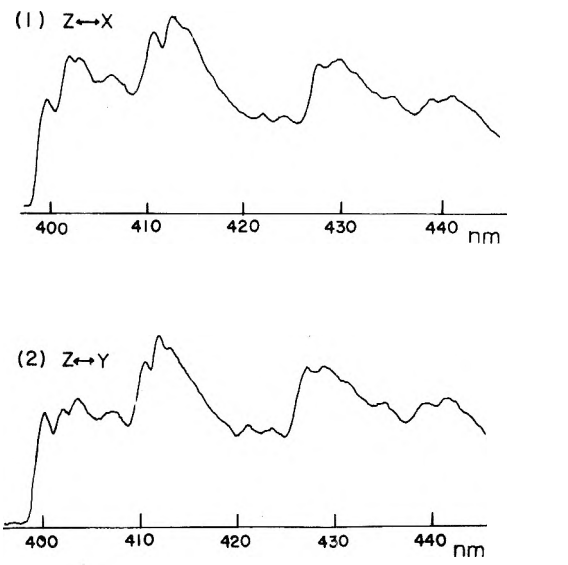

Figure 6. The phosphorescence spectra of a xanthone trap obtained with a time delay of the shutter opening and microwave saturation: (1) microwave saturation of the x ↔ z transitions of the A and B species; (2) microwave saturation of the y ↔ z transitions of the A and B species.

Discussions

(A) *Nature of the Triplet States and ZFS.* The experimental results presented here leave little doubt about the $^3\pi\pi^*$ assignment of the xanthone triplet state studied here. In fact $\Delta E_{TT}(^3n\pi^*-^3\pi\pi^*) \simeq 1450$ cm^{-1} for the present system is quite large. At present we have no experimental data to decide the origin of the two triplet species, but they may be due to the two types of xanthone molecules occupying the two different sites in crystals. Guest triplet states occupying multiple sites are quite common in mixed crystal systems.[67-70] Although the decay properties of the A and B species are very similar, D values are considerably different.

In the present systems $\Delta E_{TT}(^3n\pi^*-^3\pi\pi^*)$ and $\Delta E_{ST}(^1n\pi^*-^3\pi\pi^*)$ are about 1450 and 2500 cm^{-1}, respectively. Although we do not know the exact values of ΔE_{TT} and ΔE_{ST} for the A and B species, we may assume similar values. Then, if the spin–orbit coupling matrix element $^3G = \langle ^3\pi\pi^*|\mathcal{H}_{so}|^3n\pi^*\rangle$ is large, D should be affected strongly by the second-order effect of spin–orbit coupling.[8,38,39,71] It was found that this is the case in conjugated enones,[41] and aromatic carbonyls of the benzaldehyde type.[26,42,46] For a series of aromatic carbonyls of the benzaldehyde type ^3G was estimated empirically to be ~9 cm^{-1}.[26,42,46] When $\Delta E_{TT} = 1400$ cm^{-1} this value of ^3G predicts that the spin–orbit contribution to D is about 0.08 cm^{-1}.

In the xanthone triplet states studied here the observed D are rather small and it is likely that the spin–orbit contribution to ZFS is much smaller than in the cases of benzaldehydes. However, the difference in D of A and B species could be, at least partly, due to the difference in the contribution of spin–orbit coupling to ZFS.

In order to see whether the spin–orbit contribution to ZFS is large in the aromatic carbonyls containing two phenyl rings such as xanthone and substituted benzophenones we have further studied several systems with very different values of ΔE_{TT}. The results are shown in Table IV. In spite of large differences in ΔE_{TT} and the changes in the nature of T_1 state, the variations in ZFS are not very large. This situation is very different from benzaldehydes and acetophenones in which $|D|$ ranges from 0.1 to 0.5 cm^{-1}.[26,42,46] The above observation also seems to indicate that the spin–orbit contribution to ZFS in xanthone and substituted benzophenones are likely to be much smaller than in benzaldehydes.

In the matrix element ^3G the integration is taken over both electronic and nuclear coordinates. Hence, ^3G is affected by the changes of electronic wave functions as well as by Franck–Condon factor. Franck–Condon factor could be important in reducing ^3G in the present systems.

(B) *Total and Nonradiative Decay Rates.* $k_z \simeq 16$ s^{-1} is much larger than the sublevel decay rates of the $^3\pi\pi^*$ aromatic hydrocarbons. Thus, the presence of the C=O group must be the cause of the relatively large decay rates. The Boltzmann average of k_z, k_y, and k_x gives a lifetime of ~150 ms. This value is similar to the lifetime of the long-lived xanthone observed by Pownall et al.[47,52] $k_z \gg k_y$, k_x follow the general decay pattern of the $^3\pi\pi^*$ aromatic carbonyls so far investigated. As seen from the values given in Table III, $k_z/k_y \gg k_z^r/k_y^r$. Therefore, k_z should have a large nonradiative decay component as in many other $^3\pi\pi^*$ aromatic carbonyls with relatively large ΔE_{TT}.[46]

In the present xanthone ΔE_{TT} is rather large and the mixing with the $^3n\pi^*$ state is not likely to be important in determining k_z. Therefore, as in the other $^3\pi\pi^*$ aromatic carbonyl with relatively large ΔE_{TT}, spin–orbit mixing with the $^1n\pi^*$ state is considered as the main cause for the nonradiative decay from the z sublevel.[46] However, k_z obtained for xanthone here is much smaller than those obtained for substituted benzaldehydes with the similar value of ΔE_{ST}. In the case of para-substituted benzaldehyde we have obtained $k_z \simeq 50$ s^{-1} for the systems with $\Delta E_{ST} = 2500$ cm^{-1}. Rather small value of k_z in xanthone may also be due to the small value of spin–orbit matrix element, $^1G = \langle ^3\pi\pi^*|\mathcal{H}_{so}|^1n\pi^*\rangle$.

The value of k_y is similar to those of many other $^3\pi\pi^*$ aromatic carbonyls. The mixing with the $^1\sigma\pi^*$, $(^1\pi\sigma^*)$ state is considered to be the main cause of the y sublevel decay as in other aromatic carbonyls.

TABLE IV: ZFS and Decay Properties of the Related Molecules

	ν_{00}, cm^{-1}	ZFS, cm^{-1}		Total decay rate, s^{-1}			Character
		D	E	X	Y	Z	
Xanthone trap (B)	24 882	−0.1103	+0.0186	0.45	1.75	16.0	$^3\pi\pi^*$
4-Aminobenzophenone (DPM)	21 690	−0.0704	+0.0304	1.7		17	$^3\pi\pi^*$
4,4′-Dimethoxybenzophenone	24 470	−0.0965[a]	+0.0321[a]	51		310	$^3n\pi^*$ (?)
Benzophenone[b] (DPM)	23 780	−0.1410	+0.0426	45	42	750	$^3n\pi^*$

[a] Taken from the data by Batley and Bramley (ref 39). [b] ZFS for benzophenone obtained in DPM are somewhat different from those obtained in other hosts; Chan and Schmidt, *Symp. Faraday Soc.*, **3**, 156 (1969); Winscon and Maki, *Chem. Phys. Lett.*, **12**, 264 (1971); Shain and Sharnoff, *J. Chem. Phys.*, **59**, 2335 (1973); Hochstrasser, Scott, and Zewail (ref 40).

The value of k_x is, on the other hand, considerably smaller than those of substituted benzaldehydes. This observation is consistent with the planar structures of xanthone.

(C) $S_1 \rightarrow T_1$ *Intersystem Crossing.* In the case of xanthone in diphenylmethane and 9,10-dihydroanthracene the populating rates represent the relative populating rates via $S_1 \rightarrow T_1$ intersystem crossings. In these systems the general selection rule for the intersystem crossing in $^3\pi\pi^*$ aromatic carbonyls, $P_z \gg P_x, P_y$, also holds.

(D) *Radiative Properties.* While the pattern of the total decay rates from the sublevels of xanthone is similar to those of other $^3\pi\pi^*$ aromatic carbonyls, the radiative properties are quite different from the $^3\pi\pi^*$ aromatic carbonyls of benzaldehyde type. First, the intensity of the 0–0 band is weak. Second, the carbonyl stretching mode is not the prominent vibrational band. In the following we analyze the obtained data based on the C_{2v} symmetry. The direct spin–orbit coupling scheme under C_{2v} symmetry is given in Table V.

(1) *Radiative Decay from the z Sublevel.* There has been much discussion about the radiative mechanisms of the $^3\pi\pi^*$ aromatic carbonyls.[1-3,9,11,13-18,42,44,45] The suggested main mechanisms include spin–orbit mixing with the $^1n\pi^*$ state[9,14] and direct configurational and vibronic mixing with the $^3n\pi^*$ state.[14-16,23,42,45] In the case of aromatic carbonyl of the benzaldehyde type, the following three mechanisms were found to be important, although the relative importance of the different mechanisms depends considerably on the system:[42,45] (a) Spin–orbit mixing with $^1n\pi^*$ state

$$^3\pi\pi^*(T_1^z) \overset{SO}{\longleftrightarrow} {}^1n\pi^*$$

(b) Direct configurational mixing with $^3n\pi^*$ state

$$^3\pi\pi^*(T_1^z) \overset{electr}{\longleftrightarrow} {}^3n\pi^*(T_2^z) \overset{SO}{\longleftrightarrow} {}^1\pi\pi^*(^1A_1)$$

(c) Vibronic mixing with $^3n\pi^*$ state

$$^3\pi\pi^*(T_1^z) \overset{vibr}{\longleftrightarrow} {}^3n\pi^*(T_2^z) \overset{SO}{\longleftrightarrow} {}^1\pi\pi^*(^1A_1)$$

Although part of the z sublevel radiative decay may be due to the above mechanisms, xanthone in the present study is unique in that none of the above mechanisms are the main one for the following reasons.

First, the z sublevel emits only weakly at the 0–0 bands. Hence mechanism a or b cannot be the main one. The importance of mechanism a depends on ΔE_{ST}, ^1G, and the oscillator strength for the $^1n\pi^* \rightarrow S_0$ transition. The importance of mechanism b depends on ΔE_{TT} and the deviation from the planarity which allows the direct mixing of $^3n\pi^*$ and $^3\pi\pi^*$ states. The relatively large ΔE_{TT}, the rigid planar structure of xanthone, and the small value of ^1G are probably factors which are not in favor of mechanisms a and b.

Although the major part of the z sublevel emission is vibronic (Herzberg–Teller mechanisms) mechanism c also cannot be the main one here, since this mechanism is incompatible with the phosphorescence polarization data by Pownall and Huber.[47] These authors found that the polarization of the phosphorescence of the long lived (~120 ms) xanthone triplet state is negatively polarized with respect to the $S_0 \rightarrow {}^1\pi\pi^*(^1A_1)$ absorption at the vibronic bands indicating that the $^1\pi\pi^*(^1A_1)$ state is not the main mixing singlet state. Their work suggests that the main mixing singlet state is likely to be $^1\pi\pi^*(^1B_2)$ state. If this is the case the possible vibronic spin–orbit mechanism should be

$$^3\pi\pi_z^*(^3A_2) \overset{SO}{\longleftrightarrow} {}^1n\pi^*(^1A_2) \overset{vibr(b_1)}{\longleftrightarrow} {}^1\pi\pi^*(^1B_2)$$

The vibrations most active in the vibronic mixing are 290 and 670 cm^{-1}. If the above mechanism is correct these vibrations should be b_1 vibrations.

Thus the radiative property of $^3\pi\pi^*$ xanthone is strikingly different from those of many other $^3\pi\pi^*$ aromatic carbonyls in that both vibronic and configurational mixings between $^3n\pi^*$ and $^3\pi\pi^*$ states are rather ineffective in producing radiative activity of the z sublevel. This is probably because in xanthone the C=O group is rigidly held to the planar ring system and the carbon atoms next to the carbonyl group are fixed to rings.

TABLE V: Routes of Direct Spin–Orbit Coupling (C_{2v} Symmetry)

Triplet states	Spin states and total symmetry	Mixing singlet state and state symmetry
$^3\pi\pi^*(^3A_1)$	$T_z(^3A_2)$	$^1n\pi^*(^1A_2)$
	$T_y(^3B_1)$	$^1\sigma\pi^*(^1B_1)$
	$T_x(^3B_2)$	$^1n\sigma^*(^1B_2)$
$^3n\pi^*(^3A_2)$	$T_z(^3A_1)$	$^1\pi\pi^*(^1A_1)$
	$T_y(^3B_2)$	$^1n\sigma^*(^1B_2)$
	$T_x(^3B_1)$	$^1\sigma\pi^*(^1B_1)$

(2) *y Sublevel Emissions.* The y sublevel emission of the $^3\pi\pi^*$ aromatic carbonyl was ascribed to the direct mixing with the $^1\sigma\pi(^1\pi\sigma^*)$ state.[18,42,46]

$$^3\pi\pi_y^*(^3B_1) \overset{SO}{\longleftrightarrow} {}^1\sigma\pi^*, {}^1\pi\sigma^*(^1B_1)$$

Strong 0–0 and 1660-cm^{-1} bands of the y sublevel emission of xanthone indicate the importance of the direct mechanism and are consistent with the above mechanism. The fact that $k_z^r/k_y^r \sim 1$ at the 0–0 band indicates that direct spin–orbit mixing with the $^1\sigma\pi^*(^1\pi\sigma^*)$ state is at least as effective as that with the $^1n\pi^*$ state in producing radiative decay at the 0–0 band in spite of the large energy difference between $^3\pi\pi^*$ and $^1\sigma\pi^*(^1\pi\sigma^*)$ states.

(3) *x Sublevel Emission.* The emission from the x sublevel is the weakest. k_z^r/k_x^r was found to be ~30. This value is similar to that obtained in the $^3\pi\pi^*$ azaaromatics such as quinoxaline studied by Anteunis et al.[72] The small value of k_x^r is consistent with the planar structure of xanthone in the $^3\pi\pi^*$ state.

(E) *Connection with the Other Related Work.* It is known that xanthone exhibits dual phosphorescence:[47] one short-lived with the lifetime of ~25 ms and the other long-lived with an ~120 ms lifetime. The short-lived one has been considered as arising from the $^3n\pi^*$ state, while the long-lived one appears to originate from the $^3\pi\pi^*$ state. However, it was suggested that the dual emission in rigid media may arise from two different conformations of the $^3n\pi^*$ state.[52] The long-lived ($\tau_p \simeq 120$ ms) species in 3-MP was ascribed to $^3n\pi^*$ state xanthone which has a distorted structure. As we have shown here the long-lived xanthone triplet state observed by Pownall et al. in 3-MP at 2 K is likely to be similar in character to $^3\pi\pi^*$ state xanthone studied here and there seems little doubt about the $^3\pi\pi^*$ assignment to the long-lived xanthone. Our ODMR data also do not support the suggestion that long-lived xanthone has a very distorted structure.

The short-lived xanthone species ($\tau \sim 25$ ms) has a strong emission at the 0–0 band with positive polarization with respect to $S_0 \rightarrow {}^3\pi\pi^*(^1A_1)$ absorption. The phosphorescence spectrum is also characterized by a strong progression of the C=O stretching frequency. These properties have been generally thought of as indications of a $^3n\pi^*$ nature.[1,2] However, it has been shown that these properties also appear in the $^3\pi\pi^*$ carbonyls, if the energy separation between them is small and direct mixing between $^3n\pi^*$ and $^3\pi\pi^*$ states due to distortion from planarity is the main source of the radiative activity.[46] In our xanthone systems the energy separation between the singlet and triplet $n\pi^*$ states was found to be ~1000 cm^{-1}. On the other hand, in the short-lived xanthone triplet state in 3-MP the separation between the T_1 state and $^1n\pi^*$ was estimated to be 1144 cm^{-1} [47] which is still ~150 cm^{-1} larger than the $^1n\pi^*$–$^3n\pi^*$ separation determined in our system. Hence, it is possible that the short-lived species is also a $^3\pi\pi^*$ state with very small ΔE_{TT} (on the order of 100 cm^{-1}). In the $^3\pi\pi^*$ states with such a small ΔE_{TT} the radiative properties may resemble those of the $^3n\pi^*$ states as in the case of numerous $^3\pi\pi^*$ aromatic carbonyls of the benzaldehyde type with relatively small ΔE_{TT}.[42,46] Since the carbonyl group is rigidly held to the planar molecule in xanthone distortion from planarity in $^3n\pi^*$ and $^3\pi\pi^*$ states would be smaller than in benzaldehyde. Nevertheless such a mixing may be significant when ΔE_{TT} is very small. A lifetime of 25 ms is also consistent with the $^3\pi\pi^*$ assignment of the short-lived species. It was found that the total decay rate of a series of $^3\pi\pi^*$ aromatic carbonyl is approximately proportional to $1/\Delta E_{ST}^2$.[46] Since ΔE_{ST} for the short-lived species is about half that for the long-lived xanthone studied here, their lifetime is predicted to be about 25 ms, if a similar correlation between the total decay rate and ΔE_{ST} holds for xanthone.

In summary all spectroscopic data on the short-lived xanthone can be rationalized on the basis of the dominant $^3\pi\pi^*$ character, although we have no direct evidence in favor of such an assignment. When we compare ~25-ms lifetime of xanthone with those of $^3n\pi^*$ benzophenone (~5 ms)[1] and anthrone (2 ms)[13] the lifetime of short-lived xanthone also appears to be in favor of a $^3\pi\pi^*$ assignment.

Acknowledgment. This work was supported in parts by a NSF Institutional Science Development grant. We thank E. T. Harrigan for his help in some measurements. N.H. thanks Professor L. Goodman and his group at Rutgers University for stimulating and useful discussions. The authors are grateful to the referees for their helpful suggestions.

References and Notes

(1) S. P. McGlynn, T. Azumi, and M. Kinoshita, "Molecular Spectroscopy of the Triplet States", Prentice-Hall, Englewood Cliffs, N.J., 1969, Chapter 6.
(2) R. S. Becker, "Theory and Interpretations of Fluorescence and Phosphorescence", Wiley, New York, N.Y., 1969, Chapter 12.
(3) L. Goodman, "Excited States", Vol. 1. E. C. Lim, Ed., Academic Press, New York, N.Y., Chapter 6.
(4) G. Porter and P. Suppan, *Trans. Faraday Soc.*, **60**, 1664 (1965).
(5) R. Shimada and L. Goodman, *J. Chem. Phys.*, **43**, 2027 (1966).
(6) N. C. Yang and S. L. Murov, *J. Chem. Phys.*, **43**, 4358 (1966).
(7) N. C. Yang, D. S. McClure, S. L. Murov, J. J. Houser, and R. Dusenbery, *J. Am. Chem. Soc.*, **89**, 5466 (1967).
(8) R. M. Hochstrasser and T. S. Lin, *J. Chem. Phys.*, **49**, 4928 (1968).
(9) T. Takemura and H. Baba, *Bull Chem. Soc. Jpn.*, **42**, 2756 (1969).
(10) Y. Kanda, J. Stanislaus, and E. C. Lim, *J. Am. Chem. Soc.*, **91**, 1085 (1969).
(11) R. M. Hochstrasser and C. A. Marzzacco, "Molecular Luminescence", E. C. Lim, Ed., W. A. Benjamin, New York, N.Y., p 631.
(12) S. Dym, R. M. Hochstrasser, and M. Shafer, *J. Chem. Phys.*, **48**, 684 (1968).
(13) S. Dym and R. M. Hochstrasser, *J. Chem. Phys.*, **51**, 2458 (1969).
(14) W. A. Case and D. R. Kearns, *J. Chem. Phys.*, **52**, 2175 (1970).
(15) (a) R. Zwarich and L. Goodman, *Chem. Phys. Lett.*, **7**, 609 (1970); (b) M. Koyanagi, R. Zwarich, and L. Goodman, *J. Chem. Phys.*, **56**, 3044 (1972); (c) M. Koyanagi and L. Goodman, *ibid.*, **55**, 2959 (1971); **57**, 1809 (1972); (d) L. Goodman and M. Koyanagi, *Mol. Photochem.*, **4**, 369 (1972).
(16) Y. H. Li and E. C. Lim, *Chem. Phys. Lett.*, **7**, 15 (1970).
(17) G. Fisher, *Mol. Cryst.*, **11**, 85 (1970).
(18) Y. Tanimoto, H. Kobayashi, S. Negakura, and T. Azumi, *Chem. Phys. Lett.*, **16**, 10 (1972).
(19) E. Migirdicyan, *Chem. Phys. Lett.*, **12**, 413 (1973).
(20) M. E. Long and E. C. Lim, *Chem. Phys. Lett.*, 20, 413 (1973).
(21) L. Goodman and M. Koyanagi, *Chem. Phys. Lett.*, **21**, 1 (1973).
(22) O. R. Loufty and J. M. Morris, *Chem. Phys. Lett.*, 22, 584 (1973).
(23) C. R. Jones, D. R. Kearns, and R. M. Wing, *J. Chem. Phys.*, **58**, 1370 (1973).
(24) S. W. Mac and N. Hirota, *Mol. Phys.*, **27**, 327 (1974).
(25) N. Kanamaru, M. E. Long, and E. C. Lim, *Chem. Phys. Lett.*, **26**, 1 (1974).
(26) H. Hayashi and S. Nagakura, *Chem. Phys. Lett.*, **18**, 63 (1973); *Mol. Phys.*, **27**, 969 (1974).
(27) S. J. Sheng and D. M. Hanson, *J. Chem. Phys.*, **60**, 368 (1974).
(28) E. J. Baum, J. K. Wan, and J. N. Pitts, *J. Am. Chem. Soc.*, **88**, 2652 (1966).
(29) N. C. Yang and R. L. Dusenbery, *J. Am. Chem. Soc.*, **90**, 5899 (1968).
(30) P. J. Wagner, M. J. May, A. Haug, and P. R. Graber, *J. Am. Chem. Soc.*, **92**, 5269 (1970).
(31) P. J. Wagner, A. E. Kemppainen, and H. N. Schott, *J. Am. Chem. Soc.*, **95**, 5604 (1973).
(32) A. A. Lamola, *J. Chem. Phys.*, **47**, 4810 (1967).
(33) M. Sharnoff, *Mol. Cryst.*, **5**, 297 (1969).
(34) N. Hirota, *Chem. Phys. Lett.*, **4**, 305 (1969).
(35) A. Nishimura and D. Tinti, *Chem. Phys. Lett.*, **13**, 278 (1972).
(36) A. Nishimura and J. S. Vincent, *Chem. Phys. Lett.*, **13**, 89 (1972).
(37) T. H. Cheng and N. Hirota, *Chem. Phys. Lett.*, **13**, 194 (1972); **14**, 415 (1972).
(38) C. R. Jones, F. Rappano, A. H. Maki, and D. R. Kearns, *Chem. Phys. Lett.*, **13**, 521 (1972).
(39) M. Batley and R. Bramley, *Chem. Phys. Lett.*, **15**, 337 (1972).
(40) R. M. Hochstrasser, G. R. Scott, and A. H. Zewail, *J. Chem. Phys.*, **58**, 873 (1973).
(41) C. R. Jones, D. R. Kearns, and A. H. Maki, *J. Chem. Phys.*, **59**, 873 (1973).
(42) T. H. Cheng and N. Hirota, *Mol. Phys.*, **27**, 281 (1974).
(43) S. W. Mac and N. Hirota, *Mol. Phys.*, **27**, 309 (1974).
(44) M. A. Souto, P. J. Wagner, and M. A. El-Sayed, *Chem. Phys.*, **6**, 204 (1974).
(45) E. T. Harrigan and N. Hirota, *Chem. Phys. Lett.*, **27**, 405 (1974); *Mol. Phys.*, **31**, 681 (1976).
(46) E. T. Harrigan and N. Hirota, *Mol. Phys.*, **31**, 663 (1976).
(47) H. J. Pownall and J. R. Huber, *J. Am. Chem. Soc.*, **93**, 6429 (1971).
(48) P. Gacoin and Y. Mayer, *C. R. Acad. Sci. Paris*, **267**, 149 (1968).
(49) R. N. Griffin, *Photochem. Photobiol.*, **7**, 157 (1968).
(50) N. Y. C. Chu and D. R. Kearns, *J. Am. Chem. Soc.*, **94**, 2619 (1972).
(51) Y. Tanimoto, N. Hirota, and S. Nagakura, *Bull. Chem. Soc. Jpn.*, **48**, 41 (1975).
(52) H. J. Pownall, R. E. Conners, and J. R. Huber, *Chem. Phys. Lett.*, **22**, 403 (1973).
(53) T. H. Cheng and N. Hirota, *J. Chem. Phys.*, **56**, 5019 (1972).
(54) J. Schmidt, D. A. Antheunis, and J. H. van der Waals, *Mol. Phys.*, **22**, 1 (1971).
(55) J. Schmidt, Thesis, Leiden, 1972.

(56) A. L. Kwiram, *Phys. Chem., Ser. One., 1972–1973,* **4** (1972).
(57) M. A. El-Sayed, D. V. Owens, and D. S. Tinti, *Chem. Phys. Lett.*, **6**, 395 (1970).
(58) C. R. Chen and M. A. El-Sayed, *Chem. Phys. Lett.*, **10**, 307 (1971).
(59) A. H. Francis and C. B. Harris, *J. Chem. Phys.*, **57**, 1050 (1972).
(60) C. B. Harris, *J. Chem. Phys.*, **54**, 972 (1972).
(61) D. S. Schweitzer, J. Zuclich, and A. H. Maki, *Mol. Phys.*, **25**, 193 (1973).
(62) The attempts to obtain sublevel phosphorescence spectra of other systems have been reported recently. (a) S. Yamauchi and T. Azumi, *Chem. Phys. Lett.*, **21**, 603 (1973); (b) N. Nishi and M. Kinoshita, *ibid.*, **27**, 342 (1974).
(63) W. Rothman, A. Case, and D. R. Kearns, *J. Chem. Phys.*, **43**, 1067 (1965).
(64) N. Hirota, *J. Chem. Phys.*, **44**, 2199 (1966).
(65) N. Hirota, unpublished observation.
(66) The line width for this transition was found to be broad (~0.1 GHz). Accordingly this transition frequency has considerable uncertainty.
(67) R. M. Hochstrasser and G. J. Small, *J. Chem. Phys.*, **45**, 2270 (1966); **48**, 3612 (1968).
(68) R. E. Gerkin and A. M. Winer, *J. Chem. Phys.*, **47**, 504 (1967).
(69) E. T. Harrigan and N. Hirota, *J. Chem. Phys.*, **49**, 2301 (1968).
(70) G. Fisher, *Mol. Cryst.*, **11**, 85 (1976).
(71) H. Hayashi and S. Nagakura, *Mol. Phys.*, **24**, 801 (1972).
(72) D. A. Antheunis, J. Schmidt, and J. H. van der Waals, *Mol. Phys.*, **27**, 1571 (1974).

Electron Spin Resonance and Kinetic Studies on the Liquid-Phase Autoxidation of Tetralin with Lead Dioxide

Shun-ichi Fukuzumi and Yoshio Ono*

Department of Chemical Engineering, Tokyo Institute of Technology, Ookayama, Meguro-ku, Tokyo, Japan *(Received August 16, 1976)*

Publication costs assisted by the Tokyo Institute of Technology

The autoxidation of tetralin with lead dioxide has been studied at 291–323 K. The application of electron spin resonance (ESR) to this reaction has enabled the tetralin peroxy radical (a chain propagating agent) to be detected during the reaction. By measuring simultaneously the concentration of tetralin peroxy radical and the rate of oxygen absorption, the rate expressions for both the radical concentration and oxygen absorption have been determined under the same conditions. A reaction mechanism has been proposed such that the chain initiation involves the formation of the peroxy radical from the hydroperoxide over the catalyst surface and their desorption into the homogeneous phase, where the chain propagation and the chain termination proceed. The simultaneous measurements of the radical concentration and the rate of oxygen absorption have made the accurate determination of the absolute rate constants of the propagation and the termination possible.

Introduction

The oxidation of organic compounds is usually carried out in the gaseous phase with heterogeneous catalysts or in the liquid phase with homogeneous catalysts. Recently, however, the autoxidation of liquid hydrocarbons with heterogeneous catalysts has been studied by several investigators.[1-11] In our previous works,[9-11] we have studied the autoxidation of cumene as well as the decomposition of cumene hydroperoxide with lead dioxide and the application of electron spin resonance (ESR) to these reactions has enabled cumylperoxy radical (a chain propagating agent) to be detected in the reactant solutions. The ESR and kinetic results have lead to the conclusion that the autoxidation of cumene with lead dioxide is a radical chain reaction in which the chain initiation involves the formation of cumylperoxy radicals by the decomposition of the hydroperoxide over the catalyst surface and their desorption into the homogeneous phase, where the chain propagation and the chain termination proceed.[9] The termination process has been considered to be the first-order decay of cumylperoxy radicals.[10]

However, with regard to primary or secondary hydrocarbons, the autoxidation with heterogeneous catalysts has not been studied as extensively as that of the tertiaries, such as cumene, although the autoxidation with homogeneous catalysts has been studied extensively, especially in the case of tetralin,[12-16] which is a typical secondary hydrocarbon. The autoxidation of tetralin with manganese dioxide has been considered to be a radical chain reaction,[8] but the reaction mechanism has not been elucidated in detail and the presence of peroxy radical has not been confirmed so far either.

In the present work, we have studied the autoxidation of tetralin with lead dioxide by measuring both the concentration of tetralin peroxy radical with ESR and the rate of oxygen absorption and by examining the product distribution. A reaction mechanism, composed of elementary reactions analogous to those proposed in the autoxidation of cumene with lead dioxide[9] except for the termination step, will be proposed. The absolute rate constants and the Arrhenius parameters for the propagation and the termination reactions can be determined directly by measuring the radical concentration and the rate of oxygen absorption simultaneously.

Experimental Section

Materials. Tetralin (reagent grade), obtained from commercial sources, was distilled and percolated through an activated aluminum column prior to use. The surface area of

lead dioxide, obtained from Maeda Chemicals, was 17.6 m^2/g as determined by the BET method.

Apparatus. The apparatus has been described in detail elsewhere.[9,11] The autoxidation of tetralin with lead dioxide was carried out in a standard sample tube (0.8 cm i.d.) placed in an ESR cavity at 291 K. Oxygen gas was bubbled through the solution by use of a capillary inserted in the sample tube in order to put the catalyst powder in a uniformly suspended state. On adding lead dioxide powder to the tetralin solution using CCl_4 as a diluent, the ESR signal was registered with use of a JEOL-X-band spectrometer (JEOL-PE-1X) with 100-kHz magnetic modulation. The radical concentration was determined by comparing the absorption area of the radical and that of 1,1-diphenyl-2-picrylhydrazyl (DPPH) in benzene.

The simultaneous measurements of both the radical concentration and the rate of oxygen absorption were also carried out at 291–323 K, as follows. The autoxidation reaction was carried out in a 50- or 100-cm^3 flask immersed in a temperature-controlled bath, the solution was stirred magnetically, and the flash was attached to a wet-gasometer with which the rate of oxygen absorption was measured. At the same time, the part of the solution involving the catalyst powder was circulated with use of a roller pump through the ESR cavity. The intensity of the ESR signal was confirmed to be independent of the circulating rate over a range of 50–200 cm^3/min.

Analytical Procedure. The concentrations of the hydroperoxides and the other products were determined as follows. When the reaction was stopped, the solution involving the catalyst powder was filtered immediately and then part of the sample was titrated for hydroperoxide by the iodometric method.[17] Then, part of the filtered solution was treated with a sufficient amount of triphenylphosphine to convert the hydroperoxide into tetralol quantitatively.[18] The treated sample was then analyzed for tetralol and tetralone by chromatographic methods.

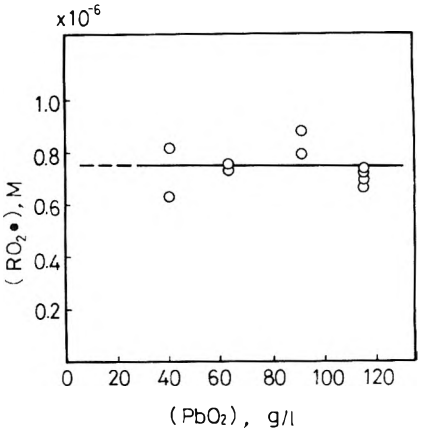

Figure 1. Steady concentration of tetralin percxy radical as a function of initial catalyst weight-to-liquid volume ratio for the autoxidation of tetralin with lead dioxide at 291 K.

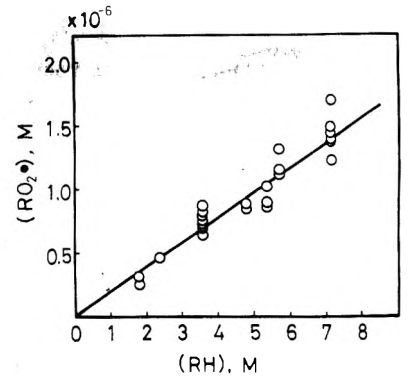

Figure 2. Steady concentration of tetralin peroxy radical as a function of initial concentration of tetralin for the autoxidation of tetralin with lead dioxide at 291 K.

Results

Steady Concentration of Tetralin Peroxy Radical. When lead dioxide powder was added to the tetralin solution, the ESR spectrum of tetralin peroxy radical was observed at 291 K. The ESR spectrum consisted of a symmetric single line with no detectable hyperfine structure; the isotropic g factor of 2.0149 ± 0.0002 is in good agreement with the literature values.[19-21] The line width (ΔH_{msl}, distance between points of maximum slope) was 0.98 ± 0.03 mT. No ESR signal was observed unless lead dioxide powder was added to a tetralin solution. The concentration of tetralin peroxy radical was almost constant with reaction time for several hours. The effects of the concentration of tetralin and the catalyst weight-to-liquid volume ratio on the steady radical concentration were investigated at 291 K. The radical concentration was found to be independent of the catalyst weight-to-liquid volume ratio over a range of 40–120 g/l. and to be proportional to the concentration of tetralin, as shown in Figures 1 and 2, respectively, and eq 1:

$$[RO_{2}\cdot] = k_a[RH][PbO_2]_0 \quad (1)$$

where k_a is the constant at 291 K as (2.33 ± 0.04) × 10^{-7} l./g.

Rate of Oxygen Absorption. The absorption of oxygen is observed when lead dioxide powder is added to a tetralin solution and the rate of oxygen absorption was constant with time for several hours. The absorption of oxygen did not occur unless lead dioxide powder was added to a tetralin solution. The effects of the catalyst weight-to-liquid volume ratio and the tetralin concentration on the steady rate of oxygen absorption were investigated at 291 K. Figure 3 shows the relation between the steady rate of oxygen absorption and the catalyst ratio for various concentrations of tetralin. Like the radical concentration, the rate of oxygen absorption is found to be independent of the catalyst ratio over the same range in Figure 1. In Figure 4, the square root of the rate of oxygen absorption is plotted against the initial concentration of tetralin. The square root of the rate of oxygen absorption is found to be proportional to the tetralin concentration. Thus, the rate of oxygen absorption is expressed as:

$$-(d[O_2]/dt) = k_b[RH]^2[PbO_2]_0 \quad (2)$$

where k_b is the constant as (5.40 ± 0.10) × 10^{-7} $l.^2\,g^{-1}\,mol^{-1}\,s^{-1}$ at 291 K, and [RH] is the initial concentration of tetralin which is almost constant during the reaction because of low conversion in our experimental conditions.

Effect of Temperature on Radical Concentration and on Rate of Oxygen Absorption. The simultaneous measurements of the radical concentration and the rate of oxygen absorption were carried out in the temperature range of 291–323 K. The results are shown in Figure 5. In each case, experiments were started with the same initial hydroperoxide and tetralin concentrations and the same catalyst weight-to-liquid volume ratio. By assuming the same kinetics as in eq 1 and 2 are op-

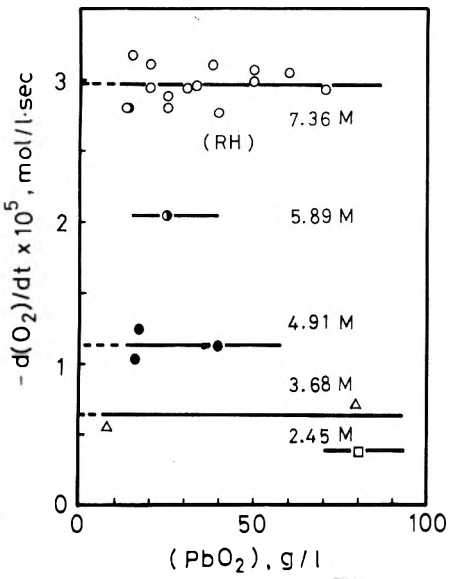

Figure 3. Rate of oxygen absorbed as a function of initial catalyst weight-to-liquid volume ratio for different initial concentrations of tetralin at 291 K.

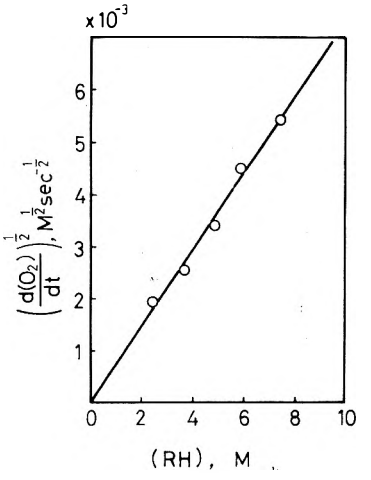

Figure 4. Square root of rate of oxygen absorbed plotted against initial concentration of tetralin at 291 K.

erative throughout the temperature range, the activation energies for k_a and k_b were determined as 0.0 and 23 kJ/mol, respectively.

Hydroperoxide Concentration during the Reaction. The concentrations of tetralin hydroperoxide during the reaction were determined at various reaction times at 291 K. The hydroperoxide concentration was almost constant with time for several 10-min periods. The steady concentration of the hydroperoxide during the reaction was found to be independent of the initial concentration of the hydroperoxide added before the reaction. These results are the same as those obtained in the autoxidation of cumene reported previously.[9] The effects of the tetralin concentration and the catalyst weight-to-liquid volume ratio on the steady hydroperoxide concentration were investigated at 291 K. The results are summarized in Figure 6 where the steady hydroperoxide concentration is plotted against $[RH]^2/[PbO_2]$. The steady hydroperoxide concentration is found to be proportional to the square of tetralin concentration and inversely proportional to the catalyst ratio. Then, the steady concentration of tetralin hydroperoxide during the reaction is expressed as:

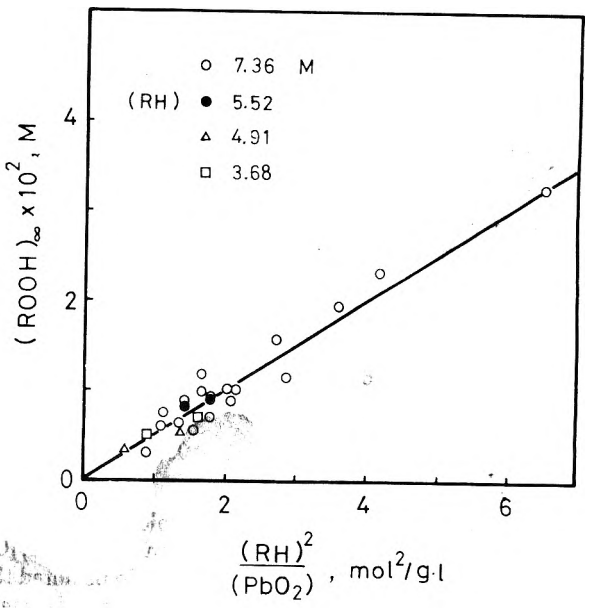

Figure 5. Steady concentration of tetralin hydroperoxide plotted against $[RH]^2/[PbO_2]$ at 291 K.

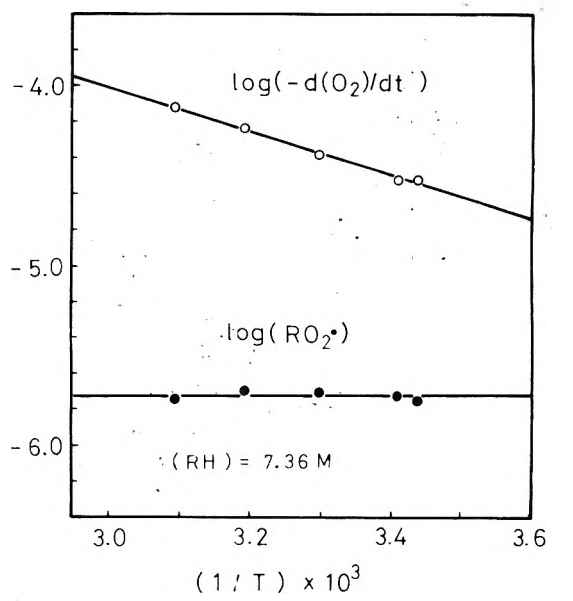

Figure 6. Arrhenius plots of the rate of oxygen absorbed and the steady concentration of tetralin peroxy radical.

$$[ROOH]_\infty = k_c[RH]^2/[PbO_2] \quad (3)$$

where k_c is the constant as 5.0×10^{-3} g/mol.

Product Distribution. The product distribution for the autoxidation of tetralin with lead dioxide was investigated at 291 K. The results are summarized in Table I, where the amount of oxygen absorption is also presented. The reaction products are found to be tetralol and tetralone as well as the hydroperoxide. The yield of tetralol is always greater than that of tetralone, irrespective of the catalyst weight-to-liquid volume ratio and the concentration of tetralin. Then, the ratio of tetralol to tetralone can be denoted as:

$$[ROH]/[R'C{=}O] = 1 + \alpha \quad (4)$$

The value of α, given in Table I as 0.72 ± 0.04, is almost constant, irrespective of the catalyst ratio and the tetralin con-

TABLE I: Product Distribution of Tetralin Oxidation with Lead Dioxide

$[RH]_0$, M	$[PbO_2]_0$, g/l.	[ROH], M	[R′C=O], M	$[O_2]$, mol/l.	([ROH] + [R′C=O])/$[O_2]$	α
7.36	71	0.151	0.086	0.144	1.64	0.76
7.36	60	0.065	0.035	0.051	1.96	0.86
7.36	51	0.158	0.084	0.144	1.68	0.88
7.36	50	0.250	0.150	0.255	1.56	0.68
7.36	40	0.045	0.024	0.038	1.82	0.88
7.36	33	0.108	0.068	0.070	2.52	0.60
7.36	25	0.156	0.105	0.143	1.82	0.50
5.88	25	0.131	0.080	0.089	2.38	0.64
4.91	67	0.071	0.040	0.056	1.98	0.78
4.91	40	0.060	0.033	0.043	2.16	0.82
3.68	80	0.068	0.040	0.053	2.04	0.70
2.45	80	0.058	0.037	0.052	1.82	0.58

centration. The ratio of the sum of tetralol and tetralone, [ROH] + [R′C=O], to the amount of oxygen absorption, $[O_2]$, is 2.0 (mean value) as seen in Table I. It should be noted that the ratio is the same as that of the concentration of dimethylphenylcarbinol to the amount of oxygen absorption in the autoxidation of cumene with lead dioxide.[9]

Discussion

Reaction Mechanism. From eq 1 and 2, the relation between the rate of oxygen absorption and the concentration of tetralin peroxy radical is given as:

$$-(d[O_2]/dt) = k_c[RH][RO_2\cdot] \quad (5)$$

where k_c is equal to k_t/k_a. Equation 5 indicates that the following chain propagation reactions proceed (eq 6 and 7) by which oxygen is absorbed.

$$RO_2\cdot + RH \xrightarrow{k_3} ROOH + R\cdot \quad (6)$$

$$R\cdot + O_2 \xrightarrow{k_4} RO_2\cdot \quad (7)$$

As in the previous study on the autoxidation of cumene with lead dioxide,[9] it can be well assumed that the initiation step of the autoxidation is the formation of peroxy radicals from the hydroperoxide decomposition on the catalyst surface. The propagation steps are given as eq 6 and 7, described above. As far as the termination step with regard to a secondary hydrocarbon such as tetralin is considered, the following bimolecular termination of secondary peroxy radicals which have an α hydrogen has frequently been postulated in the past:[22]

$$2R_2CHOO\cdot \rightleftharpoons (R_2CHOOOOHCR_2) \rightarrow R_2CHOH + R_2C{=}O + O_2 \quad (8)$$

The self-reaction of secondary peroxy radicals proceeds through a tetroxide intermediate and yields alcohol, ketone, and oxygen. Though the presence of a tetroxide intermediate has been confirmed in the self-reaction of secondary peroxy radicals, as well as in the reactions of the tertiaries,[22] there have been reported two different mechanisms for the formation of alcohol, ketone, and oxygen,[23] as discussed below.

(A) The self-reaction of secondary peroxy radicals proceeds via a highly oriented tetroxide decomposing through a cyclic transition state, a process first advanced by Russell,[24] which is not available to the tertiaries.

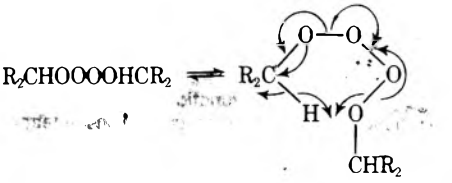

$$\rightarrow R_2CHOH + R_2C{=}O + O_2 \quad (9)$$

(B) The self-reaction of secondary peroxy radicals gives two secondary alkoxy raicals followed by their rapid disproportionation while still in the solvent cage, which is analogous to the case of the tertiaries:[25,26]

$$R_2CHOOOOHCR_2 \rightleftharpoons (R_2CHO\cdot + O_2 + \cdot OHCR_2)_{cage} \rightarrow R_2CHOH + R_2C{=}O + O_2 \quad (10)$$

According to the Russell mechanism (A), the self-reaction of the peroxy radicals should yield equal amounts of alcohol and ketone, while, according to mechanism B, a certain fraction of the alkoxy radicals may escape from the cage and more alcohol will be formed than ketone via the following reaction:

$$RO\cdot + ROOH \rightarrow ROH + RO_2\cdot \quad (11)$$

In the present case, a greater amount of tetralol than tetralone was formed and the ratio of tetralol to tetralone was constant, irrespective of the catalyst weight-to-liquid volume ratio and the tetralin concentration, as seen in Table I. Similar results (that more alcohol is formed than ketone) have been obtained in the studies on pulse radiolysis of cyclohexane saturated with oxygen[27-30] and on the decomposition of cyclohexenyl hydroperoxide in cyclohexene with manganese dioxide.[31] Thus, it is concluded in the present case that the termination step is the self-reaction of tetralin peroxy radicals which proceeds via mechanism B. The Arrhenius parameters for the rate of the self-reaction of the peroxy radicals determined in this study also indicate that mechanism B is operative in the present case, as will be discussed later.

On the basis of the above discussion, the whole reaction mechanism can be written as shown in eq 12–17.

Initiation

$$ROOH + PbO_2 \xrightarrow{R_i} RO_2\cdot \quad (12)$$

Propagation

$$RO_2\cdot + RH \xrightarrow{k_3} R\cdot + ROOH \quad (13)$$

$$R\cdot + O_2 \xrightarrow{k_4} RO_2\cdot \quad (14)$$

$$RO\cdot + ROOH \xrightarrow{k_5} ROH + RO_2\cdot \quad (15)$$

$$RO_2\cdot + RO_2\cdot \xrightarrow{k_{6p}} 2RO\cdot + O_2 \quad (16)$$

Termination

$$RO_2\cdot + RO_2\cdot \xrightarrow{k_{6d}} ROH + R'C{=}O + O_2 \quad (17)$$

Here, we have denoted the rate of the hydroperoxide decomposition on the solid surface by R_i. Tetralin peroxy radicals are formed by the decomposition of the hydroperoxide on the catalyst surface and desorb into the homogeneous phase (eq 12), where the chain propagation (eq 13–16) and the chain termination (eq 17) proceed. According to this mechanism, the following rate equations will be given:

$$-(d[O_2]/dt) = k_4[R\cdot][O_2] - k_6[RO_2\cdot]^2 \quad (18)$$

$$(d[ROOH]/dt) = k_3[RO_2\cdot][RH] + R_i - k_5[RO\cdot][ROOH] \quad (19)$$

where $k_6 = k_{6p} + k_{6t}$. Applying the steady-state approximation with respect to $[RO_2\cdot]$ and $[R\cdot]$, eq 19 can be rewritten as:

$$(d[ROOH]/dt) = k_3[RO_2\cdot][RH] - 2k_6[RO_2\cdot]^2 \quad (20)$$

The concentration of the hydroperoxide during the reaction was found to be steady. Then:

$$(d[ROOH]/dt) = 0 \quad (21)$$

From eq 20 and 21, the steady concentration of tetralin peroxy radical is given as:

$$[RO_2\cdot] = k_3[RH]/2k_6 \quad (22)$$

Equation 22 is consistent with the experimental observations that the radical concentration is proportional to the tetralin concentration but independent of the catalyst weight-to-liquid volume ratio, eq 1. The rate of oxygen absorption, eq 18, can be rewritten as follows using eq 22:

$$-(d[O_2]/dt) = k_3[RO_2\cdot][RH] - k_6[RO_2\cdot]^2 = k_3^2[RH]^2/4k_6 \quad (23)$$

Equation 23 also agrees with the experimental observations that the rate of oxygen absorption is proportional to the square of [RH] and independent of the $[PbO_2]$, eq 2.

Product Distribution. The proposed reaction mechanism can also explain the product distribution. The reaction products were tetralol and tetralone as well as the hydroperoxide, and the ratio of tetralol to tetralone, eq 4, was constant at 1.72, irrespective of $[PbO_2]$ and [RH]. According to our reaction mechanism, the free alkoxy radicals which escape from the cage, eq 16, react with the hydroperoxide, eq 15, to yield more tetralol than tetralone. With steady-state approximation with respect to $[RO\cdot]$, the rate of the formation of tetralol and tetralone is given as:

$$(d[ROH]/dt) = k_{6t}[RO_2\cdot]^2 + k_5[RO\cdot][ROOH] = (k_{6t} + 2k_{6p})[RO_2\cdot]^2 \quad (24)$$

$$(d[R'C{=}O]/dt) = k_{6t}[RO_2\cdot]^2 \quad (25)$$

From eq 24 and 25, one obtains the ratio of tetralol to tetralone:

$$(d[ROH]/d[R'C{=}O]) = 1 + 2(k_{6p}/k_{6t}) \quad (26)$$

Equation 26 agrees with the experimental observations that the ratio of tetralol to tetralone is greater than 1, and is independent of $[PbO_2]$ and [RH], eq 4. Comparing eq 26 with the experimental one (eq 4), one obtains:

$$\alpha = 2k_{6p}/k_{6t} \quad (27)$$

From eq 22 and 23, the rate of oxygen absorption is rewritten as:

$$(d[O_2]/dt) = k_6[RO_2\cdot]^2 \quad (28)$$

Then, from eq 24, 25, and 27, eq 29 is obtained. Equation 29 also agrees with the experimental observations in Table I that the ratio of [ROH] + [R'C=O] to $[O_2]$ is 2.0.

$$d([ROH] + [R'C{=}O])/-d[O_2] = 2 \quad (29)$$

Using eq 22, the rate of the hydroperoxide formation, eq 19, can be rewritten as:

$$(d[ROOH]/dt) = (k_3^2k_{6t}/2k_6^2)[RH]^2 - R_i \quad (30)$$

It is well assumed that the rate of the hydroperoxide decomposition on the solid surface, R_i, can be expressed as a function of $[PbO_2]$ and [ROOH] as follows:

$$R_i = k_1[ROOH][PbO_2] \quad (31)$$

where k_1 is the rate constant. Then, from eq 21, 30, and 31, the steady concentration of the hydroperoxide during the reaction is given as:

$$[ROOH]_\infty = \frac{k_3^2k_{6t}}{2k_6^2k_1}\frac{[RH]^2}{[PbO_2]} \quad (32)$$

Equation 32 is also consistent with the experimental observations in Figure 6 that the steady hydroperoxide concentration is proportional to the square of the tetralin concentration and inversely proportional to the catalyst ratio.

Absolute Rate Constants for Tetralin Oxidation. The elementary reactions involved in the autoxidation of hydrocarbons have received considerable attention and the values of the rate constants for the elementary reactions have been reported.[23] In order to elucidate the reaction mechanism for the elementary reactions, more precise values of "absolute" rate constants and their temperature coefficients under various experimental conditions are required. In the present study, the simultaneous measurements of the concentration of tetralin peroxy radical and the rate of oxygen absorption have permitted easy and direct evaluation of the absolute rate constants for the autoxidation of tetralin. Comparing the experimental observations, eq 1 and 2, with eq 22 and 23, one obtains the values of the propagation rate constant, k_3, and the self-reaction of the peroxy radicals, k_6, at 291 K as:

$$k_3 = 2k_b/k_a = 4.6 \pm 0.2\ M^{-1}\ s^{-1} \quad (33)$$

$$2k_6 = 2k_b/k_a^2 = (2.0 \pm 0.1) \times 10^7\ M^{-1}\ s^{-1} \quad (34)$$

From eq 27, 33, and the value of α in Table I, one obtains the values of the termination rate constant k_{6t} and the rate constant k_{6p} at 291 K given in eq 35 and 36.

$$2k_{6t} = 2(1 + \alpha/2)^{-1}k_6 = (1.5 \pm 0.2) \times 10^7\ M^{-1}\ s^{-1} \quad (35)$$

$$2k_{6p} = 2(1 + 2/\alpha)^{-1}k_6 = (5.3 \pm 0.8) \times 10^6\ M^{-1}\ s^{-1} \quad (36)$$

The apparent activation energy for k_a and k_b obtained from

TABLE II: Activation Parameters for Tetralin Oxidation

Log $A_3/M^{-1}\ s^{-1}$	E_3, kJ/mol	Log $2A_6/M^{-1}\ s^{-1}$	E_6, kJ/mol	Ref
4.74	23	11.3	23	This study
4.4	19	7.6	1.7	28
6.75	35	9.6	18	29
		10.0	19 ± 4	30
5.3[a]	30[a]	10.9[a]	30[a]	9

[a] Activation parameters for cumene oxidation determined by the same method.

Figure 5 leads to the activation parameters of the propagation rate constant, k_3, and the self-reaction of tetralin peroxy radical, k_6. The values are shown in Table II, together with the literature values.[28-30] The reported literature values of E_3 were determined from the relation[23] $E_3 = E_O - (1/2)E_i + (1/2)E_6$, where E_O is the overall activation energy and E_i is the activation energy for chain initiation, and vary over a wide range of 19–35 kJ/mol. The reported values of E_3 were considered to be inaccurate because they should reflect the errors involved in the various methods[23] used to determine E_6, E_i, and E_O. In this study, the activation parameters of k_3 and k_6 have been determined directly under the same conditions as described above.

The parameters in the autoxidation of cumene are also listed in Table II. It should be noted that the frequency factors for the self-reaction of tetralin peroxy radicals and cumylperoxy radicals are quite similar. This suggests that the mechanism of the self-reaction of teralin peroxy radicals is the same as that of cumylperoxy radicals. Thus, it is concluded that mechanism B, not mechanism A, is also operative for the self-reaction of tetralin peroxy radicals.

Acknowledgment. We wish to thank Professor T. Keii for helpful discussions.

References and Notes

(1) C. Meyer, G. Clement, and J. C. Balaceanu, *Proc. Int. Congr. Catal., 3rd, 1964*, **1**, 134 (1965).
(2) Ya. B. Gorokhovatsky, "Catalysis", Vol. 2, J. W. Hightower, Ed., North-Holland/American Elsevier, New York, N.Y., 1973, p 879.
(3) Ya. B. Gorokhovatsky, N. P. Evmenenko, M. V. Kost, and V. A. Khishnyi, *Teor. Eksp. Khim.*, **9**, 373 (1973).
(4) A. D. Breugdenhil, *J. Catal.*, **28**, 493 (1973).
(5) H. J. Neubrug, M. J. Phillips, and W. F. Graydon, *J. Catal.*, **38**, 33 (1975).
(6) A. J. Caloyannis and W. F. Graydon, *J. Catal.*, **22**, 287 (1972).
(7) G. R. Varma and W. F. Graydon, *J. Catal.*, **28**, 236 (1973).
(8) A. Mukhejee and W. F. Graydon, *J. Phys. Chem.*, **71**, 4232 (1967).
(9) S. Fukuzumi and Y. Ono, *J. Chem. Soc., Perkin Trans. 2*, in press.
(10) S. Fukuzumi and Y. Ono, *J. Chem. Soc., Perkin Trans. 2*, in press.
(11) S. Fukuzumi and Y. Ono, *J. Chem. Soc.,, Perkin Trans. 2*, in press.
(12) K. Kamiya, S. Beaton, A. Lafortune, and K. U. Ingold, *Can. J. Chem.*, **41**, 2020 (1963).
(13) Y. Kamiya, S. Beaton, A. Lafortune, and K. U. Ingold, *Can. J. Chem.*, **41**, 2034 (1963).
(14) Y. Kamiya and K. U. Ingold, *Can. J. Chem.*, **42**, 1027 (1964).
(15) Y. Kamiya and K. U. Ingold, *Can. J. Chem.*, **42**, 2424 (1964).
(16) A. E. Woodward and R. B. Mesrobian, *J. Am. Chem. Soc.*, **75**, 6189 (1953).
(17) R. D. Mair and A. J. Graupner, *Anal. Chem.*, **36**, 194 (1964).
(18) R. U. Sneeringer and V. I. Steuberg, *Anal. Lett.*, **4**(8), 485 (1971).
(19) K. U. Ingold and J. R. Morton, *J. Am. Chem. Soc.*, **86**, 3400 (1964).
(20) J. E. Bennet and R. Summers, *J. Chem. Soc. Faraday Trans. 1*, **10**, 1043 (1973).
(21) M. Melamud, S. Schlick, and B. L. Silver, *J. Magn. Reson.*, **14**, 104 (1974).
(22) J. A. Howard, *Adv. Free Radical Chem.*, **4**, 49 (1972).
(23) D. F. Bowaman, T. Gillan, and K. U. Ingold, *J. Am. Chem. Soc.*, **93**, 6555 (1971).
(24) G. A. Russell, *J. Am. Chem. Soc.*, **79**, 3871 (1957).
(25) R. Hiatt and S. Szilagyi, *Can. J. Chem.*, **48**, 615 (1970).
(26) R. Hiatt and L. Zigmund, *Can. J. Chem.*, **48**, 3967 (1970).
(27) R. Blaekburn and A. Charlesby, *Trans. Faraday Soc.*, **62**, 1159 (1966).
(28) W. A. Cramer, *J. Phys. Chem.*, **71**, 1171 (1967).
(29) C. F. Lowever, *J. Phys. Chem.*, **71**, 1112 (1967).
(30) A. Maclachlan, *J. Am. Chem. Soc.*, **81**, 960 (1965).
(31) H. J. Neuburg, M. J. Phillips, and W. F. Graydon, *J. Catal.*, **33**, 355 (1974).

Kinetics and Mechanism of Oxidation of Quinols by Hexachloroiridate(IV) in Aqueous Acidic Perchlorate Media

Ezio Pelizzetti,* Edoardo Mentasti, and Claudio Baiocchi

Istituto di Chimica Analitica dell'Università, 10125 Torino, Italy *(Received March 16, 1976; Revised Manuscript Received September 15, 1976)*

Publication costs assisted by the Consiglio Nazionale delle Ricerche, Rome, Italy

The kinetics and mechanism of oxidation of a series of quinols with hexachloroiridate(IV) have been investigated by means of a stopped-flow technique. The reaction rate showed first-order dependence on both reactants and a small effect of acidity and temperature was assessed. The data are in agreement with the Marcus theory, and a reorganizational parameter, λ, of 26 kcal mol^{-1} is derived; this value supports that the rate-determining step is a simple electron transfer. The intrinsic and extrinsic parameters for the oxidation of this class of reversible redox organic systems have been estimated.

Introduction

Relationships between free energies of activation and the corresponding free energies of reaction have provided useful information in the elucidation of redox reaction mechanisms.[1] A successful quantitative treatment has been achieved but confined almost entirely to reactions involving metal-ion complexes. In this laboratory the possibility of extension of similar relationships to organic redox systems in aqueous solution, when reacting with oxidizing aquometal ions (Mn(III), Co(III), Fe(III), Tl(III), V(V)),[2] has been investigated. Owing to the interest of such organic systems, the reactions of a series of substituted quinols with hexachloroiridate(IV) have been investigated. In such systems, the interactions between the reactive centers are probably small (outer-sphere mechanism) so that examination of the collected data can suggest useful criteria to distinguish between different possible mechanisms, such as electron-transfer or hydrogen atom transfer.

Experimental Section

Reagents. Sodium hexachloroiridate(IV) was supplied by Merck and the spectrum of fresh solutions agreed with literature data.[3] The quinols (K & K or Merck) were purified, when necessary, by recrystallization and the solutions were prepared daily. The following quinols have been investigated: benzene-1,4-diol (**1**), 2-methylbenzene-1,4-diol (**2**), 2-chlorobenzene-1,4-diol (**3**), 2,5-dihydroxybenzoic acid (**4**), 2,5-dihydroxybenzenesulphonic acid (**5**), 2,5-dihydroxy-1,4-disulphonic acid (**6**), 2,3-dicyanobenzene-1,4-diol (**7**).

Procedure. The reactions were followed with a Durrum-Gibson stopped-flow spectrophotometer at λ 487 nm ($\epsilon_{Ir(IV)}$ 4070 M^{-1} cm^{-1}).[3] Kinetic runs were performed with [Ir(IV)] = 1.0×10^{-5} M and excess organic substrate in the range $1.0\text{–}20 \times 10^{-4}$ M. Measurements were carried out at [$HClO_4$] = 1.00 M, μ = 1.0 M, and at different temperatures. Other measurements were performed at [$HClO_4$] = 0.50 M (μ = 1.0 M with $LiClO_4$ addition) and the observed rate constants showed very slight differences.

A series of kinetic runs was also carried out in the presence of sodium hexachloroiridate(III) in concentration of up to 12 times the initial concentration of Ir(IV); no kinetic effect was observed, thus the effect of any reverse reaction effect was neglected.

The rate constants were evaluated with a weighted least-squares method (based on the deviation of the single points of each run) and the other kinetic parameters were derived by assigning the weights on the basis of standard deviations.

The formal reduction potentials, E^0, of the couples quinone|quinol, for the different derivatives, were evaluated with a Metrohm E388 potentiometer, equipped with a saturated KCl–calomel electrode (saturated NaCl bridge) and a platinum electrode. A solution of quinol derivative, at [$HClO_4$] = 1.00 M, μ = 1.0 M, and 25.0 °C, was partially oxidized (25, 50, 75%) by addition of thallium(III) perchlorate (which rapidly reacts with 1:1 stoichiometry, giving the corresponding quinone),[4] and the formal potentials (compared with quinol value, 0.699 V)[5] were estimated from the emf readings.

Results

Potentiometric Data. The following reduction formal potentials were determined (literature data are reported in parentheses, when available):[5] **2**, 0.644 (0.645); **3**, 0.712 (0.712); **4**, 0.769; **5**, 0.787; **6**, 0.851; **7**, 0.910 (0.971) V.

Stoichiometry. By means of spectrophotometric measurements with Ir(IV) in excess, the following overall equation has been derived

$$2Ir(IV) + H_2Q \rightarrow 2Ir(III) + Q + 2H^+ \quad (1)$$

where H_2Q represents the quinol and Q the corresponding quinone. The values of the potentials for the couples Ir(IV)|Ir(III) (0.957 V, in 1 M acid, $HClO_4$ and H_2SO_4; 22 °C)[6b] and Q|H_2Q show that all the reactions go to completion.

Kinetic Data. Plots of ln ($A_t - A_\infty$), where A_t and A_∞ represent the absorbance at time t and at equilibrium, against time, were found linear for at least two half-lives. The observed rate constants also showed linear dependence on the concentration of the organic substrates. Thus

$$-d[Ir(IV)]/dt = k_0[Ir(IV)][H_2Q] \quad (2)$$

The k_0 values, concerning the different substrates, permit an estimation of the values of the specific rate constants collected in Table I, together with the activation parameters (obtained from kinetic measurements at 10.0 and 25.0 °C).

TABLE I: Kinetic Parameters for the Reactions of Quinols with $IrCl_6^{2-}$ at 25.0 °C, $[HClO_4]$ = 1.00 M, μ = 1.0 M

Compd	k_3[a]	$\Delta H_3^{\ddagger}$[b,c]	$\Delta S_3^{\ddagger}$[d,e]	$(\Delta G^\circ)_9$[b,e]	$(\Delta G^*_3)_{expt}$[b]	$(\Delta G^*_9)_{calcd}$[b,f]	$(\Delta G^*_{-3})_{expt}$[b,g]	$(\Delta G^*_{-9})_{calcd}$[b,f]
1	7.3×10^4	4.4	−21.4	4.1_5	8.3_5	8.7	4.2	4.6
2	2.5×10^5	4.3	−18.4	2.6	7.6	7.9	5.0	5.2_5
3	1.8×10^4	4.9	−22.5	4.5_5	9.2	9.0	4.6_5	4.4_5
4	$2.2_5 \times 10^3$	5.5	−24.8	6.3	10.4	10.0_5	4.1	3.7
5	1.9×10^3	2.2	−36.3	6.8	10.3_5	10.3_5	3.5_5	3.5_5
6	27	4.7	−36.5	8.9	13.0_5	11.7	4.1_5	2.8
7	32	4.7	−35.7	10.5_5	12.9_5	12.8_5	2.4	2.3

[a] M^{-1} s^{-1}; the error is ±3–5%. [b] kcal mol^{-1}. [c] The error is ±0.7–1.2 kcal mol^{-1}. [d] cal mol^{-1} deg^{-1}; the error is ±2.4–4.0 cal mol^{-1} deg^{-1}. [e] Calculated by assuming $K_{1(SQ)}$ = 10 M for the unsubstituted quinol. [f] Calculated from eq 7 with λ = 26 kcal mol^{-1}. [g] $(\Delta G^\circ)_9 = (\Delta G^*_3)_{expt} - (\Delta G^*_{-3})_{expt}$.

Discussion

Since Ir(IV) is a well-known one-electron oxidant, the present noncomplementary oxidation takes place through two successive one-electron steps, as follows

$$Ir(IV) + H_2Q \underset{k_{-3}}{\overset{k_3}{\rightleftharpoons}} Ir(III) + SQ \qquad (3)$$

$$Ir(IV) + SQ \xrightarrow{k_4} Ir(III) + Q \qquad (4)$$

where SQ represents the semiquinone radical, irrespective of its protonated form (the protons are omitted). If the steady-state condition is applied to the semiquinone radical, the following equation is obtained

$$-\frac{d[Ir(IV)]}{dt} = \frac{2k_3k_4[Ir(IV)]^2[H_2Q]}{k_{-3}[Ir(III)] + k_4[Ir(IV)]} \qquad (5)$$

The observed first-order plots of ln $(A_t - A_\infty)$ vs. time, and the absence of Ir(III) effect, suggest that $k_4[Ir(IV)] \gg k_{-3}[Ir(III)]$, hence

$$-d[Ir(IV)]/dt \simeq 2k_3[Ir(IV)][H_2Q] \qquad (6)$$

Thus, $k_0 = 2k_3$.

Comparison of the kinetic constants and of the activation parameters with those involving displacement of a chloride ion in the coordination sphere of the hexachloroiridate(IV) anion[3] supports the conclusion that the first oxidation step follows an outer-sphere mechanism. A similar mechanism has been found to occur in the oxidation of phenol,[6a] cyclohexanone,[6b] and in the oxidation of organolead compounds[6c] by means of the same oxidizing agent. When this mechanism is operating, a relation between the rates of reaction and the overall free energies involved is expected. A theoretical model, which relates these quantities, has been developed by Marcus[1,7] and the approximate equations (neglecting the small work terms to bring reactants and products together in the transition state) are

$$\Delta G^*_{12} = \lambda_{12}(1 + \Delta G^\circ_{12}/\lambda_{12})^2/4 \quad \text{for } |\Delta G^\circ_{12}| \leq \lambda_{12} \qquad (7a)$$

$$\Delta G^*_{12} = 0 \quad \text{for } \Delta G^\circ_{12} \leq -\lambda_{12} \qquad (7b)$$

$$\Delta G^*_{12} = \Delta G^\circ_{12} \quad \text{for } \Delta G^\circ_{12} \geq \lambda_{12} \qquad (7c)$$

where $k = Z \exp(-\Delta G^*_{12}/RT)$, Z being the collision frequency in solution (10^{11} M^{-1} s^{-1}); λ_{12} is defined as $2(\Delta G^*_{11} + \Delta G^*_{22})$, (where ΔG^*_{11} and ΔG^*_{22} refer to the self-exchange reactions of the reagents) and is approximately equal to $4\Delta G^*_0$ (that is the value of ΔG^*_{12} at $\Delta G^\circ_{12} = 0$).

These simple relations, derived originally for weakly overlapping electron transfers, have found a wide applicability also for atom or proton transfers and for strong overlapping electron transfers.[7] Besides, Marcus and Sutin have also recently extended these conclusions to reactions involving large negative activation entropy variations, as in the present experiments.[8] Equations 7b and 7c apply to reactions in solution when most of the reorganization comes from the bonds being broken and formed, rather than from all the other coordinates. Inspection of eq 7a shows that an approximately linear relationship between ΔG^*_{12} and ΔG°_{12} can be observed with slope $0.5(1 + \Delta G^\circ_{12}/2\lambda_{12})$, which reduces to 0.50 if $(\Delta G^\circ_{12}/2\lambda_{12}) \ll 1$. In order to discuss the present systems with reference to the Marcus theory, the standard free energies of the rate-determining step must be evaluated; this can be performed with an estimation of the standard redox potentials of SQ|H_2Q couples. Scheme I collects the possible species involved in the quinone|quinol system.

Scheme I

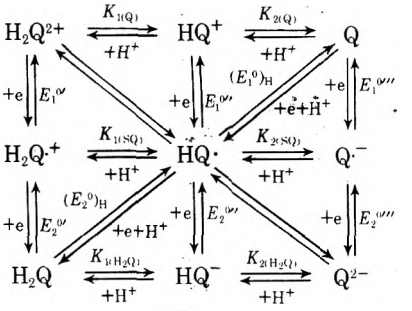

The rate-determining step (eq 3) can give rise to a semiquinone radical in the form HQ·, if one electron and one proton are released in the same step, or in the form $H_2Q^{\cdot+}$, if a simple electron abstraction takes place; eq 3 can be alternatively represented as

$$Ir(IV) + H_2Q \rightleftarrows Ir(III) + HQ\cdot + H^+ \qquad (8)$$

or

$$Ir(IV) + H_2Q \rightleftarrows Ir(III) + H_2Q^{\cdot+} \qquad (9)$$

Thus

$$K_8 = K_9K_{1(SQ)} \qquad (10)$$

For evaluation of K_8, literature data concerning reproportionation of the semiquinone anion,[9] that is

$$K_{SQA} = [Q\cdot^-]^2/([Q][Q^{2-}])$$

must be used, combined with the acid dissociation constants $K_{1(H_2Q)}$, $K_{2(H_2Q)}$, and $K_{2(SQ)}$.

We have graphed (see Figure 1) the literature data for the investigated quinols, concerning the pK's which correspond

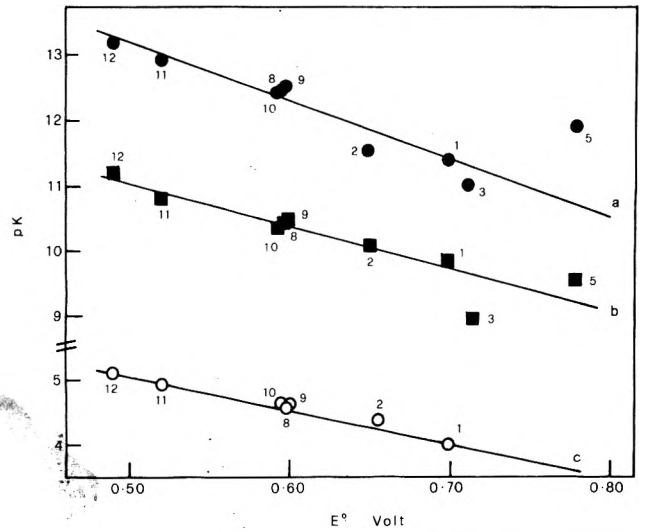

Figure 1. Plots of $pK_{2(H_2Q)}$ (a), $pK_{1(H_2Q)}$ (b), and $pK_{2(SQ)}$ (c), as a function of the reduction potential E^0. The compounds are numbered as in Table I; **8**, 2,5-dimethylbenzene-1,4-diol; **9**, 2,3-dimethylbenzene-1,4-diol; **10**, 2,6-dimethylbenzene-1,4-diol; **11**, 2,3,5-trimethylbenzene-1,4-diol; **12**, 2,3,5,6-tetramethylbenzene-1,4-diol.

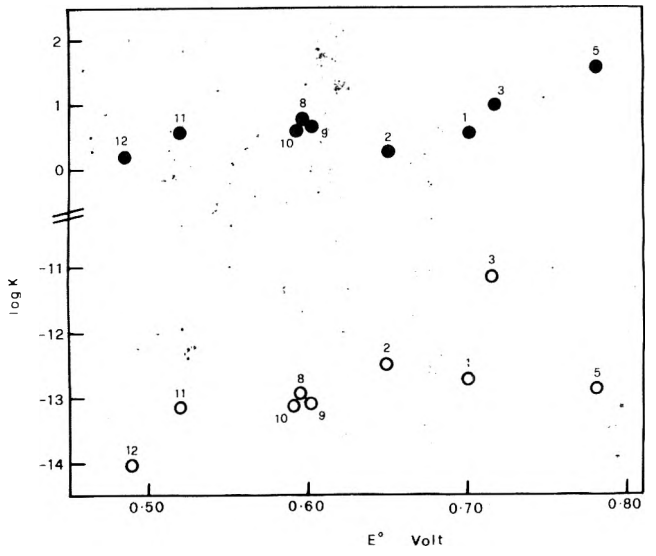

Figure 2. Plots of the logarithm of equilibrium constants K_{SQA} (●) and K_{SQ} (○) as a function of E^0.

to the above dissociation constants,[9,10] as a function of E^0 values; the points lie reasonably well on straight lines of similar slopes. Besides, Figure 2 shows the values of log K_{SQA} and log K_{SQ} (defined as $K_{SQ} = [HQ\cdot]^2/([H_2Q][Q])$), calculated from

$$K_{SQ} = K_{SQA}K_{1(H_2Q)}K_{2(H_2Q)}(K_{2(SQ)})^{-2} \qquad (11)$$

as a function of E^0. The values of $K_{2(SQ)}$ have been estimated, when necessary, from the straight line (c) of Figure 1. It is noteworthy that substantial constancy for K_{SQA} as well as for K_{SQ} is shown from the redox couples taken into consideration, in spite of their different reduction potentials.[11] The knowledge of K_{SQ} permits an estimation of the reduction potentials $(E^0_1)_H$ and $(E^0_2)_H$. In fact

$$(E^0_1)_H - (E^0_2)_H = \frac{RT}{F} \ln K_{SQ} \qquad (12)$$

and

$$(E^0_1)_H + (E^0_2)_H = 2E^0 \qquad (13)$$

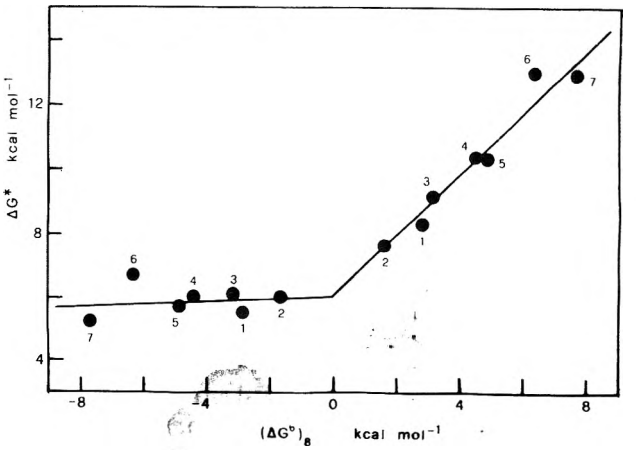

Figure 3. Plot of ΔG^*_{expt} as a function of $(\Delta G^\circ)_8$. Values with $\Delta G^\circ > 0$ pertain to reaction 8 and those with $\Delta G^\circ < 0$ to reaction −8.

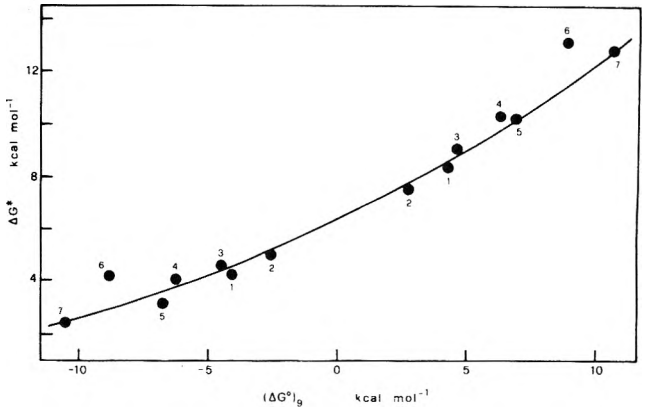

Figure 4. Plot of ΔG^*_{expt} as a function of $(\Delta G^\circ)_9$. The line was drawn according to eq 7a and $\lambda = 26$ kcal mol^{-1}. Values with $\Delta G^\circ > 0$ pertain to reaction 9 and those with $\Delta G^\circ < 0$ to reaction −9.

From the data reported in Figure 2, the value of $(E^0_1)_H - (E^0_2)_H$ can reasonably be assumed constant for different substrates, around −0.76 V. Then a potential of 1.08 V should be assigned to $HQ\cdot|H_2Q$ couple for the unsubstituted quinol, in agreement with other kinetic observations.[12] Then, the free energies for the rate-determining step (eq 8) can be calculated, for the different compounds, according to

$$(\Delta G^\circ)_8 = -RT \ln (K_1 K_{SQ})^{1/2} \qquad (14)$$

where K_1 refers to the equilibrium constant for the stoichiometric eq 1.

The dependence of ΔG^* on $(\Delta G^\circ)_8$, both for direct and reverse reaction, is depicted in Figure 3; the plot is represented by a broken line with different slopes for $\Delta G^\circ > 0$ (ca. 0.95) and for $\Delta G^\circ < 0$ (ca. 0.05). A similar situation has been found to occur in reactions of a series of quinones with $O_2\cdot^-$, and of anion radicals with aromatic hydrocarbons,[13] having slope ca. 1 for reactions with $\Delta G^\circ > 0$, and ca. 0 for $\Delta G^\circ < 0$. The authors attributed this feature to the failure of the Marcus theory for these reactions. The achievement, at least in some cases, of conditions 7b and 7c could account for the above dependences. This is not the case in the present experiments (in fact $\Delta G^*_0 \simeq 6$, and then $\lambda \simeq 24$ kcal mol^{-1}) so that the possibility that the rate-determining step is reaction 9 should be discussed.

No information about the stability of the protonated form of semiquinone, $H_2Q\cdot^+$, is available. It has been reported that

no spectral change in parent semiquinone takes place in solution when the acidity is increased;[14] thus a value ≥ 10 M has been suggested for $K_{1(SQ)}$. If, according to Figure 1, a dependence of $pK_{1(SQ)}$ on the reduction potential E^0 is assumed analogous to line c for the series of quinols (and taking $K_{1(SQ)} = 10$ M for the unsubstituted quinol), the values of K_9 can be estimated and consequently $(\Delta G^\circ)_9$ (see Table I). Figure 4 collects the experimental data with a line drawn according to eq 7a assuming $\lambda = 26$ kcal mol^{-1}.

Notwithstanding the approximations and assumptions made for the estimation of $(\Delta G^\circ)_9$, the data seem to agree with the Marcus theory, suggesting that reaction 9 could be the rate-determining step. The similarity with phenol oxidation,[6a] where a small isotopic effect suggested an electron abstraction rather than the rupture of an O–H bond, provides further support to the proposed mechanism. Moreover, since the λ value is now known (and assuming ΔG^* of self-exchange of Ir(IV)|Ir(III) to be 8.5 kcal mol^{-1}, that is $k_{exch} \simeq 10^5$ M^{-1} s^{-1})[15] ΔG^* of the couple $HQ\cdot^+|H_2Q$ can be estimated to be ca. 4.5 kcal mol^{-1}, that is $k_{exch} \simeq 5 \times 10^7$ M^{-1} s^{-1}; this value falls in the range of the observed self-exchange rate constants of radicals with the corresponding reduced species (10^7–10^9 M^{-1} s^{-1}) (ref 13 and 16). A relevant discrepancy in Figure 4 can be observed for the disulfonic derivative: this could arise from the large unfavorable entropy of activation connected with the fact that both reacting species bear a double negative charge. In the case of the monosulfonic derivative, which does not deviate from the expected behavior, the effect of its negative charge could be somewhat depressed by proper orientation of the reagents in the act of transition complex formation.

It must be noted that the rates of the reverse reactions k_{-3} have values ranging from 10^7 to 10^9 M^{-1} s^{-1} and therefore in agreement with the experimental findings $k_4[Ir(IV)] \gg k_{-3}[Ir(III)]$ for which k_4 should have values very close to the diffusion-controlled limit (ca. 10^{10} M^{-1} s^{-1}); this should be due to the large favorable free energy variations involved in step 4.

It is noteworthy that the previously assessed validity of the Marcus relationship for reactions of organic substrates with aquometal ions (Mn_{aq}^{3+} with catechols and Co_{aq}^{3+} with quinols and catechols)[2] implies that the rate-determining step in such reactions is probably the oxidation of H_2Q to $HQ\cdot$.

In conclusion, the above considerations seem to indicate that the Marcus concepts can be very useful in the suggestion of reaction mechanisms in cases where no direct experimental evidence can be drawn about the rate-determining step or the choice among different kinetically undistinguishable paths, and for an estimate of intrinsic (λ parameter) and extrinsic (standard potentials of intermediate species) parameters in the redox reactions involving these important classes of organic substrates.

Acknowledgments. We wish to thank Professor R. A. Marcus for stimulating discussion at Leeds. We also thank CNR (Rome) for financial support.

References and Notes

(1) R. A. Marcus, *Annu. Rev. Phys. Chem.*, **15**, 155 (1964); N. Sutin, *ibid.*, **17**, 119 (1966); *Chem. Brit.*, **8**, 148 (1972); W. L. Reynolds and R. W. Lumry, "Mechanisms of Electron Transfer", Ronald Press, New York, N.Y., 1966.
(2) E. Pelizzetti, E. Mentasti, and G. Giraudi, *Inorg. Chim. Acta*, **15**, L 1 (1975); E. Pelizzetti, E. Mentasti, and E. Pramauro, *J. Chem. Soc., Dalton Trans.*, **26** (1976); E. Mentasti, E. Pelizzetti, and C. Baiocchi, *J. Inorg. Nucl. Chem.*, **38**, 2017 (1976); E. Pelizzetti and E. Mentasti, *ibid.*, **38**, 2005 (1976); E. Pelizzetti, E. Mentasti, and G. Saini, *Gazz. Chim. Ital.*, **106**, 605 (1976).
(3) I. Poulsen and C. S. Garner, *J. Am. Chem. Soc.*, **84**, 2032 (1962).
(4) E. Pelizzetti, E. Mentasti, M. E. Carlotti, and G. Giraudi, *J. Chem. Soc., Dalton Trans.*, 794 (1975).
(5) W. M. Clark, "Oxidation-Reduction Potentials of Organic Systems", Williams and Wilkins Co., Baltimore, Md., 1960; W. Flaig, H. Beutelspacher, H. Reimer, and E. Kalke, *Ann. Chem.*, **719**, 96 (1968).
(6) (a) R. Cecil and J. S. Littler, *J. Chem. Soc. B*, 1420 (1968); (b) R. Cecil, J. S. Littler, and G. Easton, *ibid.*, 626 (1970); (c) H. C. Gardner and J. K. Kochi, *J. Am. Chem. Soc.*, **97**, 1855 (1975).
(7) R. A. Marcus, *J. Phys. Chem.*, **72**, 891 (1968); J. E. Earley, *Prog. Inorg. Chem.*, **13**, 243 (1970).
(8) R. A. Marcus and N. Sutin, *Inorg. Chem.*, **14**, 213 (1975).
(9) L. A. Bishop and L. K. J. Tong, *J. Am. Chem. Soc.*, **87**, 501 (1967).
(10) P. S. Rao and E. Hayon, *J. Phys. Chem.*, **77**, 2274 (1973); K. B. Patel and R. L. Willson, *Trans. Faraday Soc.*, **69**, 814 (1973).
(11) An exception is given by chloroquinol, probably due to a low value adopted for $K_{2(SQ)}$; for duroquinol, the small deviation could arise from the uncertainty about $K_{2(H_2Q)}$ (higher values are in fact available in the literature).
(12) T. W. Newton, *J. Inorg. Nucl. Chem.*, **36**, 639 (1974).
(13) I. B. Afanas'ev, S. V. Prigoda, T. Ya. Malt'seva, and G. I. Samokhvalov, *Int. J. Chem. Kinet.*, **6**, 643 (1974).
(14) J. M. Hale and R. Parsons, *Trans. Faraday Soc.*, **59**, 1429 (1963).
(15) P. J. Proll in "Comprehensive Chemical Kinetics", Vol. 7, C. H. Bamford and C. F. H. Tipper, Ed., Elsevier, Amsterdam, 1972, Chapter 2.
(16) D. Meisel, *Chem. Phys. Lett.*, **34**, 263 (1975).

Gas-Phase Methylbenzenes Isomerization

Giorgio Perez

Laboratorio di Chimica Nucleare del C.N.R., CP 10, 00016 Monterotondo Stazione, Roma, Italy *(Received December 2, 1975; Revised Manuscript Received June 15, 1976)*

Publication costs assisted by Laboratorio di Chimica Nucleare del C.N.R.

Xylenes and trimethylbenzenes were isomerized in the gaseous phase using as protonating agents D_3^+ and HeT^+ ion, obtained by γ radiolysis of D_2, and by T_2 β decay, respectively. Experiments with HeT^+ ions confirmed that methylbenzenes undergo isomerization by intramolecular 1,2-methyl shifts. A protodemethylation reaction was also observed and was ascribed to the relatively high energy of the reactant. The use of the less energetic D_3^+ ions shows that the gas phase isomerization results are qualitatively in agreement with solution isomerization data. *p*-Xylene and *o*-xylene isomerize faster than *m*-xylene; *m*-xylene rearranges faster to *p*-xylene than to *o*-xylene. Mesitylene does not undergo isomerization, while hemimellitene isomerizes to pseudocumene which, more slowly, rearranges to give mesitylene. A reaction scheme is suggested and its kinetics studied.

Introduction

In strongly acid solvents, such as $HF–BF_3$ or $HF–SbF_5$, nuclear magnetic resonance spectra of arenium ions appear;[1] the stability of an arenium ion is correlated to its resistance toward isomerization, transalkylation, and dealkylation reactions, and to its basicity. Cations of less basic isomers undergo isomerization to the more stable cations so that the *o*-xylenium and the *p*-xylenium ions, as well as the cations of pseudocumene and hemimellitene, isomerize to the more stable isomeric cation of *m*-xylene and mesitylene, respectively. Overall rearrangement reactions taking xylenium and trimethylbenzenium ions as the most stable cation of each of the methylbenzenes are

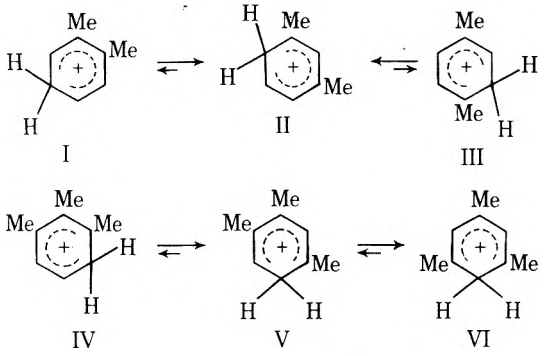

In the course of NMR spectrometric studies of the dimethylbenzenium and trimethylbenzenium ions,[2] the spectra of ions I and IV were found to change, irreversibly, into those of II and VI, respectively. Quenching the solutions, Brouwer[3] measured the ionic compositions as a function of time. As was expected both I and III gave II, while IV gave V which, more slowly, isomerized to ion VI. Disproportion products were not formed to confirm results obtained by other authors.[4-9] Kilpatrick and Luborsky[10] did not find any appreciable isomerization of the xylenes and trimethylbenzenes, following this process by the increase in conductance of the solutions. The methylbenzenium ion rearrangements proceed by successive 1,2-hydrogen and 1,2-methyl shifts with the methyl shifts as the rate-determining step. The activation energies of the methyl migration process[1,3] have been reported; according to their large values, Olah and Mo[11] did not find any xylene isomerization when the reaction temperature was below 0 °C. Determining the equilibrium constants for a proton transfer reaction Chong and Franklin[12] measured the proton affinities of xylenes in gas phase. Even if there is no precise quantitative agreement, the results are in the same order that would be expected from studies of the basicity of the xylenes as determined in solution.

In the gas phase arene alkylation, alkyl group migrations were observed[13,14] so that it seems possible to study arene isomerization by the method introduced by Ausloos and Lias:[15,16] H_3^+ ions, produced by irradiating H_2, are allowed to transfer a proton to relatively small concentrations of substrate.

In a previous communication[17] the gas phase reactions between the isomeric xylenes and the HeT^+ ions from T_2 β decay were studied.

The results confirmed that the substrate undergoes isomerization by an intramolecular 1,2-methyl shift. In the present paper the reactions of the D_3^+ ions produced by irradiating D_2 in the presence of the relatively small concentrations of xylenes and trimethylbenzenes are discussed.

Experimental Section

Materials. Tritium was purchased from CEA (France) and its purity, corresponding to a minimum T_2 content of 94%, was determined by radio-gas-solid chromatography, as described by Cacace and Caronna.[18]

Xylenes and trimethylbenzenes (C. Erba, Italy) were analyzed by gas-liquid chromatography, and the impurities were less than 0.2% for each isomer. Deuterium, oxygen, and the other chemicals were commercial Research Grade products and were used without further purification.

Procedure. In T_2 β decay runs a measured amount of xylene was introduced into a 300-ml Pyrex vessel and stored at 150 °C for 2 months.[17,18] Weighed carrier amounts were added before proceeding to the analysis of each sample. The labeled arenes were separated and collected by preparative gas chromatography on a 5-m didecylphthalate column heated at 95 °C with a helium flow rate of 2.17 l/h, and on a 4-m Bentone 34 column (80 °C, 1.28 l of He/h) to resolve *p*-xylene from *m*-xylene. The gas-chromatographic separation of each compound was repeated until a constant specific radioactivity

value was reached, as measured with a Nuclear Chicago Mark I liquid scintillation spectrometer.

The toluene tritium distribution was determined as described elsewhere.[19] In the D_2 γ radiolysis experiments weighed amounts of aromatic hydrocarbon were sealed into capillary Pyrex tubes. Each tube was introduced in a 500-ml Pyrex vessel. The vessels, connected to a vacuum line, were outgassed and then, after addition of oxygen (3 Torr), were filled with deuterium up to a pressure of 500 Torr. In some runs, the D_2 pressure was varied as reported in the next section.

The samples were irradiated with ^{60}Co γ rays at 40 ± 5 °C in a 220 Gamma cell (Atomic Energy of Canada) with a dose ranging from 4.84×10^{20} to 1.21×10^{21} eV g^{-1} of deuterium at a dose rate of 4.3×10^5 rads h^{-1}, as measured by Fricke dosimetry.

After the irradiation a fraction of the reaction mixture was analyzed by a F30 Perkin-Elmer gas chromatograph equipped with a flame ionization detector. A 5-m Bentone 34–didecylphthalate (3:4) column operating with a nitrogen flow rate of 50 cm^3/min resolved the xylenes and the trimethylbenzenes at 55 and 65 °C, respectively.

The radiation damage runs on mixtures of methylbenzenes in the presence of helium were performed by filling the ampoules with 500 Torr of helium and irradiating them with 1.21×10^{21} eV g^{-1} of He. As reported by Verdin,[20] the G values for toluene formation and substrate isomerization in the γ radiolysis of xylenes are very low. In order to approximate to the same energy transfer processes of the systems arene–deuterium the ampoules were filled with helium. The results confirm the relatively high stability of methylbenzenes toward γ radiations: the overall demethylation and isomerization G values referred to absorbed dose by helium were found in the range 1×10^{-3} to 6×10^{-3}.

Results and Discussion

Arene plus HeT^+ Ions. In a previous experiment[17] HeT^+ ions, produced during the T_2 β decay,[21,22] were allowed to react with the xylenes and the radioactivity of the aromatic reaction products measured by the isotopic dilution method.

The relative tritium content recovered in the labeled arenes is reported in Table I.

The fraction of the total radioactivity of the HeT^+ ions from the T_2 β decay recovered in the products was 0.35 ± 0.04 for each isomer.

Since the analysis of the gaseous products did not show any detectable amount of the lighter hydrocarbons and the radioactivity measurements of unpurified mixtures did not prove any presence of polymeric substances, owing to the fact that the measured activity did not exceed the tritium content found in the identified reaction products after the purification, it seems likely that all the tritium from the HeT^+ ions, not incorporated in the arenes, was present in the gaseous phase as HT.

A comparison between our yields and the results obtained in the reaction of HeT^+ ions with toluene[18] supports the idea that the fundamental reaction is a hydride ion extraction from a methyl group. The hydrogen tritide is not measurable since it is present as a relatively abundant impurity in the T_2 used to produce the HeT^+ ions; but the observed yields decrease from 60–70% to 30–40%, when the methyl groups are doubled, and this fact can be reasonably explained as an extraction of a hydride ion from a methyl group.

The statistical *m*-xylene isomerization as well as the xylene protodemethylation were ascribed to the protonating agent

TABLE I: Tritium Percent in the Aromatic Hydrocarbons after the Reaction between HeT^+ Ions and Xylenes[a]

	Aromatic tritium percent in			
Substrate	Toluene	*o*-Xylene	*m*-Xylene	*p*-Xylene
o-Xylene	19.5	74.3	6.2	<0.1
m-Xylene	8.2	2.5	86.7	2.5
p-Xylene	10.0	<0.1	6.7	83.5

[a] Substrate pressure 500 Torr.

energy. As a matter of fact the ΔH_0 of the HeT^+ ion is 323 kcal/mol.[23] Furthermore, the absence of any *p*-xylene from *o*-xylene and vice versa, and the tritium presence in the isomerized substrate confirmed the intramolecular 1,2-methyl shift.

The tritium distribution in the toluene produced by protodemethylation of *m*-xylene was determined. The radioactivity was found essentially in the ortho and para position of the methyl group to confirm the electrophilic attack of the HeT^+ ions[18,24–26] and the relatively rapid 1,2-hydrogen shift.

The relatively high substrate pressure, ca. 500 Torr, used in the experiments to avoid the radiation damage toward the labeled products, did not allow the xylenium ion to survive enough for two subsequent methyl shifts.

Additional experiments have been carried out to show that as the substrate pressure is lowered, a second methyl shift can be observed as well as higher isomerization and protodemethylation, but the dramatic reduction of the recovered tritium in the arenes, reported in Table II, probably due to the radiolysis of the labeled products, makes these results slightly useful for quantitative discussions.

Arenes plus D_3^+ Ions. In the D_2 radiolysis experiments the arenes pressure was kept low to minimize direct radiation effects; it is then also possible to observe a second methyl shift. Moreover, since the ΔH_0 of the D_3^+ ion, ca. 256 kcal/mol,[27–29] is lower than the ΔH_0 of the HeT^+ ions, no toluene formation and a higher selectivity in the isomerization processes can be observed, as shown in Table III. According to the 1,2-methyl shift model, proposed in the Introduction, o-xylene and *p*-xylene isomerize to *m*-xylene. A second methyl shift can be observed in the isomerization of o-xylene. *m*-Xylene, as observed in solution experiments,[4] undergoes isomerization to *p*-xylene more rapidly than to *o*-xylene. Owing to the fact that some products are formed in very small amounts, experimental errors in their determination could be significant. Consequently, specific runs were performed with a higher absorbed dose; the results, reported in Table IV, show that *m*-xylene isomerizes to *p*-xylene and to o-xylene as well. Similarly the isomerization data of the trimethylbenzenes are reported in Table V. Hemimellitene isomerizes to pseudocumene, which, more slowly, rearranges further to give mesitylene. Pseudocumene gives mesitylene as the only detectable product. The absence of any measurable mesitylene isomerization can be ascribed to the relatively high stability of the mesitylene ion.[3]

In Figures 1 and 2 the initial substrate concentration, [S], is plotted against the concentration of its isomerization products, [P]. Figures 1 and 2 refer to different absorbed doses.

The slopes can be explained as competitive reactions for D_3^+ ions. These ions are produced during the γ radiolysis of D_2;[21,22,30] their formation occurs via the following processes[29]

TABLE II: Fraction of Radioactivity Recovered and Its Distribution in the Arenes after Reaction between *p*-Xylene and HeT^+ Ions

Substrate pressure, mm	Yield of tritiated aromatic compounds	Percent tritium distribution			
		Toluene	*o*-Xylene	*m*-Xylene	*p*-Xylene
708	0.38	7.2	<0.1	6.9	85.9
580	0.36	8.9	<0.1	7.0	84.1
500	0.37	10.0	<0.1	6.7	83.5
395	0.29	9.9	0.3	7.6	82.3
186	0.19	11.1	1.8	8.2	78.9
19	0.10	13.3	4.7	24.2	57.8

TABLE III: Xylenes + Deuterium Ions[a]

Substrate	Concn, μM	Final isomer composition (mol %)		
		Ortho	Meta	Para
o-Xylene	2.06	98.17	1.77	0.24
	2.52	98.23	1.73	0.22
	3.77	98.20	1.76	0.22
	5.65	98.41	1.52	0.25
	8.70	98.36	1.62	0.20
	9.51	98.40	1.58	0.20
	12.00	98.54	1.46	<0.20
	14.25	98.46	1.54	<0.20
	18.00	98.48	1.52	<0.20
	31.30	98.60	1.40	<0.20
	55.57	99.00	1.00	<0.20
	105.59	99.27	0.73	<0.20
m-Xylene	2.76	0.31	98.69	1.00
	10.36	0.28	98.99	0.73
	13.32	0.25	98.94	0.81
	16.01	0.27	99.20	0.53
	32.97	<0.20	99.50	0.50
	42.38	<0.20	99.58	0.42
	59.34	<0.20	99.61	0.39
	162.00	<0.20	99.69	0.31
p-Xylene	1.52	0.40	2.24	97.36
	2.40	0.29	1.92	97.79
	2.83	0.29	1.88	97.83
	3.17	0.30	1.82	97.88
	3.73	0.21	1.65	98.14
	7.21	0.20	1.57	98.23
	7.54	0.20	1.44	98.36
	10.83	<0.20	1.35	98.65
	15.25	<0.20	1.30	98.70
	21.66	<0.20	1.15	98.85
	48.98	<0.20	1.05	98.95
	64.66	<0.20	1.00	99.00

[a] Absorbed dose 4.84×10^{20} eV g^{-1} referred to deuterium.

TABLE IV: Xylenes + Deuterium Ions[a]

Substrate	Final isomer composition (mol %)		
	Para	Meta	Ortho
p-Xylene	93.8	4.96	0.64
o-Xylene	0.42	4.67	94.61
m-Xylene	3.23	95.59	1.18

[a] Absorbed dose 1.07×10^{21} eV g^{-1}. Dose rate 2×10^5 rads h^{-1}. Deuterium pressure 700 Torr.

$$D_2 \xrightarrow{\gamma} D_2^+ + e^- \quad (1a)$$

$$D_2^+ + D_2 \longrightarrow D_3^+ + D \quad (1b)$$

TABLE V: Trimethylbenzenes + Deuterium Ions[a]

Substrate	Concn, μM	Final isomer composition (mol %)		
		1,2,3	1,2,4	1,3,5
1,2,3-Trimethylbenzene	4.70	94.2	5.2	0.6
	7.07	95.1	4.4	0.5
	18.50	96.5	3.1	0.4
	45.90	98.4	1.4	0.2
1,2,4-Trimethylbenzene	5.48		98.0	2.0
	8.35		98.3	1.7
	18.58		98.5	1.5
	38.88		99.1	0.9
	45.52		99.2	0.8
	71.21		99.6	0.6
1,3,5-Trimethylbenzene	5.15		0.3	99.7
	17.15		0.1	99.9
	22.75		<0.1	100.0
	38.28		<0.1	100.0

[a] Absorbed dose 6.09×10^{20} eV g^{-1} of deuterium.

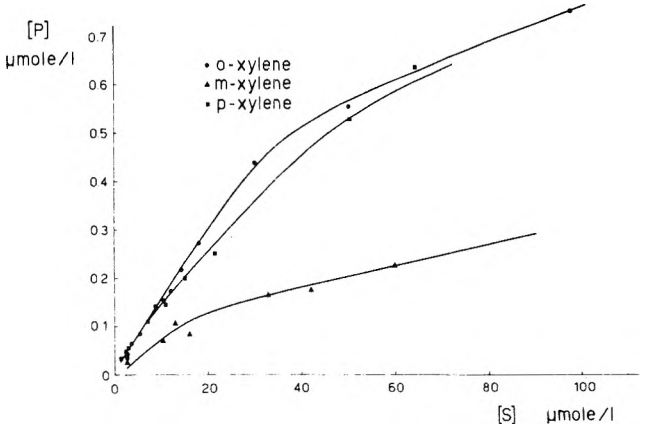

Figure 1. Variation of xylene isomerization products vs. substrate concentration.

The first step of the arene isomerization process is an exothermic deuteron transfer from D_3^+ to the arene, while the deuterium atoms are removed from the system by a low concentration of oxygen, which is a radical scavenger relatively inert toward hydrocarbons[16] and D_3^+ [31] ions.

The excited methylbenzenium ions can subsequently undergo isomerization, followed by a proton transfer to a base present in the system, or it can be collisionally stabilized and transfer a proton to a proton acceptor, B, whose nature is not well known. It can be the substrate itself or a more basic substance present in the system as impurity. Such a base acts as a quencher for the D_3^+ ions. Consequently the suggested reactions scheme is the following

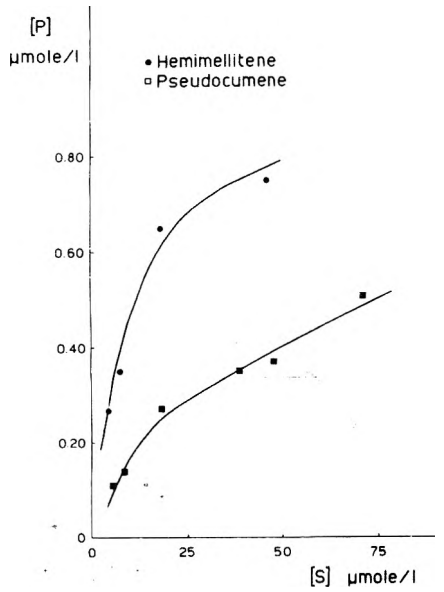

Figure 2. Variation of trimethylbenzene isomerization products vs. substrate concentration.

$$D_2 \xrightarrow[k_1]{D_2} D_3^+ \quad (1)$$

$$D_3^+ \xrightarrow[k_2]{S} SD^+ \quad (2)$$

$$D_3^+ \xrightarrow[k_3]{B} BD^+ \quad (3)$$

$$SD^+ \xrightarrow[k_4]{B} S \quad (4)$$

$$SD^+ \xrightarrow[k_5]{} PD^+ \quad (5)$$

$$PD^+ \xrightarrow[k_6]{B} P \quad (6)$$

$$D_3^+ + P \longrightarrow PD^+ + D_2 \quad (7)$$

$$PD^+ \longrightarrow SD^+ \quad (8)$$

where S and P refer to the substrate and the isomerized arene, respectively, and SD^+ and PD^+ to their deuterated ions.

For low conversions, as reported in Tables III and V, the substrate and the deuterium concentrations can be considered constant and the amount of the isomerization produced by consecutive reactions 7 and 8 can be neglected.

Therefore, under steady state conditions the following equations can be developed:

$$\frac{d[P]}{dt} = \frac{k_2 k_5 [S]}{k_5 + k_4[B]} \frac{k_1 [D_2]^2}{k_2[S] + k_3[B]} \quad (9)$$

At a given absorbed dose, it can be written in a simpler way:

$$1/[P] = \alpha + \beta 1/[S] \quad (10)$$

where

$$\alpha = \frac{k_5 + k_4[B]}{k_1 k_5 [D_2]^2} \quad (11)$$

and

$$\beta = \frac{k_3}{k_2 k_5} \frac{k_5[B] + k_4[B]^2}{k_1[D_2]^2} \quad (12)$$

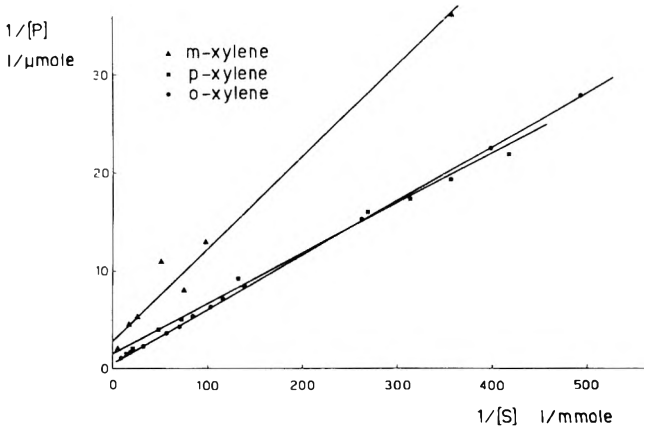

Figure 3. Xylene isomerization: plot of 1/[product] vs. 1/[substrate].

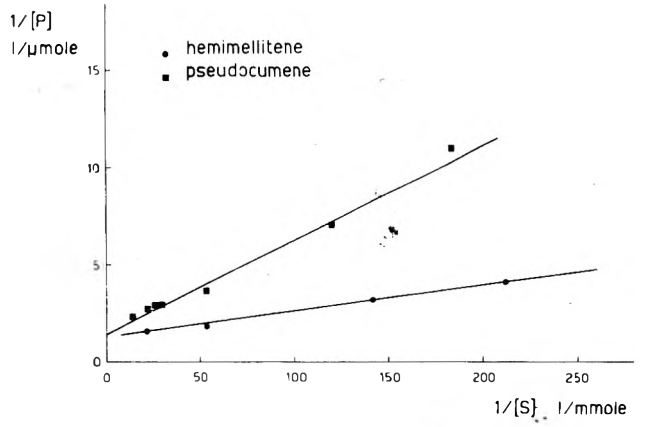

Figure 4. Trimethylbenzene isomerization: plot of 1/[product] vs. 1/[substrate].

Plotting 1/[S] against 1/[P] the straight lines, reported in Figures 3 and 4, are obtained.

Conclusions

A qualitative comparison between the isomerization rates of the xylenes, as well as the trimethylbenzenes, is possible. As in solution, o-xylene and *p*-xylene isomerize faster than *m*-xylene.

A discrepancy exists with the results obtained in the liquid phase, where it has been reported that *p*-xylene undergoes isomerization four times faster than o-xylene.[1,3] Allen and Yats found that the more basic formed *m*-xylene competed for the catalyst, lowering the isomerization rate of *p*-xylene. From this point of view these results can be explained since o-xylene is three times as basic as *p*-xylene.[32]

Qualitatively the trimethylbenzenes isomerization data confirm the results obtained by Brouwer,[1,3] since the basicity of the 1,2,3, and 1,2,4 isomers are very close.[1]

The intramolecular, rate-determining step, 1,2-methyl shift in the isomerization of the methylbenzenes has been confirmed by HeT^+ ions experiments.

For a quantitative interpretation of the data new experiments will be performed in order to establish the fraction of excited methylbenzenium ions undergoing isomerization. Furthermore, the effects of the addition of known amounts of D_2^+ ions quenchers to the system will be studied.

Acknowledgments. The author wishes to thank Professor A. Guarino and Dr. M. Speranza for helpful suggestions and for critically reading the manuscript.

References and Notes

(1) D. M. Brouwer, E. L. Mackor, and C. MacLean in "Carbonium Ions", Vol. 2, G. A. Olah and P. v. R. Schleyer, Ed., Wiley-Interscience, New York, N.Y., 1970, p 864.
(2) D. M. Brouwer, E. L. Mackor, and C. MacLean, *Recl. Trav. Chim. Pays-Bas*, **84**, 1564 (1965).
(3) D. M. Brouwer, *Recl. Trav. Chim. Pays-Bas*, **81**, 611 (1968).
(4) R. H. Allen and L. D. Yats, *J. Am. Chem. Soc.*, **81**, 5289 (1959).
(5) H. C. Brown and H. Jungk, *J. Am. Chem. Soc.*, **77**, 5579 (1955).
(6) D. A. MacCaulay and A. P. Lien, *J. Am. Chem. Soc.*, **75**, 577 (1953).
(7) G. Baddeley, G. Holt, and D. Voss, *J. Chem. Soc.*, 101, (1952).
(8) K. J. Pitzer and D. W. Scott, *J. Am. Chem. Soc.*, **65**, 803 (1943).
(9) J. F. Norris and D. Rubinstein, *J. Am. Chem. Soc.*, **61**, 1163 (1939).
(10) M. Kilpatrick and F. E. Luborsky, *J. Am. Chem. Soc.*, **75**, 577 (1953).
(11) G. A. Olah and Y. K. Mo, *J. Am. Chem. Soc.*, **94**, 9241 (1972).
(12) S.-L. Chong and J. L. Franklin, *J. Am. Chem. Soc.*, **94**, 6630 (1972).
(13) F. Cacace and E. Possagno, *J. Am. Chem. Soc.*, **95**, 3397 (1973).
(14) P. Giacomello and F. Cacace, *J. Chem. Soc., Chem. Commun.*, 379 (1975).
(15) P. Ausloos and S. G. Lias, *J. Chem. Phys.*, **40**, 3599 (1964).
(16) P. Ausloos, *Prog. React. Kinet.*, **5**, 113 (1969).
(17) G. Perez, *Radiochem. Radioanal. Lett.*, **20**, 383 (1975).
(18) F. Cacace and S. Caronna, *J. Am. Chem. Soc.*, **89**, 6848 (1967).
(19) C. L. Brett, V. Gold, and G. Perez, *J. Chem. Soc., Perkin Trans. 2*, 1450 (1967).
(20) D. Verdin, *J. Phys. Chem.*, **67**, 1263 (1963).
(21) A. H. Snell, F. Pleasonton, and H. E. Leming, *J. Inorg. Nucl. Chem.*, **5**, 112 (1957).
(22) S. Wexler, *J. Inorg. Nucl. Chem.*, **10**, (1958).
(23) W. A. Chupka and M. E. Russel, *J. Chem. Phys.*, **49**, 5426 (1968).
(24) F. Cacace and G. Perez, *J. Chem. Soc. B*, 2086 (1971).
(25) F. Cacace, R. Cipollini, and G. Ciranni, *J. Chem. Soc. B*, 2089 (1971).
(26) F. Cacace and S. Caronna, *J. Chem. Soc., Perkin Trans. 2*, 1450 (1972).
(27) R. E. Christoffersen, *J. Chem. Phys.*, **41**, 960 (1964).
(28) H. Conroy, *J. Chem. Phys.*, **41**, 1341 (1964).
(29) F. Cacace, R. Cipollini, and G. Occhiucci, *J. Chem. Soc. Perkin Trans. 2*, 84 (1972).
(30) W. A. Chupka, M. E. Russel, and K. Refaey, *J. Chem. Phys.*, **48**, 1518 (1968).
(31) F. C. Fehsenfeld, W. Lindinger, and D. L. Albritton, *J. Chem. Phys.*, **63**, 443 (1975).
(32) D. A. MacCaulay and A. P. Lien, *J. Am. Chem. Soc.*, **73**, 2013 (1951).

Spectroscopic Studies of Bicyclo[2.2.2]octa-2,5,7-triene. 2. An Interpretation of the Vibrational Spectra of Barrelene[1,2]

F. A. Van-Catledge* and C. E. McBride, Jr.

Department of Chemistry, University of Minnesota, Minneapolis, Minnesota 55455

(Received November 11, 1975)

Infrared spectra of gaseous, liquid, and polycrystalline barrelene (bicyclo[2.2.2]octa-2,5,7-triene) were recorded from 380 to 4000 cm^{-1}. Raman spectra for the liquid were measured from 100 to 4000 cm^{-1}. Vibrational assignments were made, based on group frequency correlations, ir-Raman activity, and Raman depolarization ratios. Of the 28 expected fundamental frequencies 5 were assigned by recourse to exploratory normal coordinate calculations. A 37-parameter potential function is reported which reproduces the observed frequencies with an average error of ± 2.0 cm^{-1}. The possible significance of the force constant values with regard to the strain and rigidity of barrelene is discussed.

Bicyclo[2.2.2]octa-2,5,7-triene (barrelene, 1), first prepared by Zimmerman et al.,[3] has stimulated considerable interest[1a,3a,4-12] regarding its electronic structure and properties due to the unique arrangement of p orbitals inherent in its structure. While the photoelectron spectrum of 1 seems fairly well understood,[11,12] the details of its electronic spectrum have yet to be completely unraveled.

The emphasis on electronic excited states has overshadowed the unique position of 1 as a rigid, strained bicyclic polyolefin of high symmetry (D_{3h}). Best estimates of its strain energy are 23–27 kcal/mol,[13] vs. 29 kcal/mol for bicyclo[2.2.1]hepta-2,5-diene (3).[14b] Hydrogenation of 1 to bicyclo[2.2.2]octa-2,5-diene (2) proceeds with the release of 37.57 kcal/mol,[14] one of the largest heats of hydrogenation known for a carbon–carbon double bond. This is to be compared with 34.98 kcal/mol for hydrogenation of the more highly strained 3 to bicyclo[2.2.1]heptene (4).[14] Thus we have at the outset an interesting role-reversal for 1 and 3, depending upon which thermodynamic property one examines.

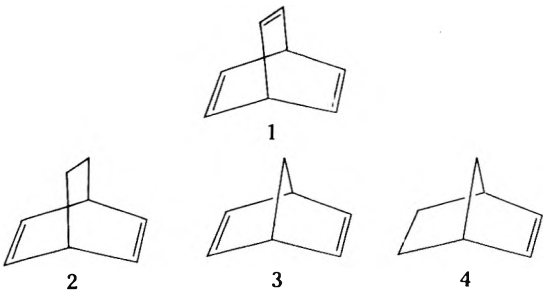

1 2 3 4

The foregoing data are but a small sample of the type of information one would like to obtain for strained systems. The alternatives available are (1) to conduct extensive thermochemical experiments, or (2) to develop some methodology for estimating heats of formation, strain energies, etc. Considerable effort has been devoted in recent years to the latter approach, particularly the calculations commonly described as molecular mechanics calculations. In this method, minimum energy configurations and conformations of molecules are calculated via methods relating to the theory of small vibrations.[15] Usually empirical force fields are parameterized to reproduce the structures and energies of small acyclic molecules, and then used for predicting properties of more complex systems. A measure of the state of the art may be

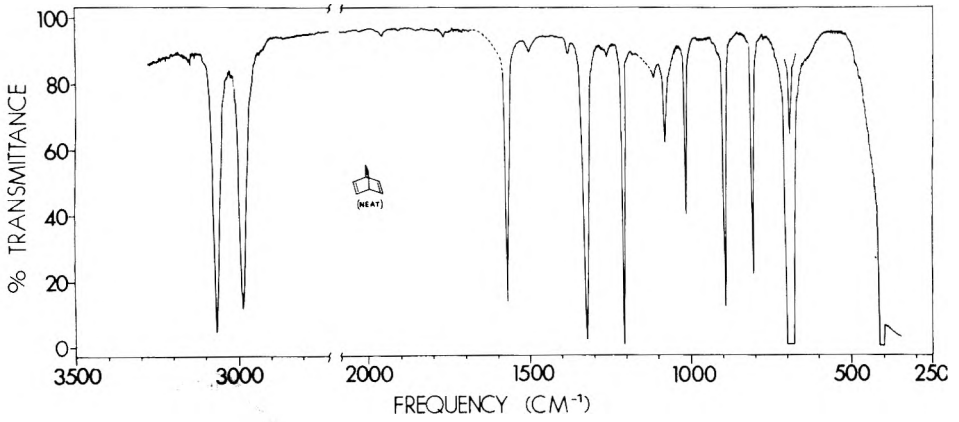

Figure 1. The infrared spectrum of liquid bicyclo[2.2.2]octa-2,5,7-triene.

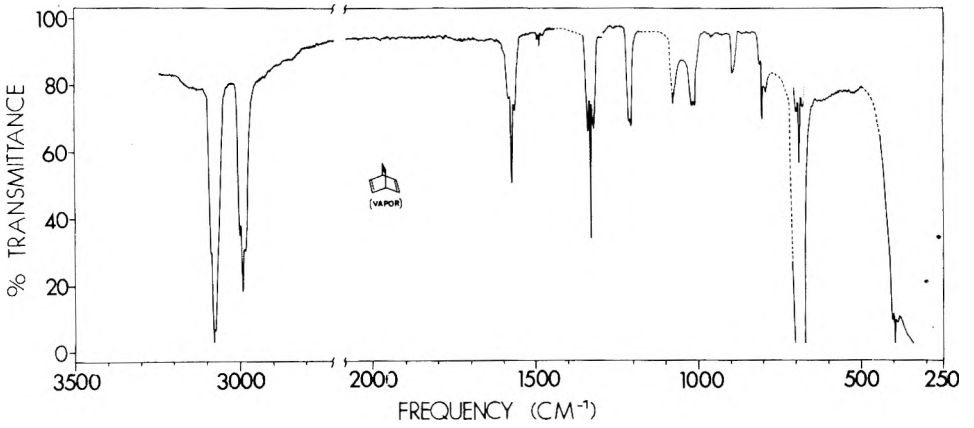

Figure 2. The infrared spectrum of gaseous bicyclo[2.2.2]octa-2,5,7-triene.

gained by considering the empirical force field results for **1** and **3**.[15d] Calculated strain energies are 25.6 and 31.6 kcal/mol, respectively, which compare reasonably well with experiment. On the other hand, this same force field fails to accurately reproduce the stepwise heats of hydrogenation for **1**. Clearly, then, the potential functions currently employed are somehow deficient.

It is important to increase our understanding of vibrations of rigid, strained molecules in order that the details of potential functions appropriate for badly deformed bond angles, bond lengths, etc., may be deduced. While such investigations have usually focused on small molecules, e.g., cyclopropane,[16] cyclopropenone,[17] recently some medium-sized, strained bicyclic systems have been studied, albeit in a preliminary fashion for some. (One potential drawback may be the difficulty associated with obtaining deuterated samples of such molecules.) For example, **3**[18,19] and its saturated analogue bicyclo[2.2.1]heptane[18,20] have been examined. Also studies of bicyclo[2.1.0]pentane[21] and bicyclo[1.1.1]pentane[22] have appeared, the latter including normal coordinate calculations. It would seem most profitable to attempt to analyze the vibrational spectrum of **1** in view of the simplifications inherent in its symmetry. In particular, a relatively small number of unique force constants would be required for a normal coordinate analysis. Thus **1** may serve as a good source of initial force constant values for less symmetrical molecules, e.g., **2**, **3**, and **4**.

Experimental Section

Bicyclo[2.2.2]octa-2,5,7-triene (**1**) was prepared by a modification[23] of the method of Zimmerman et al.[3] Vapor phase chromatography (VPC) accomplished clean separation of **1** from the usual contaminant, benzene. Preparative separations were carried out on a Prepmaster Jr. Model 776 instrument fitted with an 80 in. × 1 in. column, 15% Apiezon L on acid-washed Chromosorb P. Spectroscopic samples were purified by distillation and analytical VPC on a 200 cm × 0.65 cm column with the same packing used for preparative VPC. We estimate from VPC experiments that the *lower* limit of purity for these samples is 99.9%.

Infrared spectra were recorded on a Perkin-Elmer Model 521 double-beam grating spectrophotometer. The ir spectrum of liquid **1** (Figure 1) was recorded using KBr plates in the region 380–4000 cm^{-1}. CsI plates were used for the region 200–500 cm^{-1}. Since no noteworthy features were observed below 400 cm^{-1}, further use of CsI windows was felt to be unwarranted. Spectra of gaseous **1** were recorded in a 7.5-cm cell fitted with KBr windows over a pressure range of 10–60 Torr. Since pressure broadening was barely evident at 60 Torr, all working spectra were recorded at 30 Torr. The full scan for the gas phase is recorded in Figure 2. Polycrystalline films of **1** were examined at liquid nitrogen temperatures using a modified Wagner–Horning cell[24] equipped with KBr windows. The solid smple was repeatedly annealed until no further changes occurred in the spectrum (Figure 3).

The Raman spectrum of liquid **1** (Figures 4 and 5) was excited with 250 mW (measured at sample) of 488.0-nm radiation from a Coherent Radiation Laboratory Model 52 Ar^+ laser and recorded on a Japanese Electron Optics Laboratory Model JRS-S1 spectrometer.

The light collection system samples light scattered at an angle of 90° relative to the incident beam. The scattered light

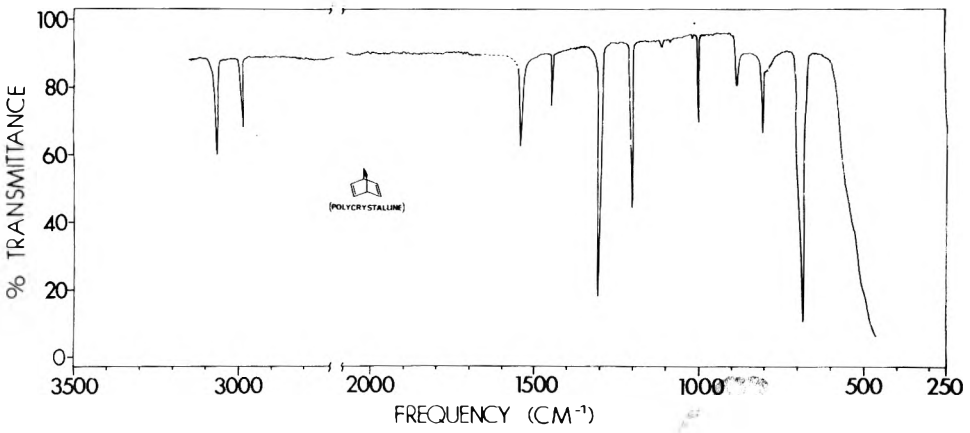

Figure 3. The infrared spectrum of polycrystalline bicyclo[2.2.2]octa-2,5,7-triene.

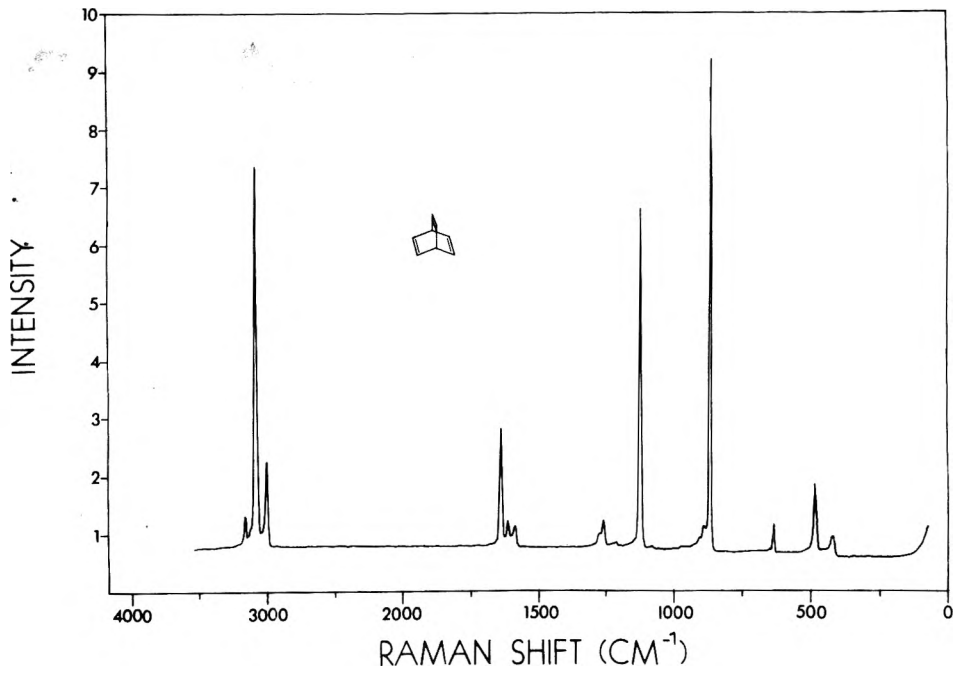

Figure 4. The Raman spectrum of liquid bicyclo[2.2.2]octatriene, $I(\|)$ observed (see Experimental Section).

passes through condensing optics and a fixed polarizer permitting passage only of light with its electric vector parallel to that of the incident beam. The polarizer is followed by a polarization scrambler through which the light passes prior to determination of the intensity, $I(\|)$. Determination of depolarization ratios, $P = I(\perp)/I(\|)$, is accomplished by passing the laser beam through a Porro-prism followed by a Glans-Thompson prism prior to sample irradiation. The electric vector of the incident light is thus rotated through an angle of 90°, and analysis of the scattered light as indicated above constitutes determination of $I(\perp)$. Narrow regions of the spectrum (100–200 cm^{-1}) were scanned several times in both modes. Depolarization ratios were calculated by equating peak height to peak intensity. Samples were examined in pyrex capillaries previously calibrated with CCl_4. We consider these ratios to be of only semiquantitative significance.

Both instruments were calibrated using indene, camphor, and cyclohexanone as frequency standards.[25] All frequencies are considered accurate to ±2 cm^{-1}. The spectral data are summarized in Table I.

Assignments

The internal coordinates for barrelene are depicted in Figure 6. No experimental determination of the structural parameters of 1 has been reported. The structural parameters we have used are obtained via molecular mechanics calculations.[26] While the method employed may have deficiencies, the molecular geometry thus obtained is more realistic than one obtained from molecular models. Further, the history of the method suggests that the true geometry is unlikely to differ severely. The structural parameters are D = 1.3416 Å; T = 1.5149 Å; d = 1.0989 Å; l = 1.0934 Å; $\theta = \epsilon$ = 113.50°; ϕ = 123.58°; ω = 102.97°. (While five significant figures may seem excessive, these structural parameters will reproduce exactly the final cartesian coordinates obtained.[26]) The moments of inertia resulting from these parameters are $I_\| = I_z$ = 283.84 × 10^{-40} g cm^2; $I_\perp = I_x = I_y$ = 295.68 × 10^{-40} g cm^2. Though barrelene is formally a prolate symmetric top, the asymmetry factor[26]

$$\beta = [(I_z/I_x) - 1] = -0.04 \quad (1)$$

TABLE I: Vibrational Assignment of Bicyclo[2.2.2]octa-2,5,7-triene

Raman,[a] neat, cm^{-1}	Ir, neat, cm^{-1}	Ir, polycrystalline, cm^{-1}	Ir, vapor, cm^{-1}	Assignment
418(0.76,46)	413 m		402 w P 411 w Q 421 w R	$\nu_{21}(E')$
485(0.79,130)				$\nu_{28}(E'')$
	613 w			$\nu_{18}(E')-\nu_{8}(A_1'')^b$
640(0.03,65)				$\nu_{6}(A_1')$
684(0.7,4)				$\nu_{27}(E'')$
698(0.91,4)	693 vs	698 s	686 s P 697 s Q 707 S R	$\nu_{20}(E')$
	811 s	811 w	802 m P 812 m Q 821 m R	$\nu_{14}(A_2'')$
870(0.02,1000)	870 vw			$\nu_{5}(A_1')$
893.5(0.44,46)	898 s	897 w	895 m QP 906 m QR	$\nu_{19}(E')$
910(0.9,11)	913 sh			$\nu_{26}(E'')$
	1016 s	1016 s 1026 sh	1012 sh P 1020 s Q	$\nu_{13}(A_2'')$
1083(0.69,15)	1081 m 1116 w	1078 w	1084[c] Q	$\nu_{18}(E')$ $\nu_{16}(E')-\nu_{8}(A_1'')^b$
1128(0.53,122)	1129 w	1137 w		$\nu_{4}(A_1'), \nu_{25}(E'')$
1169(0.4,4)	1166 vw	1189 w		$\nu_{28}(E'') + \nu_{27}(E'')$
1213(0.7,23)	1215 s	1215 m	1216 s QP 1221 s QR	$\nu_{17}(E')$
1228(0.7,80)				$\nu_{24}(E'')$
1258(0.8,57)	1262 w	1264 vw		$\nu_{23}(E'')$
1275(0.92,23)	1276 vw	1279 w		$\nu_{5}(A_1') + \nu_{21}(E')$
	1331 s	1328 vs	1328 vs P 1338 vs Q 1349 vs R	$\nu_{12}(A_2'')$
	1386 vw			$2\nu_{20}(E')$
	1498 w	1488 w	1480 w P 1490 w Q 1500 w R	$\nu_{13}(A_2'') + \nu_{8}(A_1'')^b$
	1554 sh	1562 w		$\nu_{18}(E') + \nu_{8}(A_1'')^b$
1585(0.13,34)	1578 vs	1572 s 1578 s	1573 s P 1583 s Q 1591 s R	$\nu_{16}(E')$
1611(0.03,38)	1612 w			$\nu_{3}(A_1')$, FR with $2\nu_{14}(A_2'')$
1637(0.03,164)	1642 vw 1652 vw			$\nu_{6}(A_1') + \nu_{13}(A_2'')$
2985(0.20,126)				$\nu_{2}(A_1')$
	2987 s	2984 s	2989 s P 2998 s Q 3006 s R	$\nu_{11}(A_2'')$
			3075 sh P(?)	
	3068 s	3065 s	3079 s P(?) 3086 s Q 3093 s R	
3072(0.15,580)				$\nu_{1}(A_1'), \nu_{22}(E'')$
3146(0.09,46)			3151 w	$2\nu_{16}(E')$

[a] Following the Raman frequencies in parentheses are listed the depolarization ratios and relative intensities, respectively. The Raman intensities are normalized for the most intense peak. [b] The assignments for these sum and difference combination bands are predicated upon the value $\nu_{16} = 470\ cm^{-1}$, substantially higher than the predicted value (see Table III). It should be noted, on the other hand, that the combination bands $\nu_{16} + \nu_{8} = 2053$, and $\nu_{13} - \nu_{8} = 550$ are not observed. These assignments are therefore tenuous, at best. [c] Not resolved.

reveals that the molecule is a near-spherical top. Consideration of the rotational energy levels

$$E_{J,K}(cm^{-1}) = 0.094\,66J(J+1) + 0.003\,95K^2 \quad (2)$$

shows that, although K remains a "good" quantum number, we can expect little difference in the appearance of the parallel and perpendicular bands in the ir spectrum of the gaseous molecule. PR separations are calculated[27] to be 23.5 and 24.2

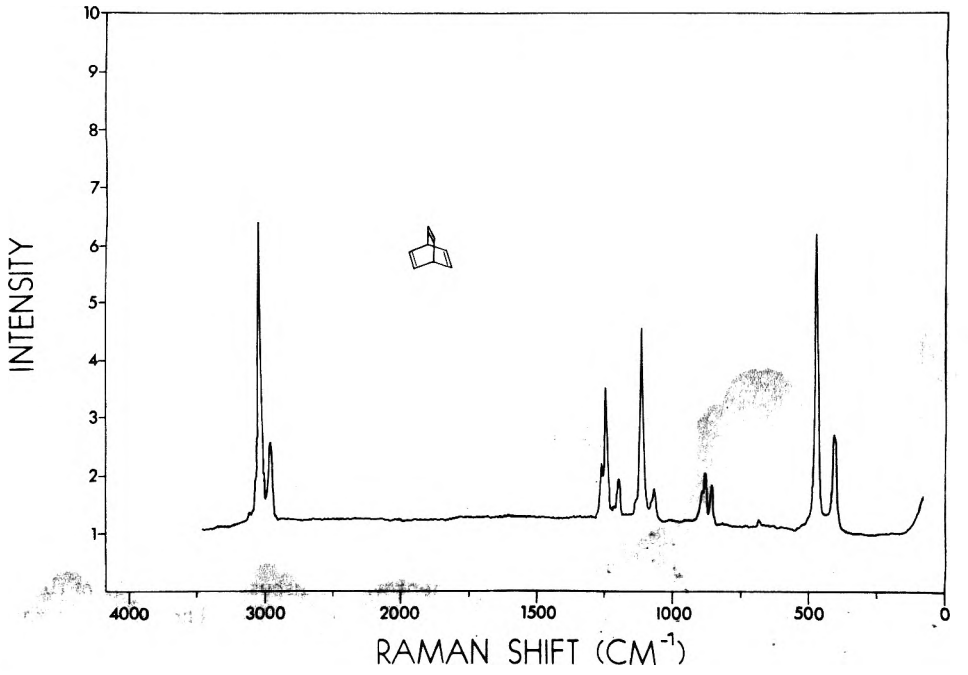

Figure 5. The Raman spectrum of liquid bicyclo[2.2.2]octatriene, $I(\perp)$ observed (see Experimental Section).

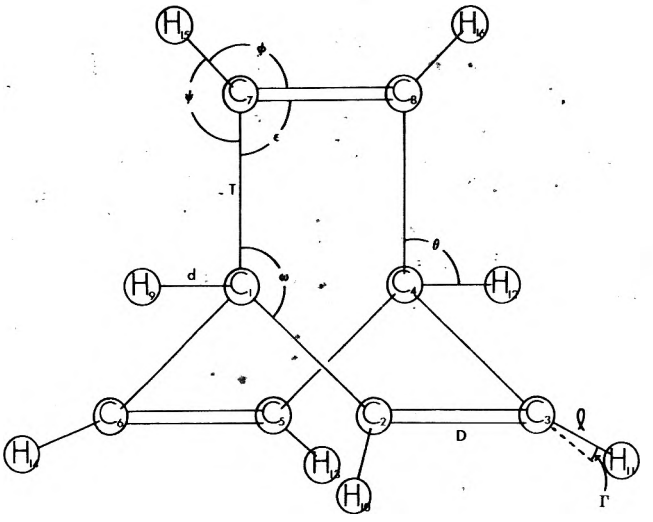

Figure 6. The internal coordinates (excluding torsions) employed for the normal coordinate analysis of bicyclo[2.2.2]octa-2,5,7-triene.

cm^{-1}, respectively. As a consequence assignments must be made without resort to band shape considerations. We have relied primarily, therefore, on ir-Raman activity and Raman depolarization values in making most of our assignments. Some few, though, required the aid of normal coordinate calculations.

The 42 normal modes of barrelene transform as

$$\Gamma_{vib}(D_{3h}) = 6A_1' + 1A_2' + 7E' + 2A_1'' + 5A_2'' + 7E''$$

We anticipate, therefore, 6 polarized (A_1') and 14 depolarized (E′ and E″) Raman lines. Seven Raman lines should have ir counterparts (E′), while 5 lines will be active in the ir only (A_2''). Three normal modes (A_2' and A_1'') will be inactive.

a. *C–H Stretching Assignments.* The structure of the representation formed by the olefinic C–H stretching modes is $A_1' + E' + A_2'' + E''$. Due to the isolation among the two-carbon bridges, we anticipated little separation between modes of A and E symmetry. We did feel that in-phase (′) and out-of-phase (″) motions on a given two-carbon bridge would give rise to observable splittings in the spectrum. Examination of the vapor phase ir spectrum (Figure 7a) shows only one strong band above 3000 cm^{-1} centered at 3086 cm^{-1}. A shoulder does appear on the P branch, however, leading us to conclude that the two modes, A_2'' and E′, have nearly the same energy. Similar overlapping appears to occur in the Raman spectrum (Figure 7b). Only one line is observed (3072 cm^{-1}) and it is polarized, leading us to associate it with the A_1' mode. Two features are worthy of note. First, the band ($I(\parallel)$ observed) shows distinct asymmetry. Second, the liquid phase ir band appears at 3068 cm^{-1}. The possible rationales reconciling these observations are as follows: (1) the A_1' and E″ appear close together in the Raman spectrum; (2) the asymmetry of the Raman line arises from the E′ mode at 3068 cm^{-1}; (3) both (1) and (2) are true. In the absence of additional information we have assigned both the E″ and A_1' modes to the 3072-cm^{-1} Raman line. Similar coincidences have been noted in the CH_2 stretching modes of bicyclo[1.1.1]pentane.[22]

The question of the splitting of the symmetric and antisymmetric C–H stretching modes is not yet resolved for (*Z*, cis) olefins. (*Z*)Butene-2 exhibits only one Raman line in this region,[28] though both modes should be Raman active. (By way of contrast, an 18-cm^{-1} splitting is reported for (*E*, *trans*)-butene-2.[29]) A substantial splitting, 38 cm^{-1}, is observed for cyclohexene,[30] but not for cycloheptene.[31] Conversely cyclohexadiene[32] reportedly shows no splitting in the vapor phase, but cyclopentadiene[33] is reported to show four peaks spanning a range of 70 cm^{-1}. As the splitting seems to be dependent upon the molecule under study, we feel justified in making the assignments outlined above.

The representation formed by the bridgehead C–H stretches is $A_1' + A_2''$. These modes should appear below 3000 cm^{-1}. The band observed at 2998 cm^{-1} in the ir vapor phase spectrum is clearly the A_2'' mode while the Raman band at 2985 cm^{-1} may be taken to correspond to the A_1' mode. These frequencies are somewhat high relative to unstrained alicyclic systems, but are consistent with observations for strained

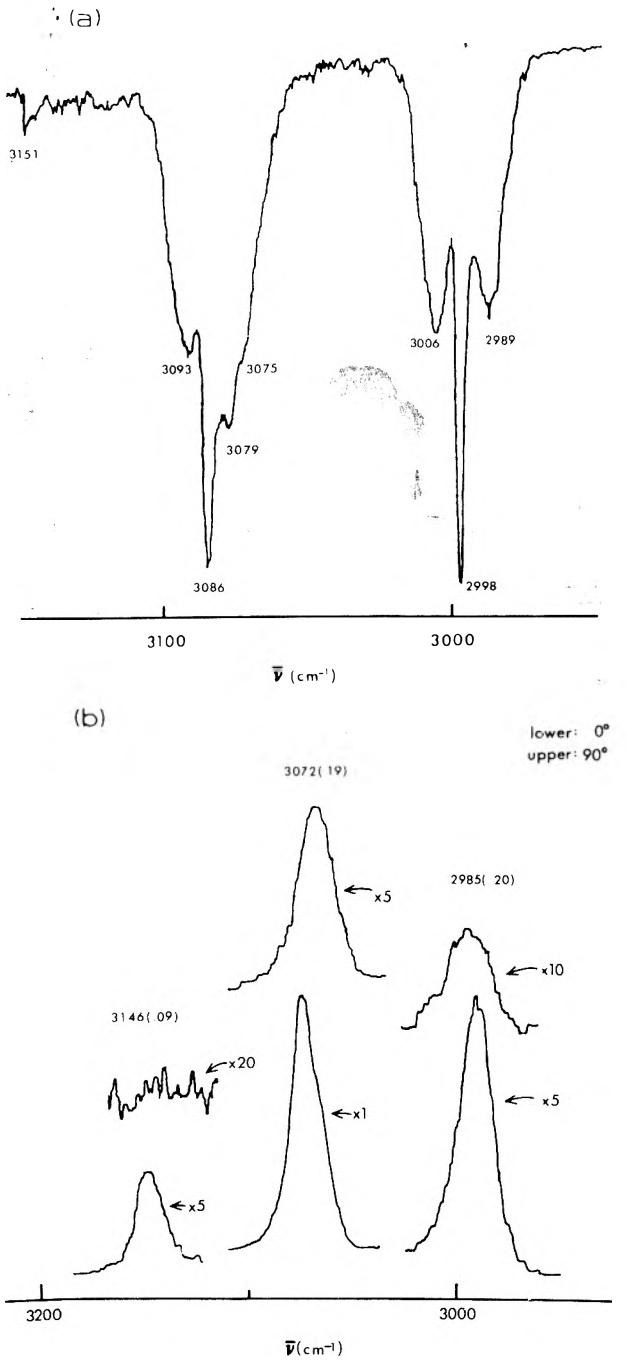

Figure 7. The vibrational spectra of bicyclo[2.2.2]octa-2,5,7-triene in the region 3150–2950 cm^{-1}: (a) gaseous infrared spectrum; (b) liquid Raman spectrum.

bicyclic systems, e.g., norbornane,[19,20] norbornadiene,[18,19] and the bicyclopentanes.[21,22]

The only remaining feature in this region occurs at 3151 cm^{-1} (ir, vapor) and 3146 cm^{-1} (Raman, liquid). We have taken this to be the overtone of the E′ C=C stretching mode appearing at 1583 cm^{-1} in the vapor phase ir spectrum.

b. *C=C Stretching Assignments.* Group frequency considerations predict the C=C stretching modes to lie in the region 1575–1650 cm^{-1}. It is not unusual in strained molecules to find these vibrational modes at lower frequencies,[17,19] but barrelene appears to be "normal" in this regard. Modes of A_1' and E′ symmetry are predicted. The latter is found in the vapor phase ir spectrum at 1583 cm^{-1} with a corresponding Raman band at 1585 cm^{-1}. The totally symmetric mode appears in the Raman spectrum at 1637 cm^{-1}, with a companion peak at 1611 cm^{-1}. As these two lines have (within experimental error) identical depolarization ratios, we postulate that these two features result from Fermi resonance interaction of the A_1' C=C stretching mode with the overtone of the fundamental at 812 cm^{-1} (A_2'', vide infra). In the absence of more detailed information we have assigned the "true" C=C stretching mode as the mean value, 1624 cm^{-1}. By way of comparison, the totally symmetric C–C stretching mode for norbornadiene, **3**, is reported to appear at 1572 cm^{-1}.[19]

c. *A_1' Assignments.* The remaining three A_1' modes should be associated with olefinic C–H in-plane bending, and the framework deformation modes corresponding primarily to C–C stretching and bridgehead C–C–C angle bending. There are two Raman lines with exceedingly low depolarization ratios (<0.05) at 870 and 640 cm^{-1}. We tentatively associate them, respectively, with the framework deformations just mentioned. We could not with confidence make an assignment at this point for the remaining A_1' mode. Hence this assignment will be discussed at the end of this section.

d. *E′ Assignments.* The remaining five E′ modes are expected to be both ir and Raman active. The basic modes to be accounted for may be described as olefinic C–H in-plane and out-of-plane bending, bridgehead hydrogen bending, and carbon framework deformation modes involving bridgehead C–C–C angle bending and C–C stretching. Three intense vapor phase ir bands have weak Raman counterparts with high depolarization ratios. The 1218-, 697-, and 411-cm^{-1} bands are associated by us with bridgehead C–H bending, olefinic C–H out-of-plane deformations, and framework deformations (angle bending), respectively. A fourth vapor phase ir band (900 cm^{-1}) exhibits medium intensity, but its Raman counterpart (893 cm^{-1}) has a somewhat low depolarization ratio. Nonetheless, the liquid phase ir band (898 cm^{-1}) is intense, and we consider this to be the C–C stretching mode. We chose to defer assigning the olefinic C–H in-plane bending mode at this point as there are a number of bands in the region 1000–1200 cm^{-1} to be sorted out.

e. *A_2'' Assignments.* The three remaining A_2'' modes are ir-active only and associated with olefinic C–H in-plane bending, and framework deformation modes best described as bridgehead angle bending and C–C stretching. The lines corresponding to these modes are assigned as 1338, 1024, and 812 cm^{-1}, respectively.

f. *E″ Assignments.* The six remaining E″ modes correspond to olefinic C–H in-plane and out-of-plane bending, bridgehead hydrogen bending, and the framework deformations encompassing C–C stretching, angle bending, and torsions. These assignments were the most difficult to make since only three of the Raman lines not already assigned are clearly depolarized and have no ir counterpart. We associate the 1228-cm^{-1} line with in-plane bending, the 684-cm^{-1} line with framework angle bending, and the 485-cm^{-1} line with torsional deformations. Since all other unassigned Raman lines had ir counterparts we felt obliged to defer the remaining 3 E″ assignments.

g. *Deferred Assignments.* In order to make the remaining assignments it was necessary to begin carrying out a normal coordinate analysis. A small force field (26 force constants) was employed for this preliminary work. The unassigned normal modes may be represented as $A_1' + E' + 3E''$. The bands as yet unassigned appear in the Raman spectrum at 910, 1083, 1128, 1169, 1258, and 1275 cm^{-1}. We were able to assign the E′ mode to the 1083-cm^{-1} line since this is the only one of

these bands having substantial intensity in the liquid phase ir spectrum. The E″ modes were best assigned as 910, 1128, and 1258 cm^{-1}, while the 1275-cm^{-1} line is felt to arise as a combination band, 870 (A_1') + 411 (E′) = 1281 (E′). The remaining A_1' mode was originally assigned to the 1169-cm^{-1} line, but attempts to refine the force constants clearly indicated that this value was too large by 30–50 cm^{-1}. The A_1' mode was, therefore, assigned to the 1128-cm^{-1} line, along with the E″ mode. This assignment helps to rationalize the low depolarization ratio observed for this line. The 1169-cm^{-1} line may then also be a combination band, 684 (E″) + 485 (E″) = 1169 ($A_1' + A_2' + E'$).

Before we conclude this section, it would be appropriate to comment on the depolarization ratios associated with some of the nontotally symmetric vibrations. The theoretical value, $\rho = 0.75$, holds rigorously only for gas phase measurements and we have made no attempt to apply refractive index corrections to our liquid phase intensity measurements. Further, the optical system of the instrument employed is likely to introduce errors in this quantity.[34] Nonetheless, most of the large deviations in ρ are readily understood. Depolarization ratio determinations for weak bands are hampered by the noise content of the spectrum, particularly in determining $I(\perp)$ (see Figure 7b). We ascribe the ρ values observed for the 698, 910, and 1275 cm^{-1} to this difficulty. In the case of the band at 893 cm^{-1} we feel the low ρ value arises from enhancement of $I(\parallel)$ by its proximity to the 870-cm^{-1} line, the most intense Raman line. We are unable, on the other hand, to satisfactorily account for the exceedingly low ρ value associated with the 1585-cm^{-1} line. The E′ assignment seems appropriate, however, in view of its strong counterpart in the infrared.

The assignment outlined above, along with the overtone, combination, and difference band assignments indicated in Table I, accounts for all observed features in the ir and Raman spectra of barrelene.

Normal Coordinate Analysis

Several general valence force fields (GVFF), only one of which will be reported in detail, were generated for barrelene. The particular computational scheme employed was originally outlined by Overend and Scherer.[35] The current versions of these programs[36] employ the **W** matrix variant[37] of the Wilson **GF** formalism.[38] An important feature of the current system is the transformation to the intrinsic force constant space for which the force constant error matrix is diagonal.[39] This facilitates identification of ill-determined force constant values in the original force constant space.

The internal coordinates utilized as a basis for the normal coordinate calculations include all those indicated in Figure 6 plus all possible framework torsions (Figure 8). This leads to an overcomplete set of 68 internal coordinates. Of the 26 redundancies contained therein, 8 are angle bending in nature, 2 arising at the sp^3 bridgehead carbons, and 6 arising at the sp^2 carbons. A kinematically complete set generated by the Decius[40] prescription would eliminate these. The bridgehead redundancies are retained for reasons of symmetry, while the C_{sp^2} redundancies are retained in the hope of maximizing transferability. The Decius set of internal coordinates contains 1 torsion for each nonterminal carbon–carbon bond (9 total) and 12 cyclic redundancies. Our set, again from symmetry considerations, contains 15 torsions. Hence our set of internal coordinates introduces 6 additional local redundancies. (A crude, but useful rationale is that this outcome results from considering such bicyclic systems as consisting of three rather than two rings.) Due to the computer methods employed (vide supra), no difficulty arises as a consequence of the redundant symmetry coordinates derived from these internal coordinates.

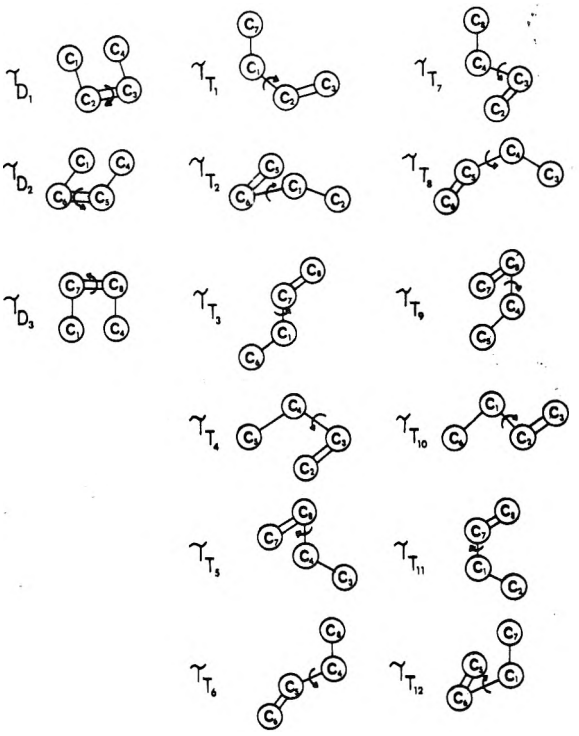

Figure 8. The torsional internal coordinates employed in the normal coordinate analysis of bicyclo[2.2.2]octa-2,5,7-triene.

The several trial potential functions were generated without constraining any force constant values.[41] Convergence was obtained by always refining the Φ_i's in two subsets constructed so as to avoid divergence problems, e.g., H_r, H_ϕ, and H_ψ could not be included in the same subset (see Figure 6). Care was taken to ensure that, apart from linear dependencies (vide supra), the various force fields corresponded to true convergence. These last tests were crucial since no more than 19 force constant values were refined in a given cycle. First a 26-parameter potential function was used to finalize the vibrational assignment. Then a more general 37-parameter potential function was subsequently developed which could also be refined satisfactorily, based on the complete vibrational assignment. It was noted, on the other hand, that several force constants in the latter potential function had relative dispersions ≥80% of the force constant value. We thus generated our final potential function by bringing to bear all possible considerations in rendering it statistically meaningful.

The selection of a final force constant set was cause for some reflection. Few GVFF calculations are truly "general". The internal coordinate set requires no more than 12 principal force constants, while the data set (28 frequencies) imposed on upper bound on the number of parameters that could be varied in a given cycle. We were concerned lest our set be too small, thereby limiting transferability. For this reason the 26 parameter potential function employed for finalizing the vibrational assignment was felt to be too restricted. We arrived at a 37-parameter potential function built up as follows: (1) Stretch–stretch interactions are included for all pairs of carbon–carbon bonds having a common atom. (2) Stretch–bend interactions are included for all angles with apices at one of

Chart I

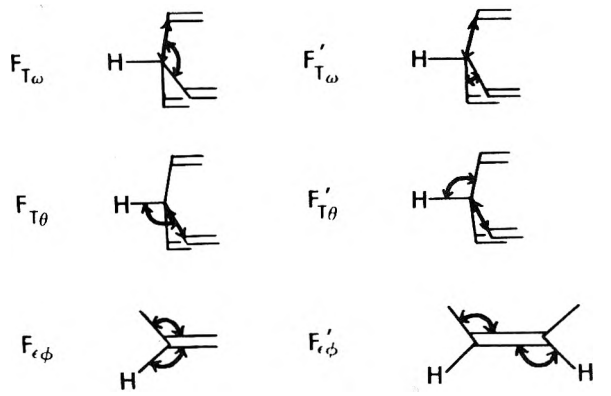

the termini of the carbon–carbon bond in question. (3) Bend–bend interactions are included for all angles about the nearest-neighbor carbon atoms where the bond is a common side for the angles in question. (4) No interaction force constants involving the C–H stretches, torsions, or out-of-plane bends were included. (This is consistent with the force fields used in studies of cyclohexene[30] and cycloheptene.[31]) (5) No next-nearest-neighbor interactions were included. It seems clear that, at least for saturated hydrocarbons,[42] these interaction force constants are exceedlingly small. The force field thus obtained possesses nomenclature problems in that several interaction force constants have the same nominal designation. The ambiguities arising for the interaction force constants are clarified in Chart I.

The cyclohexene force field of Neto et al.[30] was the principal source of our zero-order force constants $\{\Phi_i{}^0\}$. We considered using those reported by Levin and Harris[19] for norbornadiene, **3**. One noteworthy feature of this force field is a C=C stretching force constant (K_D in our notation) of 6.61 mdyn/Å. Our exploratory work with the 26-parameter potential function showed that there were two different solutions to the problem, depending upon the starting value for K_D.[41] (This problem is well-known with regard to ethylene.[43]) Since most olefin force fields lead to a value of ~8–8.5 mdyn/Å we chose to use the cyclohexene data. Some few zero-order force constants were taken from the standard hydrocarbon force field.[42] There are two interaction constants, $F'_{T\omega}$ and $F_{\theta\psi}$, for which we were unable to find reasonable starting values.

Prior to the refinement of the force constants it was necessary to impose some constraints upon the potential function with regard to the C_{sp^2} carbon angles. It is possible to construct a set of three bending coordinates in such a manner that the principal and interaction force constants for one of the three will be indeterminant. We have chosen, in the interests of retaining transferability, to retain the primitive bending coordinates and constrain the associated Φ_i's in the following manner. Since the angle ϕ (Figure 6) resembles closely a "normal" C_{sp^2}–C_{sp^2}–H angle, H_ϕ was fixed at the cyclohexene value. For stretch–bend interactions we felt it important to permit variational freedom in those cases where the bond in question also defines the angle involved. Hence $F_{D\psi}$ and $F_{T\phi}$ were likewise held constant. Finally, for bend–bend interactions, since H_ϕ is fixed, the relationship of deformations in ϵ and ψ to ϕ must be accommodated. Hence $F_{\epsilon\phi}$ and $F_{\phi\psi}$ were permitted to vary while $F_{\epsilon\psi}$ was fixed. During the refinement of the force constants, ill-determined intrinsic force constants indicated that several other interaction force constants would also have to be fixed for meaningful results to be obtained. Based on these considerations, $F_{D\phi}$, $F_{T\theta}$, $F_{T\psi}$, $F'_{T\theta}$, $F_{\epsilon\omega}$, $F_{\omega\psi}$, $F_{\theta\epsilon}$, and $F'_{\epsilon\phi}$ were fixed at the cyclohexene values.

TABLE II: Zero Order and Refined Force Constants for Bicyclo[2.2.2]octa-2,5,7-triene[a]

i	Force constant	$\Phi_i{}^0$ [b]	$\Phi_i{}^R$	$\sigma(\Phi_i{}^R)$
1	K_D	8.700	8.126	0.034[h]
2	K_T	4.384	4.017	0.039[g]
3	K_l	5.068	5.148	0.005[h]
4	K_d	4.588[c]	4.851	0.009[g]
5	H_ω	1.084[c]	0.975	0.028[g]
6	H_θ	0.657[c]	0.634	0.005[g]
7	H_ϵ	0.917	1.061	0.016[g]
8	H_ϕ	0.504	0.504	[d]
9	H_ψ	0.477	0.698	0.006[h]
10	H_Γ	0.221	0.270	0.003[h]
11	τ_D	0.222	0.458	0.041[g]
12	τ_T	0.020	0.258	0.021[g]
13	F_{DT}	0.098	0.027	0.033[g]
14	F_{TT}	0.101[c]	0.357	0.036[i]
15	$F_{D\epsilon}$	0.423	0.514	0.046[g]
16	$F_{D\phi}$	0.365	0.365	[e]
17	$F_{D\psi}$	0.077	0.077	[d]
18	$F_{T\omega}$	0.417[c]	0.508	0.032[h]
19	$F_{T\theta}$	0.360	0.360	[e]
20	$F_{T\epsilon}$	0.423	0.938	0.021[g]
21	$F_{T\psi}$	0.319	0.319	[e]
22	$F'_{T\omega}$	[f]	0.414	0.035[h]
23	$F'_{T\theta}$	0.048	0.048	[e]
24	$F_{T\phi}$	0.077	0.077	[d]
25	$F_{\theta\psi}$	[f]	0.133	0.002[h]
26	$F_{\epsilon\phi}$	−0.043	0.251	0.015[h]
27	$F_{\epsilon\psi}$	−0.043	−0.043	[d]
28	$F_{\phi\phi}$	0.122	0.006	0.004[h]
29	$F_{\phi\psi}$	0.033	0.170	0.003[g]
30	$F_{\epsilon\epsilon}$	−0.017	−0.337	0.035[h]
31	$F_{\omega\omega}$	−0.041[c]	−0.078	0.017[h]
32	$F_{\omega\theta}$	−0.034	−0.207	0.011[g]
33	$F_{\epsilon\omega}$	0.017	0.017	[e]
34	$F_{\omega\psi}$	0.062	0.062	[e]
35	$F_{\theta\theta}$	0.012[c]	0.022	0.004[h]
36	$F_{\theta\epsilon}$	−0.032	−0.032	[e]
37	$F'_{\epsilon\phi}$	0.062	0.062	[e]

[a] Stretching constants are in units of mdyn/Å; stretch–bend interaction constants in units of mdyn/radian, and bending constants in units of mdyn Å/radian². [b] From ref 30, unless otherwise noted. [c] From ref 42. [d] These force constants were not varied in order to deal with C_{sp^2} angle bending redundancy. [e] These force constants were not varied due to large contributions to ill-determined intrinsic force constants. [f] No reasonably similar force constants were found in the literature. [g] These force constants were refined together as set A. [h] These force constants were refined together as set B. [i] This force constant was varied in both sets. The dispersion reported is the larger of the two values.

Several of the refined force constants are found to differ substantially from their zero-order values (changes of 50% or more). We shall attempt to relate these changes to structural features of **1** that are absent in cyclohexene. The zero-order and refined force constant values are summarized in Table II.

Among the principal force constants, H_ψ, τ_D, and τ_T are most significantly altered. For H_ψ we believe the increase (~47%) is associated with the forced eclipsing of the olefinic and aliphatic C–H bonds. This arrangement is absent in cyclohexene, and does not generally arise in simple olefinic systems. The increase in τ_D (~100%) and τ_T (~1200%) clearly reflect the rigidity of the cage structure of **1**. The fact that the *refined* value for τ_T exceeds the *zero-order* value for τ_D serves to illustrate the powerful constraints inherent in such molecules.

It is intuitively obvious that vibrational motions in mole-

TABLE III: Comparison of Calculated and Observed Frequencies and Potential Energy Distribution of Bicyclo[2.2.2]octa-2,5,7-triene[a]

	N	ν_{obsd}, cm^{-1}	ν_{calcd}, cm^{-1}	PED
A_1'	ν_1	3072	3083	$0.99K_l$
	ν_2	2985	2991	$0.99K_d$
	ν_3	1624	1624	$0.72K_D + 0.10K_T + 0.19H_\psi - 0.10F_{D\phi}$
	ν_4	1128	1126	$0.18K_D + 0.36H_\phi + 0.57H_\psi + 0.13F_{D\phi} - 0.26F_{\phi\psi}$
	ν_5	870	872	$0.10K_D + 0.64K_T + 0.11F_{TT} - 0.15F_{T\omega} + 0.12F_{T\epsilon}$
	ν_6	640	639	$0.12K_T + 0.26H_\omega + 0.13H_\theta + 0.22H_\epsilon - 0.24H_\phi + 0.12\tau_T + 0.18F_{T\omega} - 0.15F_{T\epsilon} - 0.15F_{\epsilon\phi} + 0.19F_{\omega\theta}$
A_1''	ν_7	Not active	980	$0.67H_\Gamma + 0.19\tau_D + 0.15\tau_T$
	ν_8	Not active	415	$0.33H_\Gamma + 0.37\tau_D + 0.30\tau_T$
A_2'	ν_9	Not active	685	$1.00H_\Gamma$
A_2''	ν_{10}	3086	3080	$0.98K_l$
	ν_{11}	2998	2992	$0.98K_d$
	ν_{12}	1338	1339	$0.19H_\phi + 0.57H_\psi - 0.19F_{\phi\psi}$
	ν_{13}	1020	1024	$0.39H_\theta + 0.66H_\phi + 0.20H_\psi - 0.15F_{T\epsilon} - 0.35F_{\epsilon\phi} - 0.21F_{\phi\psi} + 0.12F_{\epsilon\epsilon}$
	ν_{14}	812	810	$0.90K_T + 0.16F_{TT} - 0.23F_{T\omega} - 0.22F_{T\epsilon}$
E'	ν_{15}	3086	3080	$0.99K_l$
	ν_{16}	1583	1583	$0.83K_D + 0.10K_T + 0.11H_\psi - 0.09F_{D\phi}$
	ν_{17}	1218	1219	$0.52H_\theta + 0.21H_\phi + 0.29H_\psi + 0.15F_{\theta\psi} - 0.14F_{\phi\psi}$
	ν_{18}	1084	1085	$0.44K_T + 0.58H_\theta + 0.15H_\phi + 0.29H_\psi - 0.23F_{T\theta} + 0.14F_{T\psi} - 0.16F_{\theta\psi} - 0.12F_{\phi\psi}$
	ν_{19}	900	899	$0.16K_D + 0.44K_T + 0.21H_\phi + 0.16H_\psi + 0.12H_\Gamma + 0.09F_{D\phi} - 0.10F_{T\epsilon} - 0.10F_{T\psi} - 0.10F_{\phi\psi}$
	ν_{20}	697	698	$0.27K_T + 0.70H_\Gamma$
	ν_{21}	411	411	$0.61H_\omega + 0.16H_\Gamma + 0.15\tau_T + 0.10F_{T\omega}$
E''	ν_{22}	3072	3076	$0.99K_l$
	ν_{23}	1258	1258	$0.27K_T + 0.14H_\omega + 0.27H_\Gamma + 0.19\tau_D + 0.22\tau_T - 0.10F_{T\omega}$
	ν_{24}	1228	1226	$0.37H_\theta + 0.32H_\phi + 0.43H_\psi + 0.16F_{\theta\psi} - 0.21F_{\phi\psi}$
	ν_{25}	1128	1127	$0.74H_\theta + 0.25H_\phi + 0.41H_\psi - 0.22F_{\theta\psi} - 0.18F_{\phi\psi}$
	ν_{26}	910	910	$0.91K_T + 0.31H_\phi + 0.13H_\phi + 0.16H_\Gamma + 0.48F_{T\epsilon} - 0.14F_{\epsilon\phi} + 0.10F_{\epsilon\epsilon}$
	ν_{27}	684	682	$0.42H_\theta + 0.23H_\phi + 0.11H_\Gamma + 0.14F_{T\epsilon} - 0.22F_{\epsilon\phi} + 0.13F_{\epsilon\epsilon}$
	ν_{28}	485	485	$0.46H_\Gamma + 0.13\tau_D + 0.27\tau_T$

[a] Average percent error = 0.13. Average error = 2.0 cm^{-1}.

cules such as 1 are likely to be more strongly coupled than in simple acyclic or monocyclic systems. A good measure of this coupling is the magnitudes of the interaction force constants. Thus, the refined interaction force constants relating the internal coordinates D, T, ϵ, and ω should exceed substantially the cyclohexene values. We find that F_{TT}, $F_{T\epsilon}$, and $F_{\epsilon\epsilon}$ are indeed larger by at least an order of magnitude. Smaller, but significant increases are noted for $F_{\omega\omega}$ and $F_{\omega\theta}$. We also find increased values for $F_{\epsilon\phi}$ and $F_{\phi\psi}$, but we do not ascribe great physical significance to these changes. These latter values most probably reflect our particular choices for handling the C_{sp^2} angle bending redundancy. Finally, we are unable to offer a rationale for the exceedingly small value of $F_{\phi\phi}$.

One principal force constant, H_ω, does not conform to our expectations in that it is slightly smaller than the zero-order value. Force field calculations for norbornadiene, 3, yield values of 1.32[19] or 1.54[2] mdyn Å/radian^2 for the analogous angle. The best estimates of the geometry of 3[44] indicate that the equilibrium bond angles are within ~4° of each other and, presumably, strained to roughly the same extent. The difference in H_ω, therefore, is inexplicable on the usual grounds. The origin of this apparent anomaly may lie in a special "electronic" effect that has been previously discussed. It is well-known that, in π-electron approximation, no net stabilization accrues from the interaction of the three double bonds in 1 in calculations neglecting overlap.[3,5-8,45] This is a consequence of the facts that (a) the π MO's of 1 are symmetry determined, and (b) all bond order terms between pπ orbitals on different bridges are identically zero. Goldstein and Hoffmann[46] have pointed out that, when overlap is included, this lack of stabilization actually corresponds to net *destabilization*. Hence a net repulsion among the ethylenic units is predicted in one-electron approximation. (This result has been recently employed in a discussion of the variation with conformation of the one-electron energy for vicinal lone pairs.[47]) Hence the low value obtained for H_ω may be the first experimental evidence for the operation of this effect in barrelene. If this is true, then the difficulties noted in accounting for the heats of hydrogenation for 1 via molecular mechanics[15d] reflect pecularities of the molecule more than deficiencies in the potential function. It is unlikely that molecular mechanics calculations would be able to incorporate such an effect in a satisfactory manner.

A comparison of the observed and calculated frequencies is presented in Table III, along with the potential energy distributions from this force field. The average errors indicate the goodness of fit. The largest values of $|\nu_i^{obsd} - \nu_i^{calcd}|$ are associated with the C–H stretching assignments. Since anharmonic corrections were not applied this is felt to be of small consequence. Examination of the PED's bears out our crude assignments with certain notable exceptions. As anticipated, the low-frequency modes clearly do not conform to the simple group frequency picture. The most obvious examples are ν_{18}, ν_{19}, ν_{12}, and ν_{23}.

Concluding Remarks

We have presented what we consider to be a reasonable and internally consistent vibrational assignment for barrelene, **1**. The normal coordinate analysis supports this assignment in that force constants differing significantly from those found for the simple cycloalkenes[30,31] are readily explicable in terms of the strain and rigidity of **1**. We feel that these force constants, with the exception noted, represent a better starting set for normal coordinate analysis of strained bicyclic olefins than has heretofore been available. A study of norbornadiene, **3**, which supports this view has been completed[2] and will be reported later.

Acknowledgments. We wish to express our appreciation to the donors of the Petroleum Research Fund, administered by the American Chemical Society for sponsoring this research. We also wish to acknowledge the helpful discussions we had with Professors Overend and Crawford of the University of Minnesota. One of us (E.C.M.) wishes to acknowledge summer fellowships granted by Eastman Kodak (1970), the National Science Foundation (1971), Dow Chemical (1972), and the Maximillian Lando Estate (1973), in addition to support over the period 1974–1975 by the donors of the Petroleum Research Fund, administered by the American Chemical Society. Finally, we express our appreciation to the University Computing Center for the generous grant which supported these calculations.

References and Notes

(1) (a) For paper 1 of the series see: F. A. Van-Catledge and C. E. McBride, Jr., *J. Am. Chem. Soc.*, **98**, 304 (1976). (b) Presented at the 170th National Meeting of the American Chemical Society, Chicago, Ill., August 24–29, 1975, Abstract No. PHYS. 104. (c) This research was supported by the Petroleum Research Fund.
(2) Taken from the Ph.D. Thesis of C. E. McBride, Jr., University of Minnesota, 1975.
(3) (a) H. E. Zimmerman, G. L. Grunewald, R. M. Paufler, and M. A. Sherwin, *J. Am. Chem. Soc.*, **91**, 2330 (1969); (b) H. E. Zimmerman and R. M. Paufler, *ibid.*, **82**, 1514 (1960).
(4) E. Wasserman, Ph.D. Thesis, Harvard University, 1958.
(5) C. F. Wilcox, Jr., S. Winstein, and W. G. McMillan, *J. Am. Chem. Soc.*, **82**, 5450 (1960).
(6) G. Giacometti and G. Rigatti, *Ric. Sci.*, **30**, 1061 (1960).
(7) J. Paldus and J. Koutecky, *Collect. Czech. Chem. Commun.*, **27**, 2139 (1962).
(8) (a) N. L. Allinger and M. A. Miller, *J. Am. Chem. Soc.*, **86**, 2811 (1964); (b) N. L. Allinger and J. C. Tai, *ibid.*, **87**, 2081 (1965); (c) N. L. Allinger, J. C. Tai, and T. W. Stuart, III, *Theor. Chim. Acta*, **8**, 101 (1967).
(9) (a) M. H. Perrin and M. Gouterman, *J. Chem. Phys.*, **46**, 1019 (1967); (b) M. H. Perrin, *ibid.*, **59**, 2090 (1973).
(10) (a) F. A. Van-Catledge, *J. Am. Chem. Soc.*, **93**, 4365 (1971); (b) F. A. Van-Catledge, Ph.D. Thesis, Wayne State University, 1968.
(11) (a) R. Hoffman, E. Heilbronner, and R. Gleiter, *J. Am. Chem. Soc.*, **92**, 706 (1970); (b) E. Haselbach, E. Heilbronner, and G. Schroeder, *Helv. Chim. Acta*, **54**, 153 (1971).
(12) N. Bodor, M. J. S. Dewar, and S. D. Worley, *J. Am. Chem. Soc.*, **92**, 19 (1970).
(13) H. Iwamura, K. Morio, and T. L. Kunii, *J. Chem. Soc. D*, 1408 (1971).
(14) (a) R. B. Turner, W. R. Meador, and R. E. Winkler, *J. Am. Chem. Soc.*, **79**, 4116 (1957); (b) R. B. Turner, *ibid.*, **86**, 3586 (1964); (c) R. B. Turner, P. Goebel, B. J. Mallon, W. von E. Doering, J. F. Coburn, Jr., and M. Pomerantz, *ibid.*, **90**, 4315 (1968).
(15) See, for example, (a) R. H. Boyd, S. N. Sanival, S. Shary-Tehrany, and D. McNally, *J. Phys. Chem.*, **75**, 1264 (1971); (b) E. M. Engler, J. D. Andrews, and P. v. R. Schleyer, *J. Am. Chem. Soc.*, **95**, 8005 (1973); (c) D. H. Wertz and N. L. Allinger, *Tetrahedron*, **30**, 2047 (1974); (d) N. L. Allinger and J. T. Sprague, *J. Am. Chem. Soc.*, **94**, 5734 (1972); and the references cited therein.
(16) See, for example, J. L. Duncan and G. R. Burns, *J. Mol. Spectrosc.*, **30**, 253 (1969), and the references cited therein.
(17) (a) F. R. Brown, D. H. Finseth, F. A. Miller, and K. H. Rhee, *J. Am. Chem. Soc.*, **97**, 1011 (1975); (b) E. C. Tuazon, D. H. Finseth, and F. A. Miller, *Spectrochim. Acta, Part A*, **31**, 1133 (1975).
(18) F. G. Baglin, *Spectrosc. Lett.*, **3**, 149 (1970).
(19) I. W. Levin and W. C. Harris, *Spectrochim Acta, Part A*, **29**, 1815 (1973).
(20) A. Meic, M. Randic, and A. Rubcic, *Croat. Chem. Acta*, **46**, 25 (1974).
(21) J. Bragin and G. Guthals, *J. Phys. Chem.*, **79**, 2139 (1975).
(22) K. B. Wiberg, D. Sturmer, T. P. Lewis, and I. W. Levin, *Spectrochim. Acta, Part A*, **31**, 57 (1975).
(23) C. E. McBride, Jr., unpublished results.
(24) E. L. Wagner and D. G. Hofning, *J. Chem. Phys.*, **18**, 296 (1950).
(25) IUPAC, "Tables of Wavenumbers for the Calibration of infra Red Spectrometers", Butterworths, Washington, D.C., 1961.
(26) N. L. Allinger, private communication. These data correspond to the calculations reported in ref 15d.
(27) W. A. Seth-Paul and G. Dijkstra, *Spectrochim. Acta, Part A*, **23**, 2861 (1967).
(28) C. M. Richards and J. R. Nielsen, *J. Opt. Soc. Am.*, **40**, 442 (1950).
(29) I. W. Levin, R. A. R. Pearce, and W. C. Harris, *J. Chem. Phys.*, **59**, 3048 (1973).
(30) N. Neto, C. di Lauro, E. Castellucci, and S. Califano, *Spectrochim. Acta, Part A*, **23**, 1763 (1967).
(31) N. Neto, C. de Lauro, and S. Califano, *Spectrochim. Acta, Part A*, **26**, 1489 (1970).
(32) C. di Lauro, N. Neto, and S. Califano, *J. Mol. Struct.*, **3**, 219 (1969).
(33) K. E. Blick, J. W. de Haan, and K. Niedenzu, *Spectrochim. Acta, Part A*, **26**, 3219 (1970).
(34) D. F. Burow, private communication.
(35) J. Overend and J. R. Scherer, *J. Chem. Phys.*, **32**, 1289 (1960).
(36) We thank Professor Overend for making copies of the programs available to us. We found it advantageous to generate an overlay version of the force constant refinement program (appropriately named OVEREND). Use of these programs for GVFF calculations is equivalent to assuming that the **Z** matrix of ref 33 is the identity matrix **E**.
(37) (a) J. H. Schachtschneider and R. G. Snyder, *Spectrochim. Acta*, **19**, 117 (1963); (b) T. Miyazawa, *J. Chem. Phys.*, **29**, 246 (1958).
(38) E. B. Wilson, Jr., J. C. Decius, and P. C. Cross, "Molecular Vibrations", McGraw-Hill, New York, N.Y., 1955.
(39) J. Overend, Ohio State Symposium on Molecular Structure Spectroscopy, June 1961.
(40) J. C. Decius, *J. Chem. Phys.*, **17**, 1315 (1949).
(41) The preliminary (unconstrained, see text) results are perhaps of interest with regard to the effect of the different starting values of K_D (mdyn/Å). With the 26-parameter potential function a zero-order value of 6.61 refined to a final value of 6.81, while a zero-order value of 8.70 refined to a final value of 8.12. When the 37-parameter potential function was employed, a zero-order value of 6.61 refined to a final value of 7.21, while the zero-order value of 8.70 refined to a final value of 8.35. In this case, however, the smaller final value of K_D was accompanied by an unusually large bending force constant, $H = 1.72$ mdyn Å/radian^2.
(42) R. G. Snyder and J. H. Schachtschneider, *Spectrochim. Acta*, **21**, 169 (1965).
(43) See, for example, (a) B. L. Crawford, Jr., J. E. Lancaster, and R. G. Inskeep, *J. Chem. Phys.*, **31**, 678 (1953); (b) J. M. Comerford, W. H. Snyder, and H. S. Kimnel, *Spectrosc. Lett.*, **4**, 9 (1971); (c) P. Pulay and W. Meyer, *J. Mol. Spectrosc.*, **40**, 59 (1971); (d) J. L. Duncan, D. C. McKean, and P. D. Mallinson, *ibid.*, **45**, 221 (1973).
(44) (a) G. Dallinga and L. H. Toneman, *Recl. Tray. Chim. Pays-Bas*, **87**, 795, 805 (1968); (b) A. Yokozeki and K. Kuchitsu, *Bull. Chem. Soc. Jpn.*, **44**, 2356 (1971).
(45) J. Hine, J. A. Brown, L. H. Zalkow, W. E. Gardner, and M. Hine, *J. Am. Chem. Soc.*, **77**, 594 (1955).
(46) M. J. Goldstein and R. Hoffmann, *J. Am. Chem. Soc.*, **93**, 6193 (1971).
(47) F. A. Van-Catledge, *J. Am. Chem. Soc.*, **96**, 5693 (1974); **97**, 4151 (1975).

ADDITIONS AND CORRECTIONS

1975, Volume 79

Hsin-Chou Chiang and Aaron Lukton: Interaction of Sodium Dodecyl Sulfate with the Hydrophobic Fluorescent Probe, 2-*p*-Toluidinylnaphthalene-6-sulfonate.

We have to correct some of our data which was published in ref 1 as follows:

(1) The $\Delta H = -3.245$ kcal/mol should be changed to $\Delta H = -3.245$ kcal/mol $\times$ 2.303 = -7.473 kcal/mol.[2] Thus, the original ΔS values of Table II should be corrected as follows:

Temp, °C	Ionic strength of added salt 0	0.05	0.10
15	−10.10	−9.049	−7.753
25	−10.10	−8.963	−7.503
35	−9.946	−8.893	−7.685

Therefore, the SDS micelle–TNS interaction is exothermic and involves a negative entropy change. However, an increase in NaCl concentration increases the association constant for the interaction by increasing the positive entropy change, that is, as noted in the corrected Table II, that salt makes the ΔS value less negative. The conclusion that the SDS micelle–TNS interaction should be hydrophobic in nature is still valid. A similar ΔS value change has been observed for the interaction of TNS with phosphatidylcholine vesicle.[3]

(2) If cmc/$[M]_{total} > 5\%$, then eq 4 in ref 1 should be changed to

$$[Mn_{total}] = \frac{1}{n}([M]_{total} - cmc)$$

with the result that the $[M]_{total}$ term of eq 7 in ref 1 should be changed to $([M]_{total} - cmc)$. Thus, the points of I at 1/SDS = 29.5 in Figure 5a–c (without NaCl) now fall on the lines. The $([M]_{total} - cmc) = [M]_{total}$ can be assumed when $[M]_{total}$ is very large, which was the case in the experiments of Figure 5a–e or when the cmc is very small so that the ratio is cmc/$[M]_{total} < 5\%$.

(3) Some of the cmc values in Table I are significantly smaller than the literature data cited, as noted in Birdi's comment in this issue of the Journal. Our results show that the higher the salt concentration, in the range 0.033–0.10 M, the greater the deviation of cmc values obtained by TNS fluorescent measurement as compared to other methods. One possible explanation is that at these ionic strengths, TNS may induce SDS oligomer formation resulting in SDS oligomer–TNS complexes, which show TNS fluorescence enhancement at the SDS concentrations lower than literature cmc values. However, SDS oligomer–TNS complexes do not represent SDS micelle–TNS complex. Higher salt concentrations may facilitate SDS oligomer formation by the effect of increasing the hydrophobic interaction of SDS monomer and TNS. The results would show larger deviations of the cmc values reaching a maximum effect at ionic strengths higher than 0.2 M.

In our study of TNS interacting with dodecyltrimethylammonium chloride (DoTAC) (unpublished data), we found that TNS could induce the formation of DoTAC oligomer–TNS complex and that DoTAC oligomer induced by TNS could be composed of more than three monomers. It should be noted here that TNS has been found to induce self-association of human luteinizing hormone[4] and human chorionic gonadotropin[5] respectively at the concentration ranging from 1.0×10^{-5} to 8.0×10^{-4} M. We find that the absorbance of TNS in the concentration range 1×10^{-5} to 1.2×10^{-4} M in 0.5 M NaCl still follows Beer's law (366 nm, ϵ 4.1×10^3)[6] and that there is no eximer formation detectable. Therefore, the possible formation of ground state or excited state dimer of TNS can be ruled out.

References and Notes

(1) H.-C. Chiang and A. Lukton, *J. Phys. Chem.*, **79**, 1935 (1975).
(2) We are grateful to Dr. A. Yoshimura of the Institute of Chemistry, Osaka University, for this correction.
(3) C. Huang and J. P. Charlton, *Biochemistry*, **11**, 735 (1972).
(4) K. C. Ingham, M. A. Saroff, and H. Edelhoch, *Biochemistry*, **14**, 4745 (1975).
(5) K. C. Ingham, H. A. Saroff, and H. Edelhoch, *Biochemistry*, **14**, 4751 (1975).
(6) W. O. McClure and G. M. Edelman, *Biochemistry*, **5**, 1908 (1966).

—H.-C. Chiang and A. Lukton

1976, Volume 80

Eli Grushka, E. J. Kikta, Jr., and H. T. Cullinan, Jr.: Binary Liquid Diffusion Prediction in Infinitely Diluted Systems Using the Ultimate Volume Approach.

Page 757. The data for octaphenone were omitted from Table II, causing a transposition of data between octaphenone data and heptaphenone. Also, the correlation coefficient for nonaphenone is in error. The corrected table should read as follows:

TABLE II: Data from the Linear Regression D_{ij}/RT Vs. $(\rho - \rho_0)$ Forced through the Origin

Compound	$10^{15}S$	Corr coef	F test	10^{-16} a_{ij}
Acetophenone	−8.71	0.992	251	5.17
Propiophenone	−8.11	0.993	274	5.56
n-Butyrophenone	−7.63	0.986	177	5.90
Isobutyrophenone	−6.96	0.995	438	6.47
Valerophenone	−6.96	0.993	278	6.47
Isovalerophenone	−6.51	0.996	531	6.92
Hexaphenone	−6.64	0.994	351	6.78
Heptaphenone	−6.41	0.997	580	7.08
Octaphenone	−6.18	0.998	917	7.29
Nonaphenone	−5.94	0.998	1140	7.58
Decaphenone	−5.74	0.996	450	7.85
Myristophenone	−5.53	0.996	558	8.15
Benzene	−16.04	0.999	1491	2.81

It should be noted that the headings in Tables II and III which read $10^{16}a_{ij}$ should read $10^{-16}a_{ij}$.

—Edward J. Kikta, Jr.

E. J. Hamilton, Jr., and C. A. Naleway: Theoretical Calculation of Strong Complex Formation by the HO_2 Radical: $HO_2 \cdot H_2O$ and $HO_2 \cdot NH_3$.

Page 2038. In the left-hand column, line 7, substitute "... on the H atom ..." for "... on the atom ...".
—E. J. Hamilton, Jr.

AUTHOR INDEX to Volume 80, 1976

Note: In this Author Index, titles of papers are listed after the name of each author of the paper. Multiple authorship is not indicated. Complete authorship may be ascertained by consulting the original paper.

KEYWORD INDEX to Volume 80, 1976

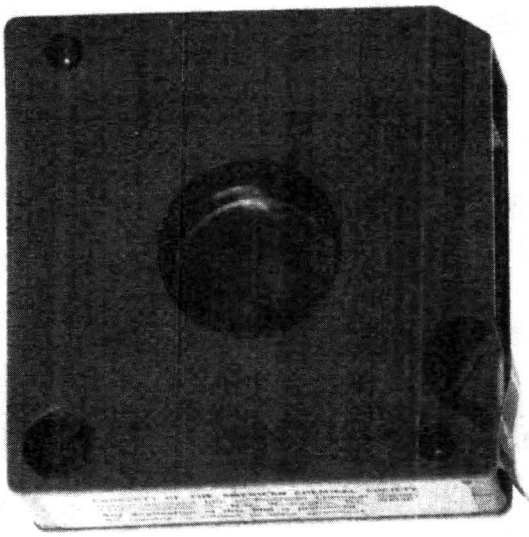

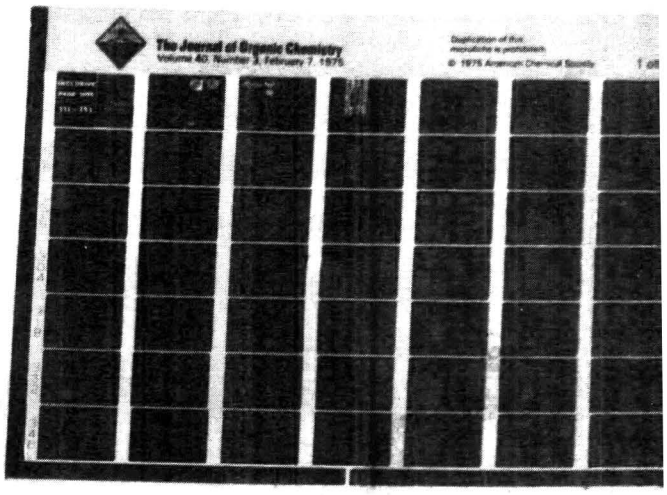

MICROFORMS

American Chemical Society publications in microform

MICROFILM OR MICROFICHE?

With the ACS microform program you can receive either, or both

Microfilm

All periodical publications back to volume one

Copying privileges included with current subscriptions

All non-print supplementary materials provided free on microfiche

Archival quality silver halide film supplied as you request; positive or negative; 16 or 35mm; cartridge, reel, or cassette.

Microfiche

Current issues of primary journals, beginning with January 1975

Individual issues or full volumes available

Supplementary materials also available on microfiche

Fiche supplied are archival quality silver halide, negative, 105 x 148mm (4" x 6"); 24x, with eye legible headers, start and end targets, and page numbers

For information about our microfilm/microfiche write:

Microform Program
Special Issues Sales
American Chemical Society
1155 16th Street, N.W.
Washington, D.C. 20036
(202) 872-4363

Not just a book...

A Celebration!

The American Chemical Society celebrates its one hundredth birthday with a present for you.

"Taking Things Apart & Putting Things Together" is lively, informative, colorful and imaginatively illustrated. It sums up the vital role chemistry plays in our lives with easy-to-read case histories . . . . cartoons . . . . magnificent photographs . . . . and illustrations.

And because the book is in celebration of the ACS role in chemistry, the price is only $2.50!

Students, teachers, laymen, librarians, even chemists—all will want *"Taking Things Apart & Putting Things Together"*. All you have to do is complete the coupon below and mail it back to us today! We'll do the rest.

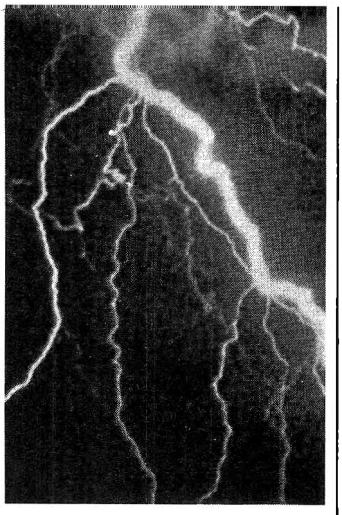

Without Us: The Nature of Chemistry

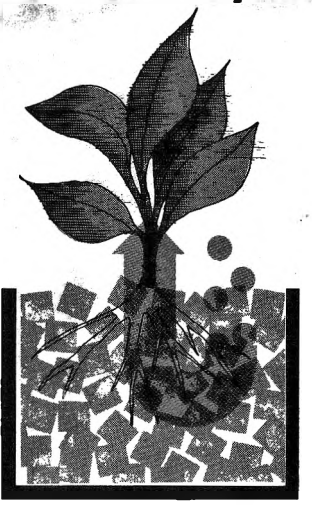

Supporting Us: The Chemistry of Farming

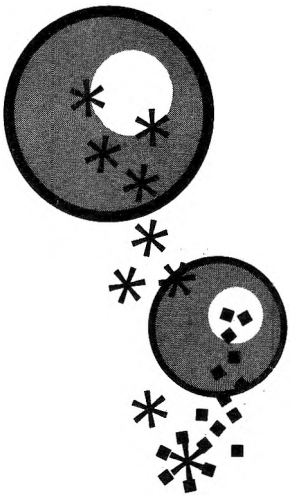

Inside Us: The Chemistry of Staying Well

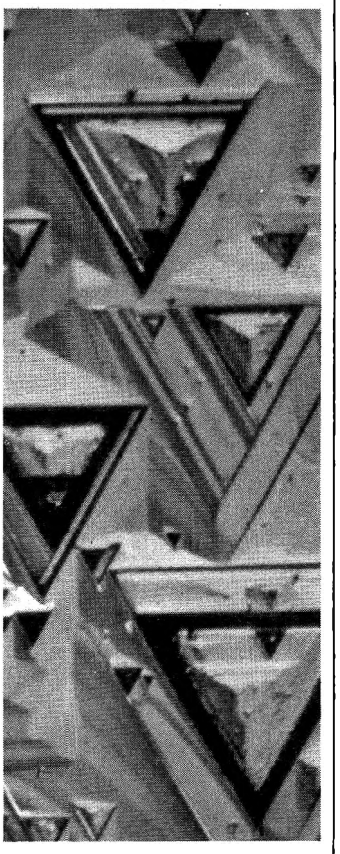

Extending Our Senses: Seeing Further With Chemistry

Around Us: What Chemists Make for People

Amplifying Our Power: The Chemistry of Energy

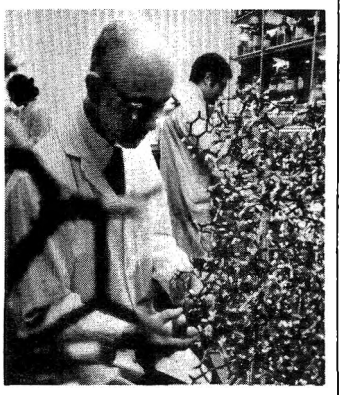

Choices Through Chemistry

Special Issue Sales, American Chemical Society
1155 Sixteenth Street, N.W., Washington, D.C. 20036

Please send me _____ copies of *"Taking Things Apart & Putting Things Together"*.

☐ Paperback $2.50 ☐ Hardback $6.00

Name _____

Address _____

City _____

State _____ Zip Code _____

Check must accompany order. Bulk rates available on request.

AX

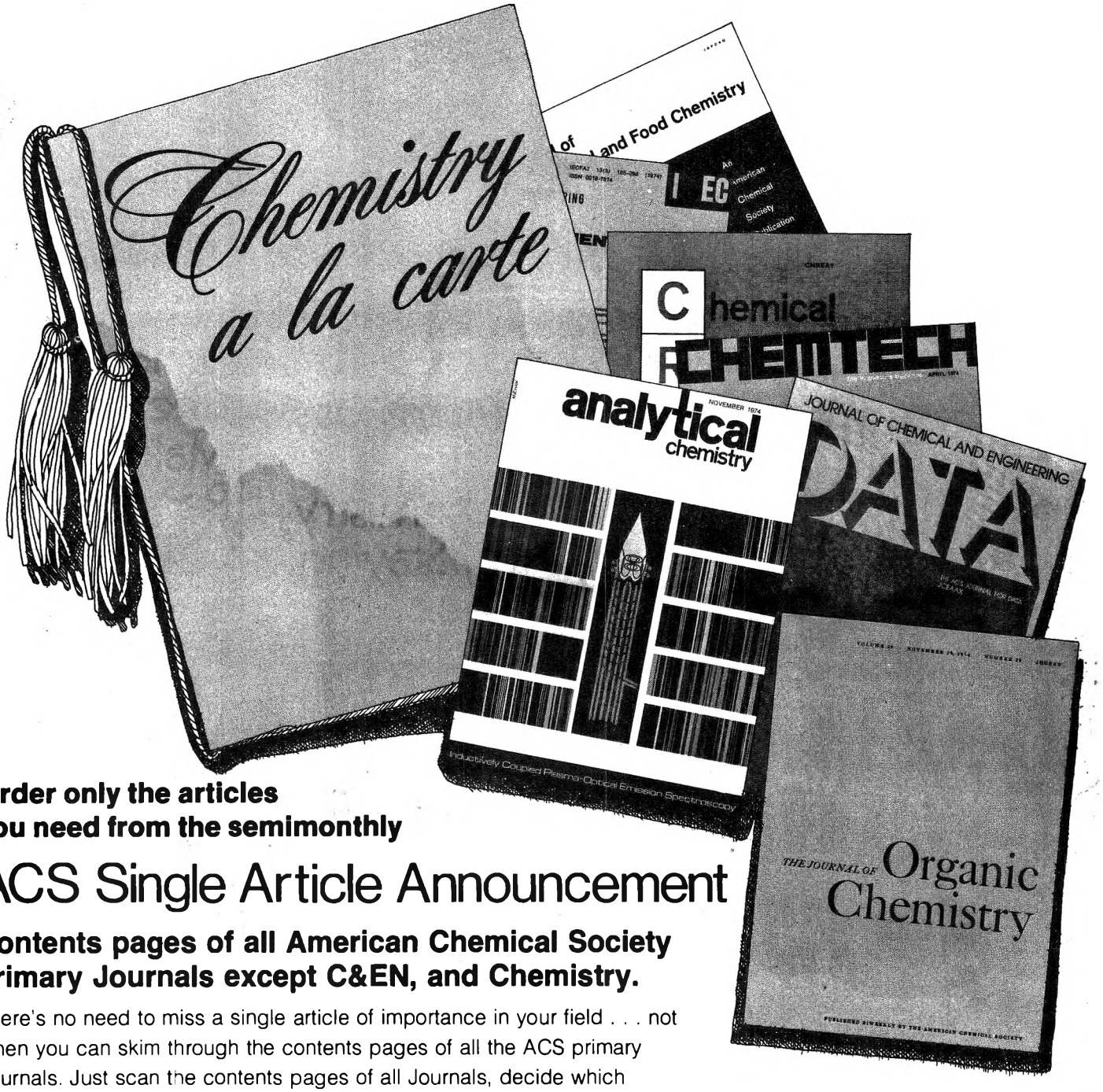

Order only the articles you need from the semimonthly

ACS Single Article Announcement

Contents pages of all American Chemical Society primary Journals except C&EN, and Chemistry.

There's no need to miss a single article of importance in your field . . . not when you can skim through the contents pages of all the ACS primary Journals. Just scan the contents pages of all Journals, decide which articles are important to you and order them. A special form is provided so that you can let us know the material you want, and we will rush it to you! Send the coupon now and start receiving your subscription to the time-saving ACS SINGLE ARTICLE ANNOUNCEMENT.

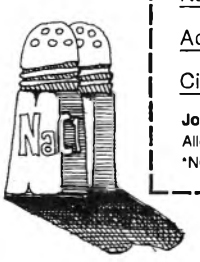

SINGLE ARTICLE ANNOUNCEMENT **1977**
American Chemical Society
1155 Sixteenth Street, N.W.
Washington, D.C. 20036

Yes—I wish to receive the ACS SINGLE ARTICLE ANNOUNCEMENT at the one-year rate checked below:

	U.S.	Canada Foreign	PUAS
ACS Member*	☐ $12.00	☐ $16.50	☐ $16.00
Nonmember	☐ $24.00	☐ $28.50	☐ $28.00

☐ Payment enclosed ☐ Bill me ☐ Bill company ☐ I am an ACS member
☐ I am not an ACS member

Air freight rates available on request.

Name _____ Position _____
(Specific title please)

Address ☐ Home ☐ Business _____

City _____ State/Country _____ Zip _____

Journal subscriptions start in January '77.
Allow 90 days for your first copy to be mailed.
*NOTE: Subscriptions at ACS member rates are for personal use only.

Prof.
Prof.

College

ssoc. Prof.
oc. Prof.
Asst. Prof.
sst. Prof.
D, Asst. Prof.

rsity

) 658-2261

C), PhD, *Professor*
PhD, *Professor*
D, *Professor*
PhD, *Assoc. Prof.*
D, *Assoc. Prof.*
D, *Assoc. Prof.*
r., PhD, *Assoc. Prof.*
D, *Assoc. Prof.*
PhD, *Assoc. Prof.*
ose H., MS, *Assoc. Prof.*
n B., PhD, *Assoc. Prof.*
., PhD, *Asst. Prof.*
., PhD, *Asst. Prof.*
hD, *Asst. Prof.*
d, PhD, *Asst. Prof.*
PhD, *Asst. Prof.*
d L., PhD, *Asst. Prof.*
id, PhD, *Asst. Prof.*

Georgia

mistry,

mistry

on C., PhD, *Professor*
ce C., PhD, *Professor*
S., PhD, *Professor*
obert A., PhD, *Professor*
D., PhD, *Professor*
Hilton J., PhD, *Res. Prof.*
William L., PhD, *Res. Prof.*
ohn M., PhD, *Assoc. Prof.*
y, W. Scott, PhD, *Assoc. Prof.*
nian, Daniel V., PhD, *Assoc. Prof.*
nard V., BS, *Assoc. Professor*
n W., PhD, *Assoc. Prof.*
Jean, PhD, *Assoc. Prof.*
ahl, Lars G., PhD, *Assoc. Prof.*
Robert E., PhD, *Assoc. Prof.*
cino, Joseph F., PhD, *Assoc. Prof.*
, James, PhD, *Assoc. Prof.*
Ronald S., PhD, *Asst. Prof.*
, Richard J., PhD, *Asst. Prof.*
ng, Norman G., PhD, *Asst. Prof.*
stava, Prakash N., PhD, *Asst. Prof.*
npler, John E., PhD, *Asst. Prof.*

sity of Georgia

30602
stry Dept., (404) 542-2626
D, Chemistry

elton, Charles E. (H), PhD, *Professor*
ill, Richard K., PhD, *Professor*
elletier, S. William, PhD, *Professor*
hilbrook, George E., PhD, *Professor*
Allinger, Norman L., PhD, *Res. Prof.*
King, R. Bruce, PhD, *Res. Prof.*
Baldwin, Winfield M., PhD, *Assoc. Prof.*
Cox, Richard H., PhD, *Assoc. Prof.*
Garst, John F., PhD, *Assoc. Prof.*

P Handler, George S., PhD, *Assoc. Prof.*
A Hercules, David M., PhD, *Assoc. Prof.*
P Heric, Eugene L., PhD, *Assoc. Prof.*
O Janzen, Edward G., PhD, *Assoc. Prof.*
P Johnston, Francis J., PhD, *Assoc. Prof.*
I King, Allen D., PhD, *Assoc. Prof.*
P Ruff, John K., PhD, *Assoc. Prof.*
O Smith, Darwin W., PhD, *Assoc. Prof.*
I Stammer, Charles H. PhD, *Assoc. Prof.*
G Waggoner, William H., PhD, *Assoc. Prof.*
A Whitten, Kenneth W., PhD, *Assoc. Prof.*
O Carr, Peter W., PhD, *Asst. Prof.*
A Cassen, Tom, PhD, *Asst. Prof.*
A Hautala, Richard R., PhD, *Asst. Prof.*
O Kelly, Patrick C., PhD, *Asst. Prof.*
P Klatt, Leon N., PhD, *Asst. Prof.*
I Nelson, Robert F., PhD, *Asst. Prof.*
P Newton, Gary M., PhD, *Asst. Prof.*
A Schelly, Zoltan A., PhD, *Asst. Prof.*
A Wynne, Kenneth J., PhD, *Asst. Prof.*
A Bobbio, Stephen M., PhD, *Instructor*
Carreira, Nionel A., PhD, *Instructor*
Kutal, Charles R., PhD, *Instructor*
Leyden, Donald E., PhD, *Instructor*
Seitz, William R., PhD, *Instructor*

University of Georgia

Athens 30602
Dept. of Medicinal Chemistry,
(404) 542-3077
B, M, D, Medicinal Chemistry

X LaRocca, Joseph P. (H), PhD, *Professor*
OX Blanton, DeWitt C., Jr., PhD, *Assoc. Prof.*
OX Honigberg, Irwin L., PhD, *Assoc. Prof.*
AX Stewart, James T., PhD, *Assoc. Prof.*
BX Thompson, Bobby B., PhD, *Assoc. Prof.*
BX Martinelli, Louis C., PhD, *Asst. Prof.*
AX Sternson, Larry A., PhD, *Asst. Prof.*

Gordon Junior College (2)

Barnesville 30204
Dept. of Math-Science, (205) 358-1700,
Ext. 72

AGO Smith, Maurice R., MS, *Instructor*

LaGrange College

LaGrange 30240
Dept. of Chemistry, (404) 882-2911,
Ext. 71
B, Chemistry

ABGO Hicks, Artaur M. (H), PhD, *Professor*
AIPX Hicks, Patrick M., MS, *Assoc. Prof.*
ABOP Cooper, Kenneth, PhD, *Asst. Prof.*

Macon Junior College (2)

Macon 31206
Div. of Natural Sciences and Mathematics,
(912) 745-8551, Ext. 262, 263

G Dever, David F., PhD, *Assoc. Prof.*

Mercer University

Macon 31207
Dept. of Chemistry, (912) 743-1511,
Ext. 287
B, Chemistry

AG James, Franklin W. (C), PhD, *Professor*
AIG Furse, Clare T., PhD, *Professor*
GP Marquart, John R., PhD, *Assoc. Prof.*
OX Wiesler, Donald P., PhD, *Asst. Prof.*
GO Taylor, Robert E., MEd, *Instructor*

Mercer University in Atlanta

Atlanta 30341
Dept. of Science and Mathematics,
(404) 451-0331, Ext. 46
B, Chemistry

AIGO Edwards, Henry L. (C), PhD, *Professor*

Tape Recordings for Lab Professionals

☐ **TLC—Best for Drug Abuse Screening**
Low-cost alternative to immunoassays

☐ **Microcomputers in Biochemistry Research**
New computers make possible hitherto impossible measurements

☐ **Data Analysis in the Lab**
Today and tomorrow in chem lab data analysis methods

☐ **Use of Enzymes in Immunology**
Detection of bound and free antigen without separation

☐ **Elemental Analysis of Blood: Cancer Patients & Controls**
Detailed comparisons, plus evaluation of analytical methods used

☐ **Polarographic Analysis in Drug Development**
D.P.P. assays of drugs in biological fluids

☐ **Bioanalysis with Membrane Electrode Probes**
Recent advances in electrode development

☐ **In Vivo Electrochemistry for Monitoring Drugs**
Reveals drug's chemical fate in the brain

☐ **Detection of Lipids & Amines in Biological Samples**
Chemical ionization mass spec speeds assay of closely related chemicals

☐ **Pulse Polarography Analysis in Environmental Toxicology**
Solves tough problems in human and animal poisoning

☐ **New Developments in Measurement of Proteins**
Light scattering of immune complexes provides a specific method for proteins in body fluids

☐ **Direct Determination of Drugs in Plasma & Urine**
Non-chromatographic procedure uses chemical ionization mass spec & stable isotope labeling

☐ **DSC: New Developments in Clinical Analysis**
Differential Scanning Calorimetry—a new analytical tool

☐ **Serum Electrolytes Using Vidicon Flame Spectrometry**
Fast, simultaneous determination of sodium, potassium, and calcium

☐ **Enthalpimetric Analysis of Immunological Reactions**
Thermometric enthalpy titration may revolutionize serological analysis

☐ **Clinical Application of Titration Calorimetry**
Thermochemical methods look very promising for clinical work

☐ **GC Determination of Apomorphine in Urine**
Study of apomorphine metabolism

☐ **Metals in Liver & Kidney Tissue by AA**
AA determination of copper, zinc, magnesium, and calcium

☐ **Bromazepam in Blood by Electron Capture GLC**
A sensitive, specific assay

☐ **Drug Analysis by Direct Multiple-Ion Detection**
Unique computerized system analyses drugs without use of GC

☐ **Thermochemical Analysis in Clinical Chemistry**
Total protein content in biological material can be determined with a precision of better than 0.6%

☐ **Amperometric Measurement of Enzyme Reactions**
Enzyme reactions are monitored by amperometric measurement of substrate depletion, product formation

☐ **Homovanillic Acid by GC-MS**
A simple procedure for HVA in urine

☐ **Kinetic Assay of Enzyme Activity**
Centrifugal fast analyzer provides data at output rate suitable for direct input into small computer

☐ **Automated Photochemical Analysis of Phenothiazines**
Samples were assayed by this system at the rate of 20 per hour

☐ **Automation in Clinical Medicine**
A Bureau of Standards colloquium

☐ **Analysis of Trace Elements**
Sensitive, reliable analytical methods are needed for trace elements

☐ **Electrochemical Approaches to Clinical Instrumentation**
Precise, accurate, highly specific analyses using ultramicro samples

☐ **Standardization of Protein & Enzyme Assays**
Biuret reaction as standard for measuring total serum protein

☐ **Pharmacologic Studies Using GC-MS**
Utility of GC-MS is emphasized in a report of two pharmacologic studies

☐ **Method Evaluation Studies in Clinical Analyses**
Method evaluation studies on precision and accuracy of lab methods

ORDER FROM:
American Chemical Society
1155 16th St., N.W.
Washington, D.C. 20036
ATTN: Dept. AP

PRICE: $8.95 per title, includes visual materials. **CASSETTES ONLY** **CHECK TITLES DESIRED**
(Allow 4 to 6 weeks for delivery)

Name _____

Address _____

17 S.P. 2520